CRIS SDR OVERVIEW

Yong Han

NOAA/STAR

Outline

- Team Members
- J1 CrIS status
- S-NPP CrIS status
- Issues and ongoing work
- Summary and Path Forward

Team Members

PI	Organization
Yong Han	NOAA/STAR
Dave Tobin	U. of Wisconsin (UW)
Larrabee Strow	U. of Maryland Baltimore County (UMBC)
Deron Scott	Space Dynamic Lab (SDL)
Dan Mooney	MIT/LL
Dave Jonson	NASA Langley
Lawrence Suwinski	Harris
Joe Predina	Logistikos
Carrie Root	JPSS/AMP
Wael Ibrahim	Raytheon

J1 CrIS Readiness

- J1 CrIS status at the 2015 annual meeting
  - Successfully completed environmental test campaign
  - Determined the pre-launch version of the calibration coefficients and parameters
  - Characterized the instrument performance with the pre-launch data
  - Delivered the first version of the J1 CrIS SDR processing algorithm
- J1 CrIS current status
  - The instrument is undergoing S/C level testing and has successfully completed the EMI testing
  - Mounting matrix for the SDR algorithm was computed and delivered
  - Improved SDR algorithm was delivered in July 2016
  - There is no critical issue

Algorithm Updates Delivered in July 2016

- On top of the J1 CrIS algorithm delivered on January 30, 2015, the following updates were delivered last month,
  - A4 algorithm implementation (spectral calibration prior to radiometric calibration) to improve calibration accuracy
  - Use of longer interferogram to reduce ringing artifacts
  - Use of wider post calibration filter to increase the usage of the guard band signals
  - Correction of the geolocation algorithm
  - Band-dependent lunar intrusion threshold added to the PCT file

SNPP CrIS Status: SDR processing

- CrIS transition to extended FSR mode on 11/02/2015 (CrIS transition to FSR mode on 12/4/2014)
- NOAA operational TSR SDRs (IDPS)
- NOAA FSR SDRs (STAR)
  - IDPS SDR format
  - bufr format converted by Walter's team
- Both TSR and FSR performances are monitored with ICVS

SDR Processing Time Line

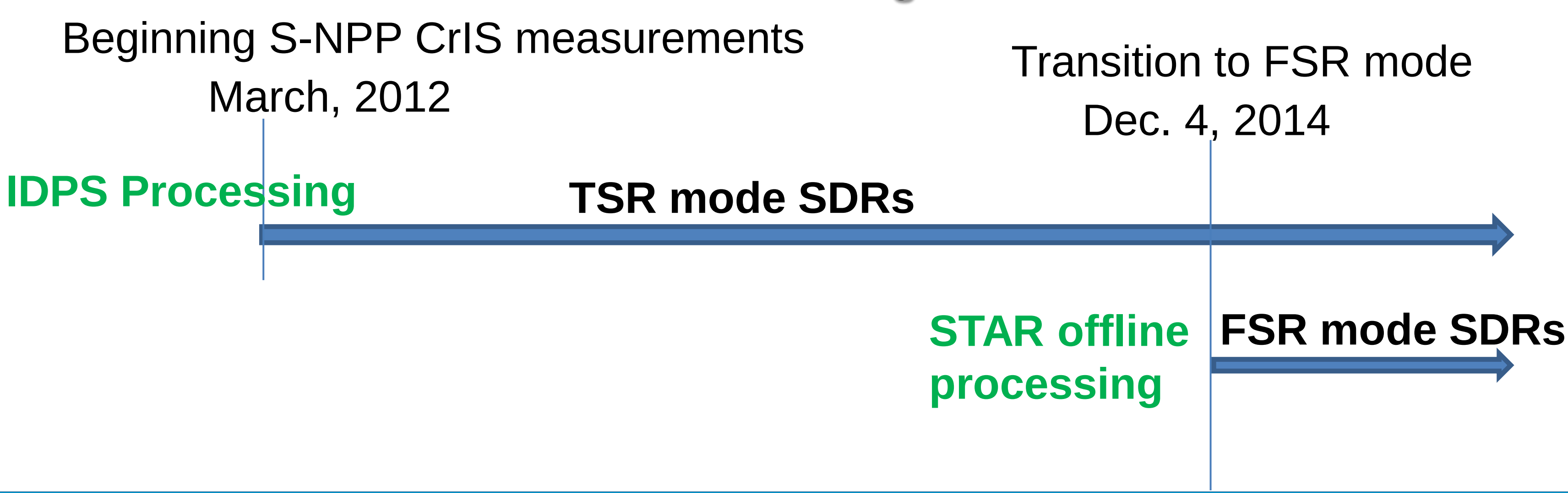

SNPP CrIS Status: stable NEdN

STAR ICVS

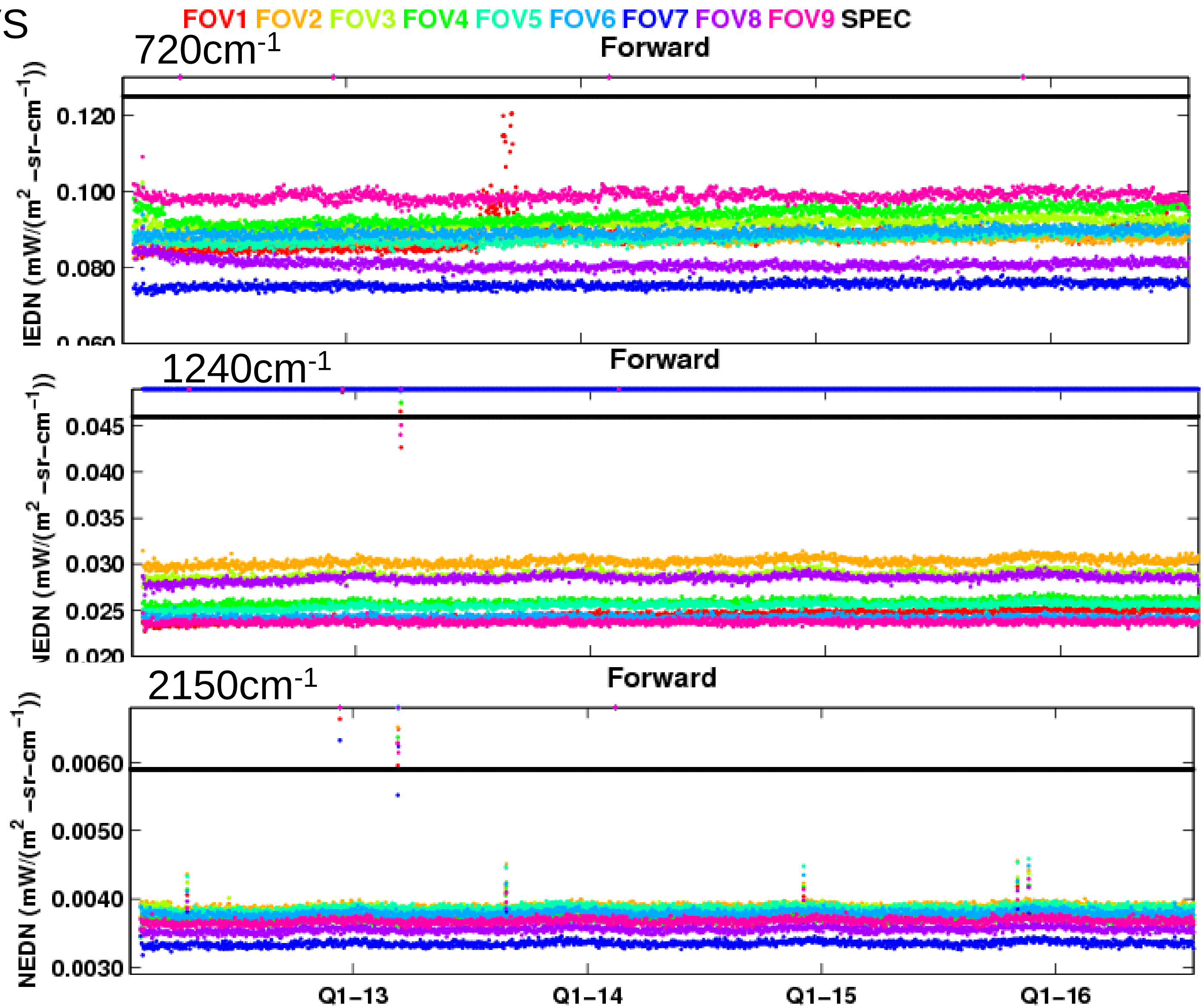

SNPP CrIS Status: stable Gain

STAR ICVS

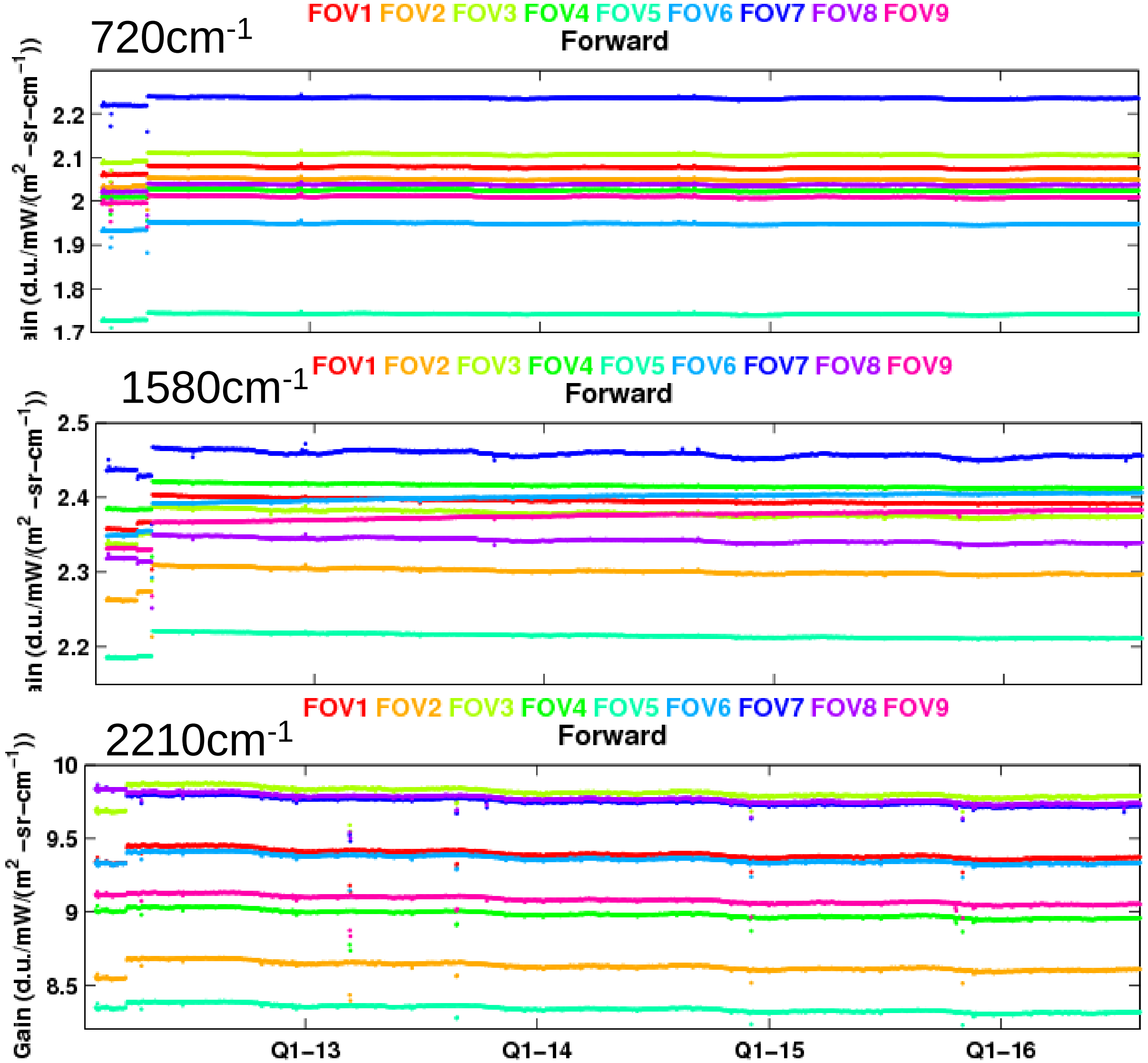

STAR CrIS Data Reprocessing

- Engineering packet version 36 (the latest) with geolocation mapping parameter updates and new MW FOV7 NL a2 coefficient
- ADL with A4 calibration algorithm and improved geolocation algorithm
- SDR truncation spectral resolution (TSR) mode for the whole history
- SDR full spectral resolution (FSR) mode since December 4, 2014
- Latest RDR version
- Processing system capability: 1 year data / 6 days
- CrIS data reprocessing will be completed by the end of this month

Team Activities: Telecon Presentations

- 23 bi-weekly telecons (8/16/2015 – 8/3/2016)
- 51 telecon presentations

Presentation subjects	Presenter (# of presentations)
Calibration equation	STAR(3), UMBC(2), MIT/LL(4), Logistikos(2), SDL(2)
Extended IFG & FIR convolution correction	SDL(1), STAR(1), UW(2), MIT/LL (2), UMBC (1)
LW FOV5 cold scene anomaly	SDL(1), UW(2)
Polarization	UW(3), Harris(1), STAR(1)
Geolocation	STAR(2)
J1 S/C level data analysis	SDL(3), STAR(2), MIT/LL(1)
SNPP anomaly analysis	STAR(2)
FIR, a2 & FOV size optimizations	UW(4), STAR (2), Logistikos(2), UMBC(1)
SNPP & J1 environmental models	SDL(2), UW(1)
Noise & O-B correlation	SDL(1), UMBC(1)

Issues and Ongoing Work

- FIR convolution correction
- LW FOV-5 cold radiance anomaly
- Channel SRF consistency
- Polarization signals and correction
- FCE correction module efficiency

FIR Convolution Correction

- Issue: FIR digital filtering (convolution) is not performed circularly and consequently the FIR gains can not completely removed from the spectra, causing ringing artifacts
- The team has been working on methods to correct the non-circular convolution error
- Two correction methods were implemented in the ADL code, delivered in July 2016 (neither turned on yet).
- The remaining work: compare and validate the methods

Raw spectrum difference from truth

Ringing artifacts

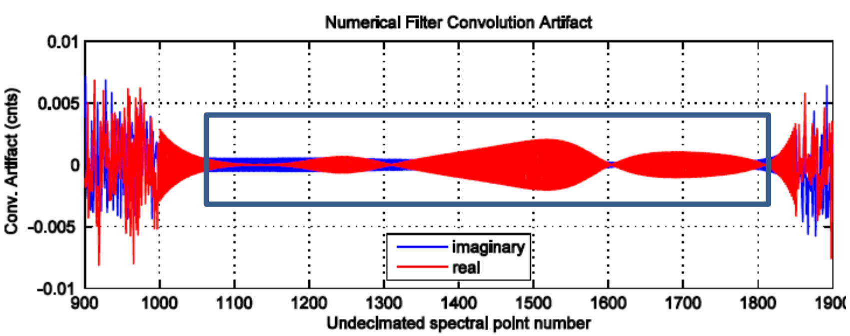

Ringing reduction by truncating IFG

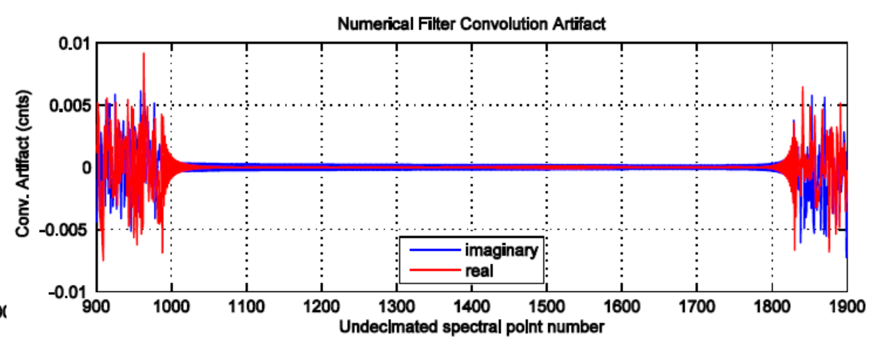

UW

LW FOV-5 Cold Scene Anomaly (1/2)

- It was noticed a year ago that SNPP CrIS LW FOV5 radiance near 668 cm-1 is out-of-family with the other 8 FOVs over tropical high cold cloud or over Greenland and Antarctica

Anomaly over high cold clouds

NOAA Algorithm #1: FOR 15 FOV 2, 5, 8 Tropical Atmosphere (ITCZ)

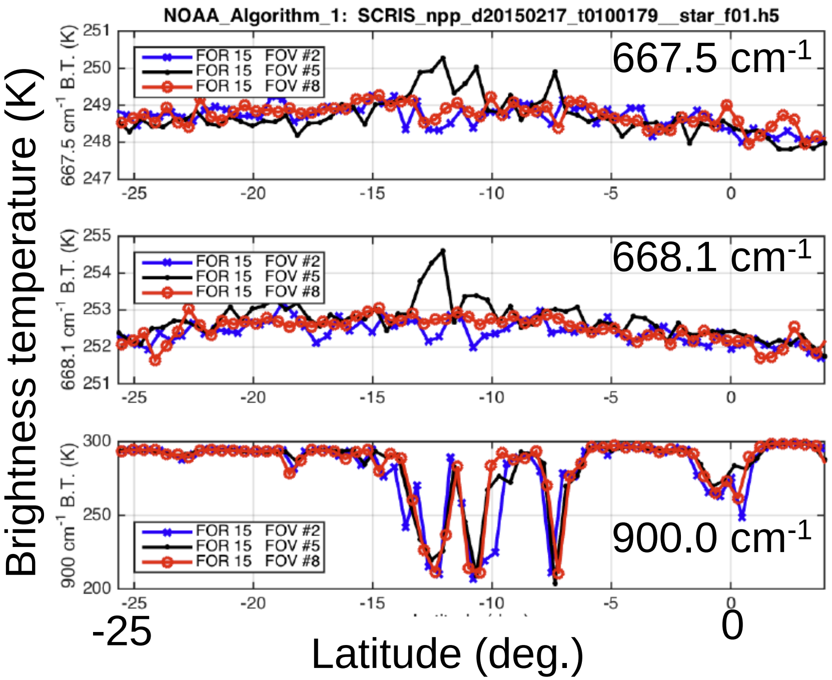

UW

Anomaly over Antarctic scene in both sweep direction

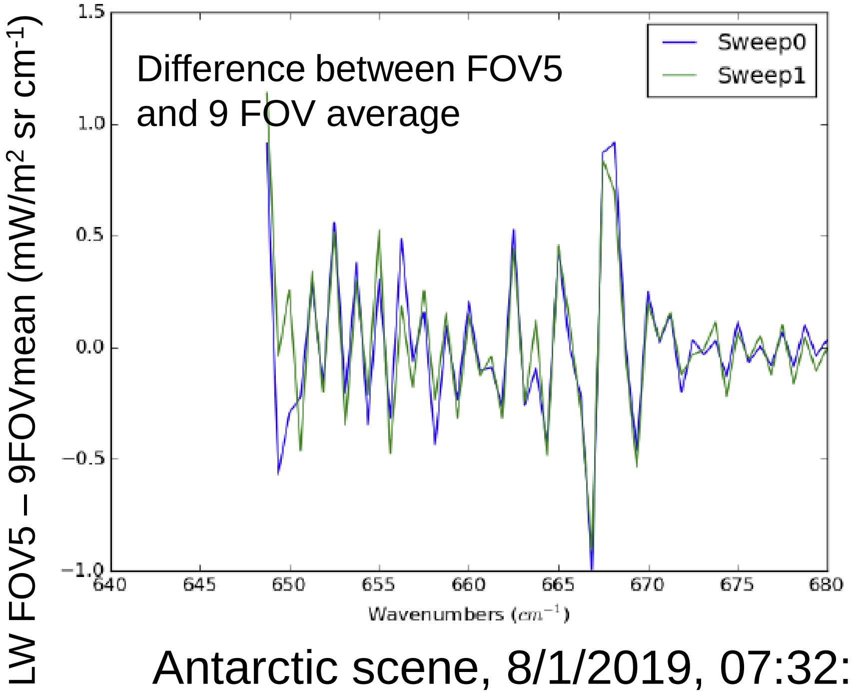

Antarctic scene, 8/1/2019, 07:32:48

SDL

LW FOV-5 Cold Scene Anomaly (2/2)

- The team has been working to understand the cause and developing mitigation solutions
- Unresolved channeling from beamsplitter as the mechanism was investigated by UW and SDL
- Results:
  - both of beamsplitter /componsator ZnSe substrates and air gap could give unresolved channeling from internal reflection
  - Simulation results qualitatively fit the symptoms; however, the simulated artifact magnitude is much smaller than the observed
- Investigation is ongoing

Channel SRF Consistency

- Due to the band limiting by the sensor responsivity, the SDR edge channels have slightly different spectral response function (SRF) from the defined Sinc function
- An RT model built with the CrIS responsivity functions can accurately model the channel SRFs
- However, since the responsivity may differ slightly among different CrIS instruments, the channel SRFs may also differ slightly across different CrIS sensors
- The team has been working to assess the impact of the responsivity variations and possibly develop calibration methods to address the SRF consistency issue

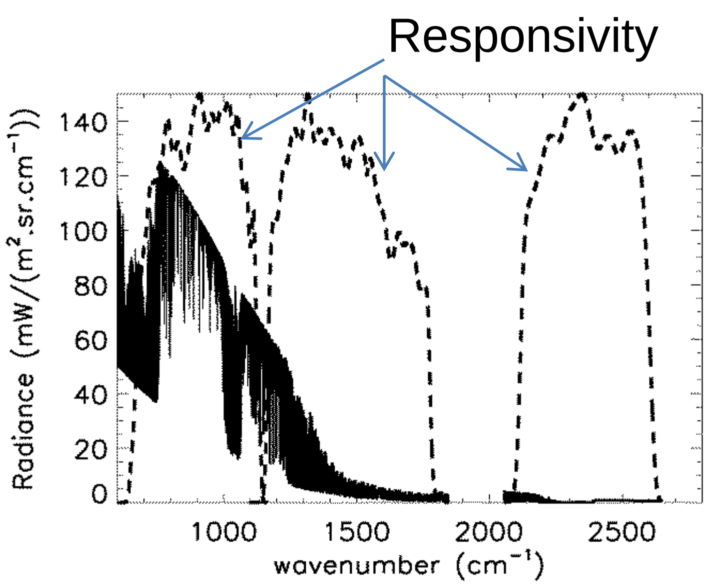

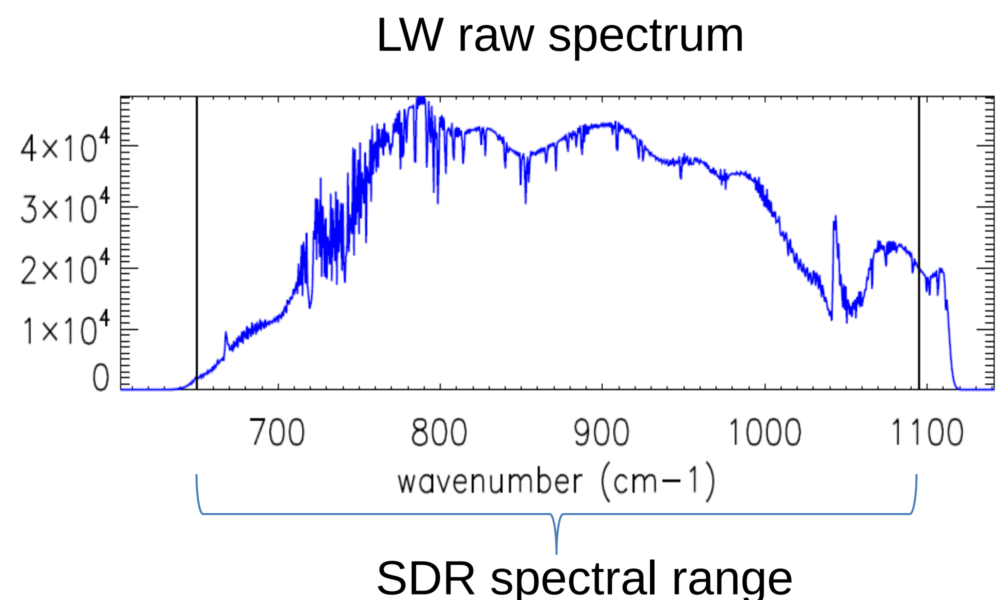

Polarization Signals & Correction

- On 9/16/2015, UW presented an analysis showing scan dependent difference between CrIS and VIIRS, possibly due to CrIS SSM and sensor polarization
- Subsequently, two investigation reports were provided by STAR and UW on the analysis of SNPP pitch maneuver data (deep space scan observations)
- Polarization correction has been formulated
- The team will further characterize the impact of the polarization and validate the benefit of polarization effect correction

Polarization signals in LW band pith maneuver data

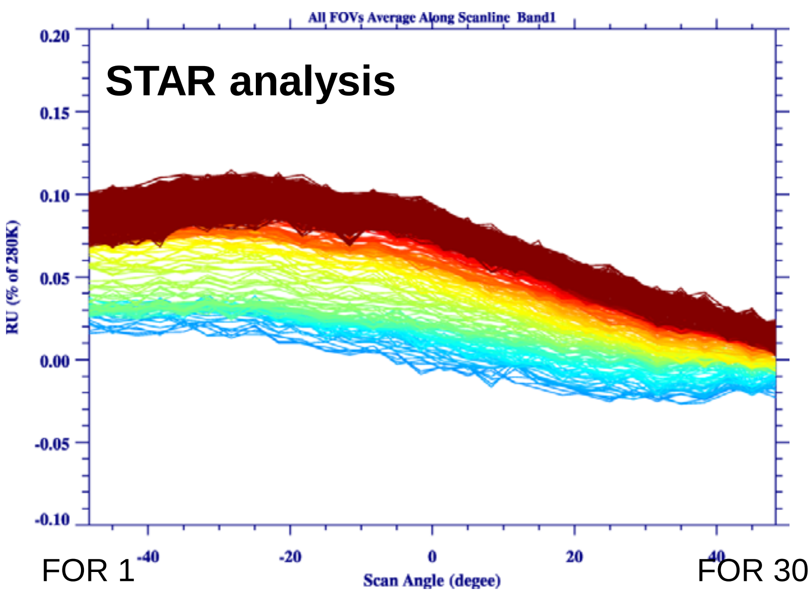

UW analysis

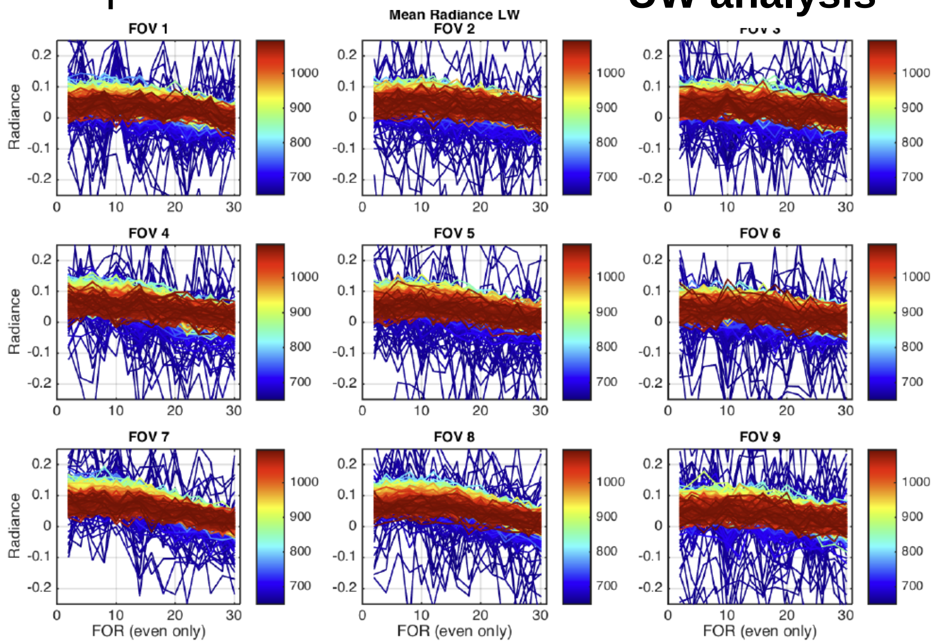

FCE Correction Latency

- Fringe Count Error (FCE) correction module has been turned off so far for SNPP due to software errors and the inability to work for cold scenes
- Fortunately, there has been no FCE event detected so far from SNPP CrIS data
- A new FCE module based on an iteration process to minimize the imaginary part of the calibrated spectrum was implemented and delivered in March 2016 for the J1 SDR processing software
- Unfortunately, the latency of the SDR processing with the FCE module does not meet IDPS requirement
- Since the improvement of the FCE module latency requires a large effort, the solution of latency issue will depend on the following considerations:
  - Whether there will be any FCE events seen from the S/C level TVAC
  - Whether IDPS can increase the number of parallel processing jobs
- The team will make a decision before the end of this year on the need to improve the FCE correction module

Summary

- The J1 CrIS SDR algorithm/software is ready for J1 mission
- SNPP CrIS performance is stable and there is no significant SDR performance degradation
- FSR SDRs are routinely generated for the NWP and retrieval communities
- Great progress was made in advancing CrIS SDR science, including calibration algorithm, digital filtering, FOV size optimization, and polarization

Path Forward

- For the J1 mission, the team will
  - analyze the S/C TVAC data
  - support validation of the operational SDR software
  - execute post-launch CalVal plan
  - Provide the Beta, Provisional and Validated SDR products on schedule
- The team will continue working to address the issues: FIR convolution correction, LW FOV5 cold scene anomaly, polarization, and FCE latency
- SNPP CrIS observation approaches 5 years; the team will
  - analyze the history of the data
  - continue monitoring its performance and SDR health

Space Dynamics LABORATORY
Utah State University Research Foundation

LW FOV5 Update

Introduction

- For S-NPP CrIS LW FOV5 has higher radiance than other FOVs at 668.125 cm^{-1} for cold scenes
- Numerous presentations on this anomaly
- Latest was from UW exploring unresolved channel spectrum
  - March 16, 2016
  - Beamsplitter gap causes a secondary “ZPD” spike at 0.88 cm OPD
- UW did analysis in the interferogram domain
- Spectral domain analysis should be identical
- Larabee provided monochromatic spectra for hot and cold scenes
- Results ambiguous
- Joe Predina proposed electrical crosstalk as root cause

Beamsplitter Gap Wedge Reduces Amplitude

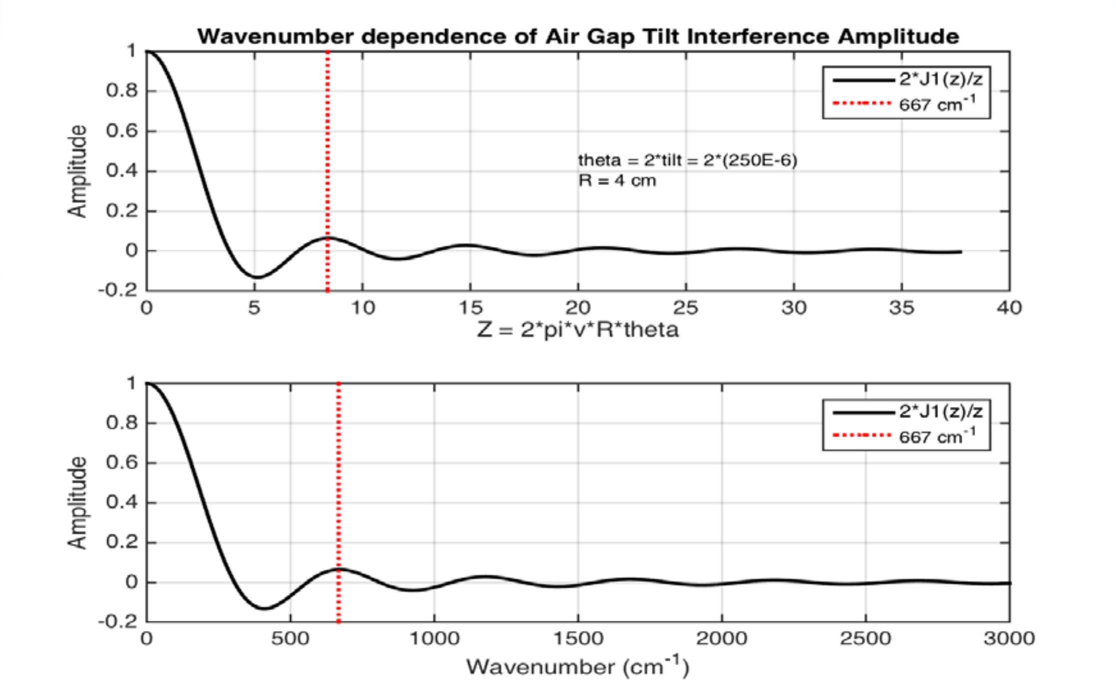

Normalization: 0.5*r ≅ (0.5) * [(n-1)/(n+1)]^2 =0.085 with n = 2.4

- From March 16, 2015 UW presentation
- Didn't use normalization (conservative analysis)

Effect of Beamsplitter Gap Reflection

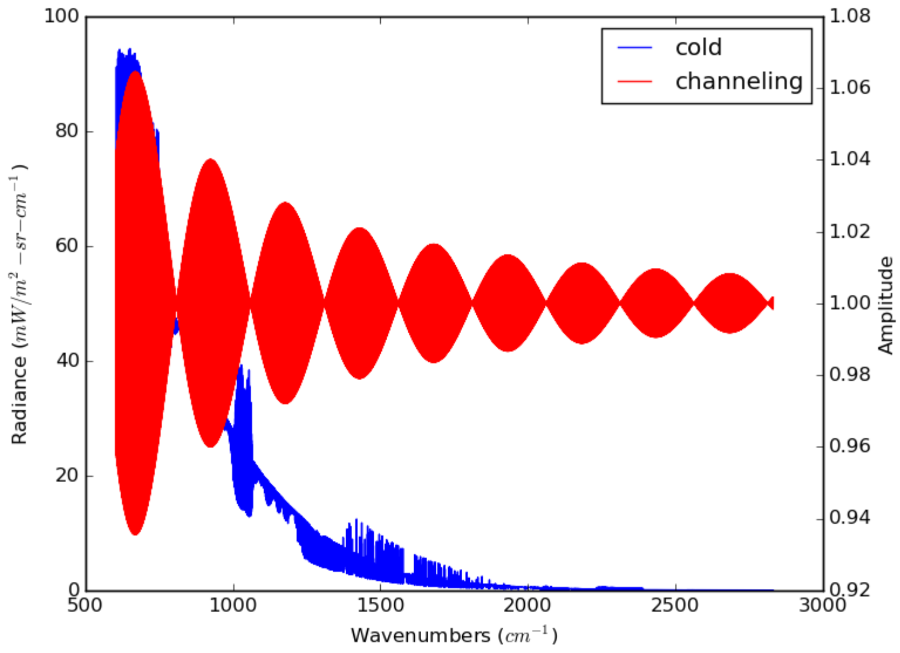

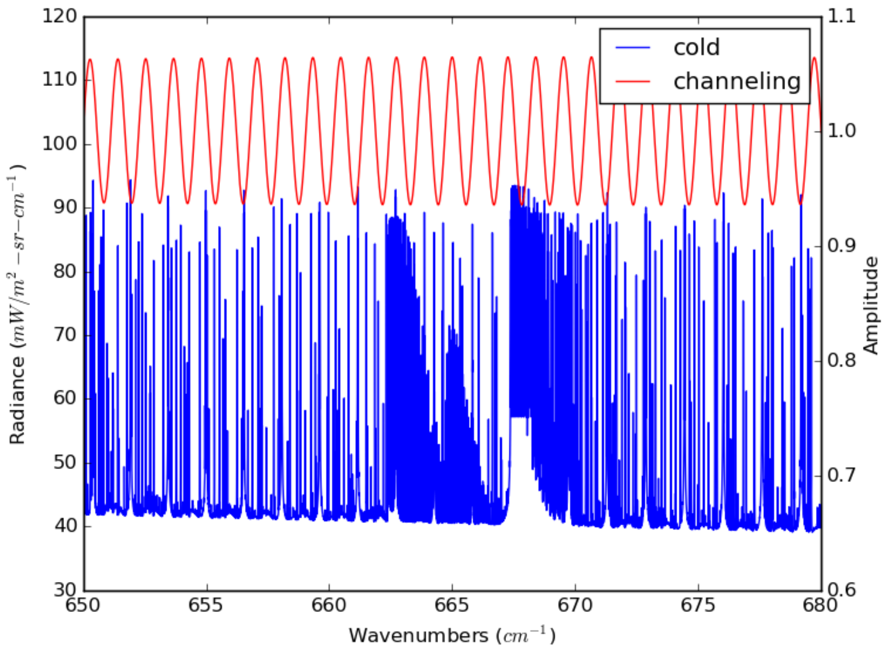

- High resolution spectra is modulated by channeling
- Phase of channeling is unknown

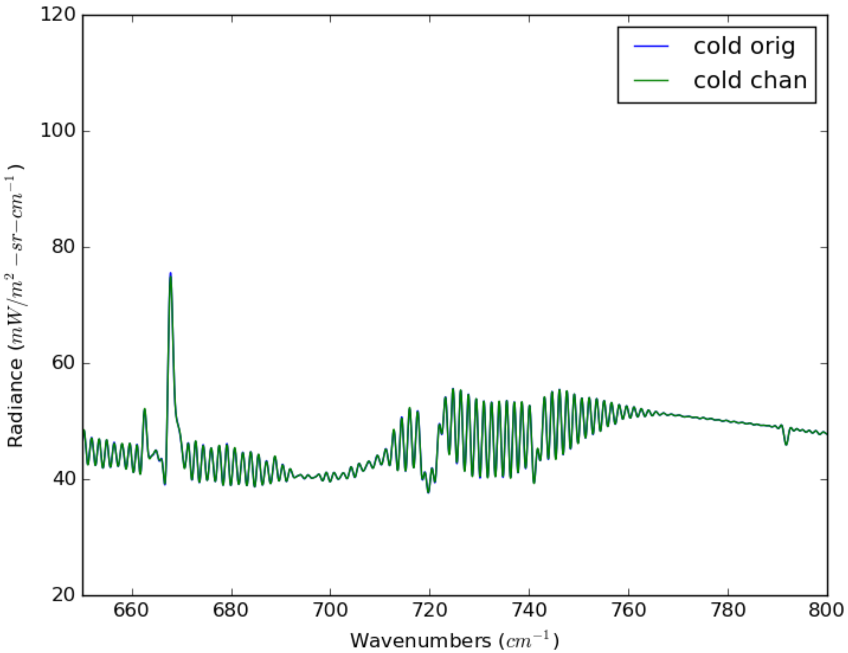

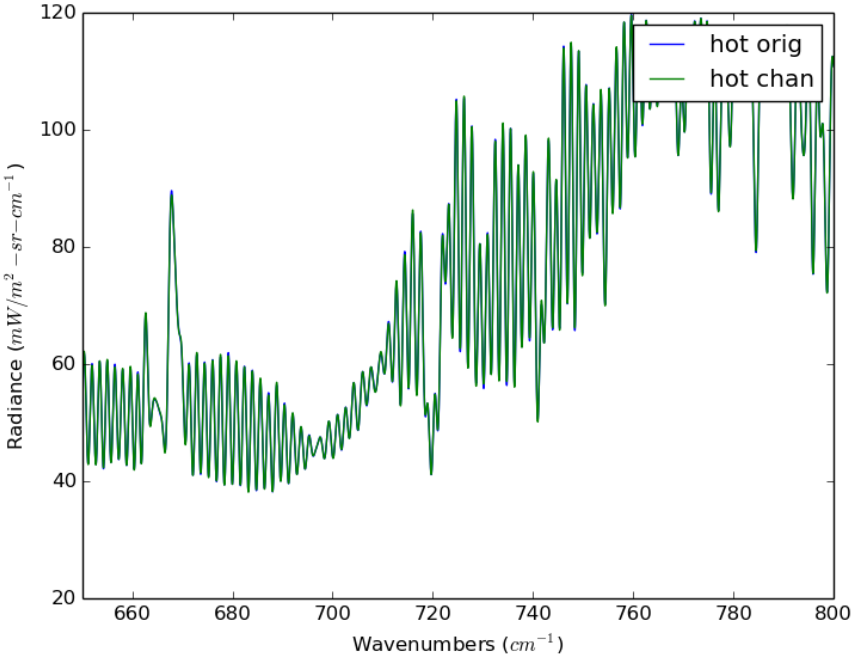

- Monochromatic spectra from Larrabee Strow
- Spectral resolution reduced to CrIS
- Modulation does not have a big affect

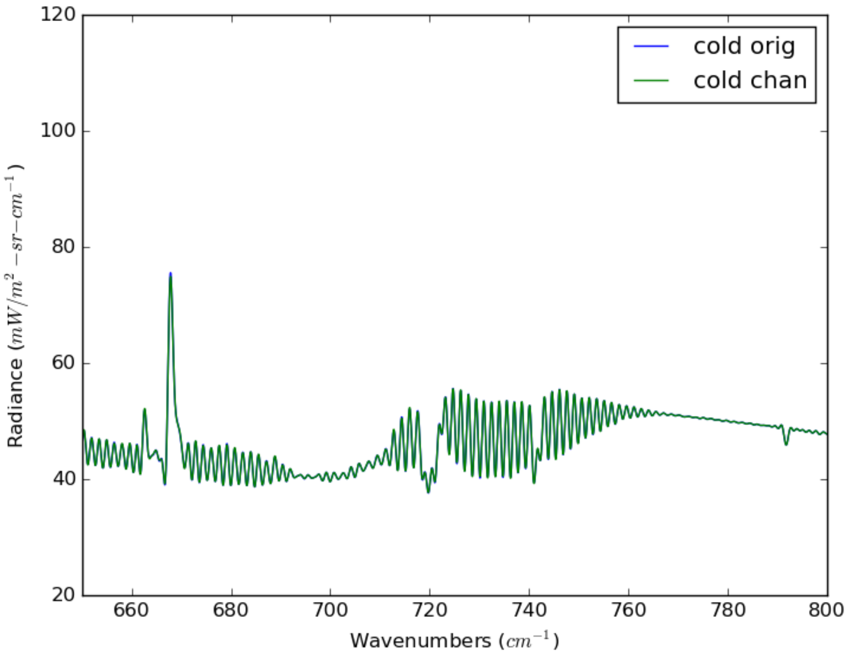

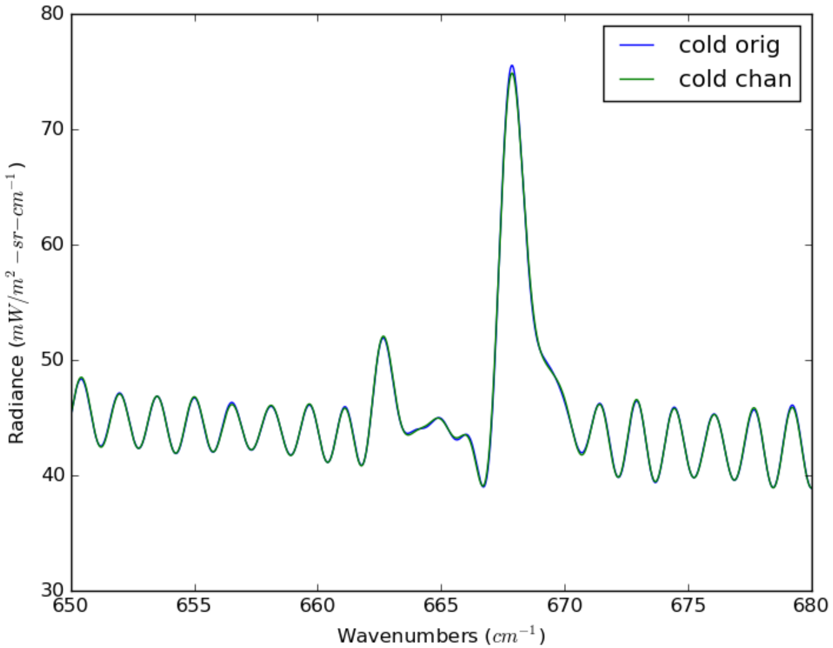

- Spectral resolution reduced to CrIS
- Modulation does not have a big affect

Observed Anomaly Doesn't Match Model

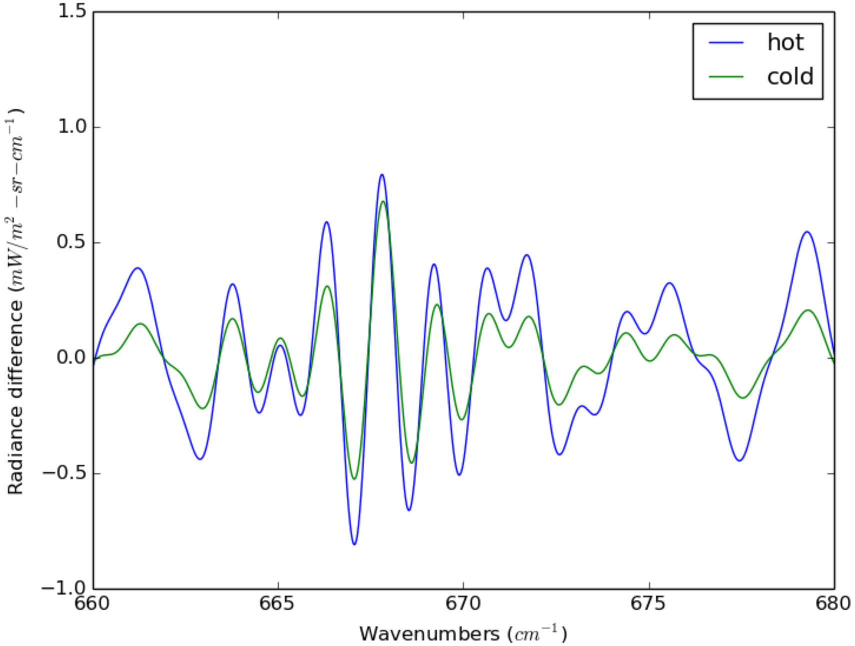

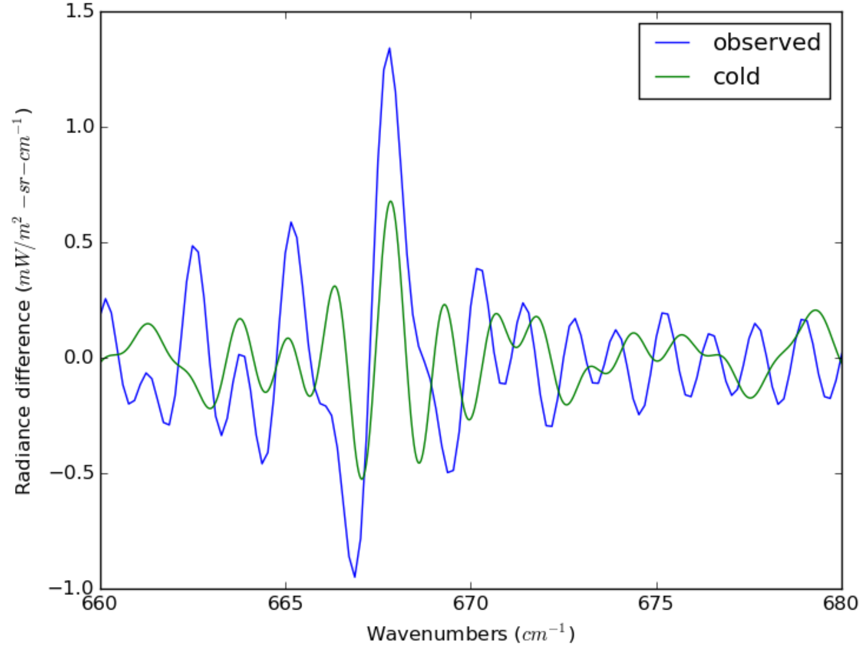

- Observed anomaly larger than modeled
- Larger affect seen for hot spectra than cold
- Shape not a very good match
- Could there be a non-LTE spectral line not in model

Spectral Shift of Anomaly

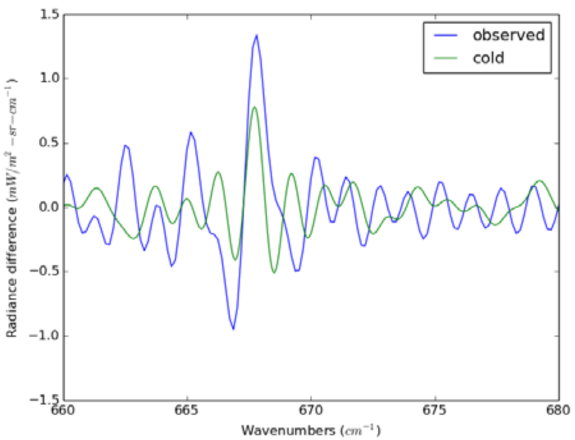

Phase 0

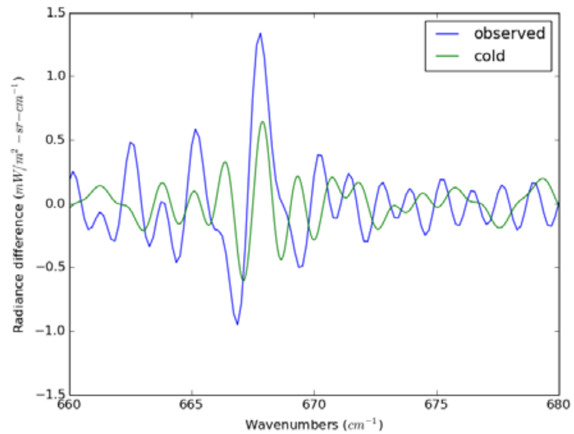

Phase -30

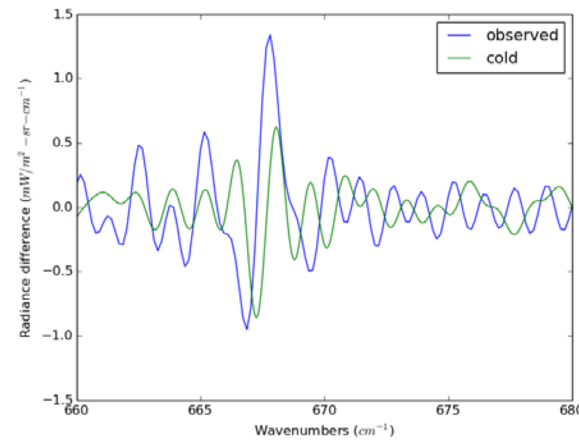

Phase -60

- Position of peak sensitive to the modulating phase
- Beamsplitter gap OPD is 0.88 cm^{-1} or 8800 μm
- Aluminum has thermal expansions of $24 \times 10^{-6}/^{o}C$ at 20 C
- Change in length for 1 C change 0.21 μm compared to wavelength of 15 μm (5 degrees of phase)
- On orbit OMA temperature change not large enough to expect to see change

Electrical Cross-Talk

- Joe Predina proposed the effect could be due to electronic cross-talk
- General electronic pickup would likely not have same phase as optical signal and would show in imaginary spectra

Anomaly Only Visible in Real Spectrum

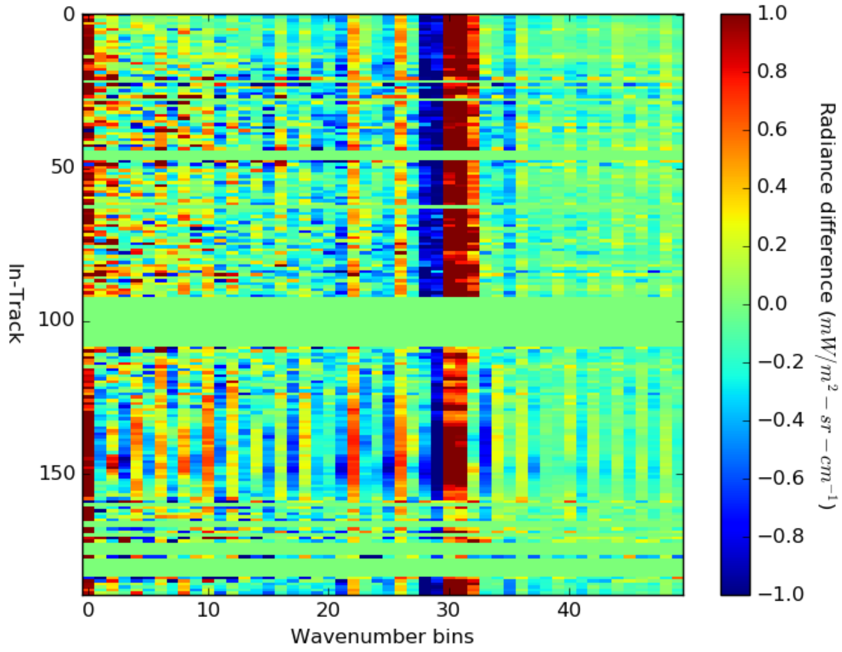

real

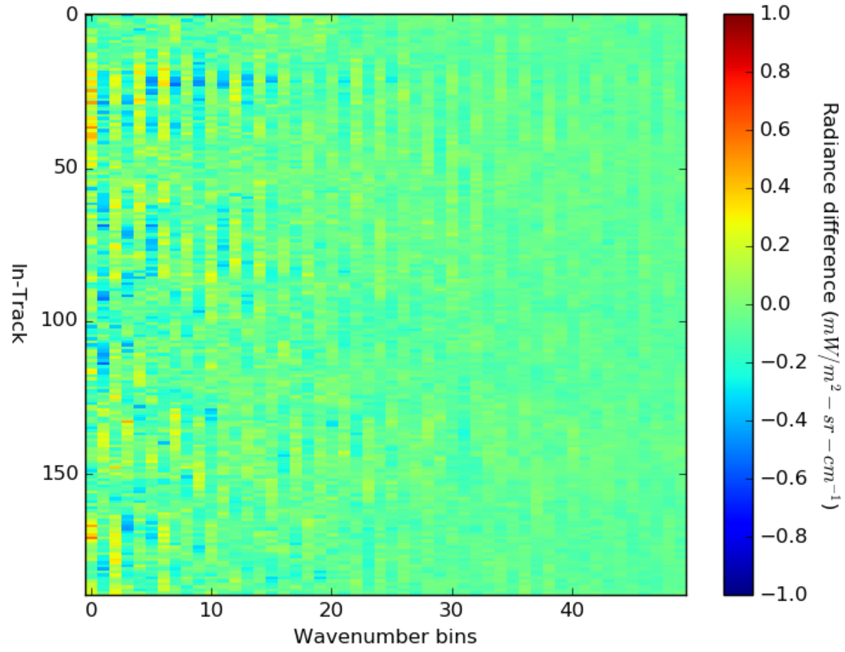

imaginary

- Difference between FOV5 and FOV6
- Anomaly shows up in real but not imaginary spectra
- August 1, 2015 orbit 19478

Electrical Cross-Talk

- If optical or detector electrical cross-talk were getting into FOV5 the line shape would be incorrect
- Synthesized spectra including SA matrix effects
  - From Larrabee Strow's high resolution spectrum
- Added small amount of FOV1 and FOV2 into FOV5
- Applied inverse SA matrix for FOV5
- Plot difference between correct FOV5 spectra

Adding Cross-Talk Not Consistent with Anomaly

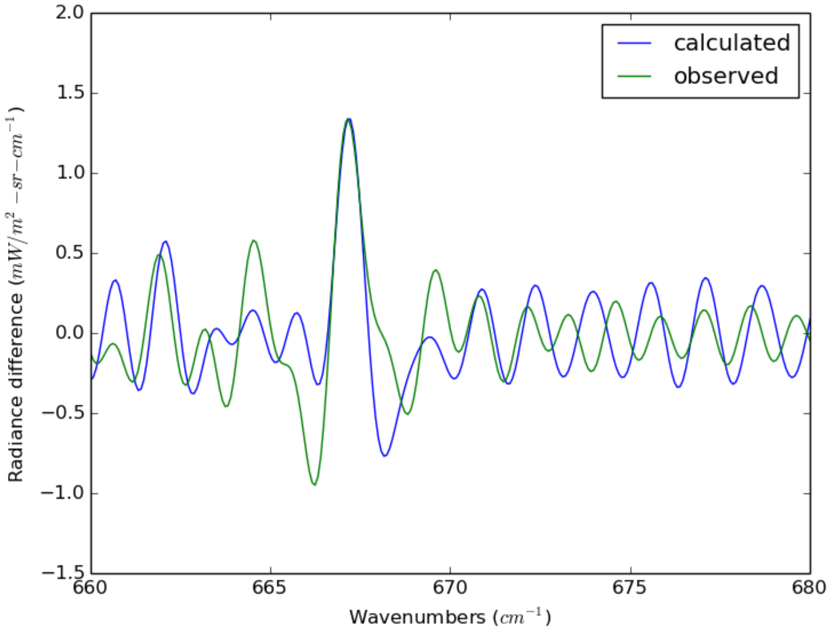

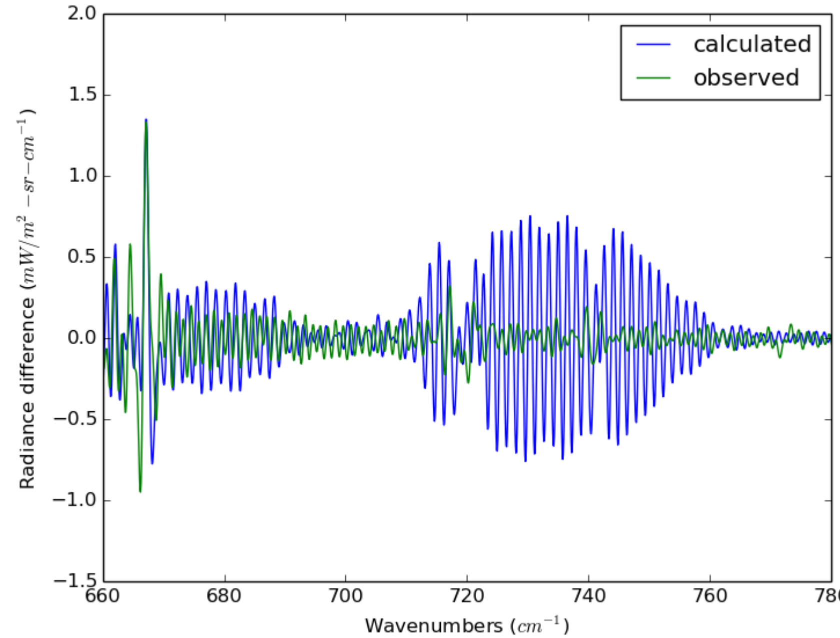

- 0.07 of FOV1 & FOV2 added to FOV5
- Biggest effect in 720 to 760 cm^{-1} region not 668 cm^{-1}
- Other combination of cross-talk also not a good fit

BACKUP

How Large is Anomaly?

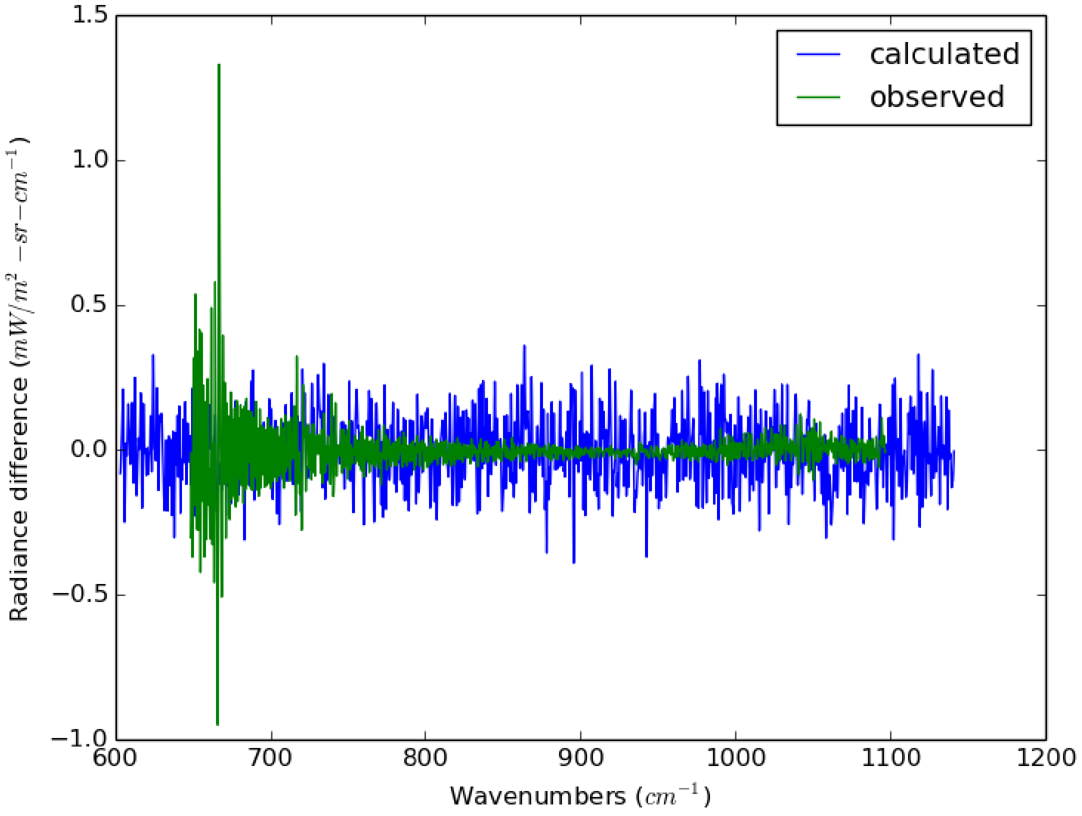

- Anomaly compared to a single pixel noise
- Anomaly was averaged over a granule

Anomaly Spectral Position not Constant

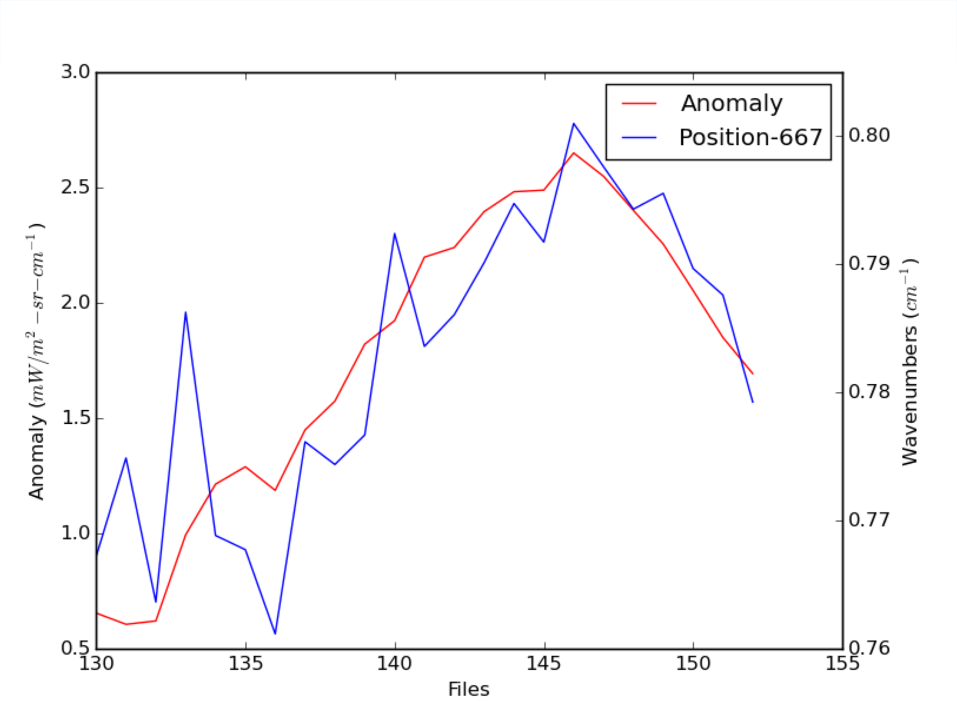

- Spectral position of anomaly correlated with amplitude
- Anomaly amplitude uses left axis, position right axis
- South pole region, averaged over each granule
- August 1, 2015 orbit 19480

Anomaly Spectral Position not Constant

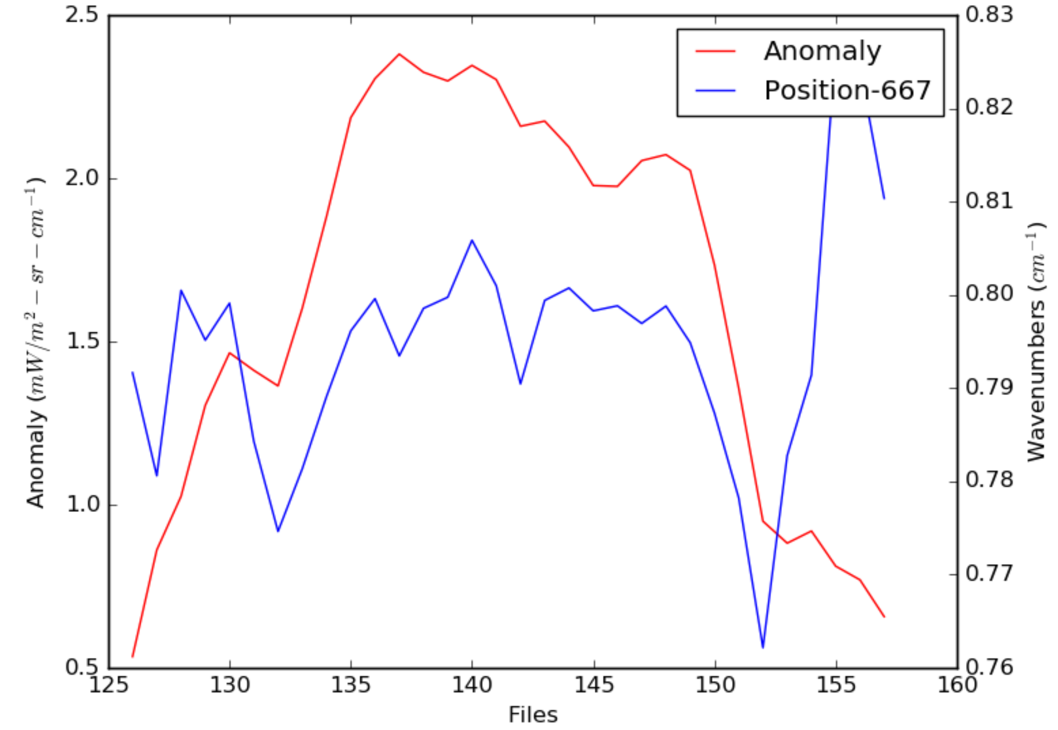

- Spectral position of anomaly correlated with amplitude
- Anomaly amplitude uses left axis, position right axis
- South pole region, averaged over each granule
- June 21, 2015 orbit 18900

Anomaly Spectral Position not Constant

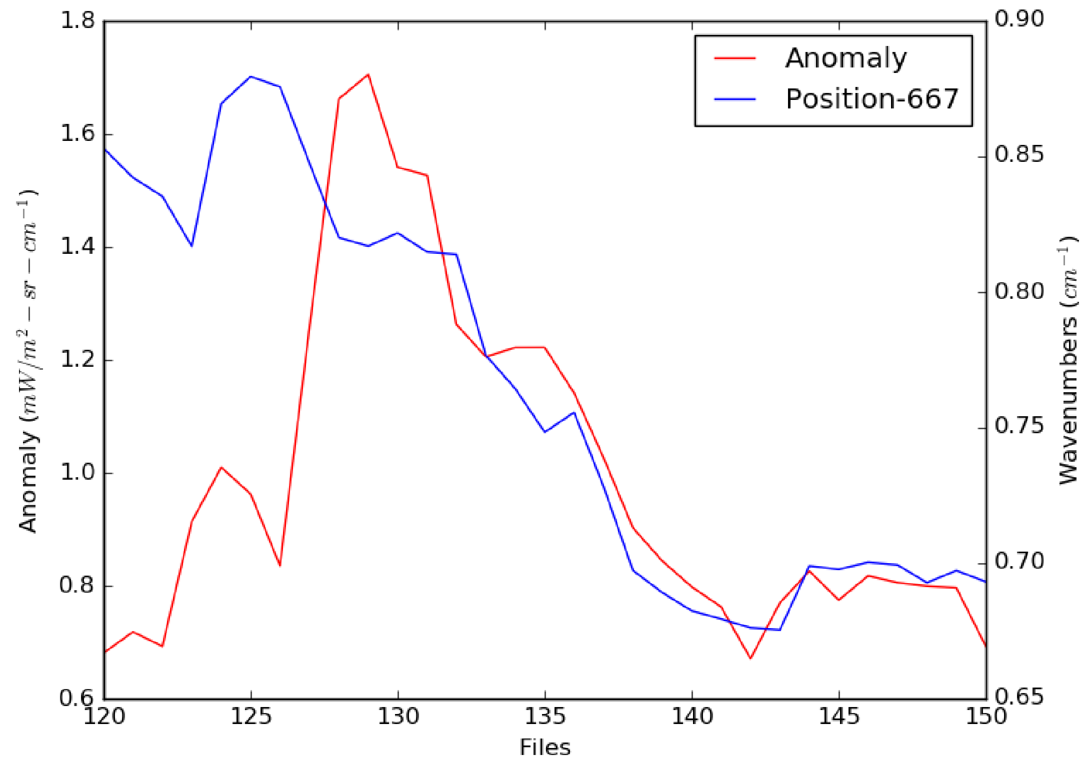

- Spectral position of anomaly correlated with amplitude
- Anomaly amplitude uses left axis, position right axis
- South pole region, averaged over each granule
- December 21, 2015 orbit 21496

Space Dynamics Laboratory
Utah State University Research Foundation

J1 CrIS System Level Testing, Results and Preparation for Launch

Mark Esplin, Deron Scott, Kori Moore, and Ben Esplin

Outline

- Preparations for J1 CrIS Spacecraft level test and early on orbit checkout
  - Differences in data format since sensor TVAC
  - Reading J1 test data
  - Exercising analysis software
- J1 CrIS sensor level TVAC performance
- S-NPP on-orbit status
  - Typical NEdN
  - Standard deviation verses Allan deviation
  - Response trending
  - Bit-trim errors due to bright scenes
  - Extended interferogram operation

PREPARATIONS FOR J1 CRIS SPACECRAFT LEVEL TEST AND EARLY ON ORBIT CHECKOUT

Plan for CrIS Spacecraft TVAC Test

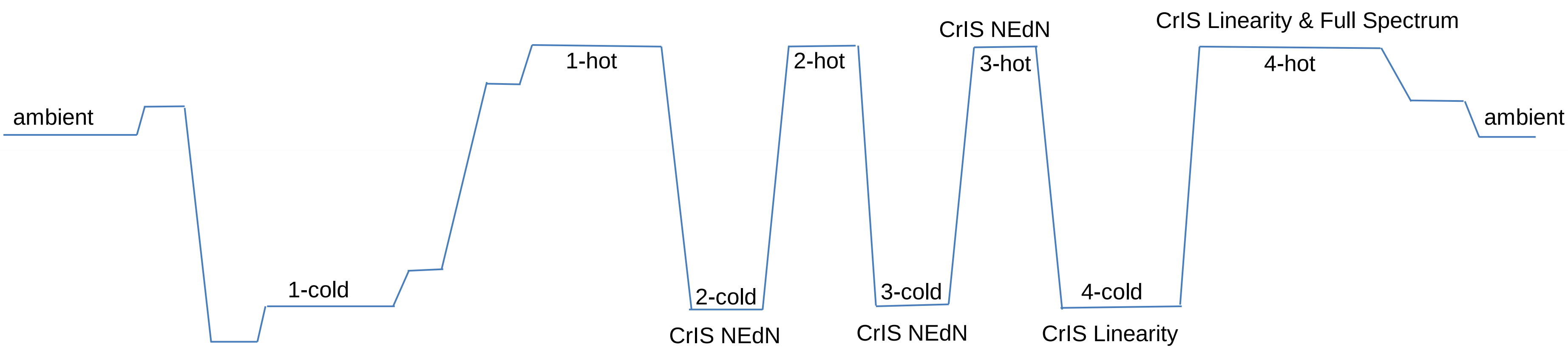

- Four hot and cold cycles planned during TVAC
- Several opportunities to evaluate CrIS NEdN and linearity
- CrIS will be active during other times as well

J1 CrIS Planned Activities

- During Spacecraft TVAC
  - Verify proper functionality of CrIS sensor
  - Investigate any unexpected behavior
  - Determine NEdN at high and low temperature plateaus
  - Check for ice buildup on optical surfaces
  - Evaluate nonlinearity changes from diagnostic mode data
  - Compare sensor performance with previous sensor level TVAC
- Early on orbit checkout in addition to above tasks
  - Evaluate occurrences of radiation spikes
  - Optimize bit-trim mask
  - Trend degradation of system responsivity

Software Tools Ready for Spacecraft TVAC

- Ability to unpack CCSDS packets from HDF5 formatted files
- Ability to read and plot telemetry data
- Plot raw interferograms both normal and diagnostic mode
- Determine FOR, FOV, sweep direction etc. from interferogram data (check for missing data)
- Convert raw interferograms into magnitude and phase spectra
- Process raw interferograms into calibrated spectra (Harris SDR generator)
- Determine NEdN and Allan deviation
- Derive nonlinearity coefficients from diagnostic mode data

J1 Preliminary Spacecraft Data

- Files have 15 granules per file
- Interferogram length LW 876, MW 1052, SW 808
- Data from all FOVs present
- For some files there is one less earth scene interferogram than expected (1799 instead of usual 1800)
  - No gaps in time stamps
  - Short granule not missing data
- Packet trackers not consistent with documentation
  - Issue currently being worked
  - Possible to get needed information from binary CCSDS packet headers

Example J1 Telemetry Data

ICT PRT3

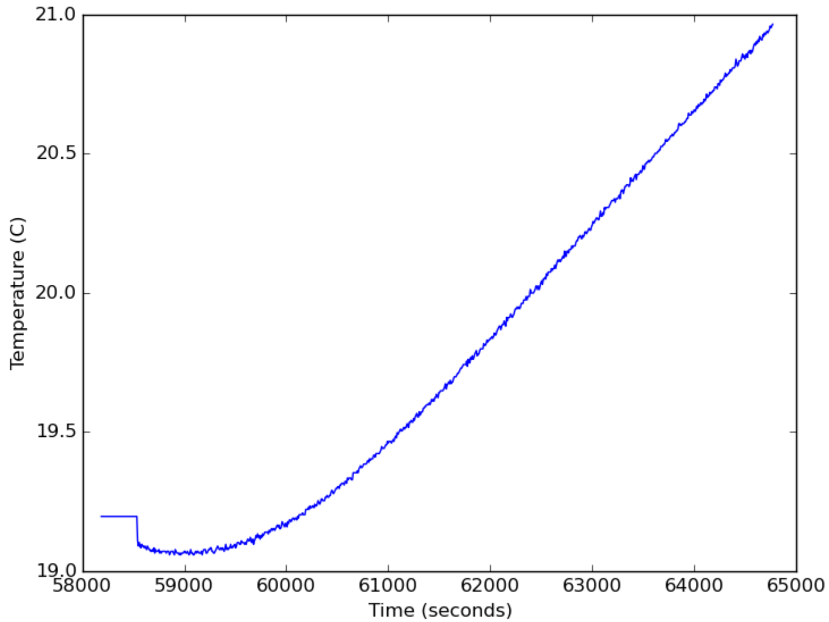

SSM Electronics Temperature

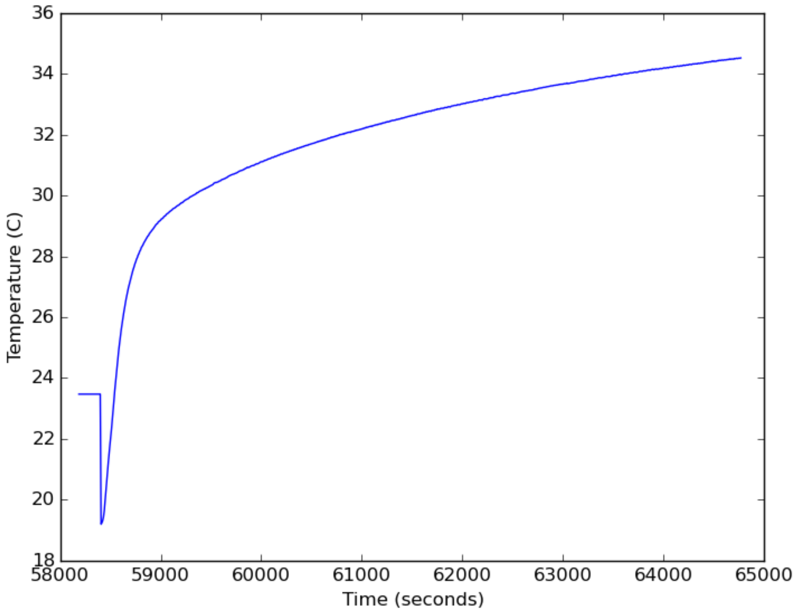

- Software able to read and decode telemetry data
- Telemetry as expected for a CrIS system turn on

RCRIT_j01_d20151014_t1609422_e1800055_b00001_c20160118222721609000_all-_dev.h5

Uncalibrated Test Spectra

Magnitude

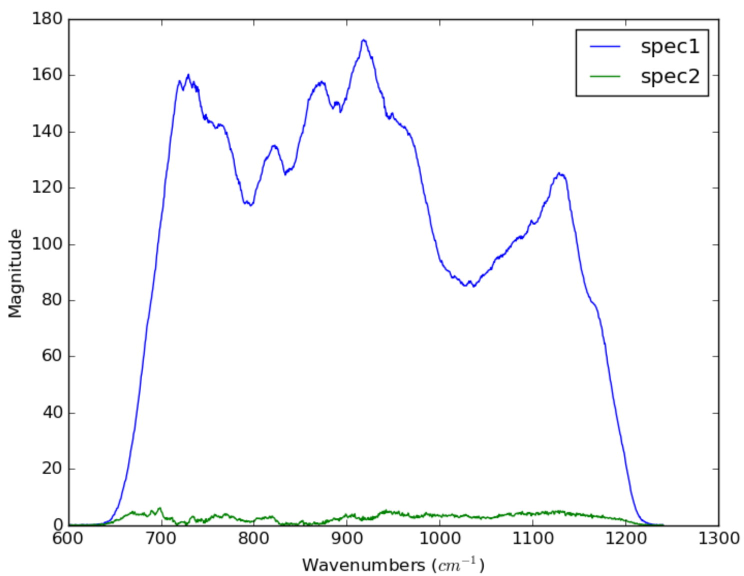

Phase

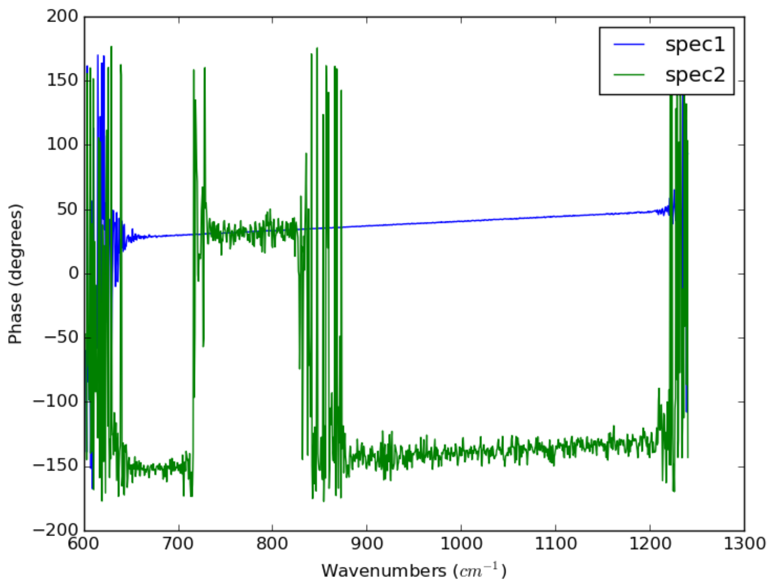

- Playback of representative interferograms
- All FOVs of a given FOR are equal
- Scan direction 1 is small amplitude
- Scan direction 0 is large amplitude
- These two spectra are replicated over and over again

J1 CRIS SENSOR LEVEL TVAC TESTING

J1 CrIS TVAC During Fall of 2014

- Basic functionality checks
- NEdN from both operational and staring modes
- Three sensor plateaus
  - (PFL) Proto Flight Low (ICT at about 262 K)
  - (MN) Mission Nominal (ICT at about 287 K)
  - (PFH) Proto Flight high (ICT at about 314 K)
- Both electronic sides and different supply voltages
- NEdN with induced vibration
- Nonlinearity Characterization
  - Diagnostic mode interferograms
  - Normal mode CrIS operation with stepped ECT temperatures

Example Staring MN NEdN

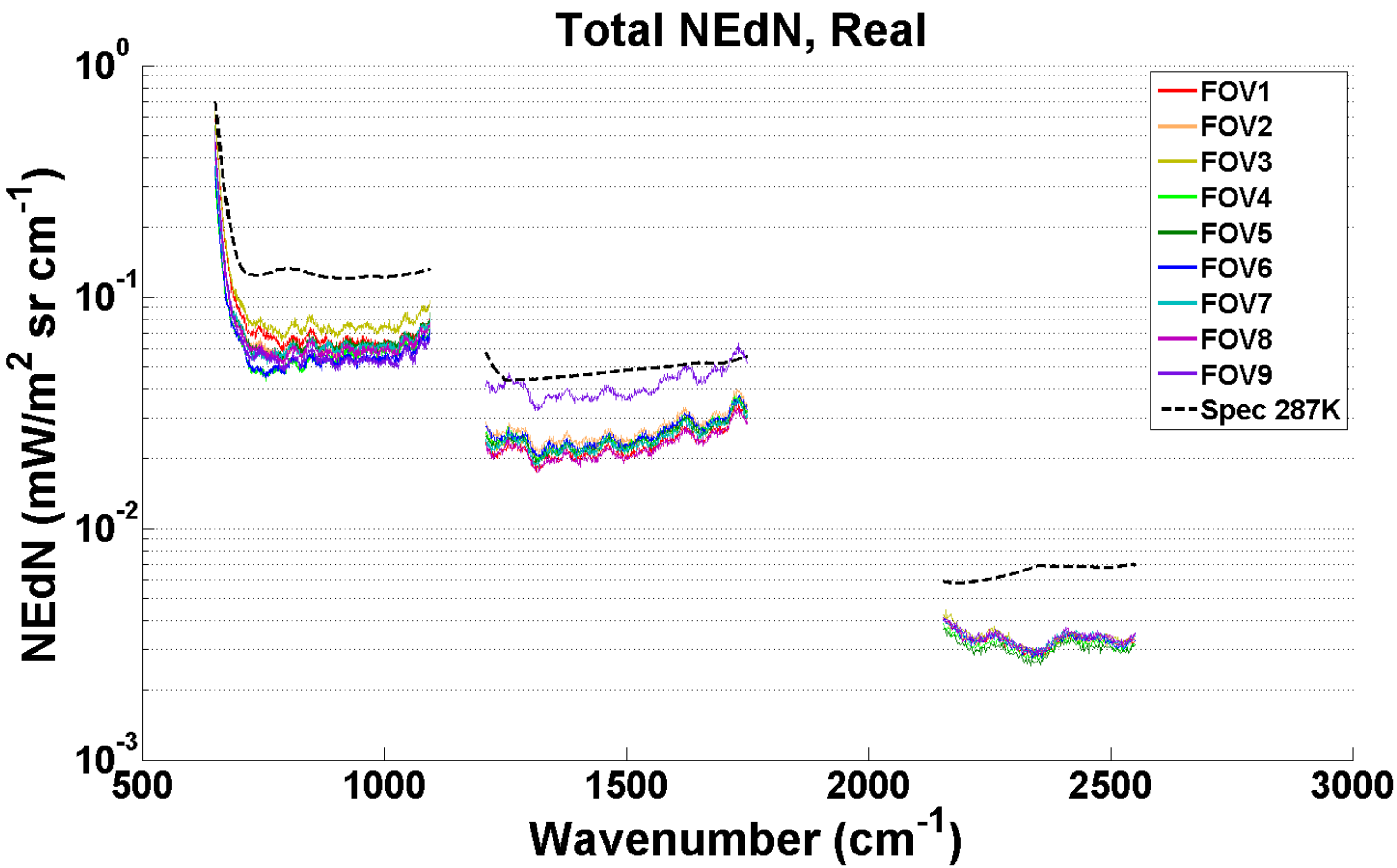

- MW FOV9 out of family with other FOVs
- MW FOV9 slightly above spec value
- MN (Mission Nominal) plateau staring mode

Operational Mode MN NEdN

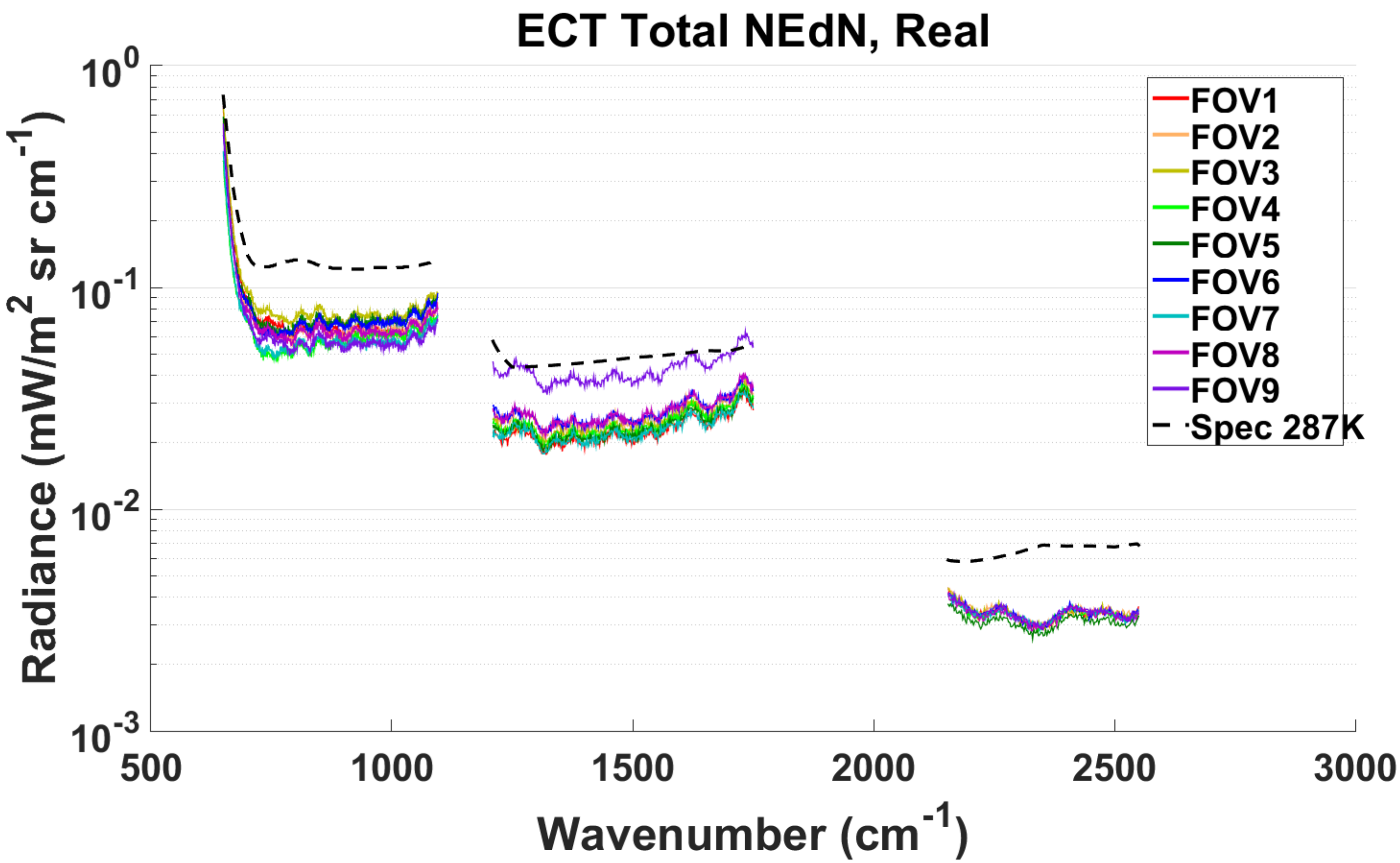

- Staring and operational mode NEdN nearly identical
- MN 287 K ECT, side 1

Nonlinearity a_2s Characterized

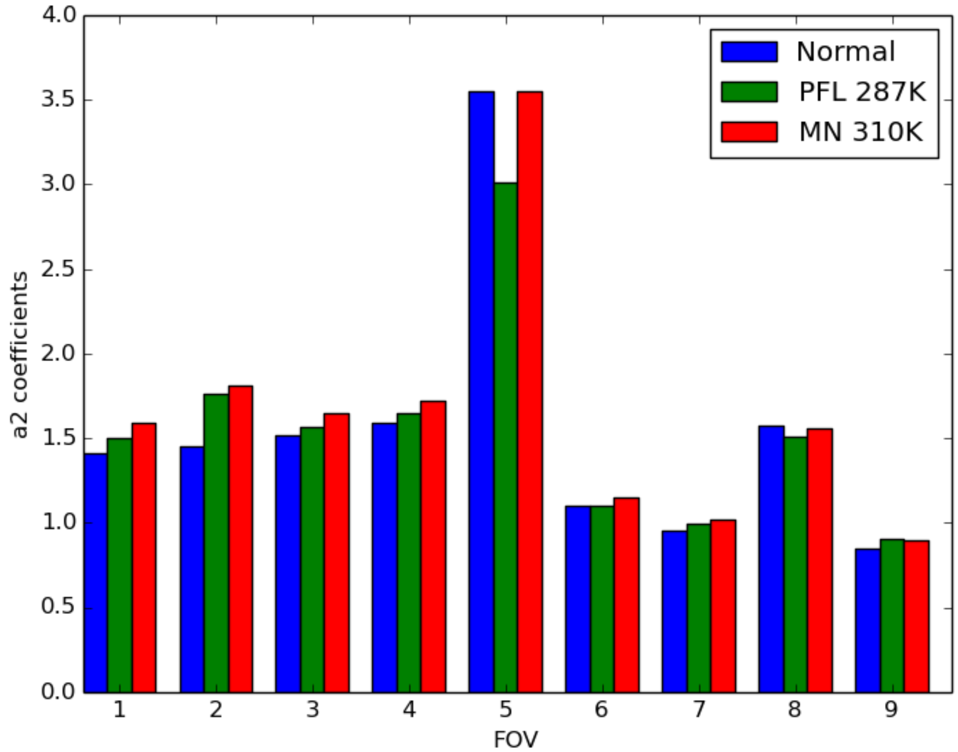

- Normal is using stepped ECT temperatures
- Relative coefficient magnitude shown
- Diagnostic mode a_2s scaled so MN 310K matched normal FOV5

S-NPP ON-ORBIT STATUS

Typical S-NPP On-Orbit NEdN

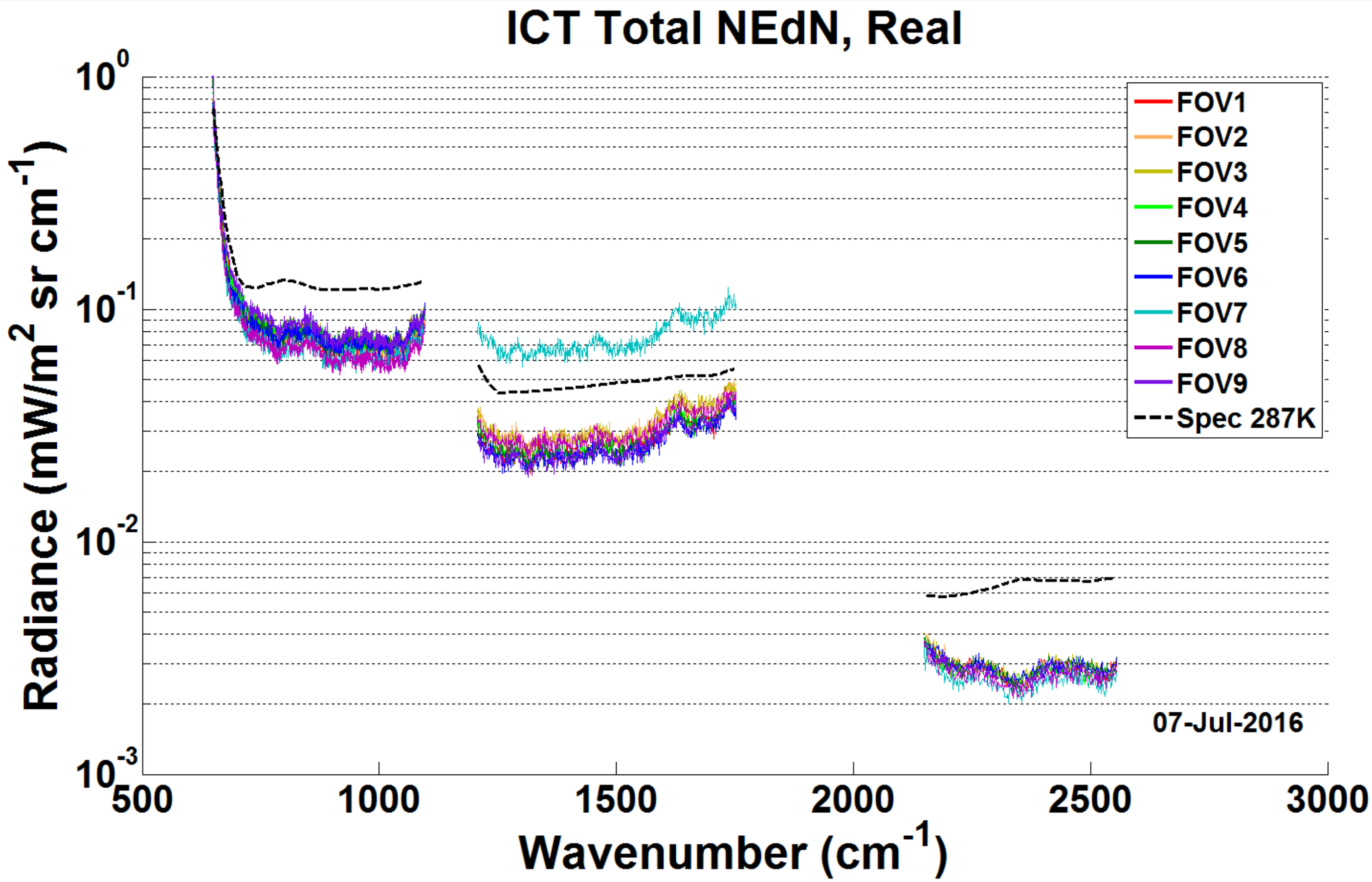

- ICT interferograms substituted for earth scenes
- Nominal resolution
- July 7, 2016

Typical S-NPP On-Orbit NEdN

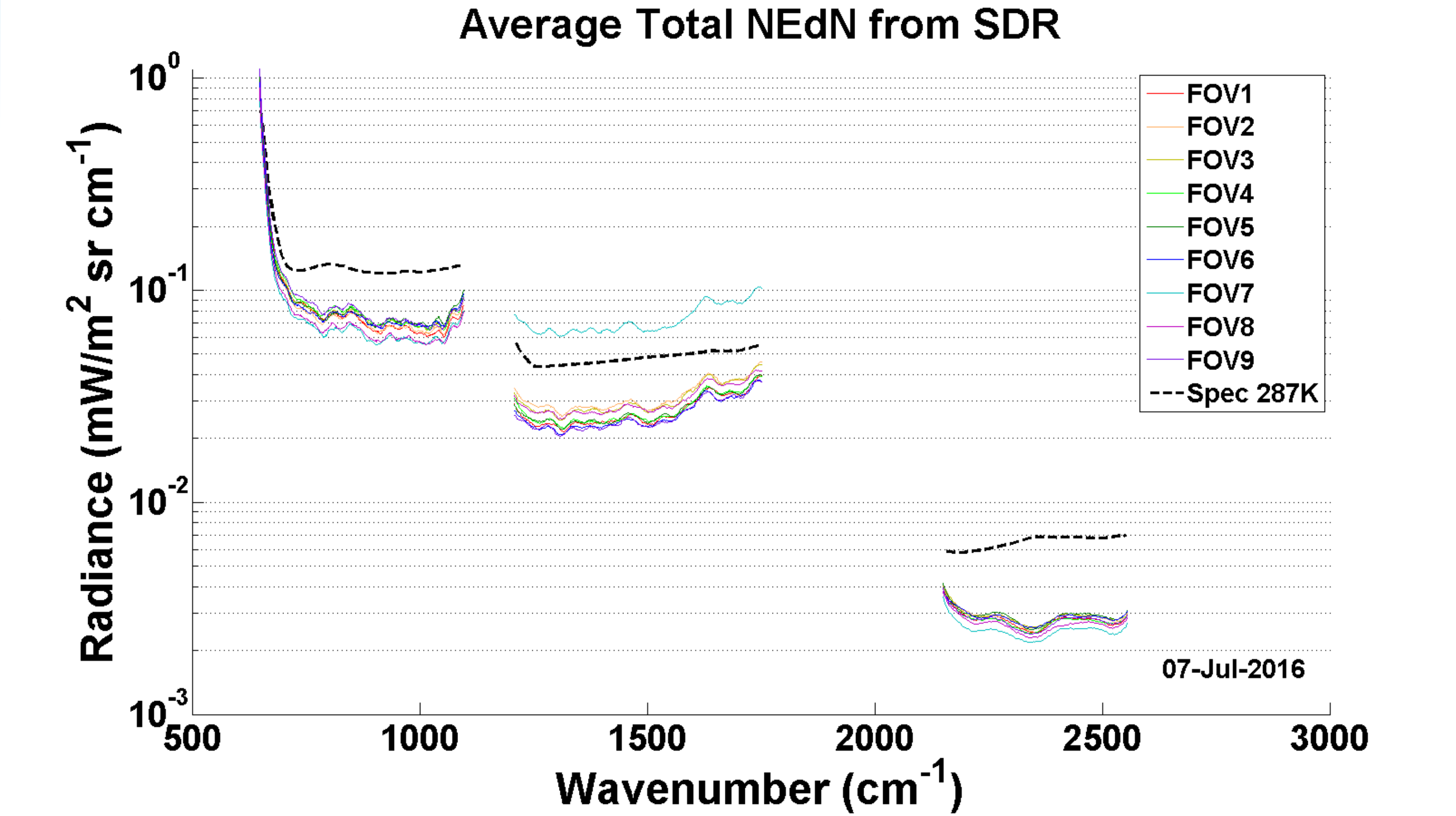

- NEdN produced by IDPS and imbedded in SDR files
- July 7, 2016

Standard Deviation vs. Allan Deviation

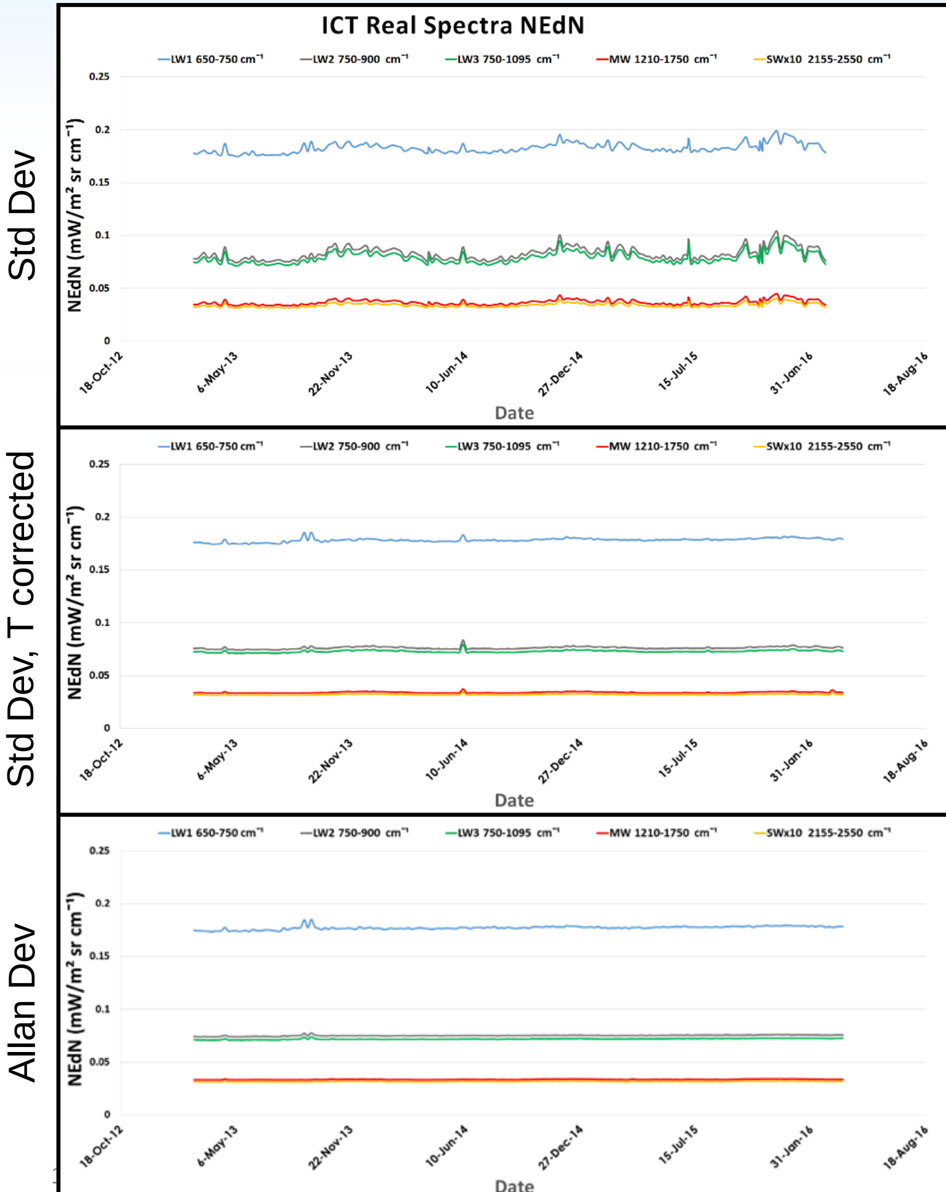

- CrIS NEdN is calculated using Std Dev of Internal Calibration Target (ICT) measurements with a temperature (T) correction applied
  - T correction normalizes response with varying ICT T
- Std Dev is sensitive to changing mean, Allan Dev is <u>not</u>
- Std Dev with T correction and Allan Dev are of similar magnitude and show CrIS instrument has been very stable
- ICT T is largest contributor to NEdN variation

CrIS Relative Response Degradation

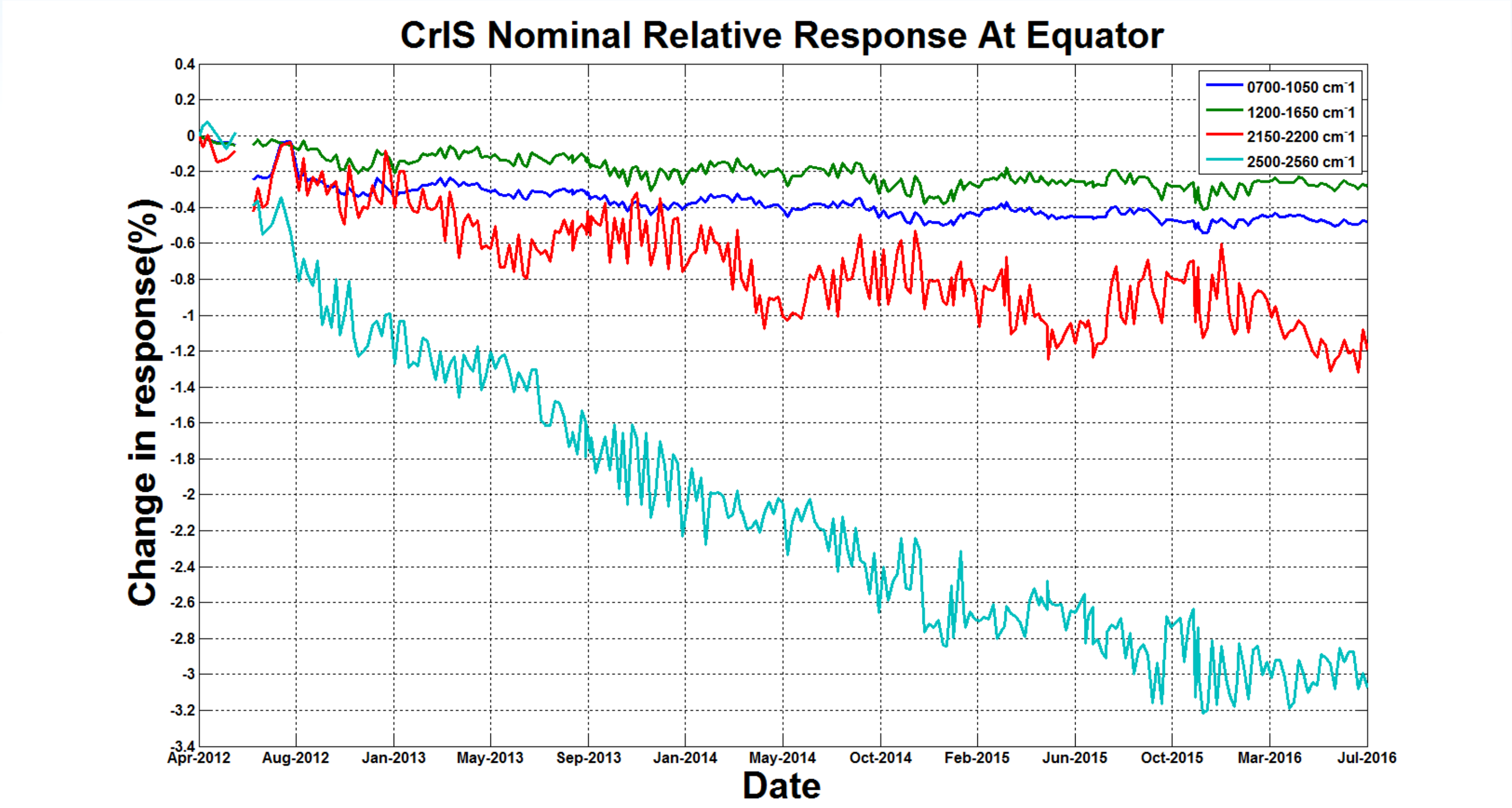

- Degradation is only about 3% after 4.5 years at most sensitive wavenumbers
- Response degradation appears to be leveling off

Bit-Trim Check

- CrIS uses bit-trim compression for interferograms
  - Different number of bit are used to encode interferogram zones
  - More bits used near center of interferogram (zero path difference or ZPD) while lower number of bits in the wings of interferogram
- Bit-trim errors occur when interferogram amplitude exceeds allocated number of bits – resulting in loss of information
- Causes of bit-trim errors: hot scenes, fires, sun glints, radiation spikes, etc.
- MW margin for bit-trim errors low for hot dry scenes
- During 2015 three cases found with bit-trim errors caused by bright scenes found (all in Lut desert in Iran)
- No bright scene bit-trim errors found in 2016 through July

Extended Mode Operation

- November 2, 2015 extended lengths of S-NPP interferograms
- Truncating interferogram ends leads to spectral ringing
- Interferogram lengths changed:
  - LW 866 to 874
  - MW 1052 (unchanged)
  - SW 799 to 808
- Additional points can be used to taper interferogram ends while maintaining required spectral resolution
- Ongoing work on optimizing ground based SDR software to take advantage of these additional points

Conclusions

- Software tools and procedures are in place for J1 spacecraft level TVAC
- Practiced reading and analyzing preliminary J1 data
- Results from spacecraft TVAC with be compared with pervious sensor level TVAC results
- S-NPP has been operating very well on orbit
- Standard deviation and Allan deviation produce essentially identical results if an ICT temperature drift correction is used
- S-NPP response degradation very low after 4.5 years
- No bit-trim errors caused by too bright desert scenes in 2016

BACKUP

MWIR Bit-Trim Error Caused by Bright Scene

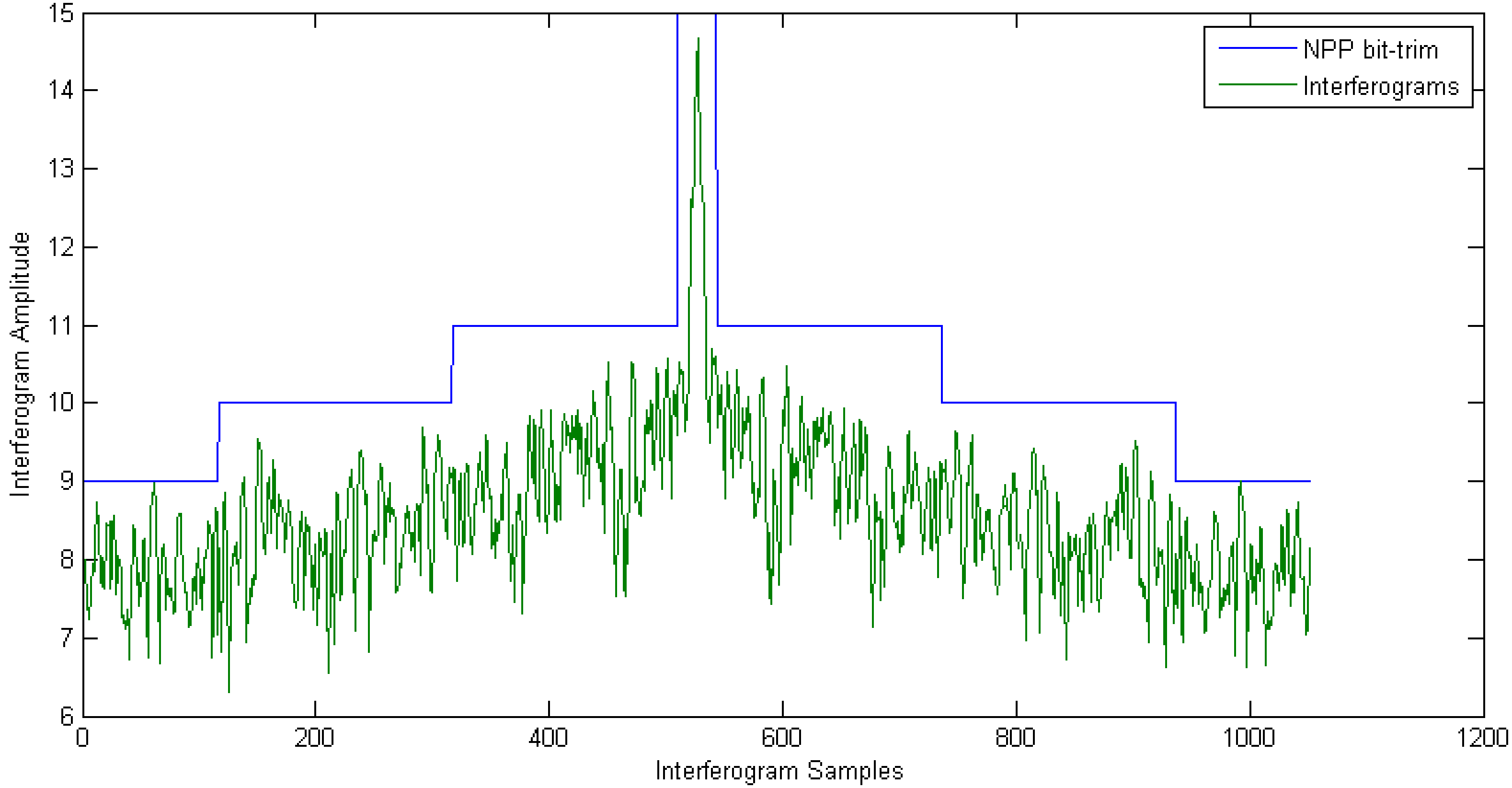

- June 11, 2015 Lut desert Iran
- Bit-trim errors occur in first and last zone

SDR Comparison

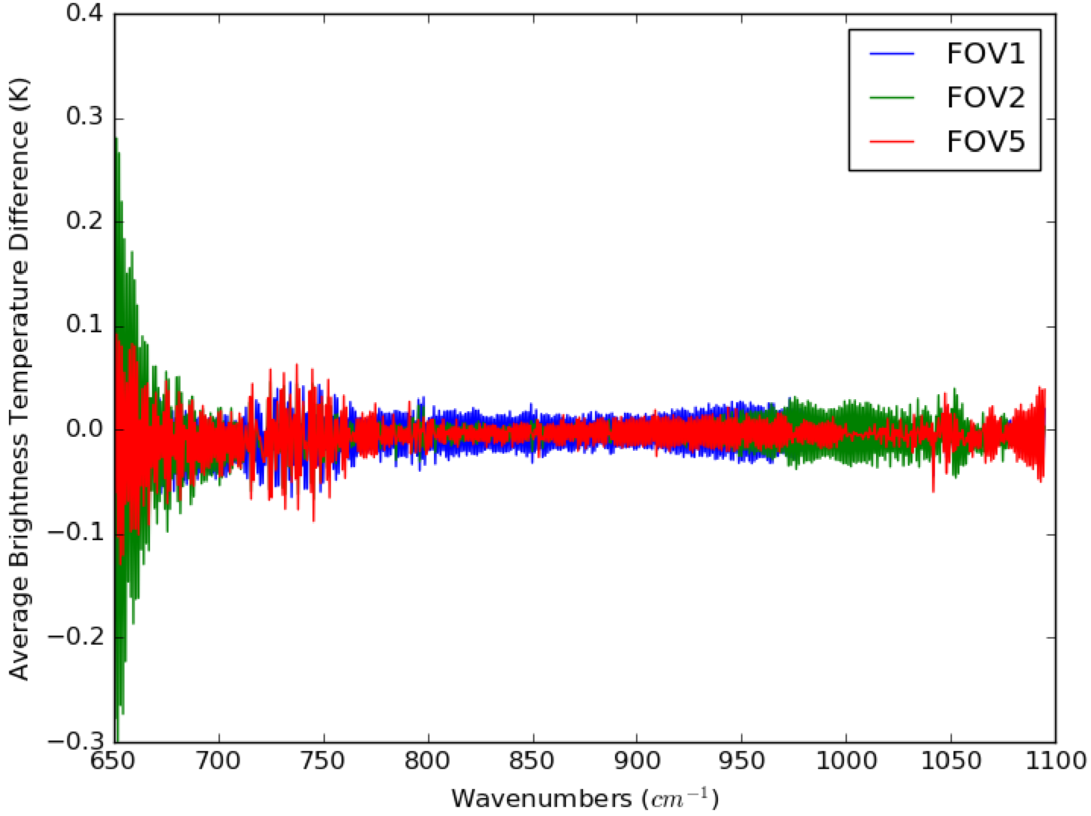

- UMBC A4 algorithm minus STAR A4 algorithm
- Clear Scenes only

PFL NEdN

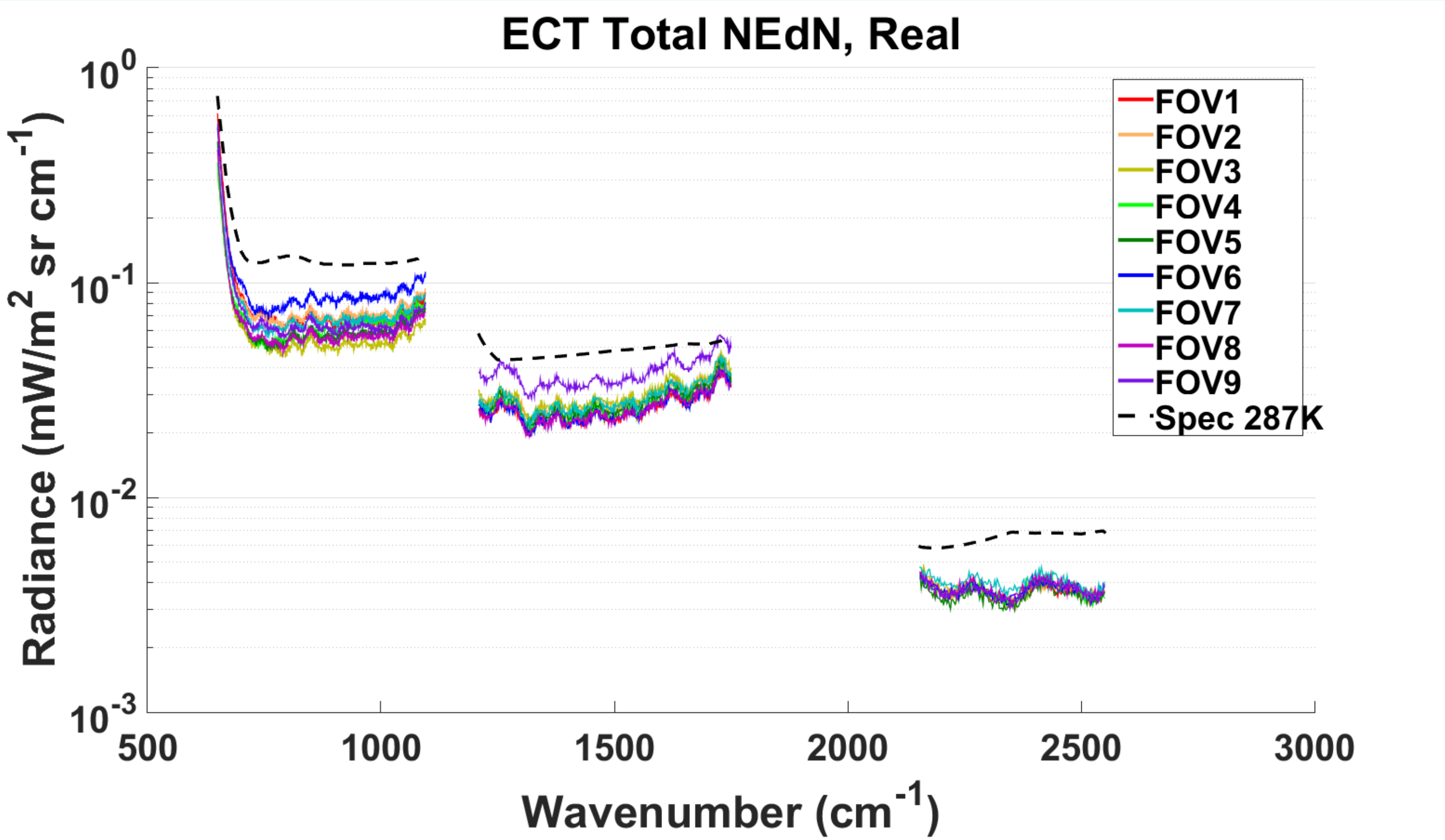

- PFL (Proto Flight Low) temperature plateau
- Operational mode, 287 K ECT, side 1

NEdN Slightly Higher for PFH

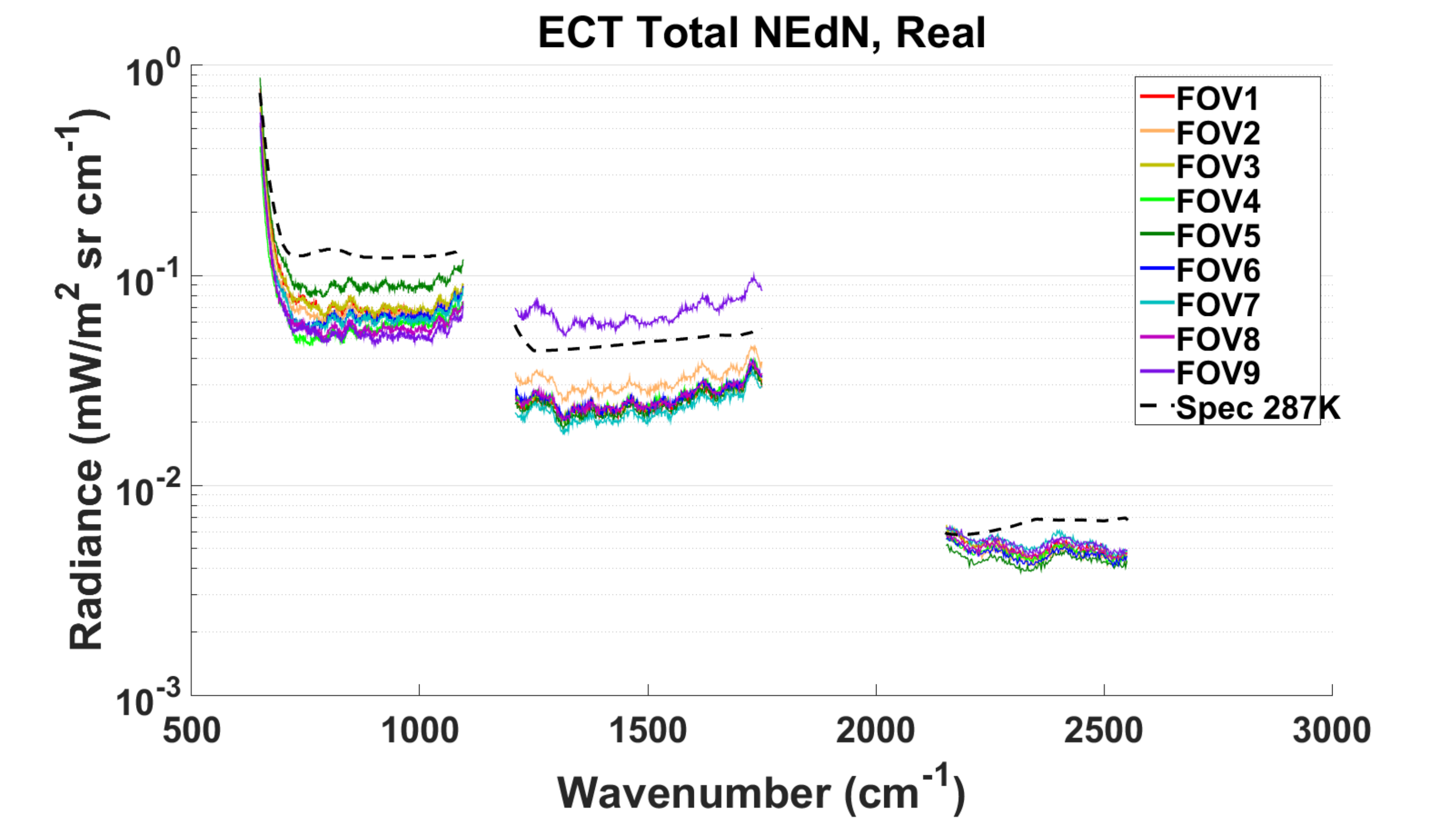

- PFH (Proto Flight High) temperature plateau
- Slightly higher NEdN
- Operational mode, 287 K ECT, side 1

CrIS Calibration Accuracy and its role as an Inter-calibration Reference

Dave Tobin, Greg Quinn, Hank Revercomb, Joe Taylor, Bob Knuteson,
Dan DeSlover, Lori Borg, Graeme Martin
Space Science and Engineering Center, University of Wisconsin-Madison

2016 JPSS Science Teams Annual Meeting
NOAA Center for Weather and Climate Prediction, College Park, MD
August 2016

Selecting, Transferring and Combining GSICS Inter-Calibration Reference Instruments

In response to CGMS action WGII/A43.02

Table 1 – Draft Scoring Scheme for GSICS Near-Real-Time Correction for 2014 Geostationary Imager IR Channels

		Threshold		Goal			Metop-A/IASI		Aqua/AIRS		SNPP/CrIS (in FSR mode)		NOAA-14/HIRS		CLARREO-1A/IR	
	Unit	Min	Max	Min	Max	Weight	OK?	Score	OK?	Score	OK?	Score	OK?	Score	OK?	Score
Date Range	Year	2014	2014	2006	2030	10	OK	7.5	OK	4.2	OK	5.8	NOK	0.4	NOK	0.0
Spatial Coverage: Lat	deg	-10	10	-90	90	1	OK	1.0	OK	1.0	OK	1.0	OK	1.0	OK	1.0
Spatial Coverage: Lon	deg	-10	10	-180	180	1	OK	1.0	OK	1.0	OK	1.0	OK	1.0	OK	1.0
Dynamic Range	K	270	300	180	330	2	OK	1.7	OK	1.7	OK	1.7	OK	1.7	OK	1.7
Spectral Range SWIR	µm	3.75	3.92	3.48	4.36	2.2	OK	1.6	OK	1.2	NOK	1.1	OK	1.4	OK	1.8
Spectral Range MWIR	µm	6.25	7.35	5.35	7.85	2.6	OK	2.6	OK	1.4	OK	2.1	NOK	0.2	OK	2.6
Spectral Range LWIR	µm	8.70	13.40	8.30	14.40	5.2	OK	5.2	NOK	2.6	NOK	2.6	NOK	2.6	OK	5.2
Geometric Range: VZA	deg			0	60	1	OK	0.9	OK	0.9	OK	0.9	OK	0.9	OK	0.0
Diurnal Coverage	hr			0	12	5	OK	1.4	OK	1.4	OK	1.4	OK	1.4	OK	5.0
# Collocations	/d	1		10000		4	OK	4.0	OK	4.0	OK	4.0	OK	4.0	OK	4.0
Spatial resolution	km		100		10	1	OK	0.8	OK	0.7	OK	0.7	OK	0.5	OK	0.2
Spatial sampling	km		1000		10	1	OK	0.4	OK	0.7	OK	0.6	OK	0.4	OK	0.1
Geolocation accuracy	km		10		0.1	5	OK	0.2	OK	0.2	OK	0.2	OK	0.2	OK	0.2
Radiometric Stability	K/yr		1		0.001	10	OK	0.2	OK	0.2	OK	0.2	OK	0.2	OK	10.0
Radiometric Noise	K		10		0.1	1	OK	0.7	OK	0.5	OK	0.5	OK	0.5	OK	0.2
Uncertainty from SBAF	K		1		0.01	10	OK	10.0	OK	1.0	OK	1.0	OK	0.3	OK	10.0
Spectral Resolution	cm-1		100		0.5	1	OK	1.0	OK	0.5	OK	0.8	NOK	0.0	OK	1.0
Spectral Stability	cm-1/yr		2		0.01	1	OK	1.0	OK	1.0	OK	1.0	OK	1.0	OK	1.0
Absolute Cal Acc	K		1		0.01	10	OK	2.0	OK	2.0	OK	2.0	OK	0.2	OK	3.0
Documented Traceability	Score 0-6	1		6		6	OK	2.0	OK	2.0	OK	3.0	OK	1.0	OK	6.0
Total						**100.0**	**100%**	**55%**	**93%**	**38%**	**90%**	**42%**	**87%**	**29%**	**97%**	**62%**

Characterization of the ability of the Climate Absolute Radiance and Refractivity Observatory (CLARREO) to serve as an infrared satellite intercalibration reference

by Tobin, Holz, Nagle, Revercomb, in press in JGR-Atmos

"… presents a new infrared intercalibration methodology that minimizes intercalibration uncertainties and provides uncertainty estimates resulting from the scene spatial variability and instrument noise. … The results are encouraging and suggest that biases between CLARREO and sounder observations can be determined with low uncertainty and with high time frequency during a CLARREO mission."

CLARREO/Sounder SNOs simulated with MODIS data

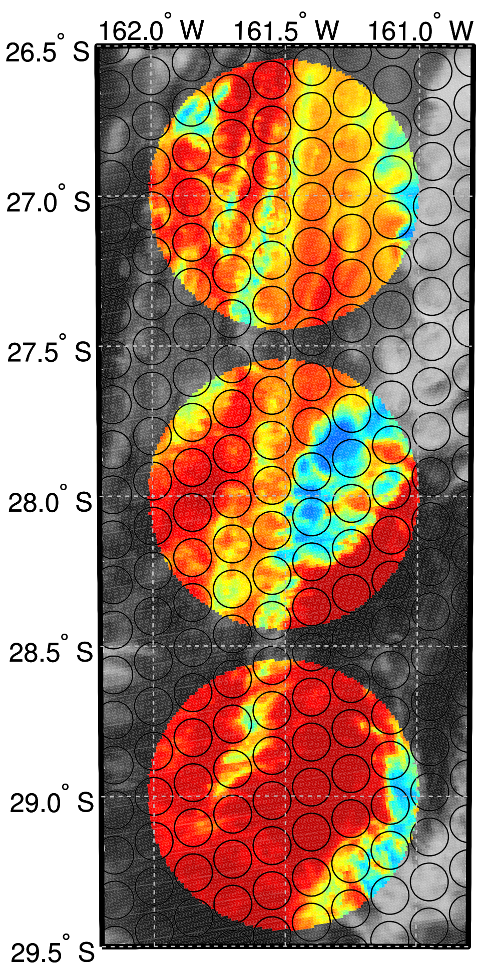

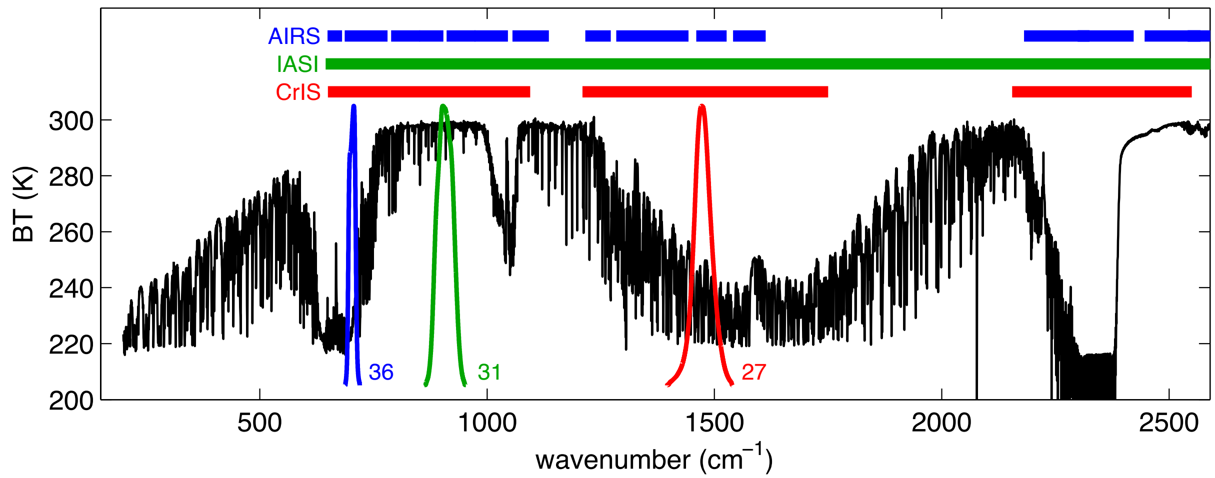

Simulation results

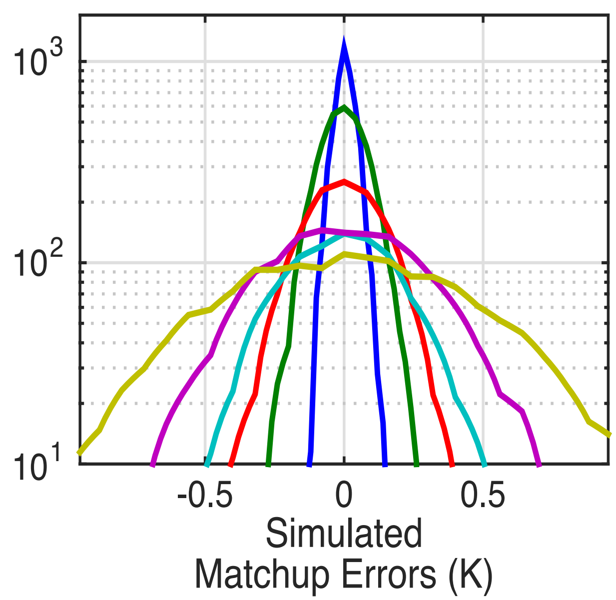

Observed (CrIS/AIRS SNOs)

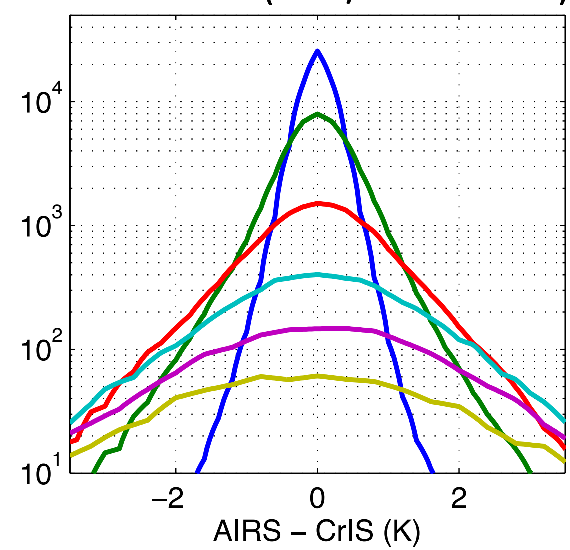

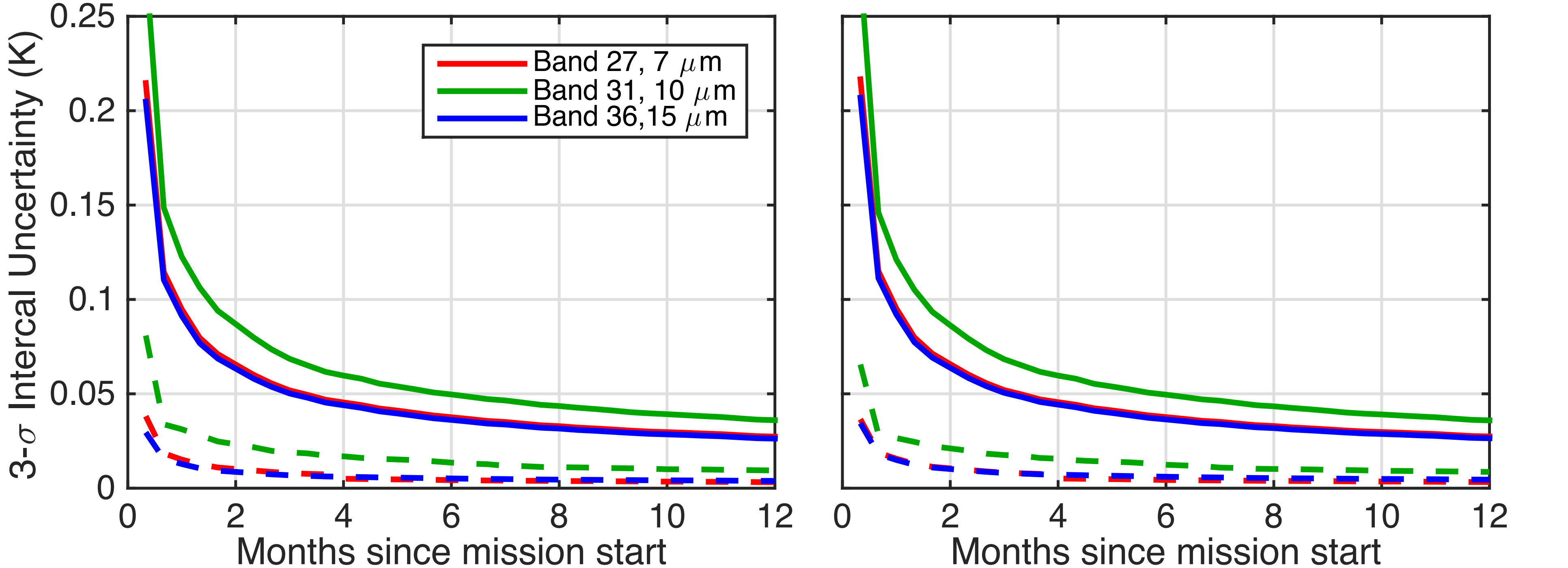

Figure 9. CLARREO Intercalibration (3-sigma) uncertainty as a function of mission length for single spectral channels in the 7, 10, and 15 mm regions for CLARREO/CrIS SNOs (left panel) and CLARREO/IASI SNOs (right panel). Solid curves include spatial and temporal colocation errors and CLARREO and sounder detector noise; dashed curves do not include CLARREO or sounder detector noise. Simulations include CLARREO in 90 degree polar orbit, CLARREO FOV diameter of 50 km, and 20 seconds between adjacent CLARREO FOVs.

Suomi-NPP CrIS Radiometric Uncertainty Estimates

Simplified On-Orbit Radiometric Calibration Equation:

$$R_{scene} = \mathcal{R}e\{(C'_{scene} - C'_{SP}) / (C'_{ICT} - C'_{SP})\}\, R_{ICT} \quad \text{with:}$$

Nonlinearity Correction: $C' = C \cdot (1 + 2\, a_2\, V_{DC})$

ICT Predicted Radiance: $R_{ICT} = \varepsilon_{ICT}\, B(T_{ICT}) + (1-\varepsilon_{ICT})\, [\, 0.5\, B(T_{ICT,\ Refl,\ Measured}) + 0.5\, B(T_{ICT,\ Refl,\ Modeled})]$

Parameter Uncertainties:

Parameter	Nominal Values	3-σ Uncertainty
T_{ICT}	280K	112.5 mK*
ε_{ICT}	0.974-0.996	0.03
$T_{ICT,\ Refl,\ Measured}$	280K	1.5 K
$T_{ICT,\ Refl,\ Modeled}$	280K	3 K
a_2 LW band	0.01 – 0.03 V^{-1}	0.00403 V^{-1}
a_2 MW band	0.001 – 0.12 V^{-1}	0.00128 – 0.00168 V^{-1}

- **Results provide estimates of the absolute calibration accuracy of the CrIS observations and, combined with the accuracy/precision of inter-calibration techniques, the level to which CrIS can be used as an inter-calibration reference.**

Suomi-NPP CrIS, example 3-sigma RU estimates

For a typical warm, ~clear sky spectrum

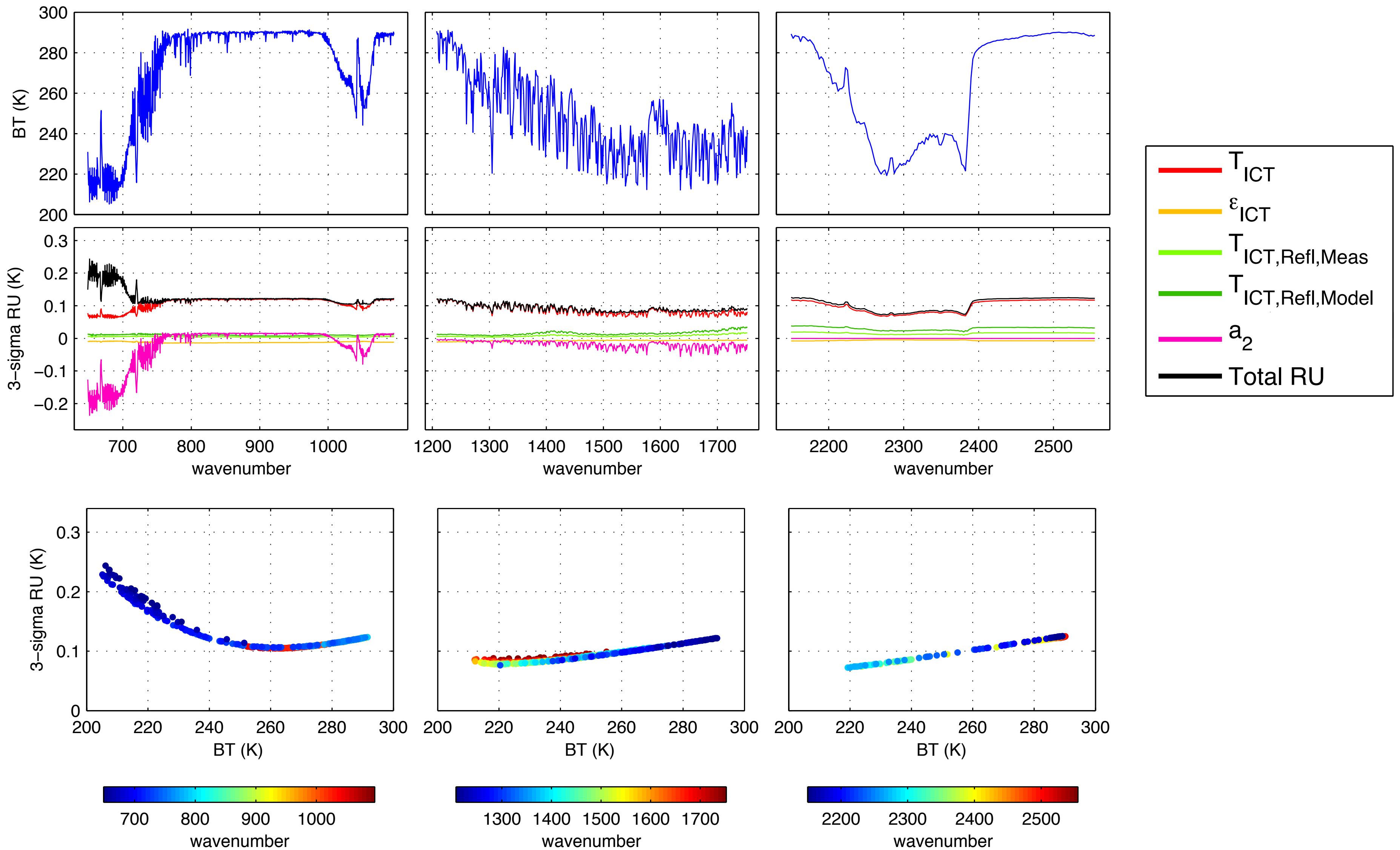

Suomi-NPP CrIS, example 3-sigma RU estimates

For a cold, high cloud spectrum

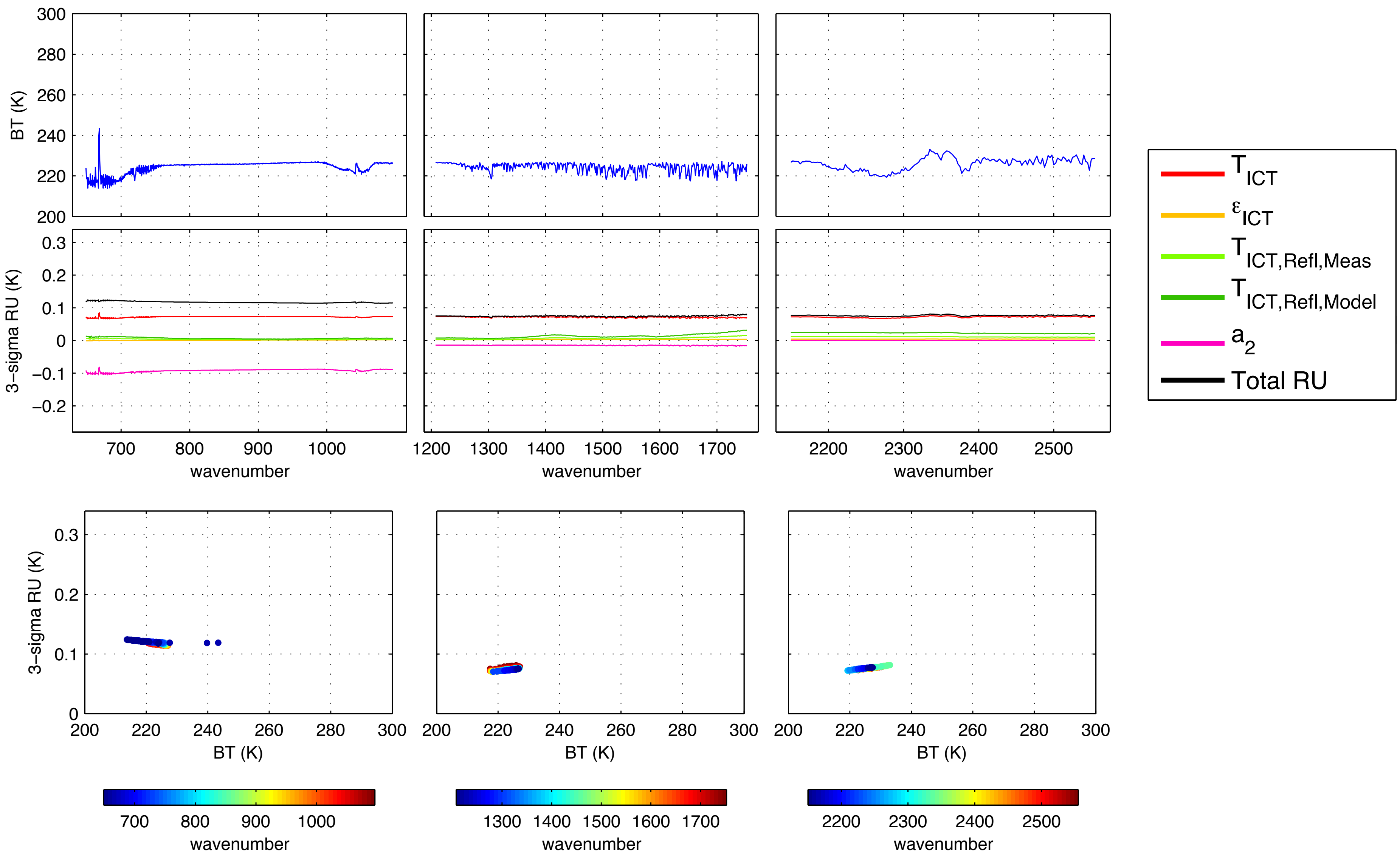

JPSS-1 Calibration Accuracy is very similar to Suomi-NPP CrIS

Main differences are: 1) Improved ICT emissivity, and 2) Different Nonlinearity magnitudes:

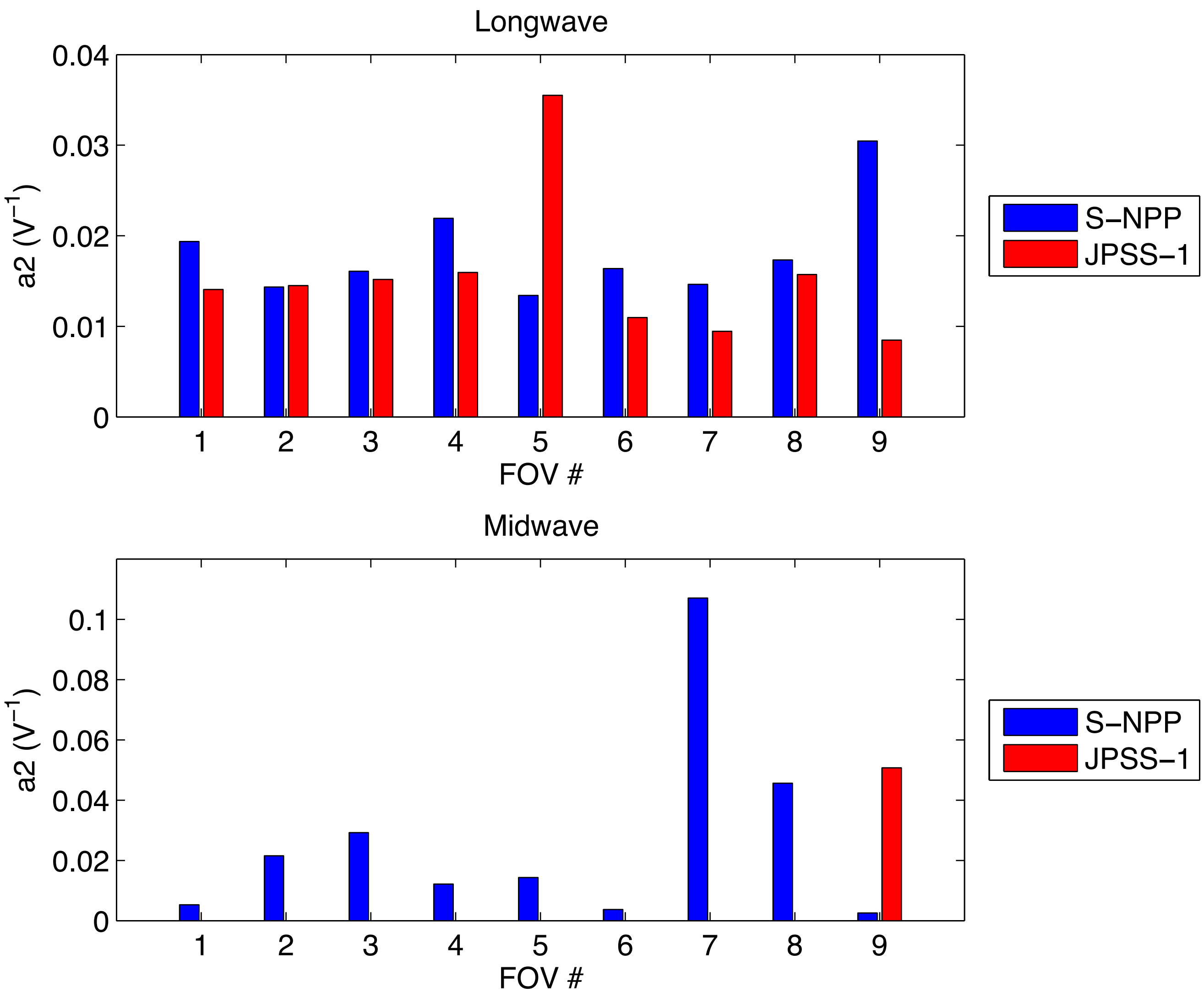

On-going Radiometric Calibration Refinements

- **Suomi-NPP Nonlinearity coefficients**
  - Primarily, reduce MW FOV7 a2 value by ~12%

- **T_{ICT} uncertainty**
  - Current values are too large because axial gradients are overestimated in current analyses. Results in change from 112 mK to ~88 mK 3-sigma.

- **Polarization**
  - Calibrations do not include polarization corrections although recent analyses suggests corrections should be included. Currently working to finalize polarization characterization and include in future processing.

Polarization

- Incident radiance is partially polarized by reflection from the scene select mirror (SSM); small degree of polarization in the IR for uncoated gold mirrors. The orientation of the polarization axis of the scene select mirror changes with scene mirror rotation. When coupled with the polarization sensitivity of the sensor, this produces a radiometric modulation of the detected signal that is dependent on the rotation angle of the scene select mirror and creates a calibration error
- In summary: SSM and sensor act as a polarizer and analyzer pair
- Corrention formalism following Pagano et al., 2000 ("Scan Angle Dependent Radiometric Modulation due to Polarization for the Atmospheric Infrared Sounder (AIRS)")

➢ 2012 Pitch maneuver data is being used to estimate polarization parameters $p_r p_t$ and α

➢ Earth view calibration effects are expected to be generally small but potentially larger for cold scene SW band radiances.

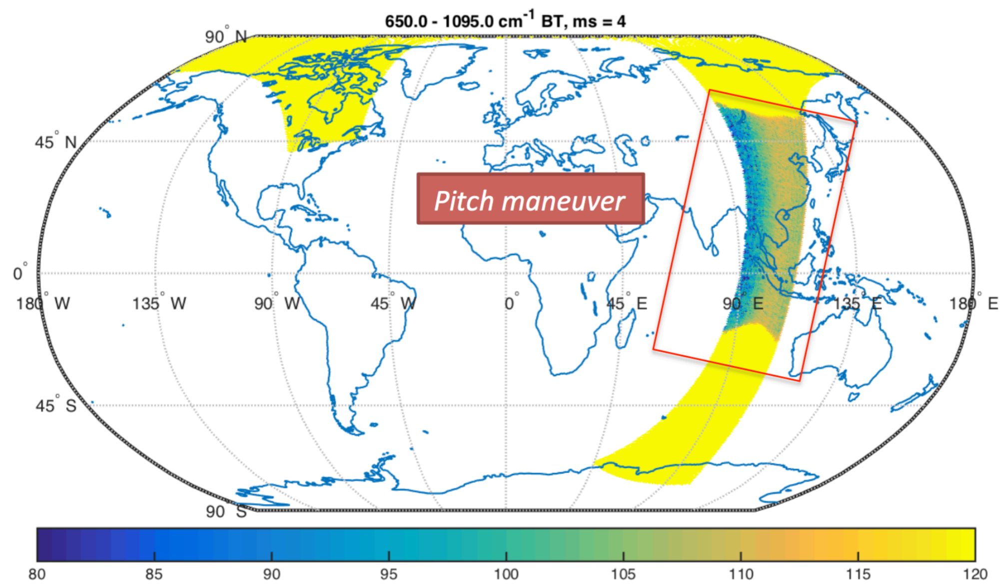

JPSS-1 Pre-launch calibration Traceability; Comparison to CrIS near ICT temperature

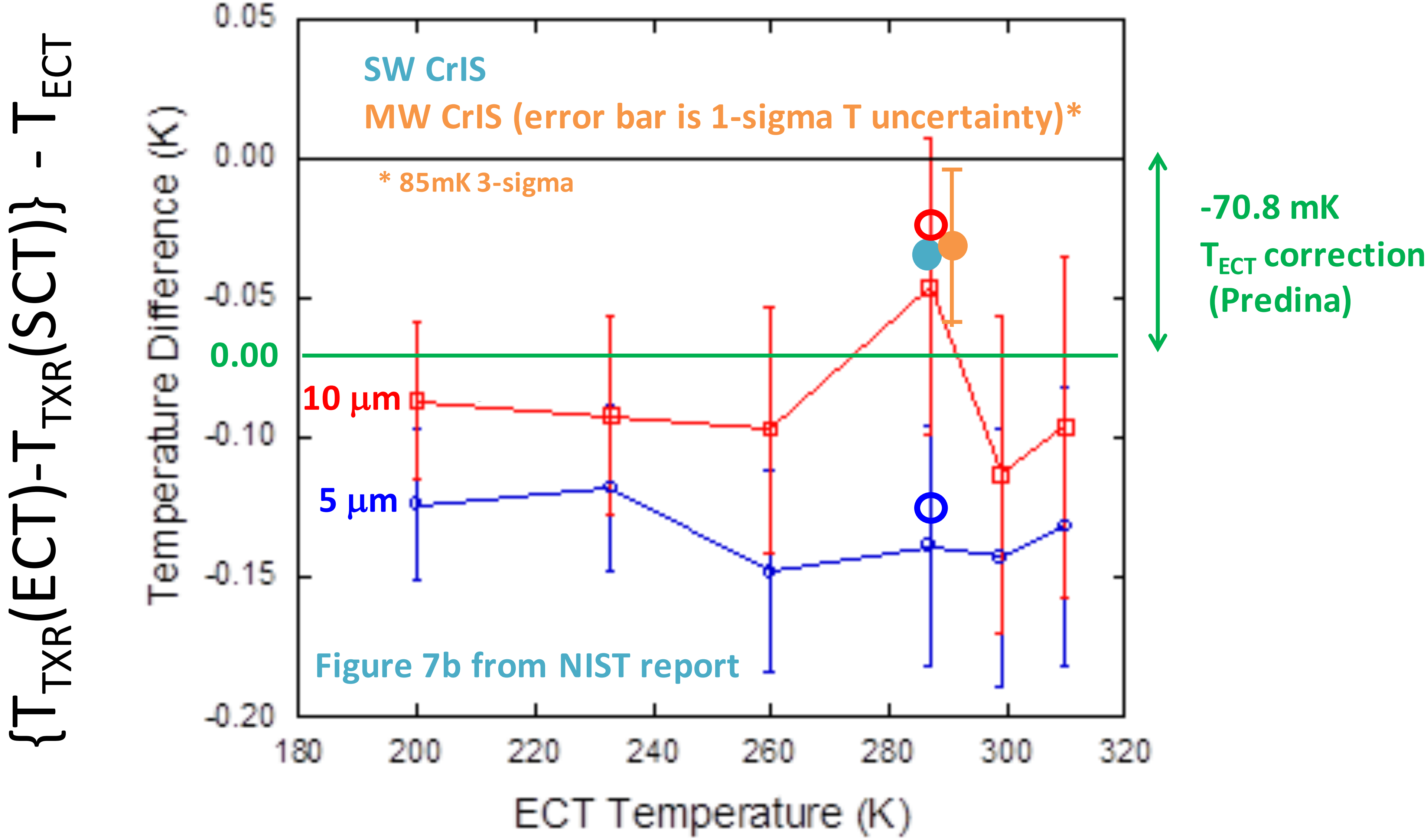

Demonstrates reasonable agreement with TXR 10 micron channel

(5 micron channel seems to have a small negative bias of 40-50 mK)

JPSS-1 Pre-launch calibration Traceability, Basic Summary

- These NIST TXR results provide valuable validation of ECT and CrIS absolute calibration
- The results do not suggest any adjustment to the CrIS calibration is necessary
- The results also validate the expected emissivity of the ECT and SCT and the ECT gradients characterized by CrIS (not shown here)

➢ Other post-launch traceability chains involve various intercomparisons, including high altitude aircraft underflights, with uncertainties typically on the same order or larger than the CrIS RU.

Four years of CrIS/VIIRS inter-comparisons

Results show:

- **Overall very small biases which are very stable with time**
- **Relatively small dependencies on signal level, scan angle, and orbit phase.**
- **Small biases become even smaller on the days when VIIRS performs its quarterly nonlinearity tests.**

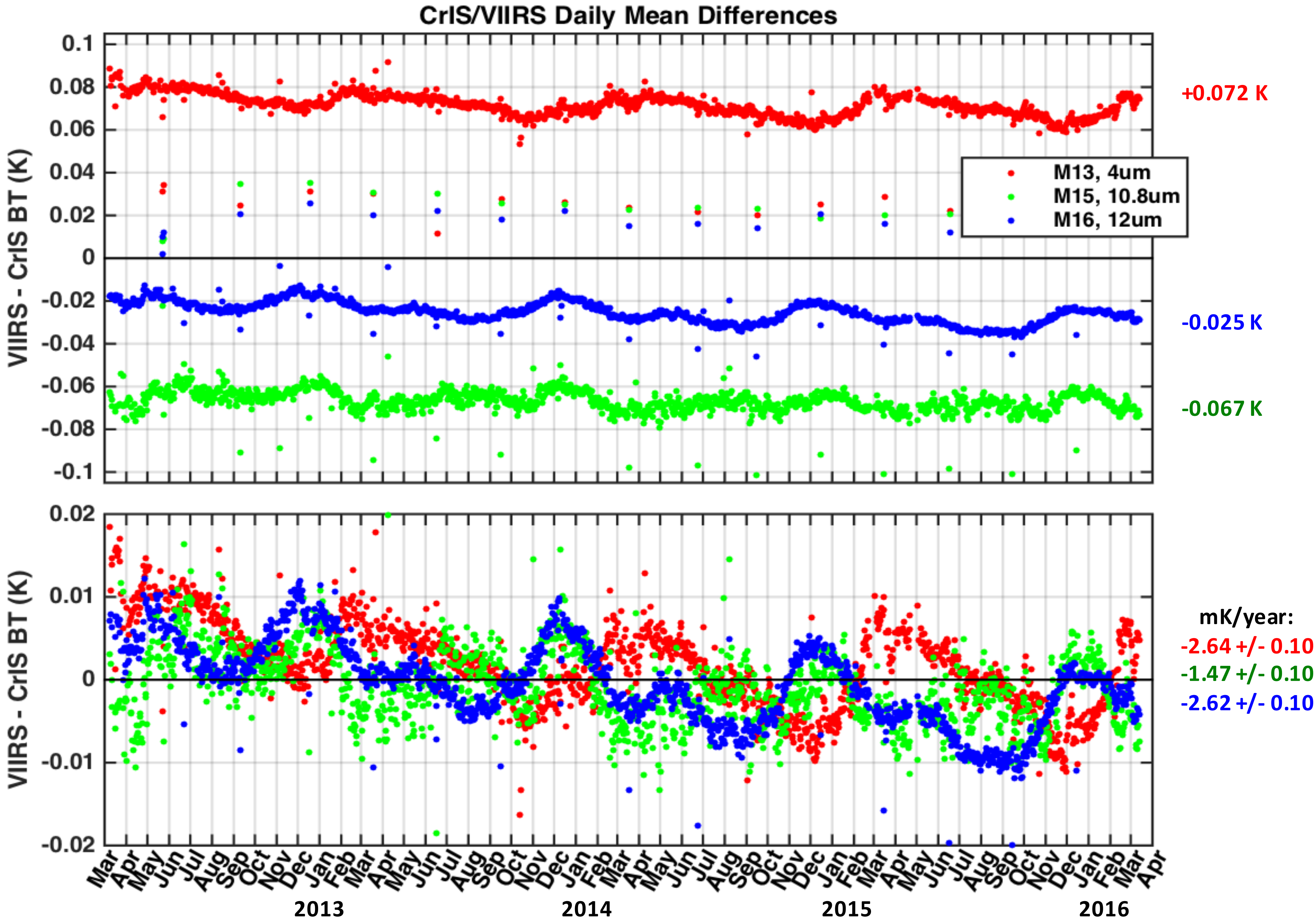

CrIS/VIIRS Daily Mean Differences
VIIRS - CrIS BT (K)
M13, 4um
M15, 10.8um
M16, 12um
+0.072 K
-0.025 K
-0.067 K
mK/year:
-2.64 +/- 0.10
-1.47 +/- 0.10
-2.62 +/- 0.10
2013
2014
2015
2016

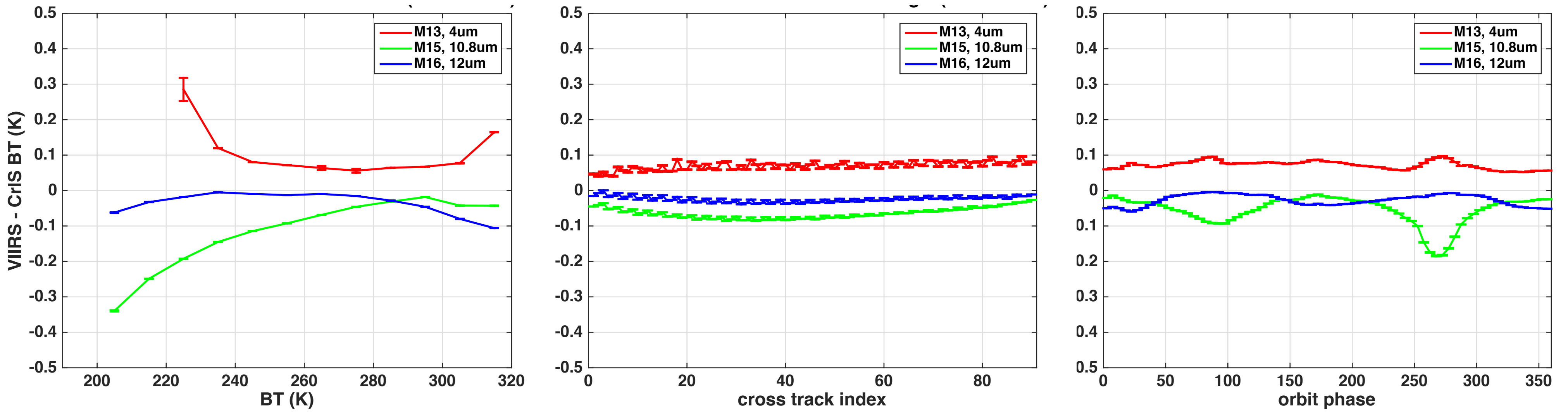

VIIRS - CrIS BT (K)
BT (K)
cross track index
orbit phase
M13, 4um
M15, 10.8um
M16, 12um

Time dependence of M12 band biases

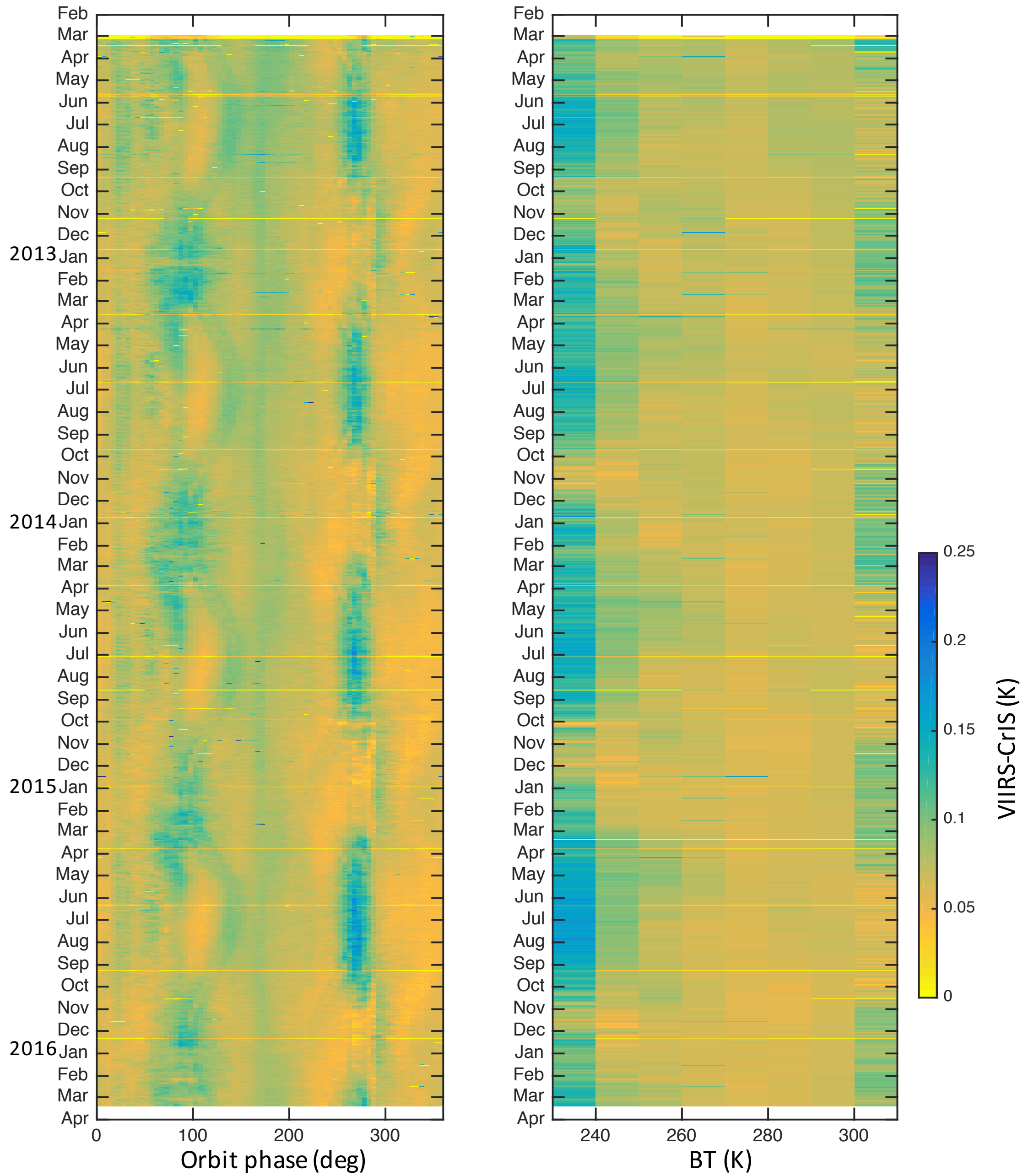

Four years of CrIS/IASI inter-comparisons

Results show:

- **Overall very small biases which are very stable with time**
- **Small but noticeable dependencies on signal level for some LW and some SW band channels.**
- **IASI-A / IASI-B differences which are generally consistent with potential changes to the IASI LW band nonlinearity corrections.**

"Big circle" SNOs with matchup criteria: +/- 20 min, 50 km radius

IASI-A/CrIS: 15,553 SNOs from 11-May-2012 to 30-June-2016
IASI-B/CrIS: 10,788 SNOs from 01-Aug-2013 to 08-June-2016

Sample SNO

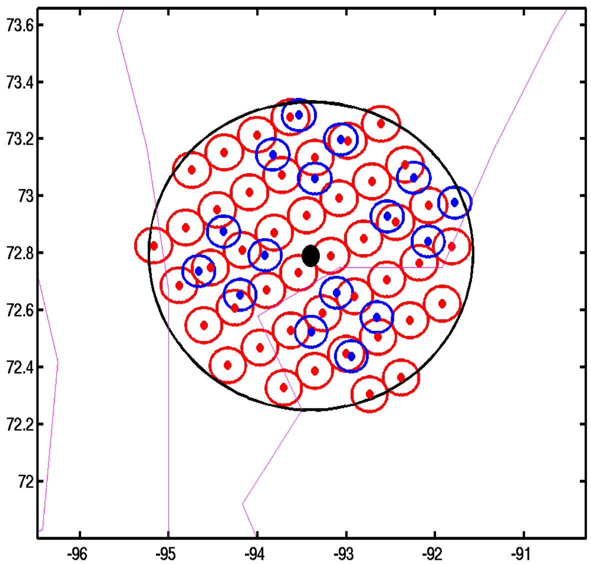

CrIS / IASI-B SNOs @ 900 cm^{-1}

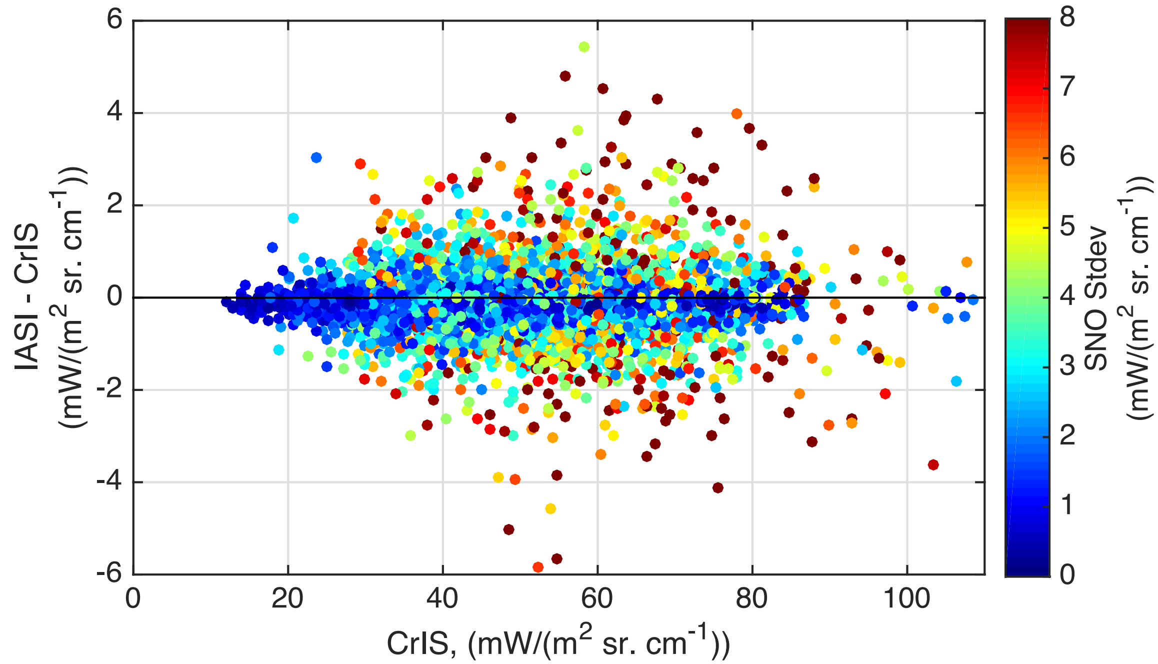

CrIS / IASI SNOs @ 680 cm^{-1}

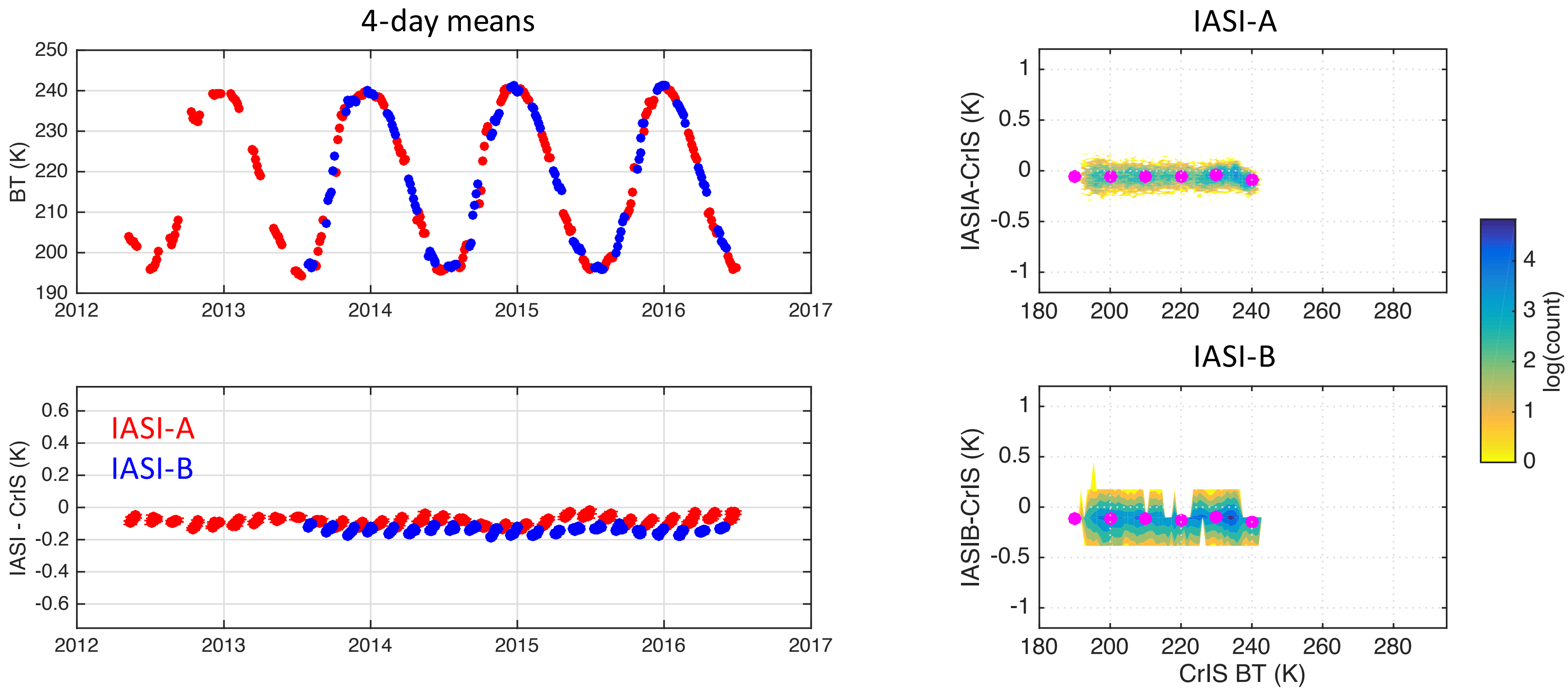

Hamming apodization, Conversion to BT at scene radiance, Southern SNOs

CrIS / IASI SNOs @ 900 cm^{-1}

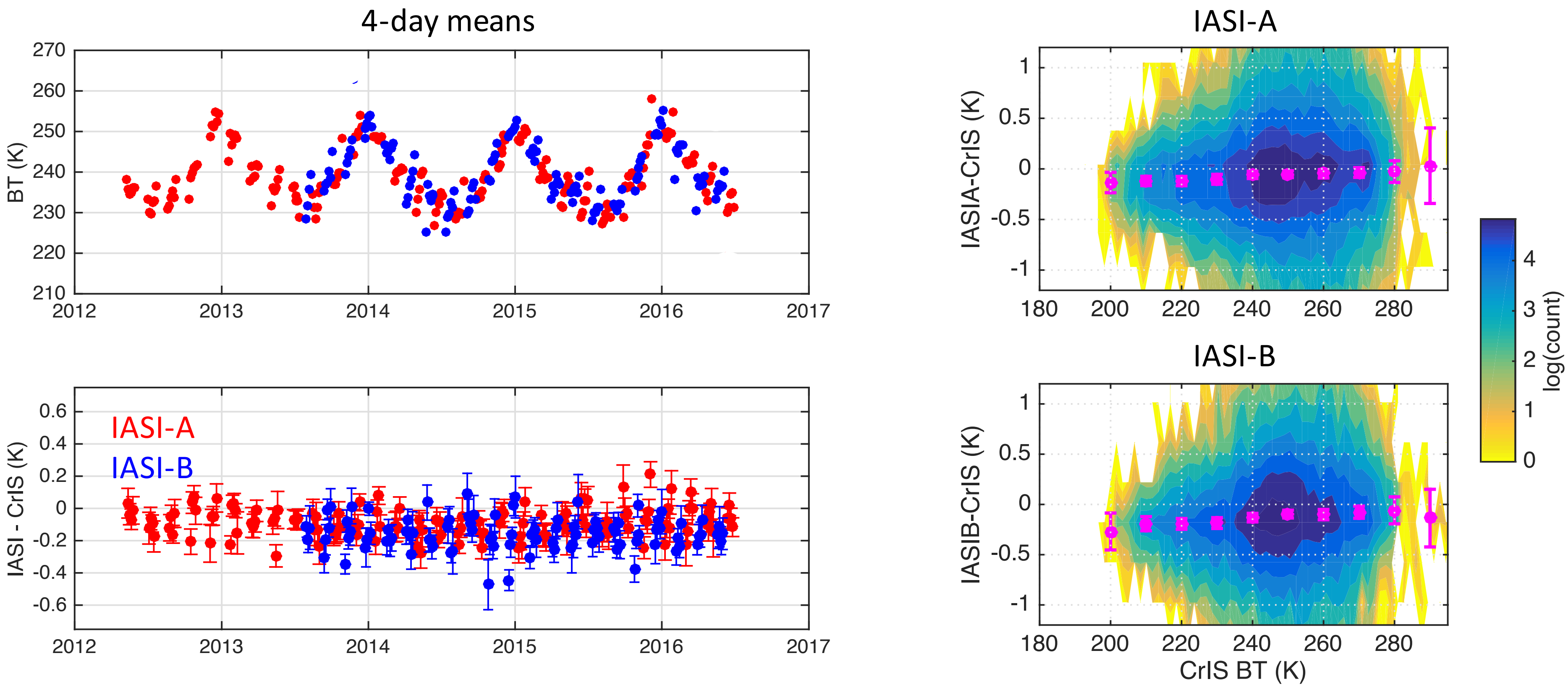

Hamming apodization, Conversion to BT at scene radiance, Southern SNOs

CrIS / IASI SNOs @ 1585 cm^{-1}

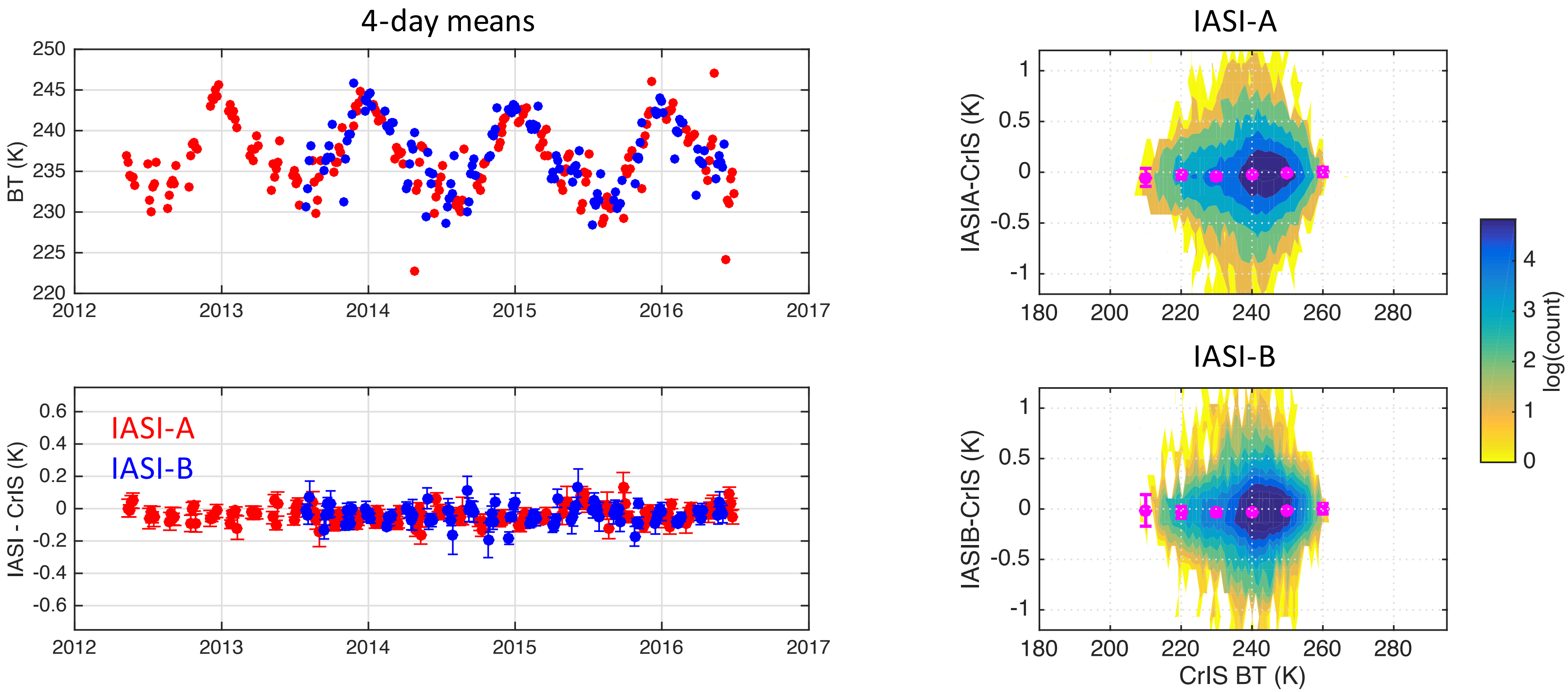

Hamming apodization, Conversion to BT at scene radiance, Southern SNOs

CrIS / IASI SNOs @ 2185 cm^{-1}

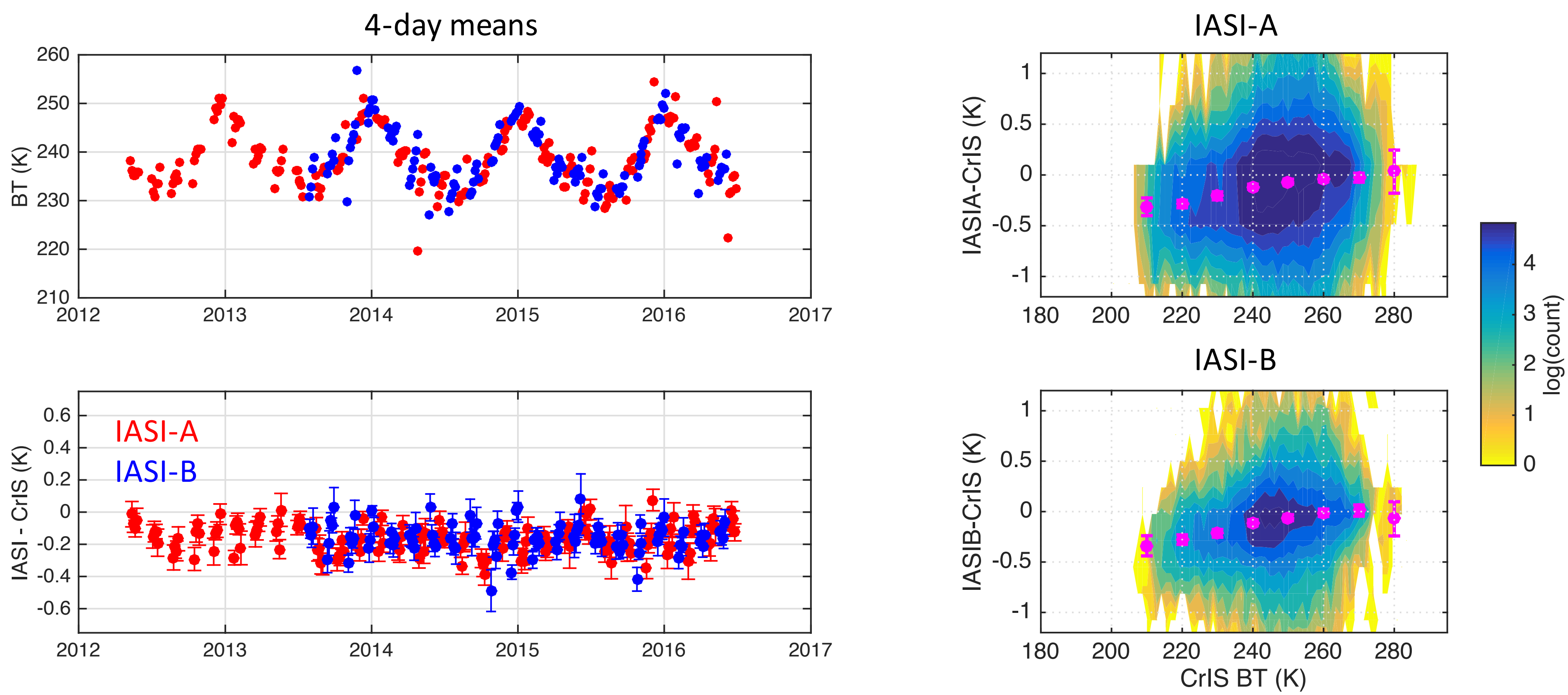

Hamming apodization, Conversion to BT at scene radiance, Southern SNOs

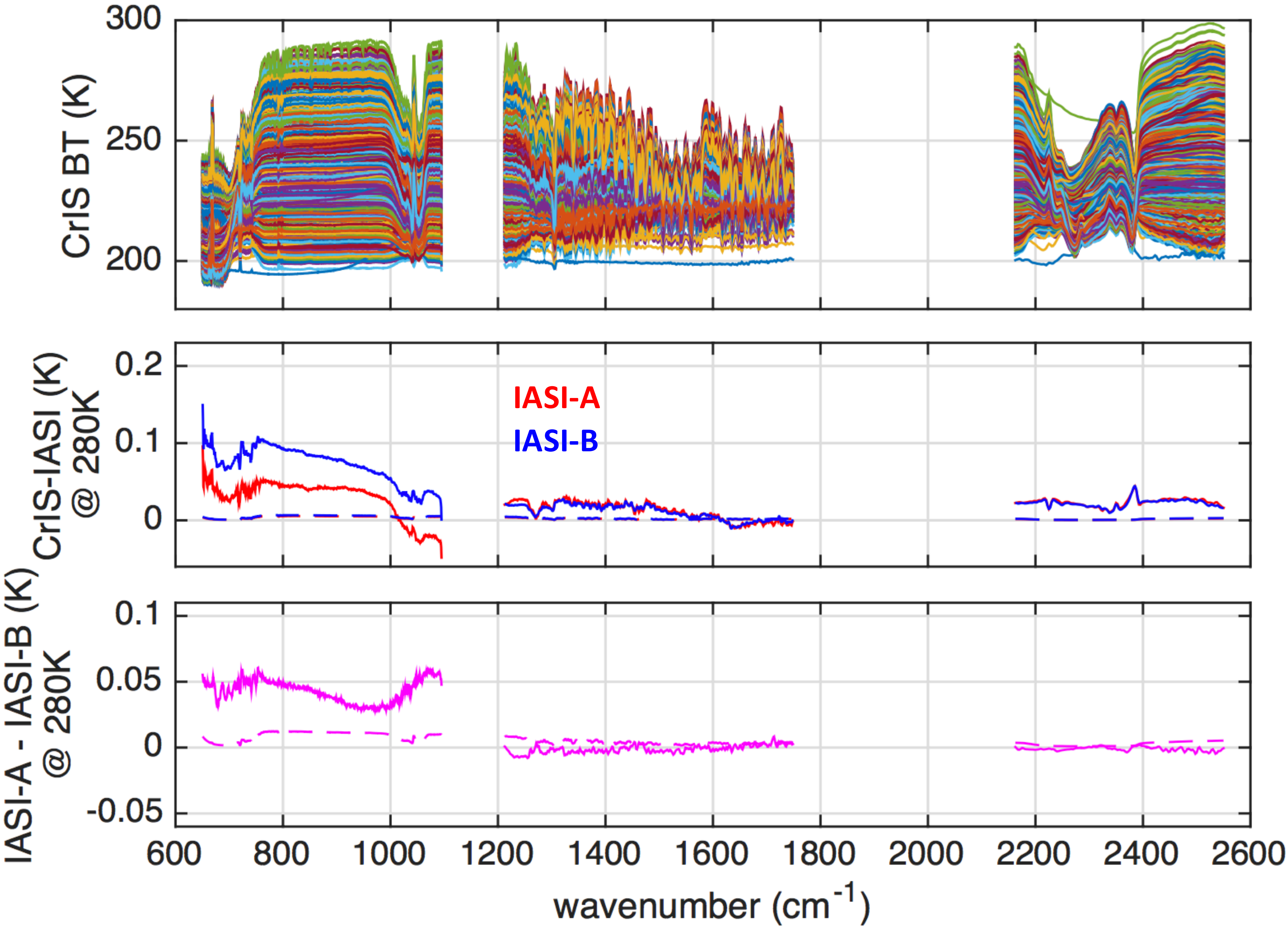

Hamming apodization, Conversion to BT at 280K, all SNOs

900 cm^{-1} Radiance Distributions, Nadir FORs 2012-2016

IASI, log(counts)

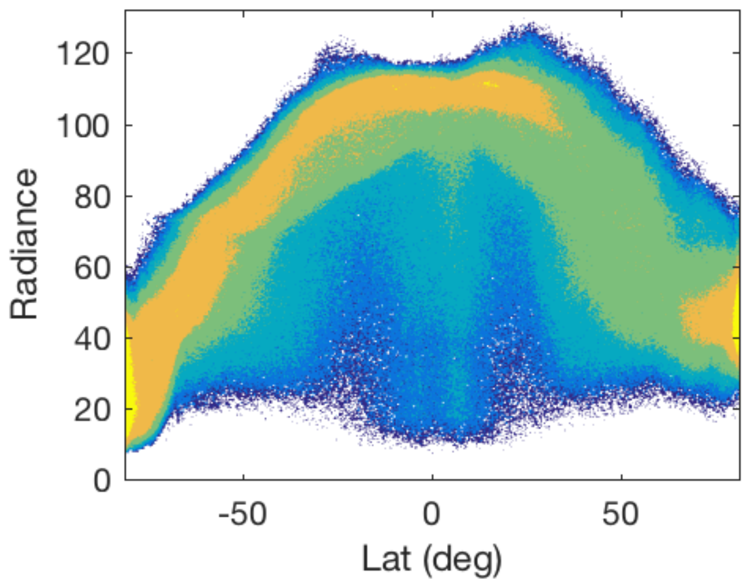

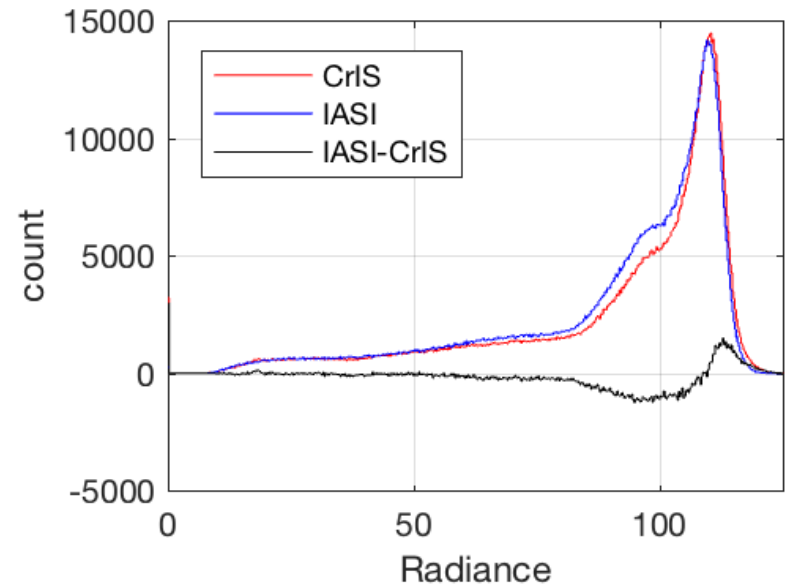

CrIS, log(counts)

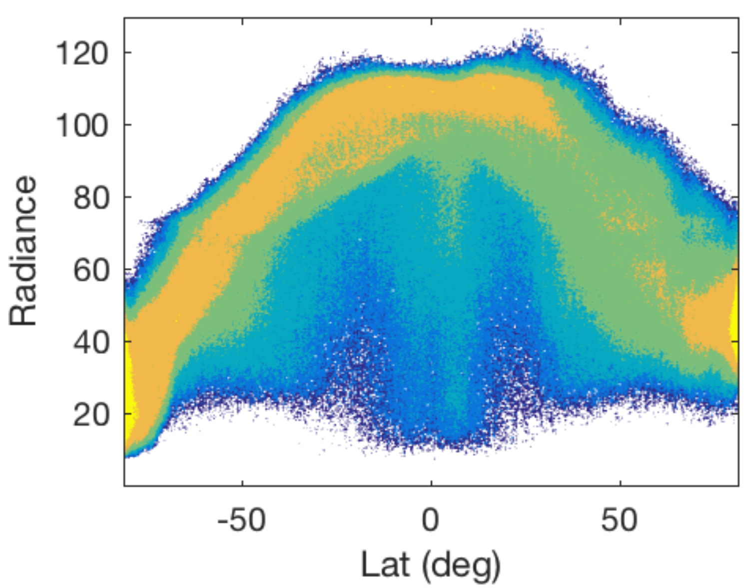

Mean Radiance vs. latitude

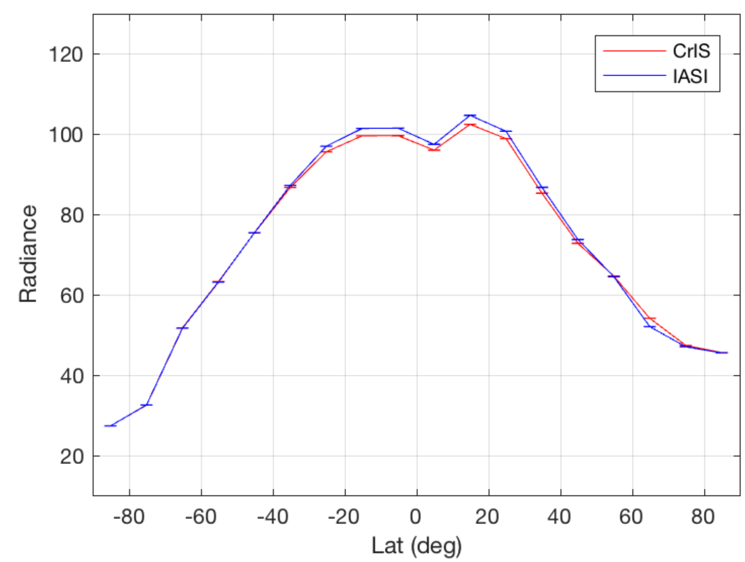

Overall Summary

- **CrIS is well suited to serve as an intercalibration reference**
  - **Radiometric calibration accuracy is generally small and well understood and documented**
  - **Pre-launch traceability via NIST testing of the ECT and various on-going efforts to establish post-launch traceability as well**
  - **Several calibration refinements underway (e.g. MW nonlinearity, polarization, ICT temperature)**
  - **Full spectral coverage would provide intercalibration of other sensors/bands**

CrIS Noise and Moldel Error Covariance

L. Larrabee Strow, Howard Motteler, and Sergio De-Souza Machado

UMBC
Department of Physics *and*
Joint Center for Earth Systems Technology

STAR Science Meeting
Aug. 9, 2016

NWP Centers: CrIS Covariance Higher than IASI

Derive CrIS Noise Covariance

- Using 1 day of ICT data, derive noise error covariance

Mimic?? NWP (Noise+Model) Error Covariance

- Match ECMWF analysis/forecast to IASI, CrIS clear scenes
- Convert IASI observations (different noise) to CrIS
- Compare bias error covariances
- Try to convert CrIS error covariance to (IASI -> CrIS) error covariance and compare

- Day: Jan 18, 2016
- SDR Code: CCAST standard

NWP Data Assimilation

Data assimilation ingests the observations y and minimizes a cost function J

$$J = (x - x_b)^T B_x^{-1} (x - x_b) + (y - K(x))^T (E + F)^{-1} (y - K(x))$$

in order to find the best analysis increment to the model background $x - x_b$.

- B_x: Background error covariance
- K: CrIS RTA
- $E + F = R$: Observation error covariance (often diagonal)
- E: Instrument error covariance
- F: Representativeness, nonlinearity, RTA covariances

NPW centers are finding R is larger for CrIS than IASI. *But* this is generally presented as correlations rather than covariances.

Present Status

- A diagonal R was/is the norm in the past.
- Many centers working towards off-diagonal R
- This should lead to better use of sounder data, using lower error estimates.
- If practical, I hope this then leads to using more channels, esp. for CrIS which has low noise, but slightly wider Jacobians

Recent Relevant Journal Articles

- *Effect of self-apodization correction on Cross-track Infrared Sounder radiance noise*, Han et. al. (Applied Optics, 2015)
- *Infrared atmospheric sounder interferometer radiometric noise assessment from spectral residuals*, Carmine Serio et. al. (Applied Optics 2015)
- *Enhancing the impact of IASI observations through an updated observation-error covariance matrix*, Niels Bormann etc. al (QJRMS 2016)

NWP “Correlation” Observations for CrIS, IASI

NRL CrIS/IASI Error Correlation

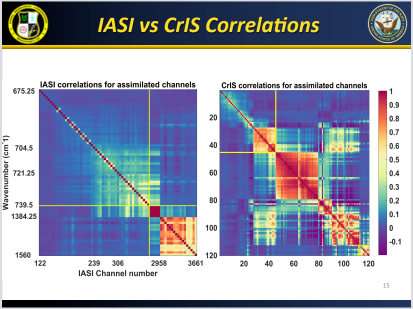

ECMWF IASI Error Correlation

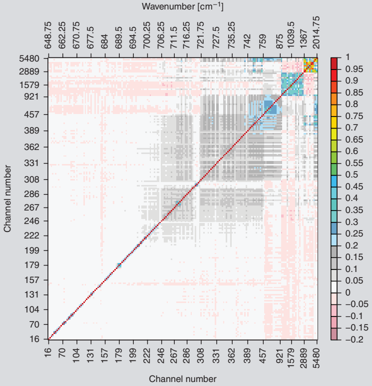

Figure 3. Observation-error correlations used in this study for assimilated IASI channels. See main text and Appendix A for further details.

Noise Correlation

- Following Han et. al., reproduce noise figures
- Expand from 512 points to 1-day (either Jan 18 or 20, 2016)
- Do SVD analysis to determine correlated noise, about 1-2% for Hamming (see Additional Material at end of talk)
- Effect of hamming on covariance and correlation matrices

Keep in mind:

- noise = $\sqrt(cov_{i,i})$
- $corr_{i,j} = \frac{cov_{i,j}}{\sqrt(cov_{i,i} \cdot cov_{j,j})}$
- CrIS has lower noise than IASI
- CrIS Hamming has lower noise than Sinc

Noise Correlation Data Analysis

- One day of ICT (blackbody) calibrated data.
- Just substitude ICT_i into SDR equation instead of ES_i
- Remove resulting slow variation in ICT B(T) with a 31-point moving average smoother
- For SVD correlated noise analysis divide by nominal noise

LongWave Noise Correlations

Sinc Noise Correlation

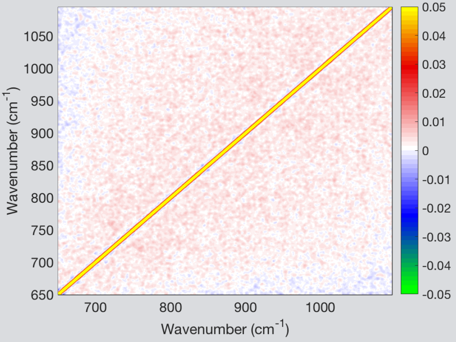

Hamming Noise Correlation

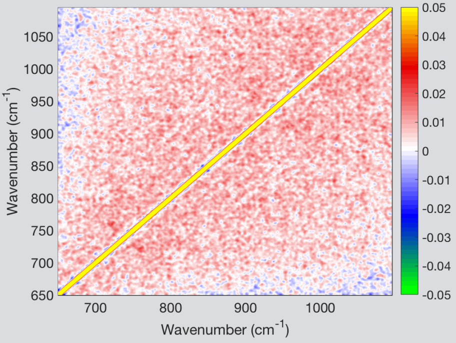

These smoothed correlation matrices suggest off-diagonal correlated noise at the 2% level. Higher for hamming.

LongWave Noise Covariance

Sinc (or Hamming) Noise Covariance

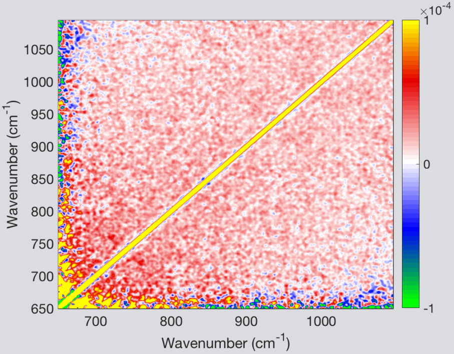

Hamming - Sinc Covariance

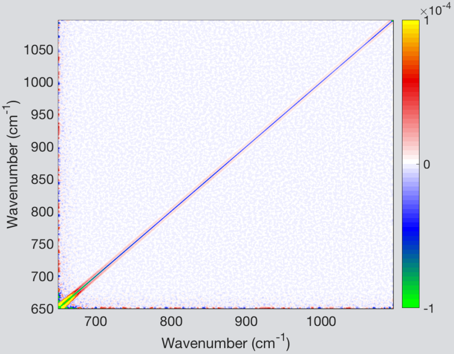

No difference between Sinc and Hamming off-diagonals!
Lower Hamming noise increases off-diagonal correlations.

Other Sources of Correlation?

- ICT environmental model? (in longwave ± -0.04 to -0.01K)
- ICT calibration variability, esp. over orbit?
- **Small** orbital calibration errors *could* produce these correlations; TVAC results (day in the life?)
- IASI blackbody has a constant temperature

ICT Calibrated Temperature vs Time

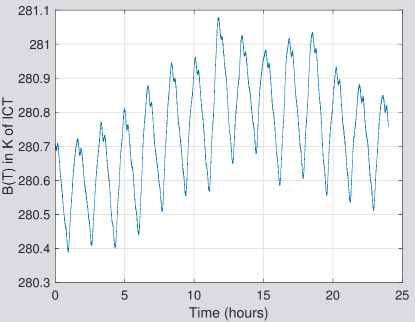

Scaled ICT T-sensor vs (ICT-SP) Counts

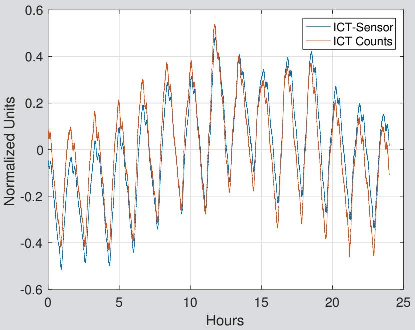

Bias Correlation Data Analysis

- Clear ocean scenes, tropical to keep *F* smaller
- Convert IASI to CrIS ILS "IASI->CrIS"
- Modify CrIS to have "IASI->CrIS" noise
- Concentrate on 650-750 cm^{-1}
- *F* covariance clearly dominates rest of LW and MW (SST, water vapor)
- ??? Our *F* is *larger* than NWP and mixes background and observation errors, and has no integration of the model to the observation time, etc etc. We are using ECMWF 3-hour forecast/analysis
- ??? Consequently, our results are, at most, only useful for relative comparisons

Clear Scene Locations for CrIS

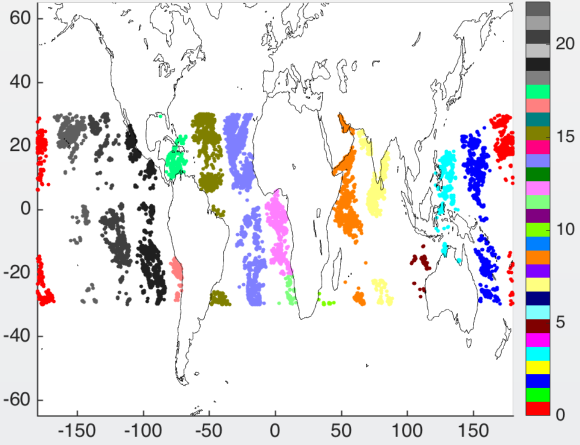

Color is hour.

CrIS and IASI Clear Biases

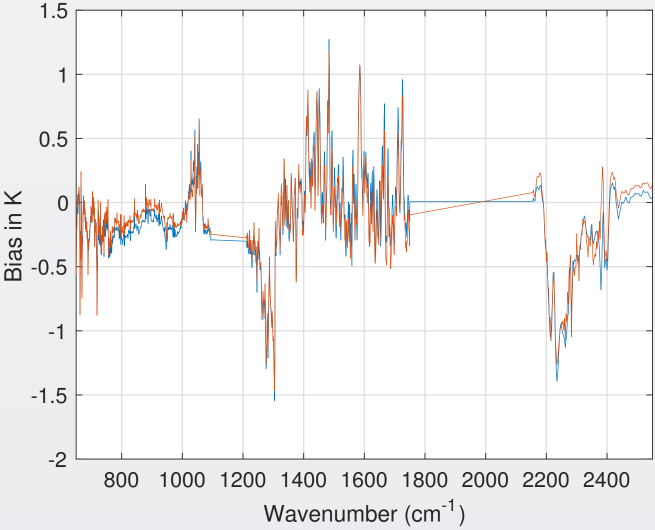

Night is similar, IASI 0.2K warmer in window region.

Bias Std and Noise

Bias Std

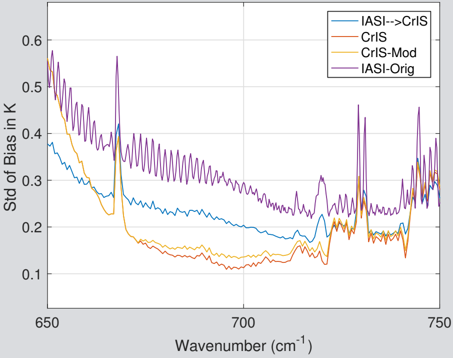

Noise

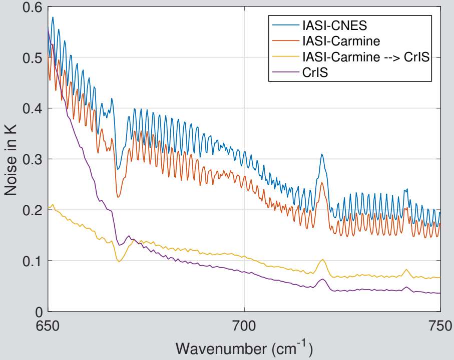

Covariance Ratios (IASI/CrIS)

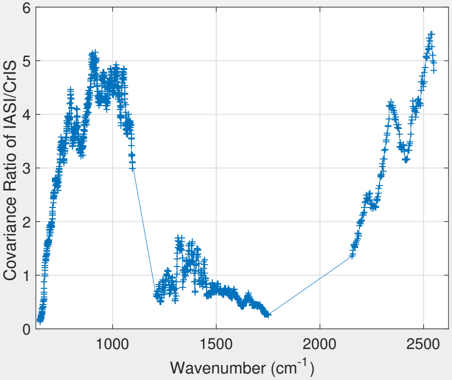

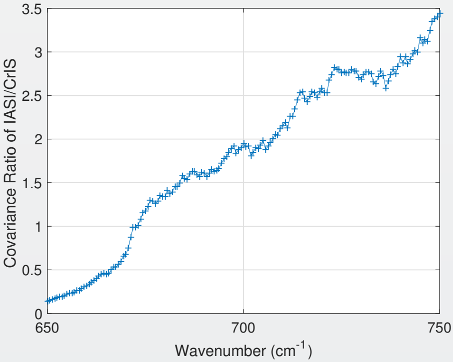

F covariances (Representativeness, RTA, etc.) constant between instruments

E covariances scale with instrument noise

Low noise implies higher off-diagonal correlations

Effective Model Error

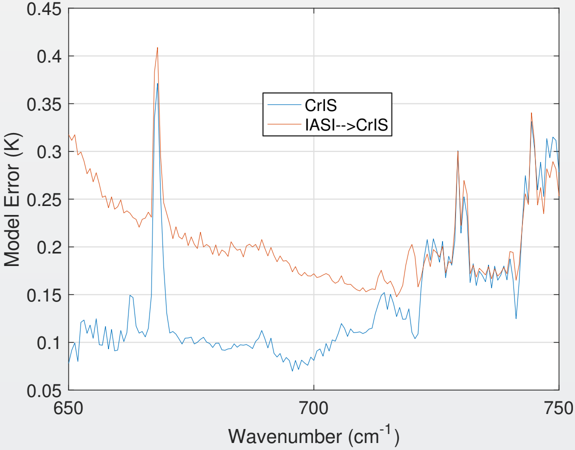

IASI model error up to 3X larger than CrIS??

$$F = \sqrt{(std^2 - inoise^2)}$$

CrIS vs IASI Correlations

CrIS

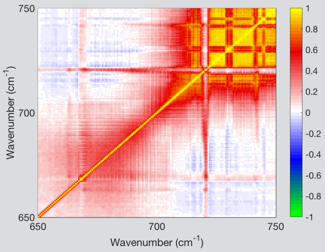

IASI

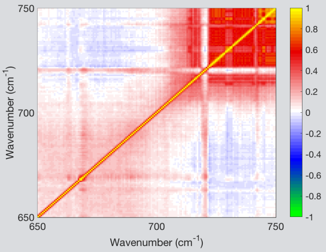

(CrIS + IASI Noise) - IASI

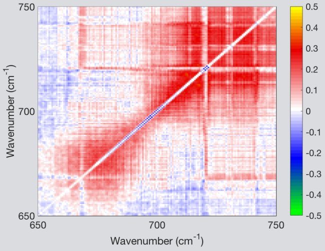

(CrIS + IASI Std) - IASI

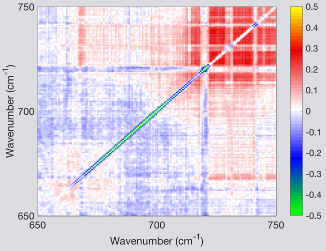

Day vs Night Correlations

CrIS Night

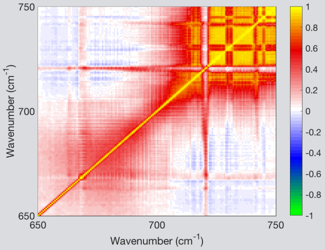

IASI Night

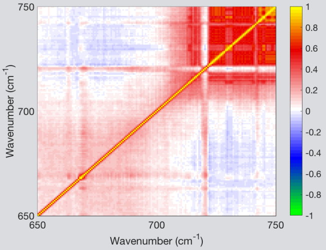

CrIS Day

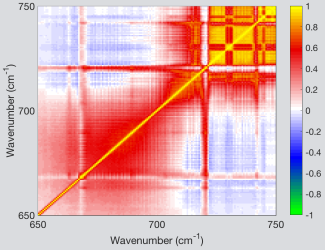

IASI Day

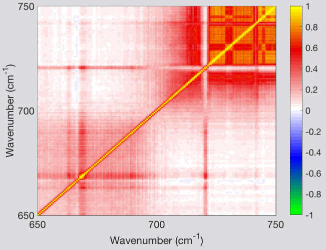

Corrected Day Correlations

CrIS

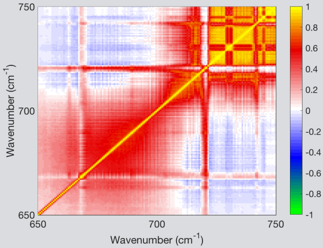

IASI

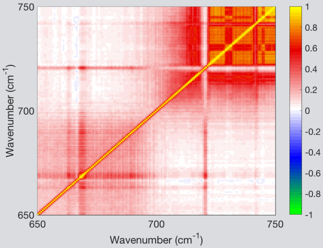

(CrIS + IASI Noise) - IASI

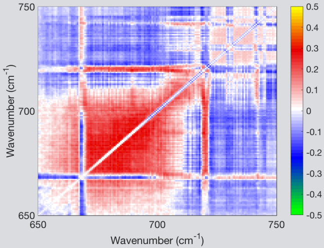

(CrIS + IASI Std) - IASI

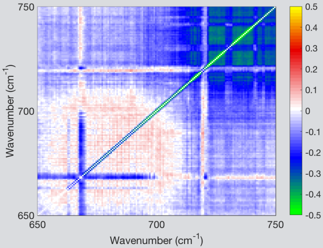

Problem with LongWave IASI Biases?

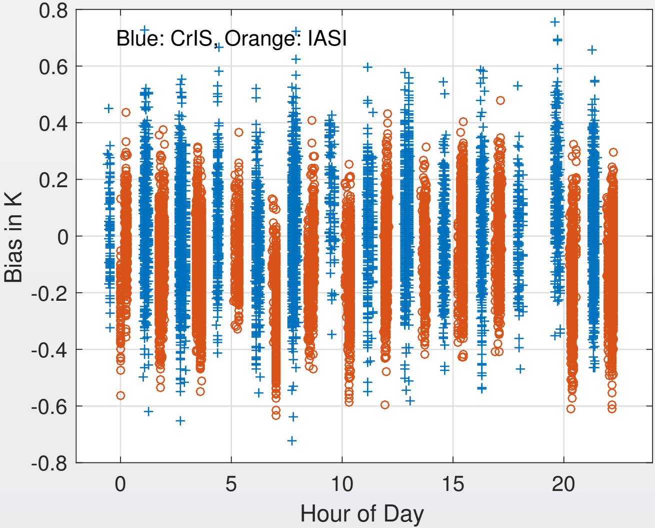

Problem with LongWave IASI Biases?

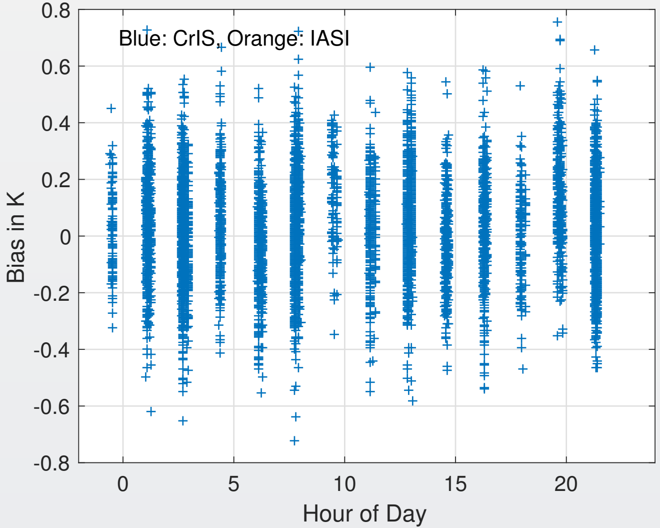

Problem with LongWave IASI Biases?

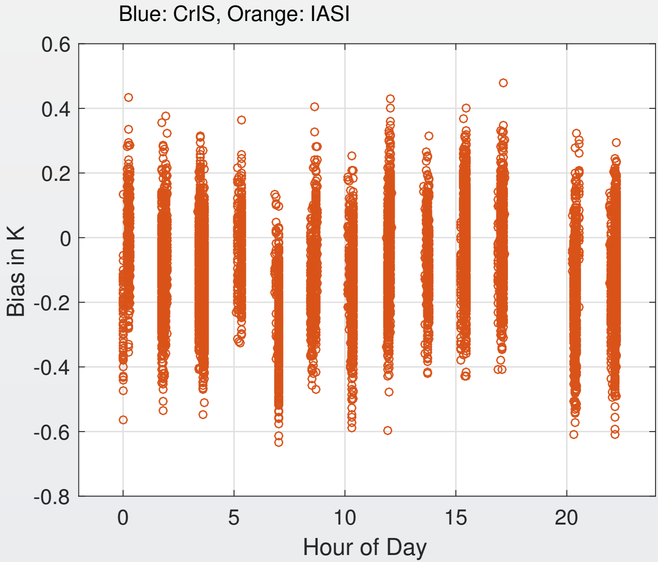

CrIS Radiometric Stability: dBT/dt Rates

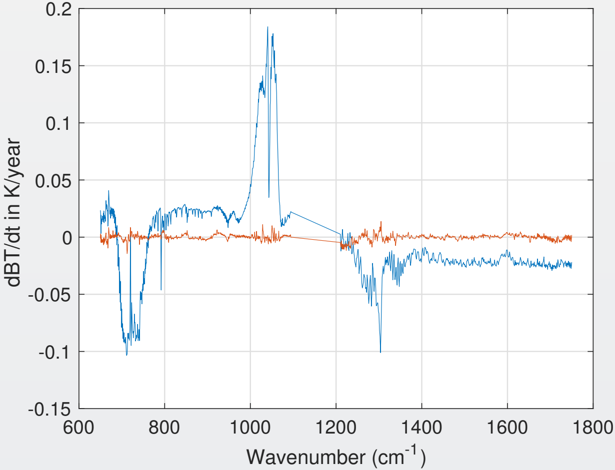

Blue: Observed Rate Red: Fit residuals

CrIS Stabliity from dBT/dt Rate Fits

- Do an OEM fit of dBT/dt (K/year) CrIS rates for tropical clear ocean spectra bias versus ERA.
- Fits for T(z) and H_2O (z) are close to ERA
- OEM fit for CO_2
  - CO_2 CrIS = 2.45 ± 0.006 ppm/year (error is wrong)
  - NOAA ESRL CO_2 = 2.39 ± 0.09 ppm/year
  - (NOAA ESRL CO_2- CrIS CO_2) = -0.002K/year ± 0.004 K/year
- OEM fit for CH_4 (just final result)
  - -0.0008 K/year ± 0.002 K/year

Need to include observation covariance to get correct OEM errors!

Conclusions

- How can NWP utilize low noise of CrIS?
- Could CO_2 be the cause of some of these correlations? Rd-do analysis in Spring when N/S gradient exists.
- Need closer interactions between instrument, RTA, and NWP researchers?
- If NWP includes observation covariances, can they now increase the number of channels used?
- CrIS channels *may* have slightly higher correlations than IASI, but maybe due to other IASI issues?
- IASI calibration appears to vary slightly with some orbits?
- JPSS-1 CrIS will have a better blackbody, will that change these observations?
- Exactly how well does the CrIS ICT temperature match the ICT emission over time? What can TVAC tell us?

Additional Material

SVD analysis of CrIS correlated noise is shown on the next three slides.

LongWave Noise Correlations

Sinc

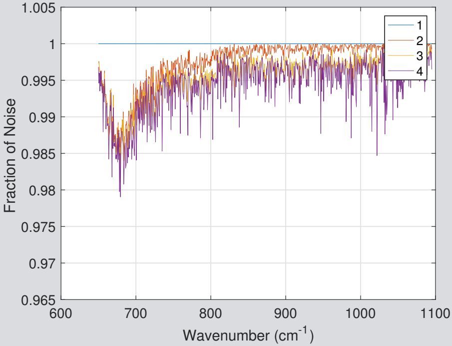

Hamming

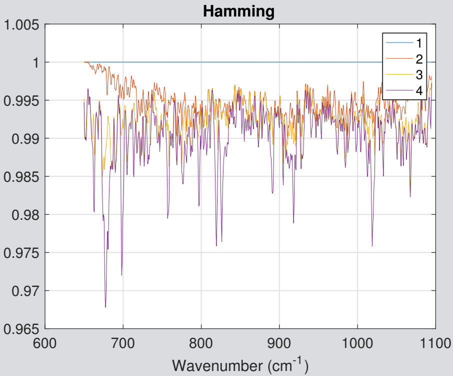

MidWave Noise Correlations

Sinc

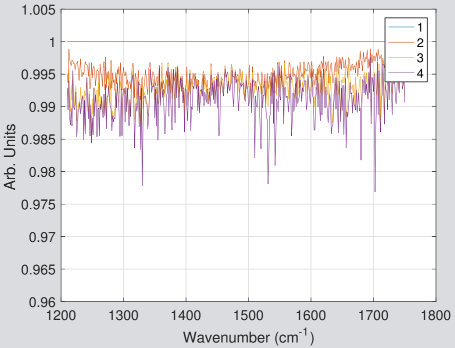

Hamming

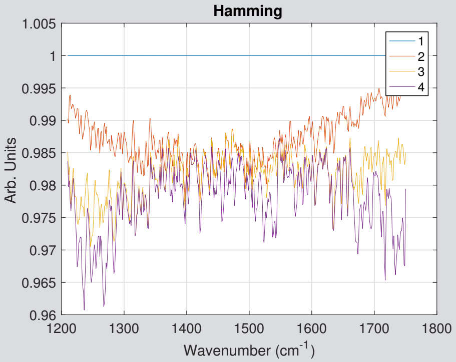

ShortWave Noise Correlations

Sinc

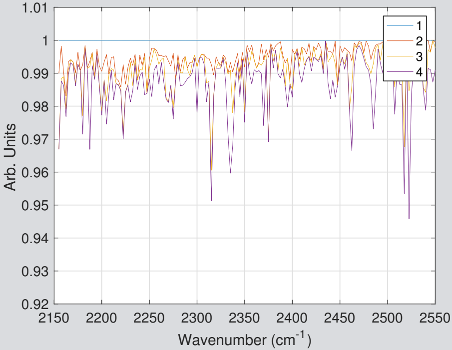

Hamming

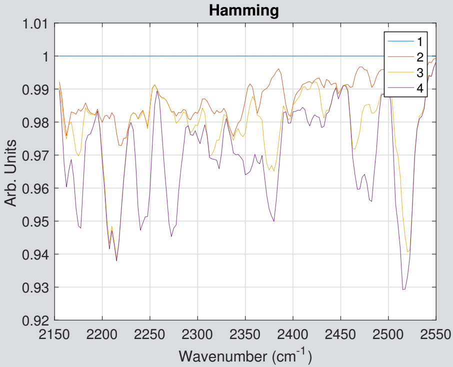

True CrIS ILS - Consequences of Unapodized SDR Processing

Joe Predina

Perry Falk

Logistikos Engineering LLC, Fort Wayne, IN

STAR JPSS Science Team Annual Meeting

Session 4, Part 1: CrIS SDR

August 8-12, 2016

College Park, MD

Introduction – True CrIS ILS

- **It is desirable for interferometer systems to produce an unapodized ideal Sinc ILS after completion of all SDR calibration operations**
- **Deviation from ideal Sinc ILS (excess spectral ringing) is common in FTS systems**
- **Spectral Ringing can be caused by many factors**
- **Suppression of Sinc ILS sidelobes & other forms of spectral ringing is commonly achieved by applying an external apodization function such as Hamming or Blackman-Harris**

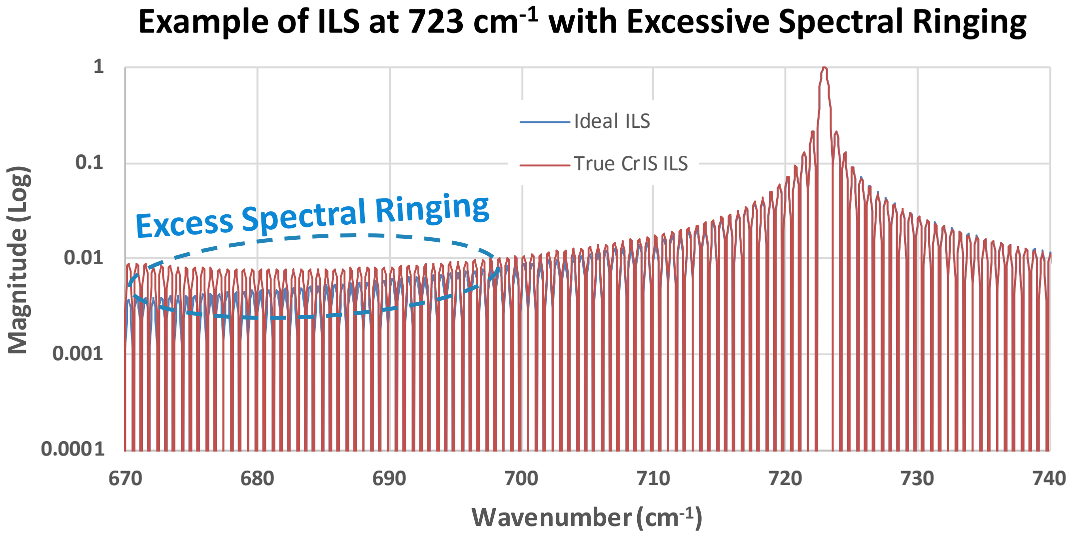

NPP SDR Processing

Radiometric Calibration Precedes Spectral Correction – Hamming Applied in EDR

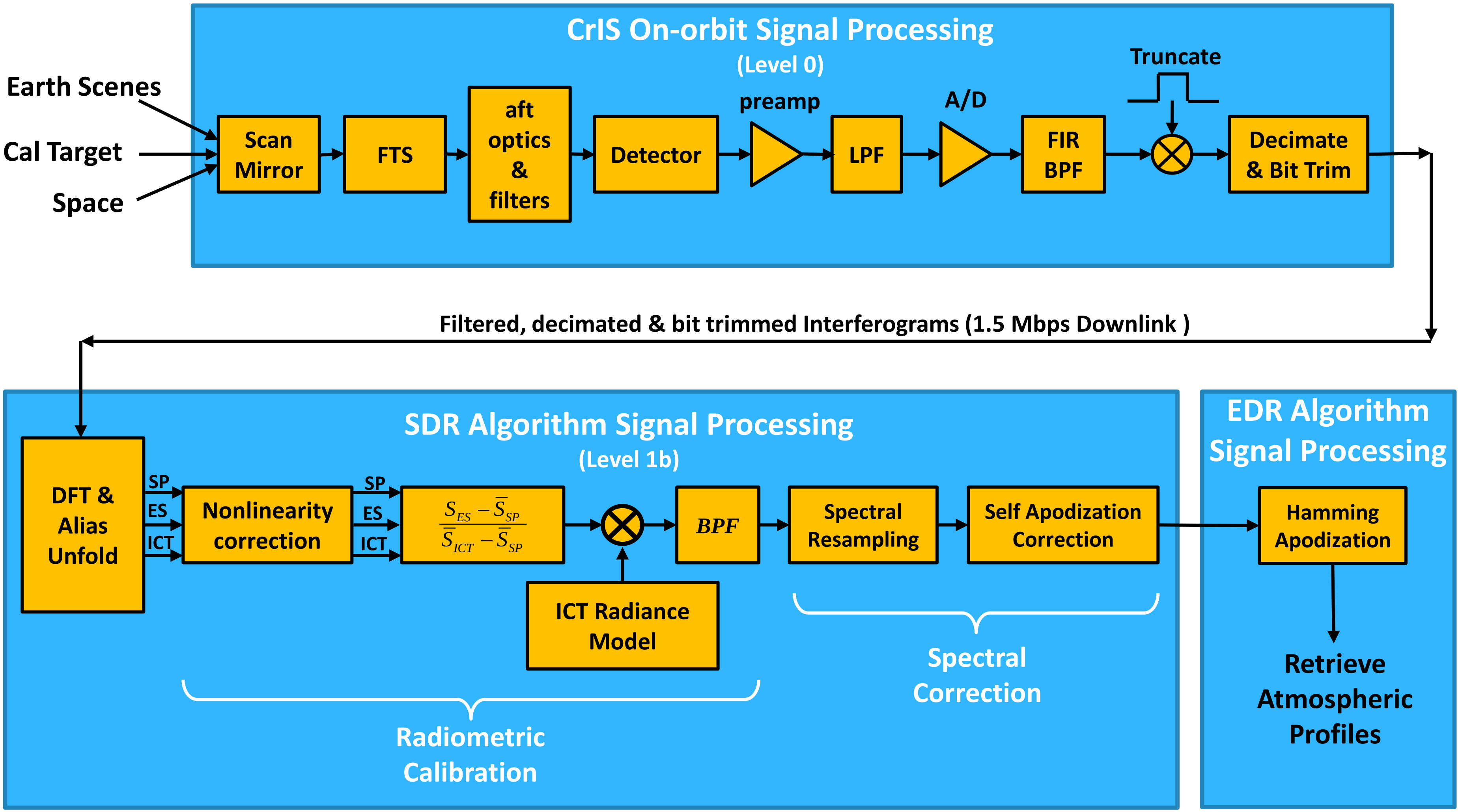

Sidelobe Spectral Ringing Typically Suppressed with Apodization Function

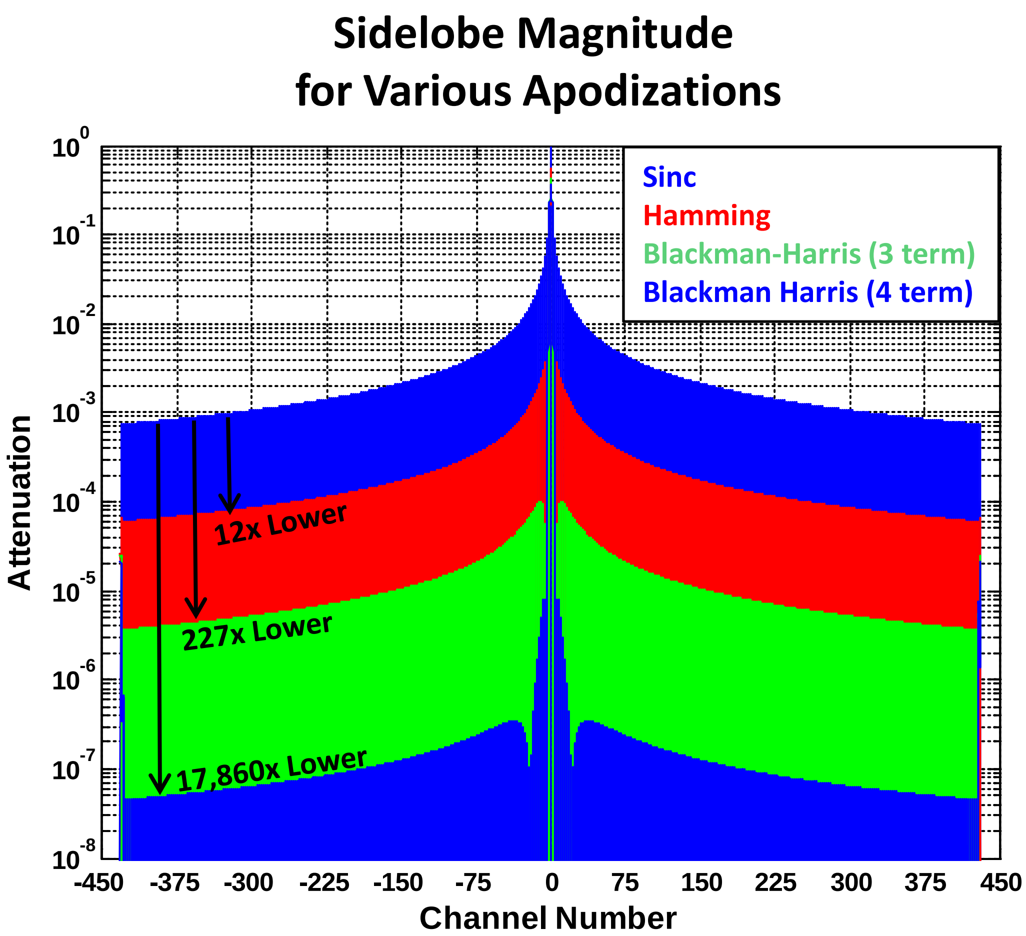

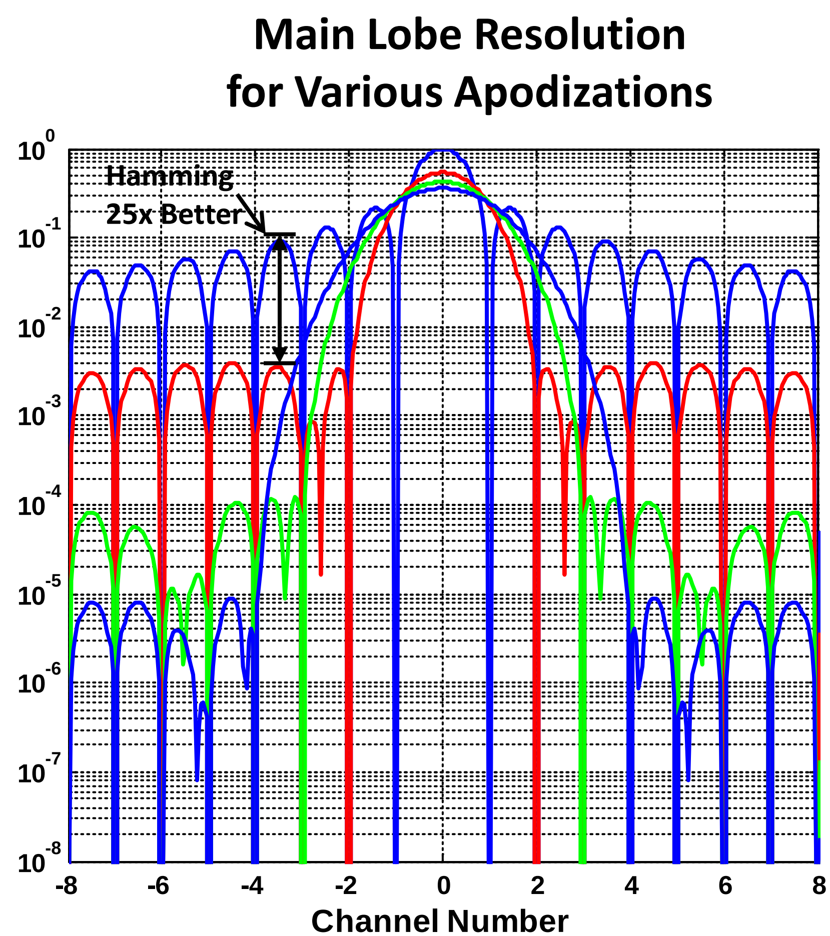

ILS Sidelobe Uncertainty Also Reduced when Using Apodization Functions

Can Current Hamming Apodization Be Eliminated?

CrIS CAL/VAL Team Focus Areas for Reducing Spectral Ringing & Improving ILS Knowledge

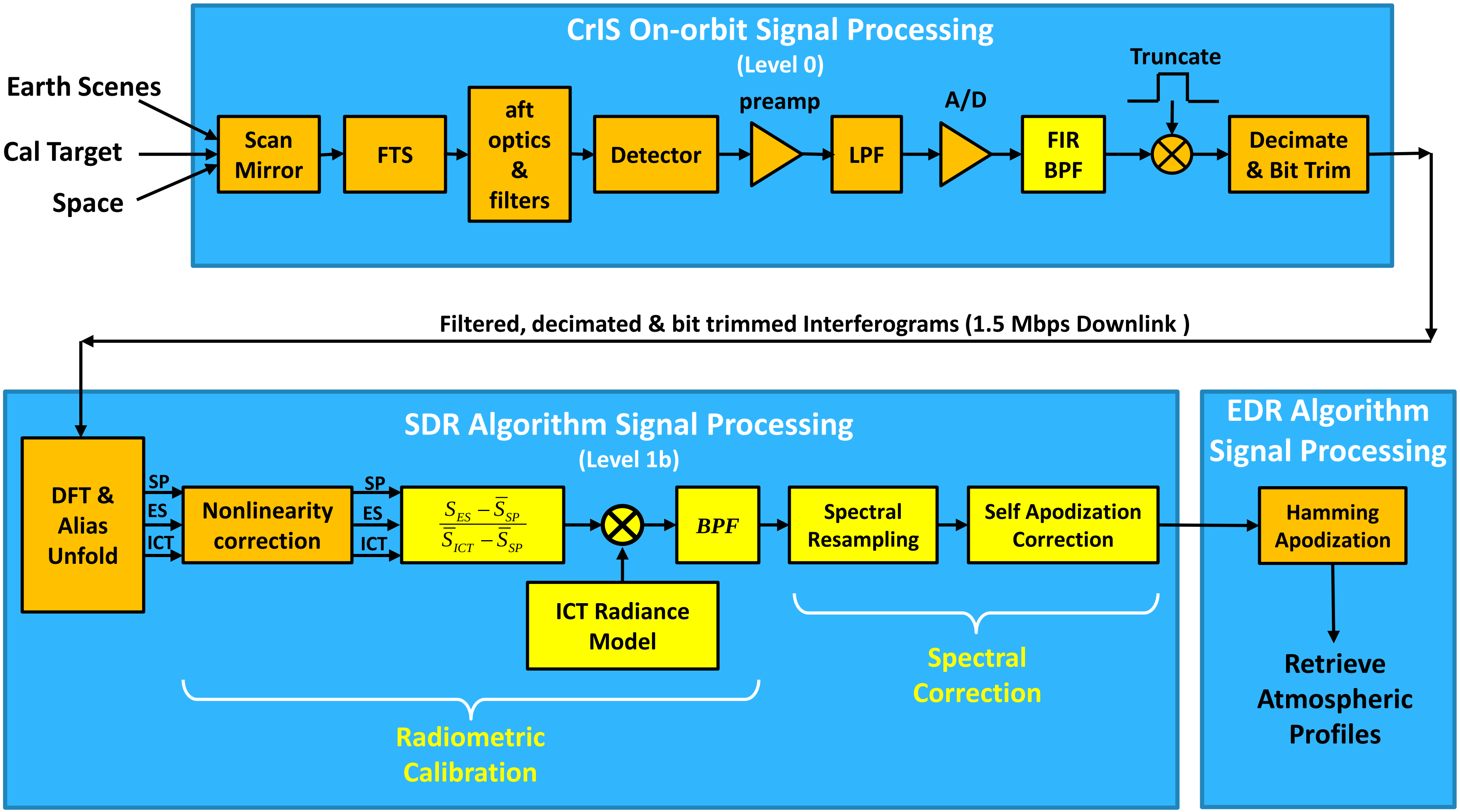

Key CAL/VAL Team Findings

Reordering of NPP CrIS SDR Calibration Operations Will Improve ILS Knowledge for J1 Instrument

- Self Apodization correction should precede Radiometric Calibration
- Self-apodization (SA^{-1}) correction should precede Spectral resampling ($F_{s\text{-}u}$)
- Spectral resampling function must use large number of samples "N_0" in computation
- Processing of extended length interferograms through full calibration and with truncation to shorter MPD as a last step helps
- Truth Spectrum must include the effect of instrument optical responsivity

Other Consequences of Suggested Changes

- Must compensate for CrIS FIR filter (FIR^{-1}) prior to spectral correction
    - In-band amplitude ripple
    - ZPD centering or delay
- Must phase correct spectrum prior to spectral correction

Improved Level 1b Algorithm Performs Spectral Correction on Extended Length Interferogram <u>Prior to</u> Radiometric Calibration

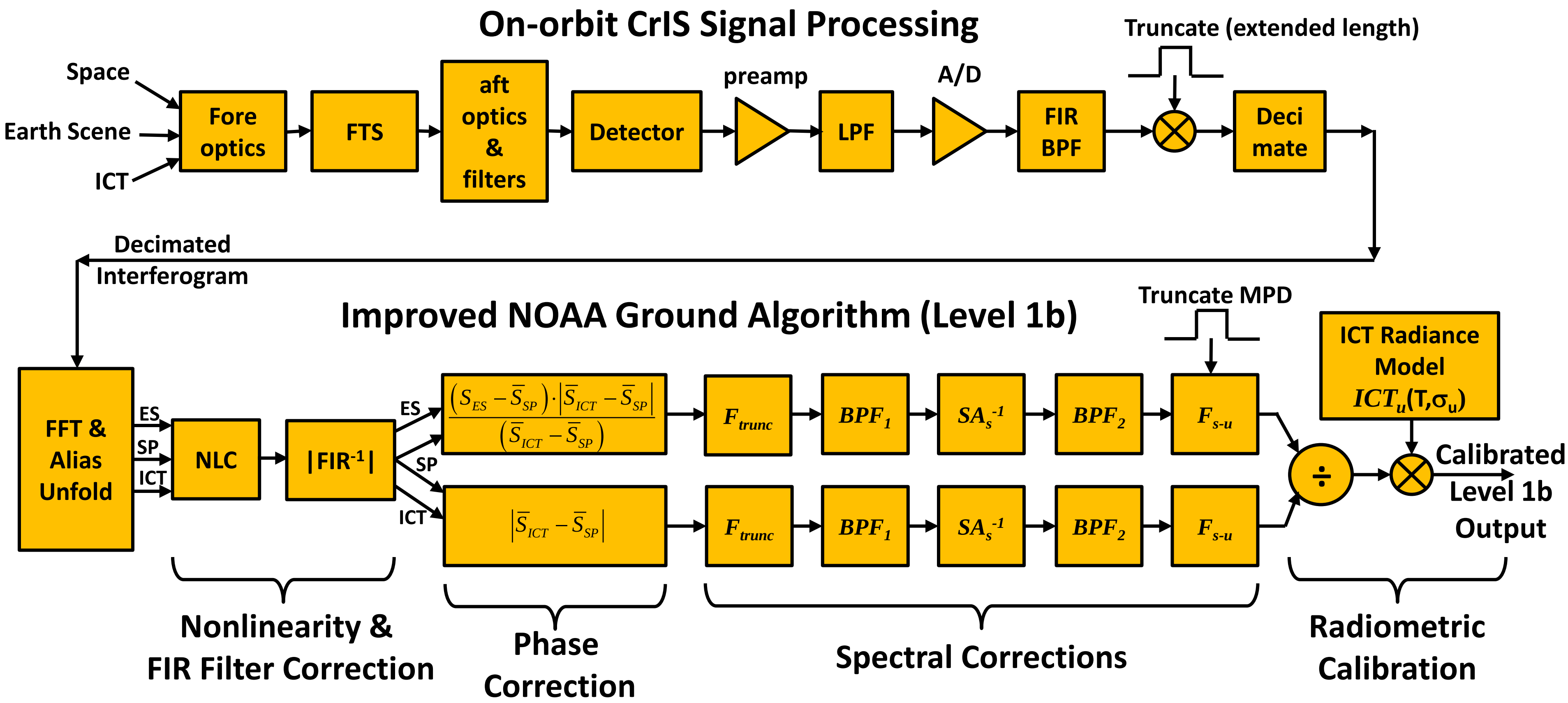

$$L_{ES} = ICT_u \cdot \frac{F_{s\to u} \cdot f_{BPF2} \cdot SA_s^{-1} \cdot f_{BPF1} \cdot F_{trunc} \cdot \left[\frac{\left(S_{ES} - \bar{S}_{SP}\right) \cdot \left|\bar{S}_{ICT} - \bar{S}_{SP}\right|}{\left(\bar{S}_{ICT} - \bar{S}_{SP}\right)} \right]}{F_{s\to u} \cdot f_{BPF2} \cdot SA_s^{-1} \cdot f_{BPF1} \cdot F_{trunc} \cdot \left|\bar{S}_{ICT} - \bar{S}_{SP}\right|}$$

$$S_{ES} = \left|FIR^{-1}\right| \cdot NLC \cdot CRIGHT\left[FFT\left(CRIGHT\left[I_{ES}, \frac{N_{Eb}}{2}\right]\right), N_{unwrap}\right]$$

$$S_{ICT} = \left|FIR^{-1}\right| \cdot NLC \cdot CRIGHT\left[FFT\left(CRIGHT\left[I_{ICT}, \frac{N_{Eb}}{2}\right]\right), N_{unwrap}\right]$$

$$S_{SP} = \left|FIR^{-1}\right| \cdot NLC \cdot CRIGHT\left[FFT\left(CRIGHT\left[I_{SP}, \frac{N_{Eb}}{2}\right]\right), N_{unwrap}\right]$$

LWIR Optical/Electrical Responsivity

Linear Magnitude | Log Magnitude | Phase

Interferometer Sweep Direction 0

Interferometer Sweep Direction 1

Interferometer Sweep Direction Difference

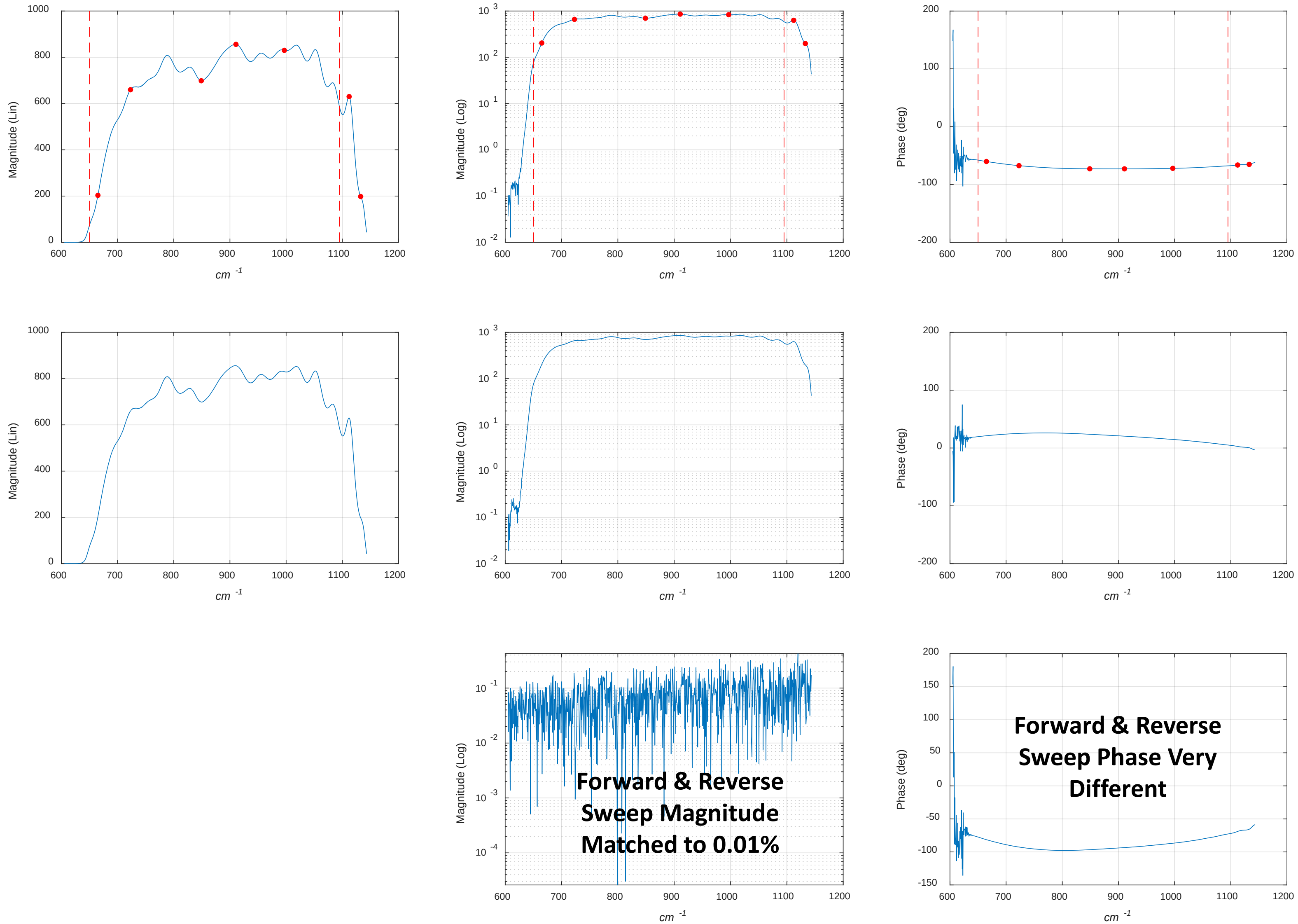

MWIR Optical/Electrical Responsivity

Linear Magnitude | Log Magnitude | Phase

Interferometer Sweep Direction 0

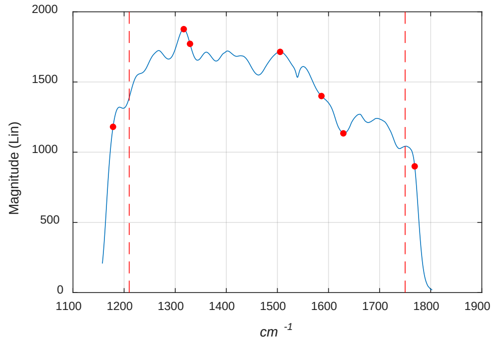

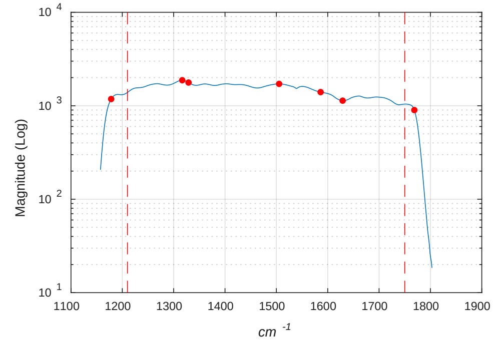

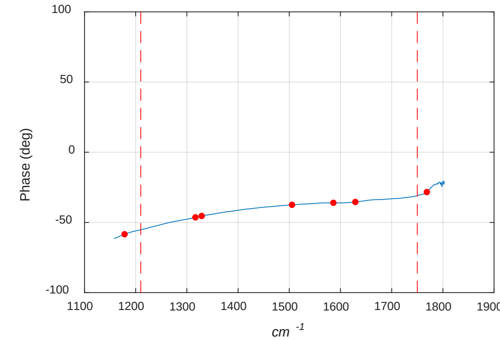

Interferometer Sweep Direction 1

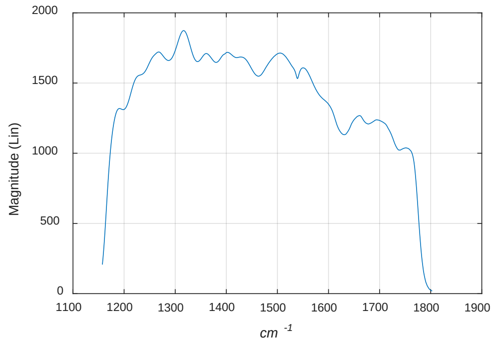

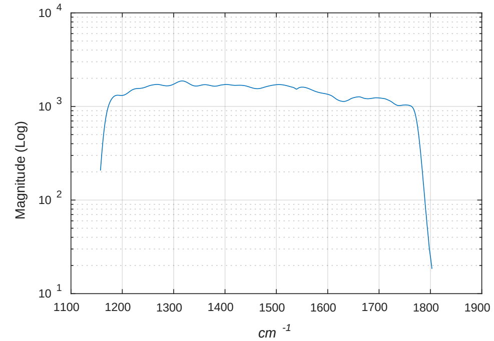

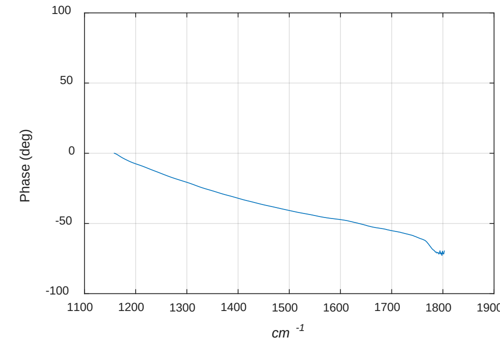

Interferometer Sweep Direction Difference

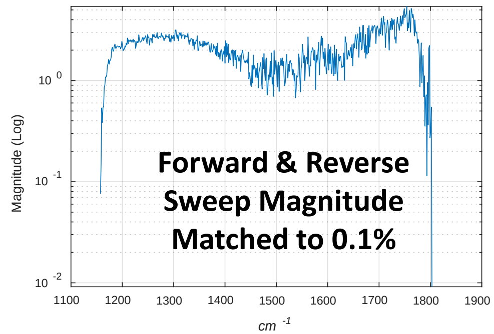

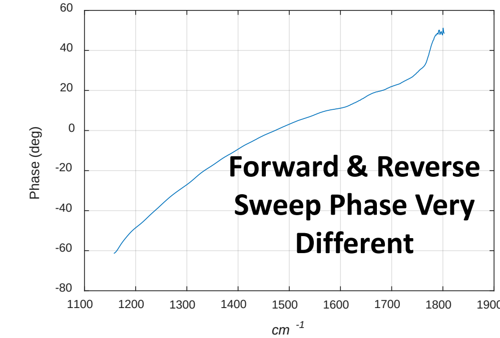

SWIR Optical/Electrical Responsivity

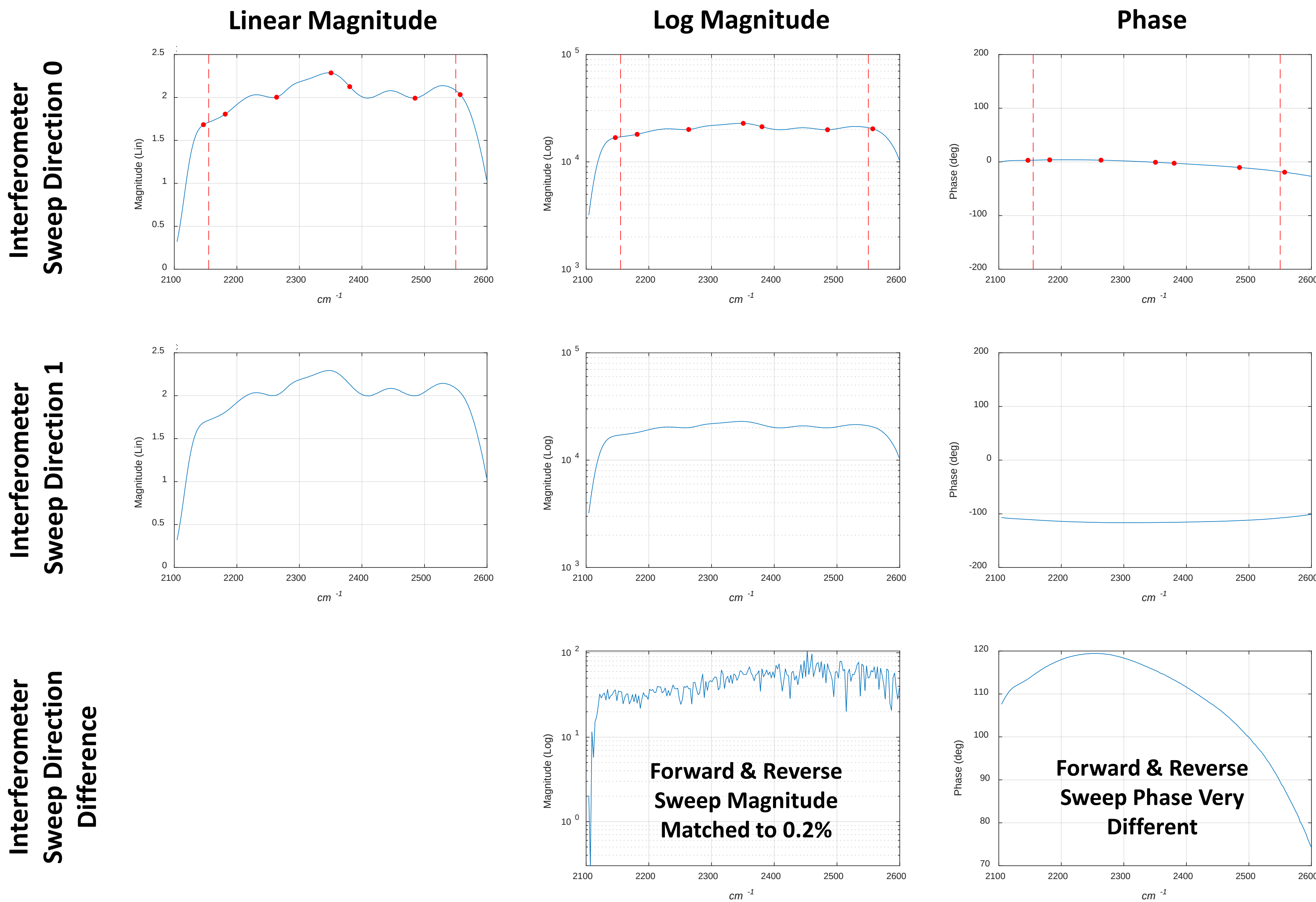

True CrIS Instrument ILS Depends Upon Optical/Electrical Responsivity Properties

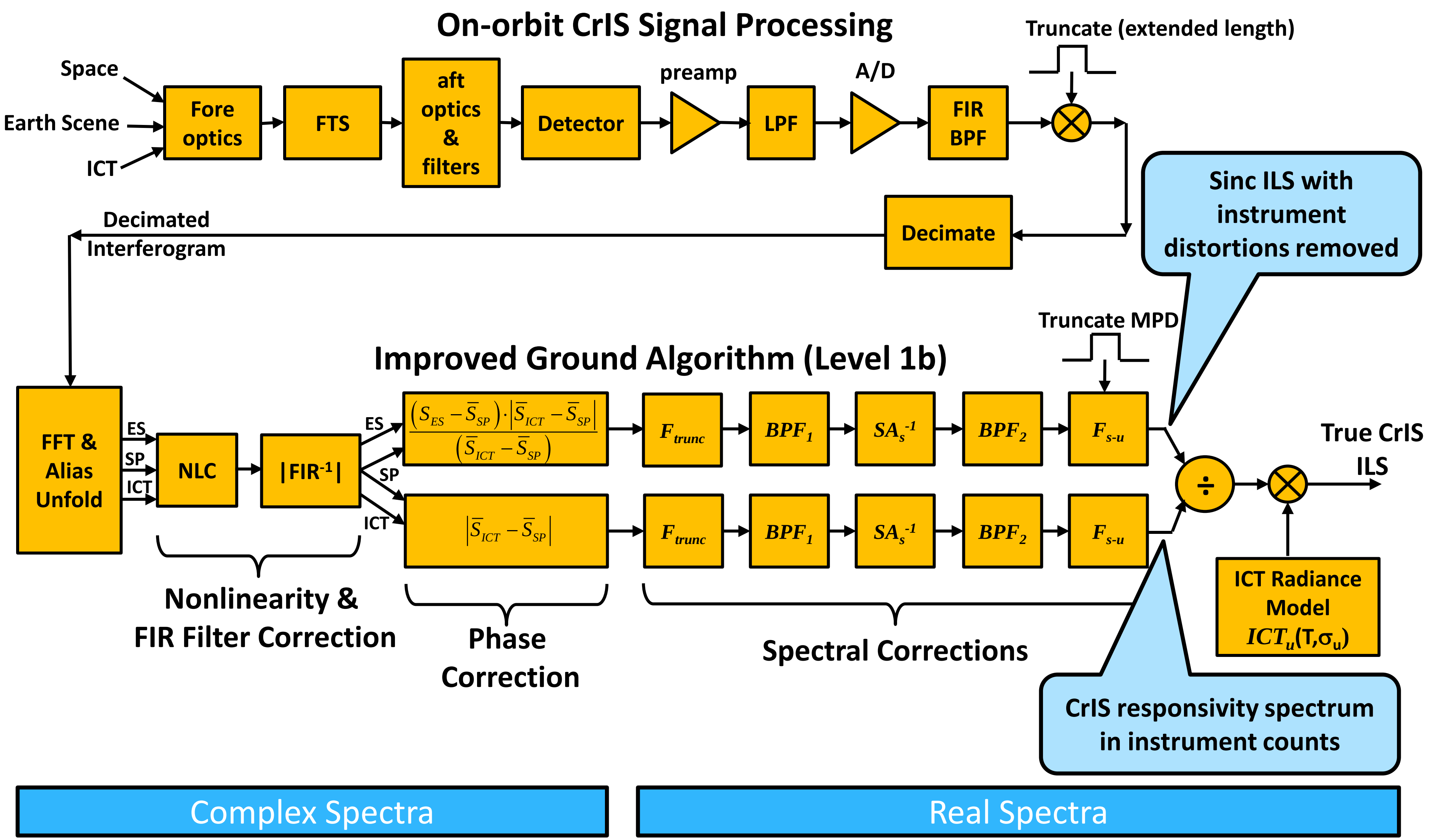

CrIS Optical/Electrical Responsivity Will Impact the Post Calibrated Instrument Line Shape (ILS)

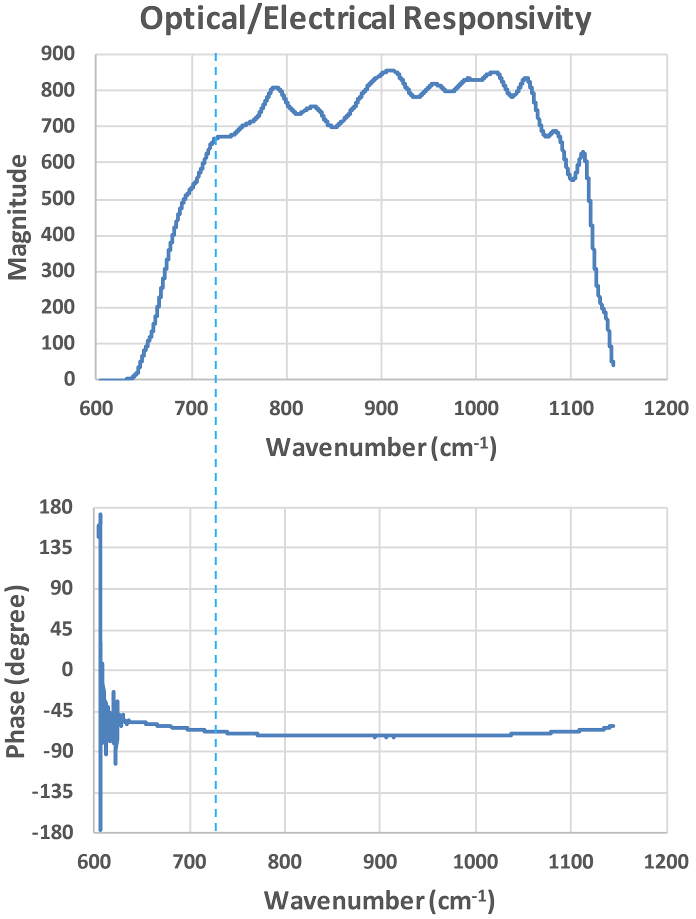

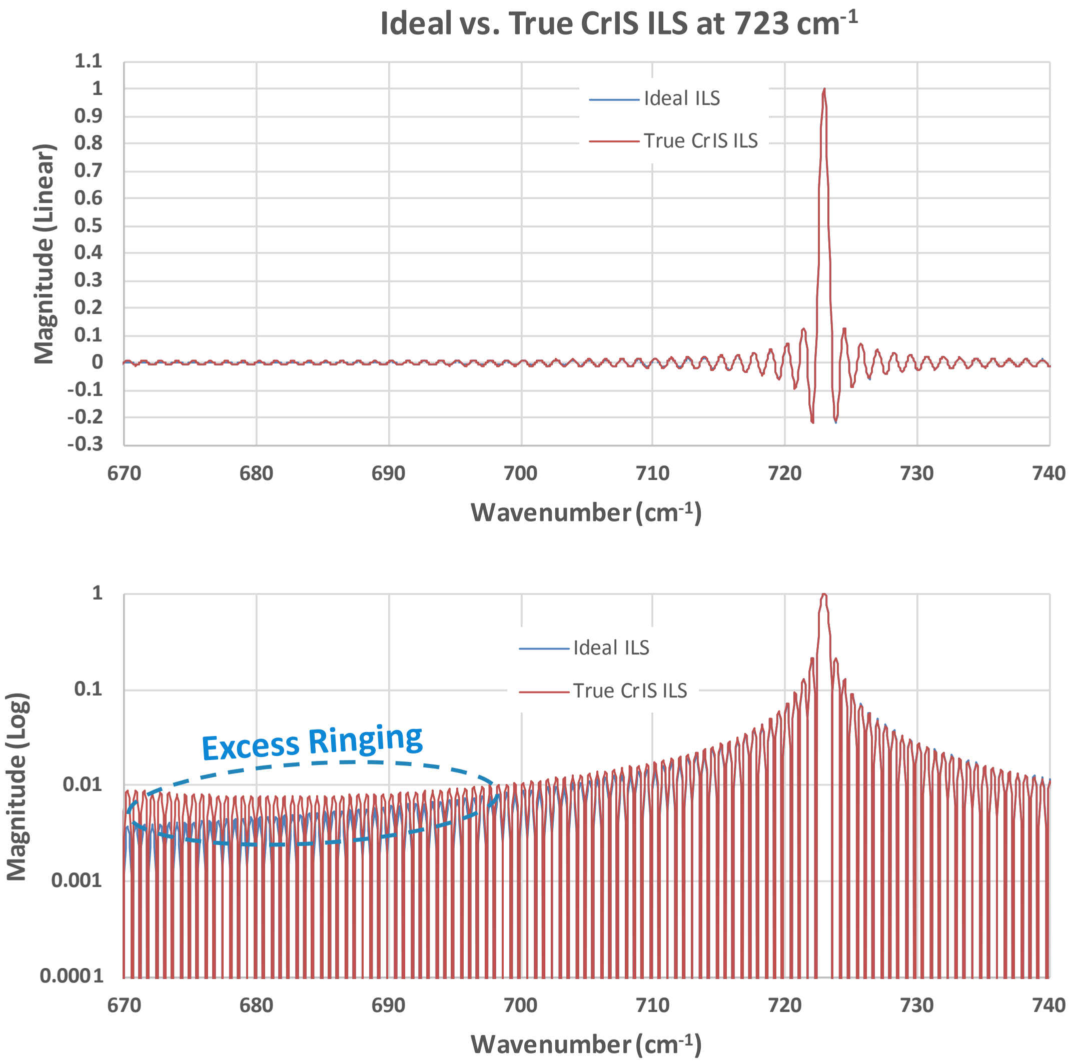

Broadband ILS Comparison at 723 cm^{-1}
(Complex ILS if Phase Correction Not Performed)

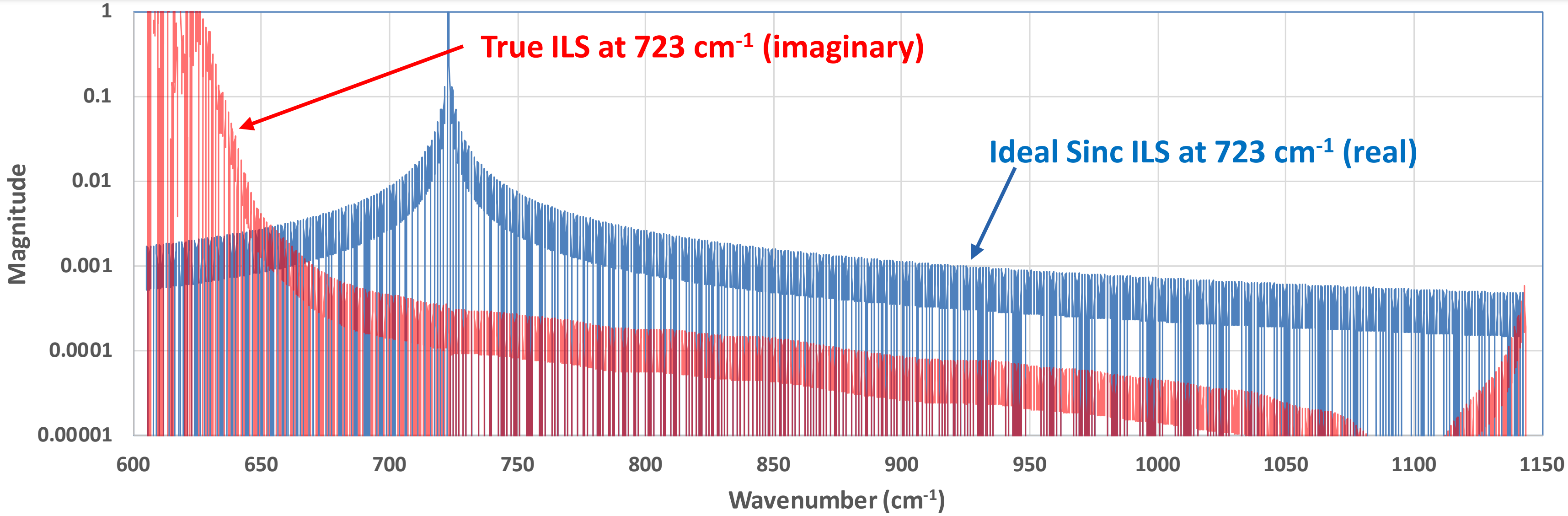

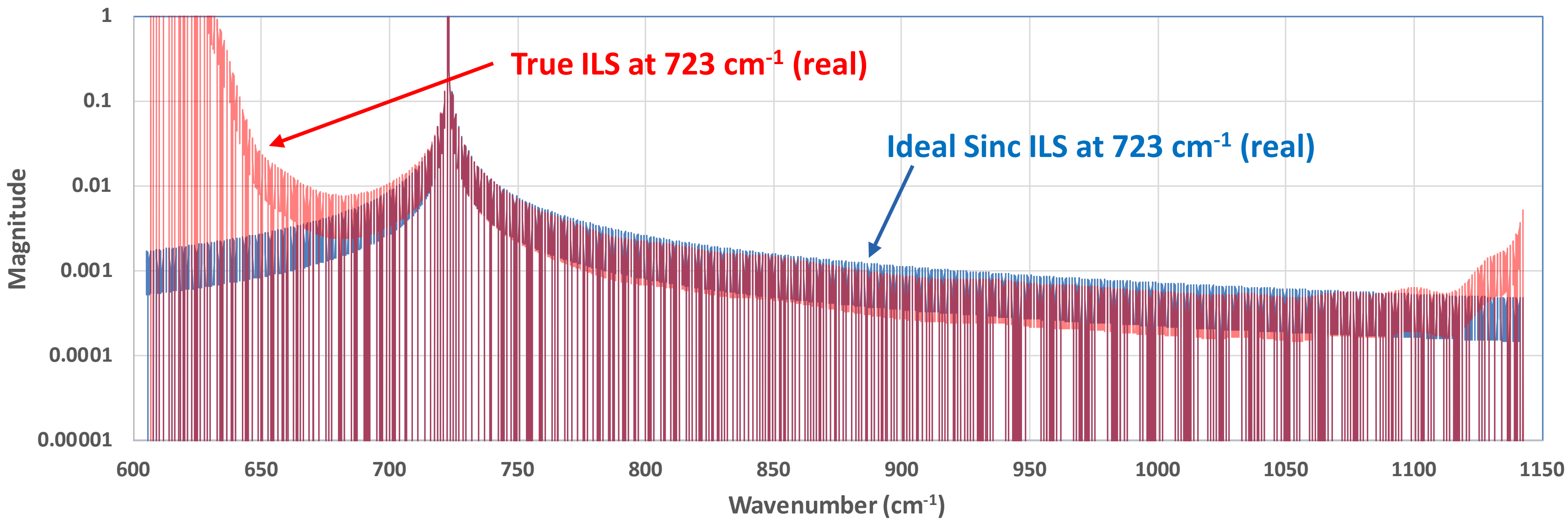

True CrIS ILS Sidelobe Error Relative 30 mK Brightness Error
(Phase corrected – 7 Channel Centers – Unapodized & Hamming Cases)

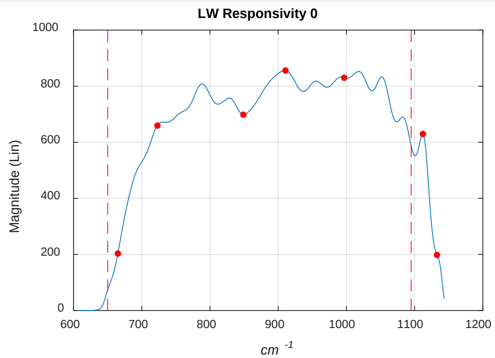

LWIR Band

Unapodized

Hammming

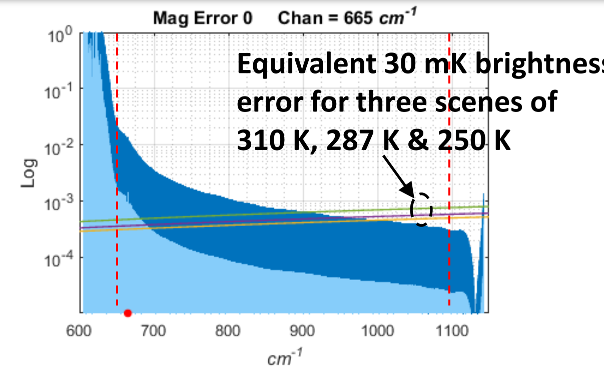

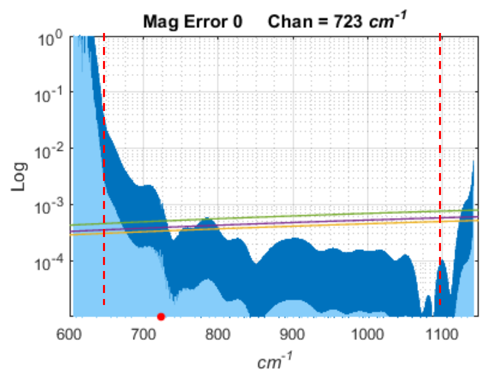

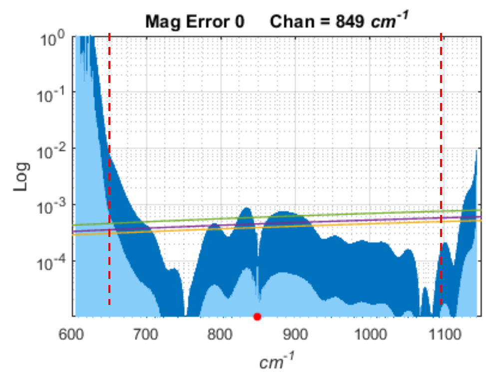

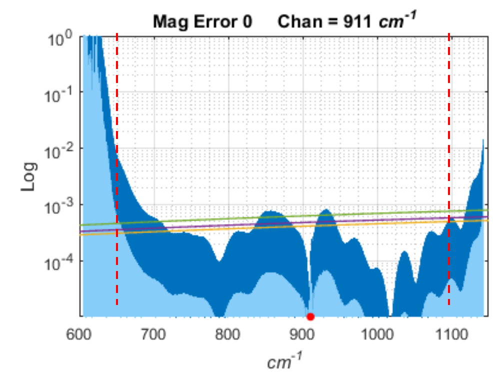

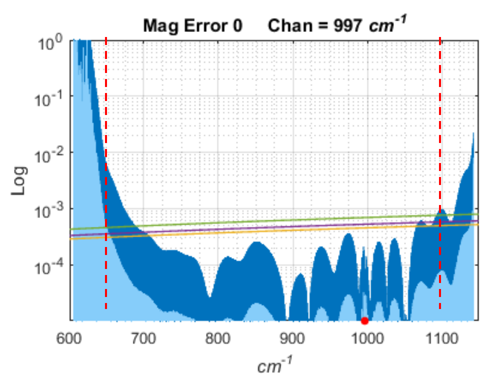

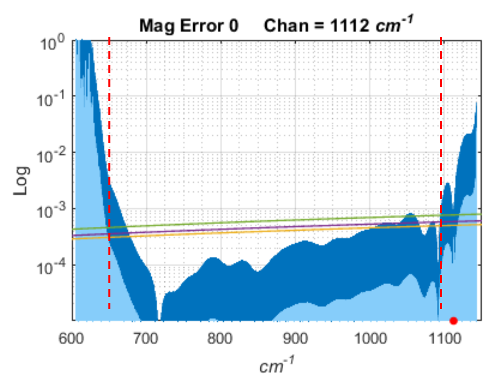

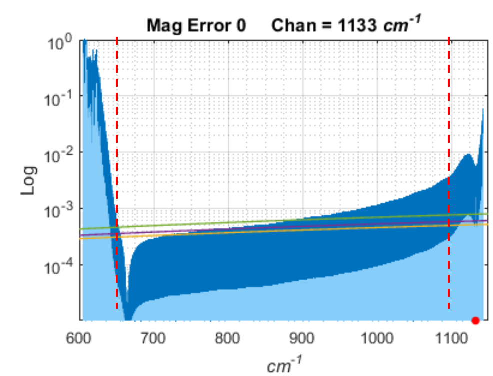

True CrIS ILS Sidelobe Error Relative 30 mK Brightness Error

(Phase corrected – 7 Channel Centers – Unapodized & Hamming Cases)

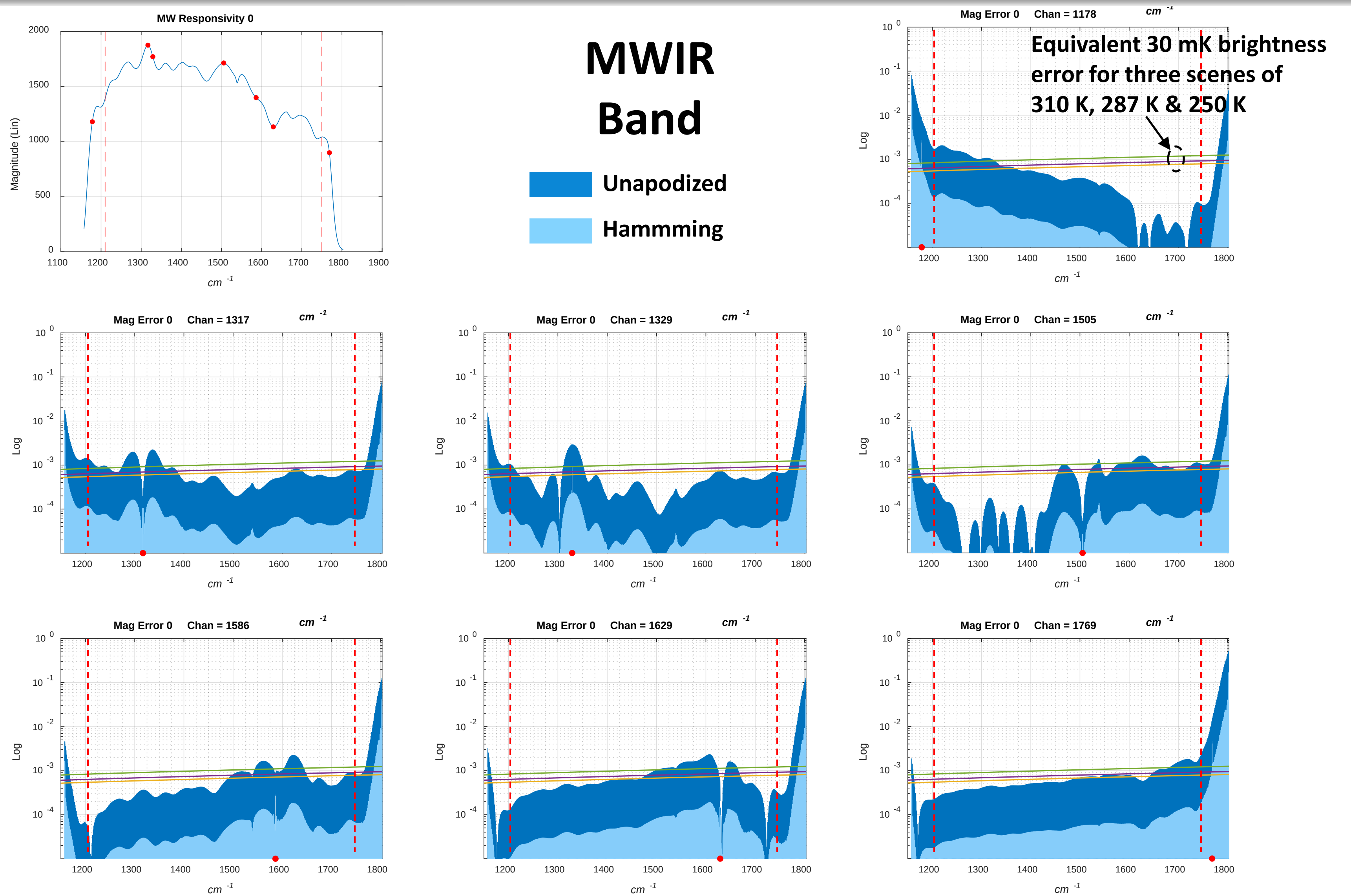

True CrIS ILS Sidelobe Error Relative 30 mK Brightness Error

(Phase corrected – 7 Channel Centers – Unapodized & Hamming Cases)

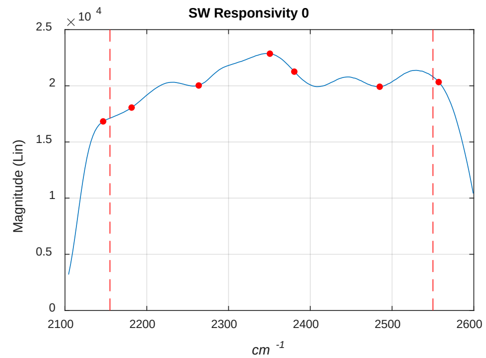

SWIR Band

Unapodized

Hammming

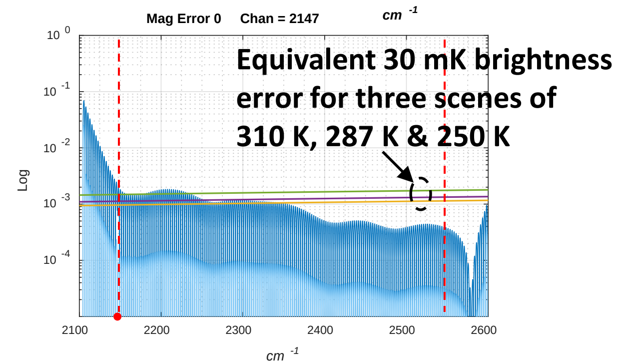

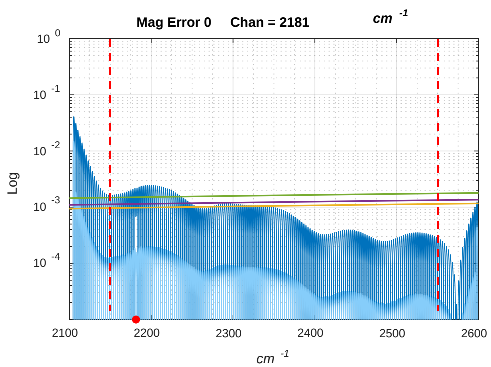

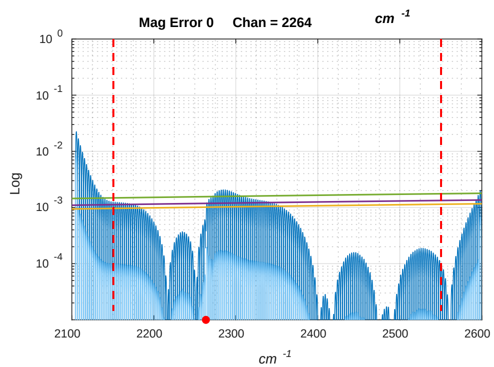

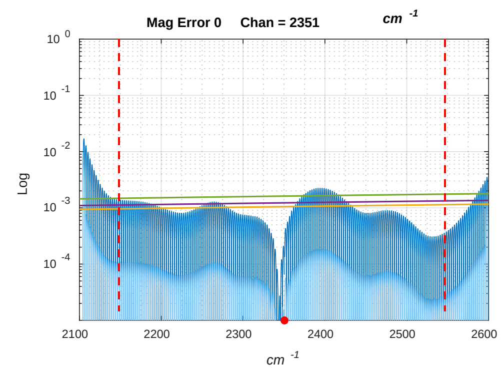

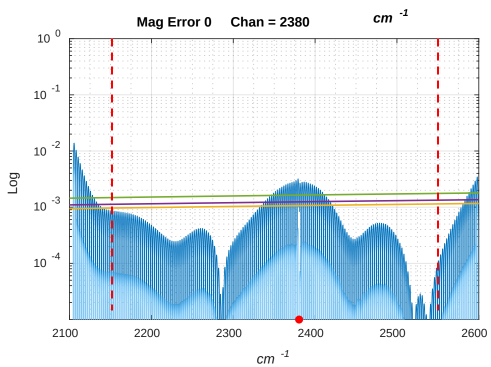

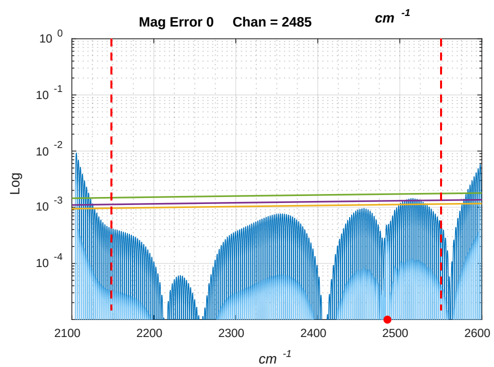

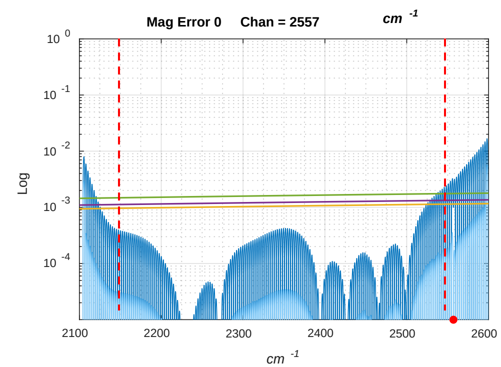

Conclusions

- **Phase correction prior to spectral correction makes the CrIS ILS sweep direction independent**
- **Fully calibrated CrIS SDR has ILS sidelobe response that even under best conditions deviates from an ideal Sinc ILS ("True ringing")**
- **Hamming apodization brings the "True Ringing" error below an equivalent 30 mK brightness temperature ILS sidelobe error for all earth scene temperatures 250 K – 310 K in the MWIR & SWIR bands & over all LWIR wavenumbers (except 650 – 680 cm^{-1})**
- **True ringing can be compensated at SDR output & in forward EDR model by multiplying spectrum by the CrIS responsivity magnitude**
  - **If this is done, Hamming apodization is not needed to meet a 30 mK brightness temperature knowledge error threshold for ILS sidelobes**

Combination of VIIRS with CrIS toward Extending Data Utilization

Likun Wang,

Yong Chen, Denis Tremblay, Yong Han

- ESSIC/Univ. of Maryland, College Park, MD; wlikun@umd.edu

Acknowledgment CrIS SDR Team

Motivation

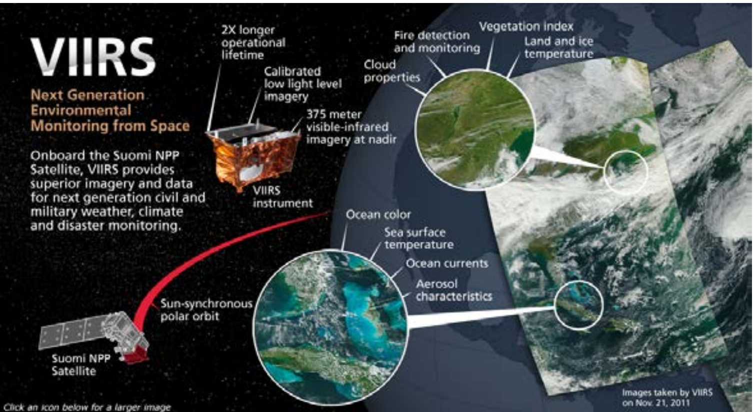

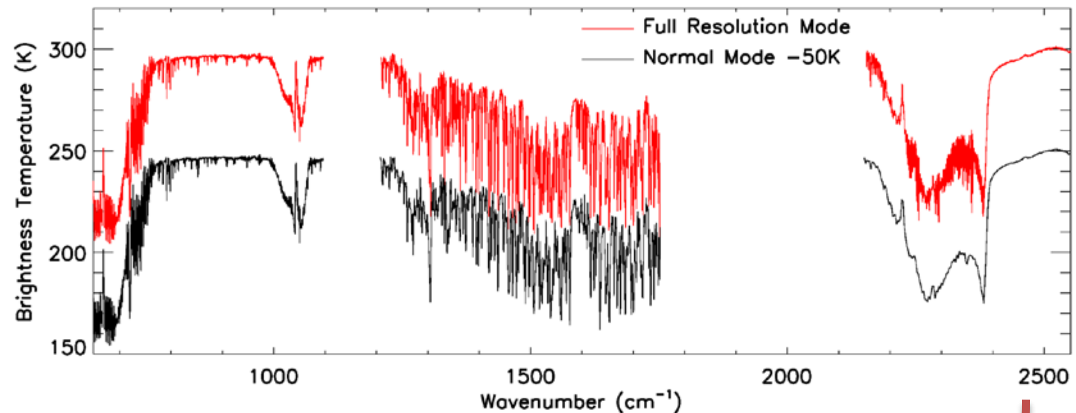

land surface
cloud properties

Combination of CrIS Spectra and VIIRS Products

NWP Data assimilations
Geophysical parameter retrievals

Purpose: Providing sub-pixel information for CrIS observations using collocated high-spatial resolution VIIRS radiances or products

Outline

- CrIS and VIIRS are two independent instruments, though on the same platform
  - Not like IASI and AVHRR on MetOp
  - No alignment requirements
  - Separate geolocation fields
- Fast and accurate collocation algorithm suitable for operational use
- Are CrIS and VIIRS perfect align together?
  - If not, collocated products can introduce errors and uncertainties, making applications even worse.
- Applications
  - Cloud detection
  - Effects of FOV size on the number of clear sky pixels
  - Cluster analysis (on-going)

VIIRS vs. CrIS: Spatially

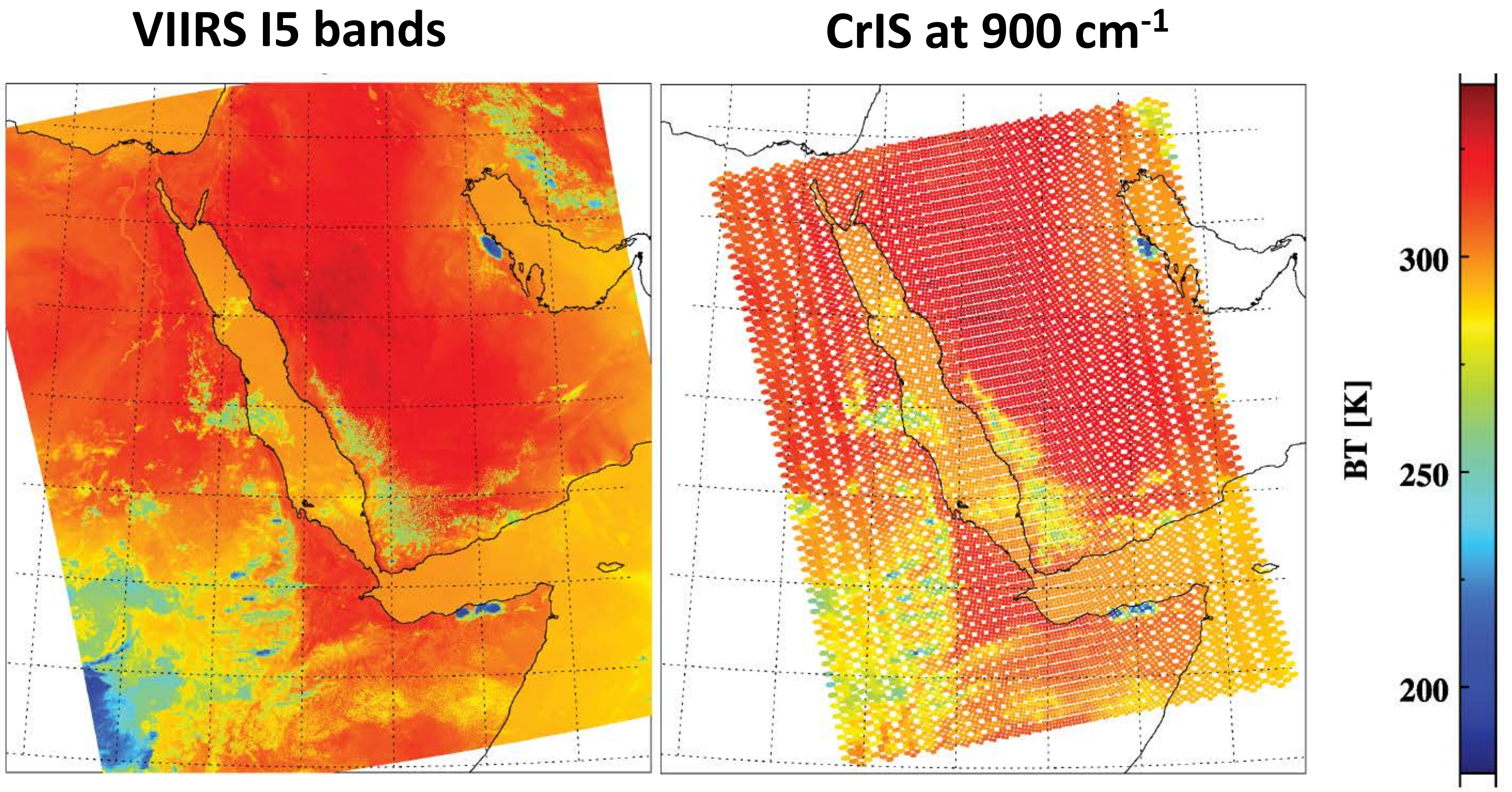

Resolution:	**375m (I) or 750m (M)**	**14.0km nadir**
Scan Angle:	**58.3°**	**48.3 °**
Sampling:	**Continuous**	**Sub-sample**

Collocation of CrIS with VIIRS

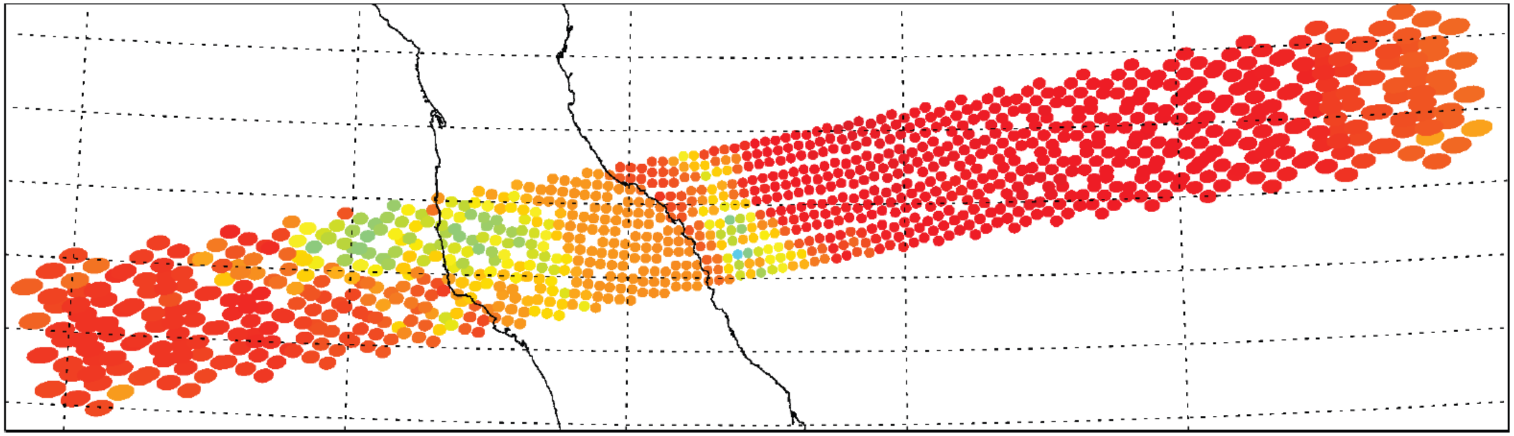

CrIS Footprints

Collocation of the measurements from two satellite sensors (either on the same satellite platform or not) involves pairing measurements from two sensors that observe the same location on the Earth but with different spatial resolutions.

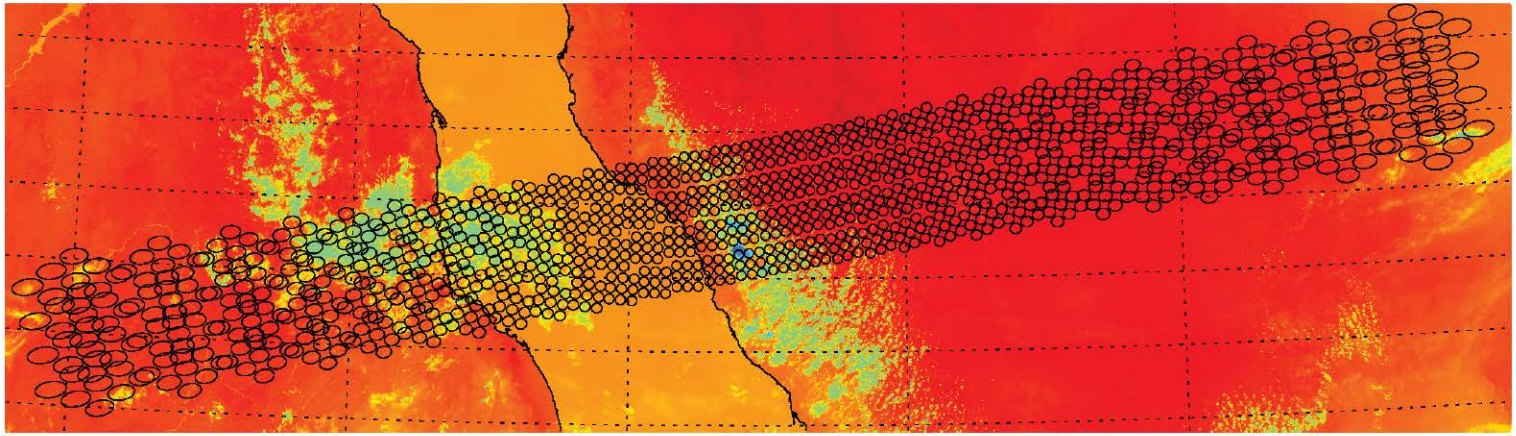

CrIS Footprints overlapped with VIIRS image

It is challenging to do it on the Earth Surface using latitude and longitude.
1) Footprint rotation and distortion off nadir; 2) Searching! Searching! Searching!

Collocation of CrIS with VIIRS Using line-of-sight vector

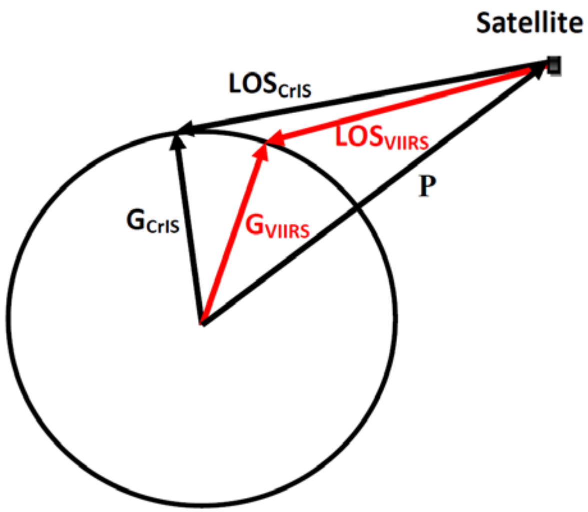

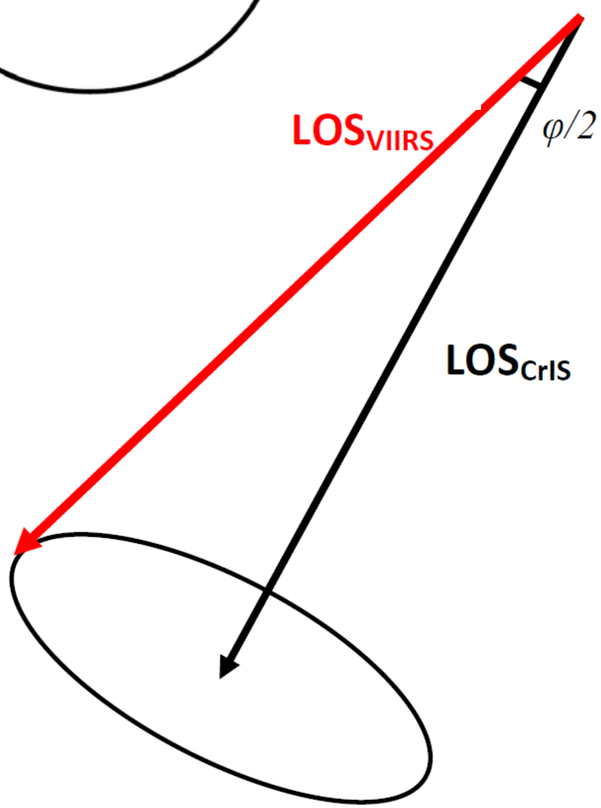

- It is better to collocate CrIS and VIIRS in space instead of on the Earth Surface
- If we can retrieve line-of-sight vector of CrIS and VIIRS
- The collocation of VIIRS and CrIS can be simplified as examining the angles between two vectors.
  - No worry about FOV distortion

Misalignment between CrIS and VIIRS at the end of scan

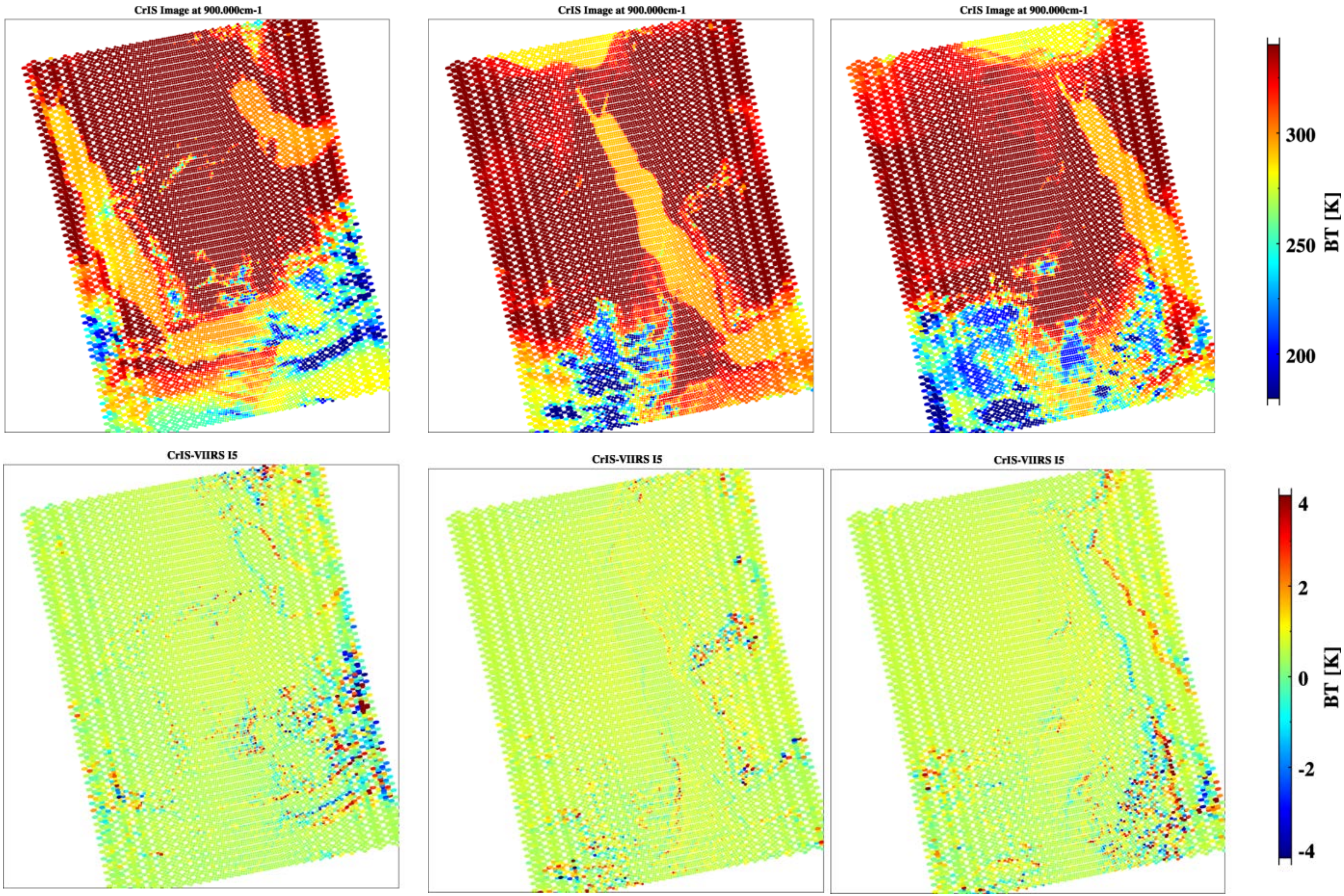

VIIRS Geolocation Very Accurate ! (I5 band: 375m resolution)

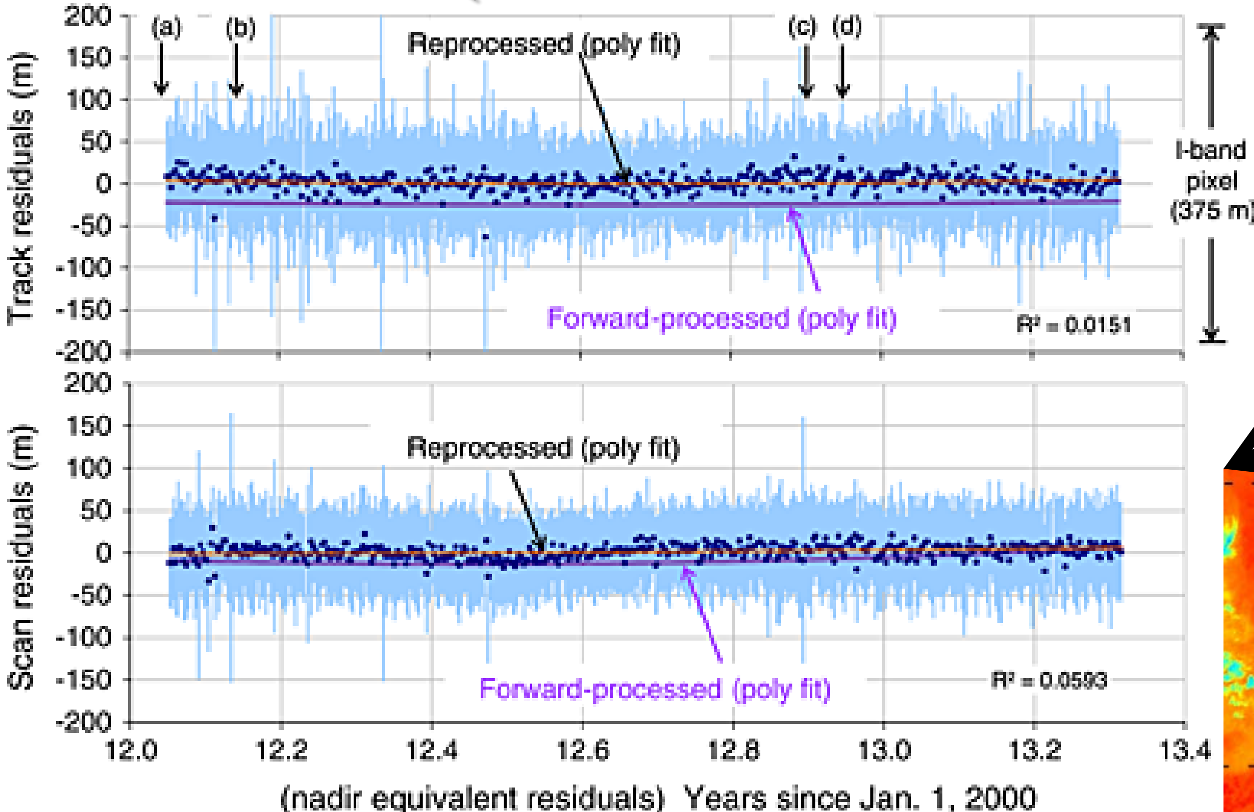

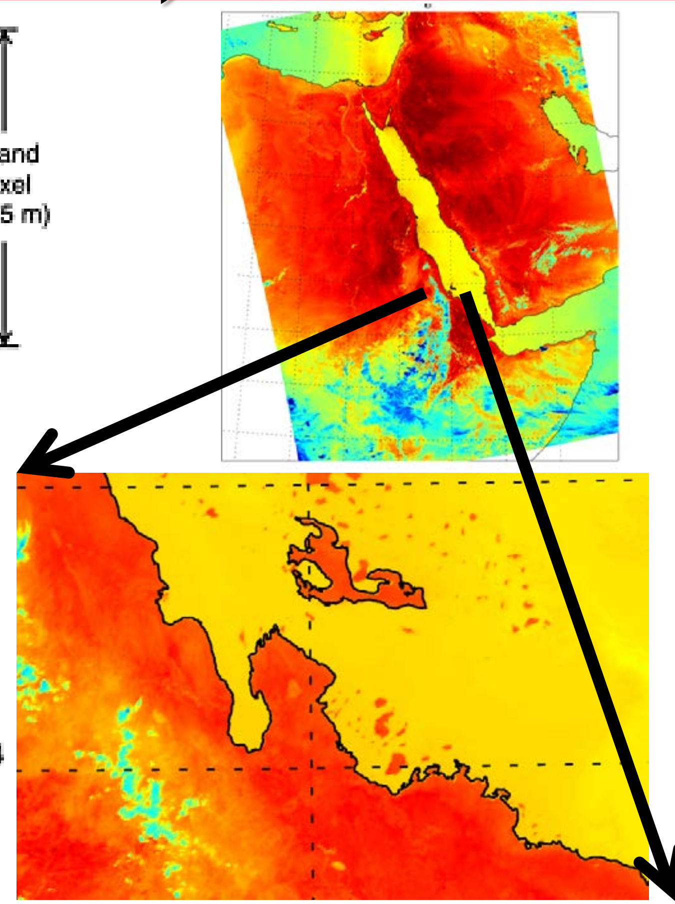

from Wolf et al. 2013

Table 2. VIIRS Geolocation Accuracy

Residuals	First Update 23 February 2012	Second Update 18 April 2013
Track mean	−24 m, −7%	2 m, 1%
Scan mean	−8 m, −2%	2 m, 1%
Track RMSE	75 m, 20%	70 m, 19%
Scan RMSE	62 m, 17%	60 m, 16%

CrIS Geolocation Assessment Using VIIRS as a reference

- The misalignment between CrIS and VIIRS can be caused by the CrIS geolocation error.
- Can we use VIIRS as a reference to check CrIS geolocation accuracy?
- The purpose is to identify the error characteristics of CrIS LOS pointing vector by comparing them with the truth.
- Furthermore, if the systematic errors are found, a new set of co-alignment parameters should be retrieved based on assessment results to improve the geolocation accuracy.

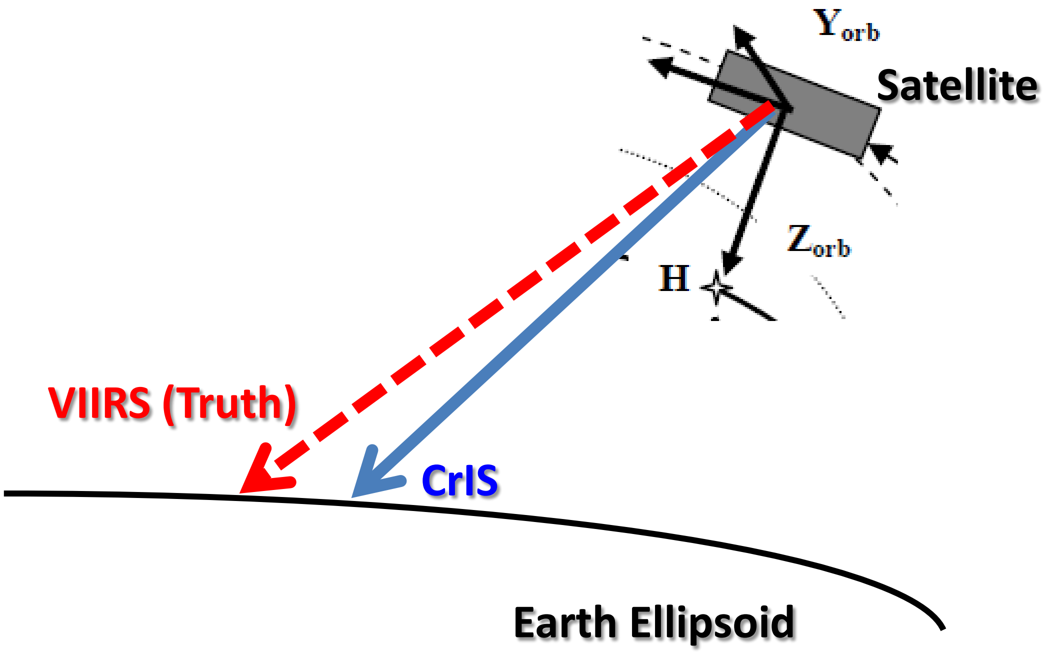

Overview of NPP/JPSS Geolocation Algorithms

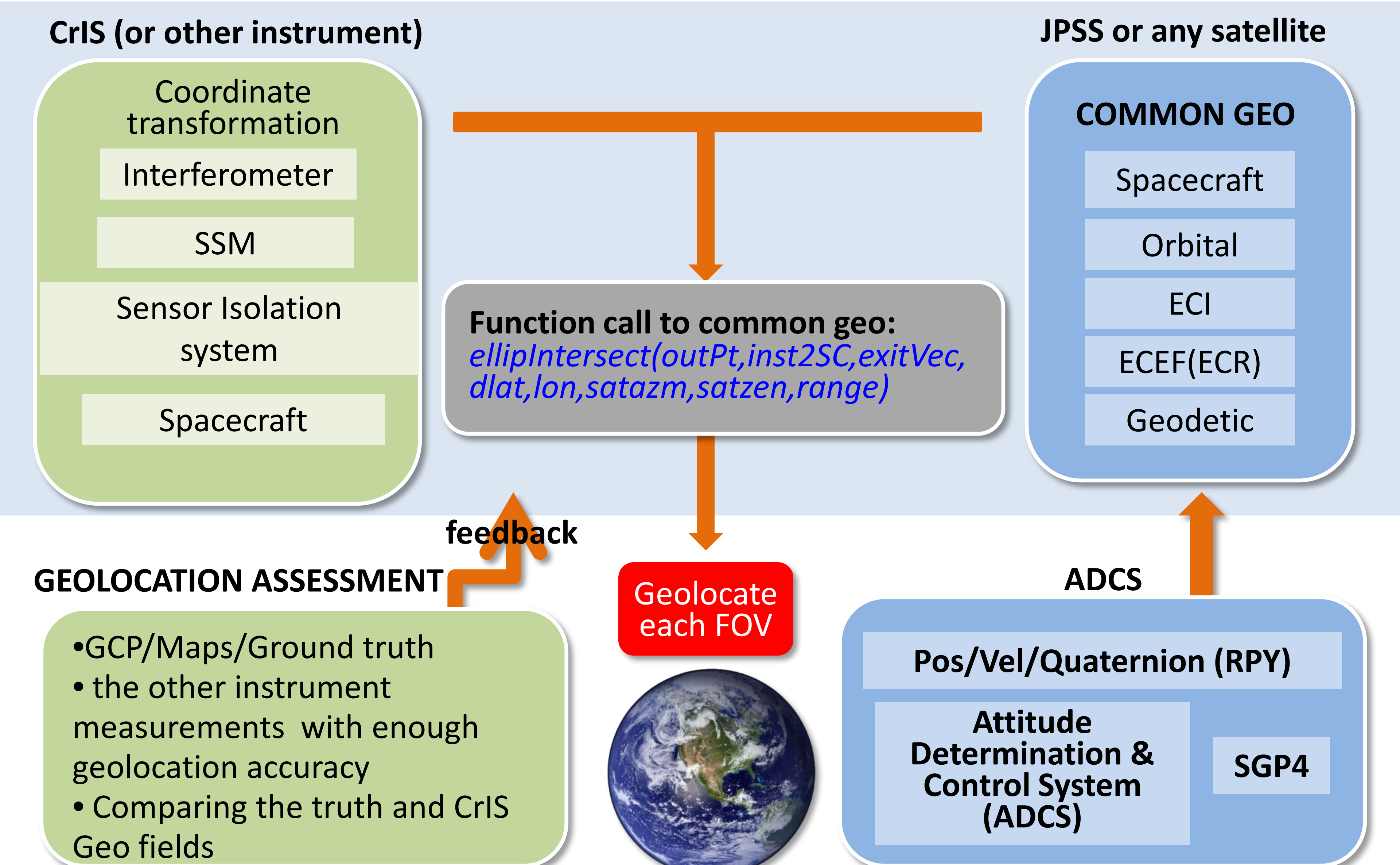

Modified from C. Cao

Inverse Geolocation Computation

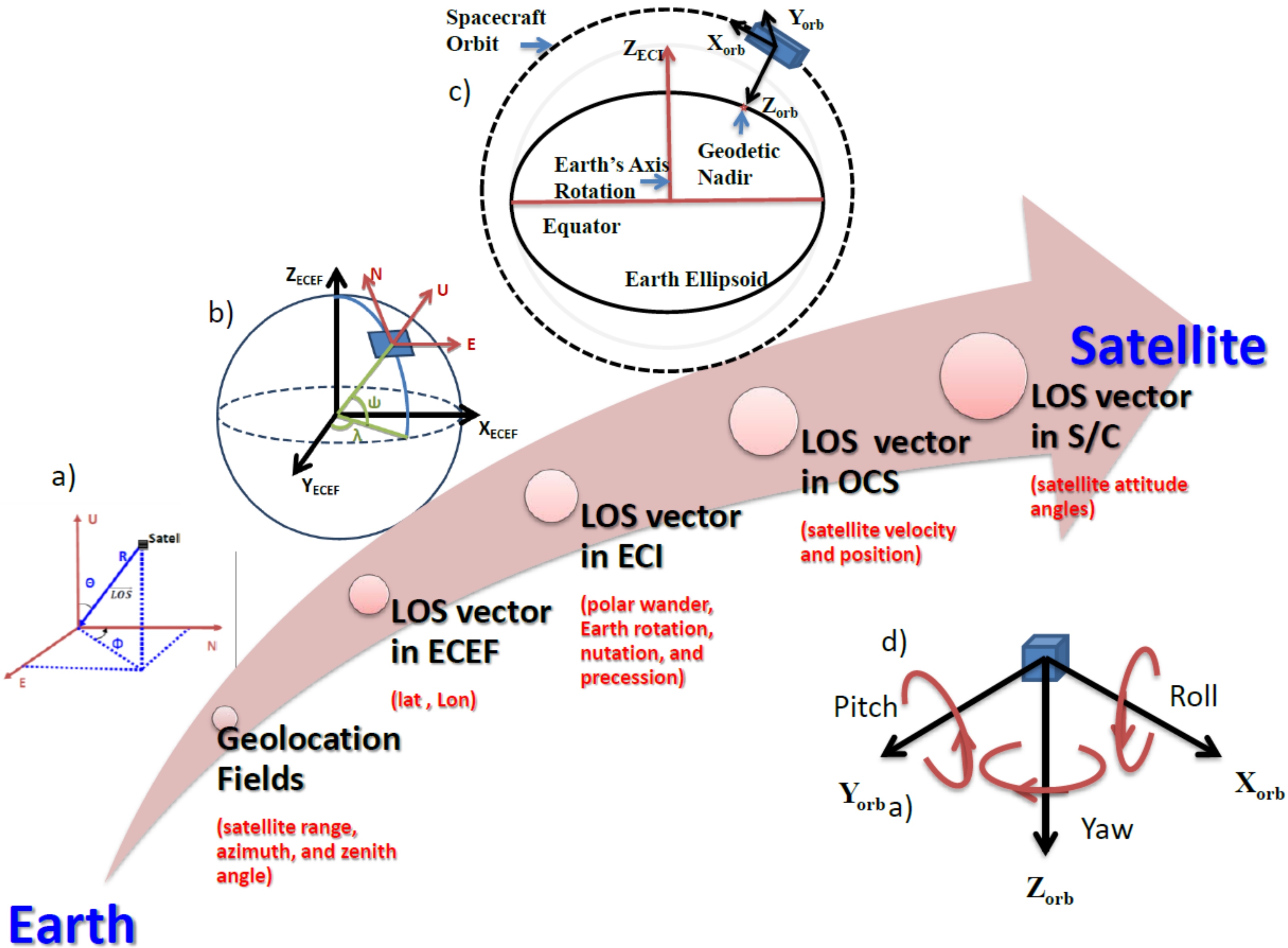

Defining α and β angles of CrIS LOS vector in Spacecraft Coordinate

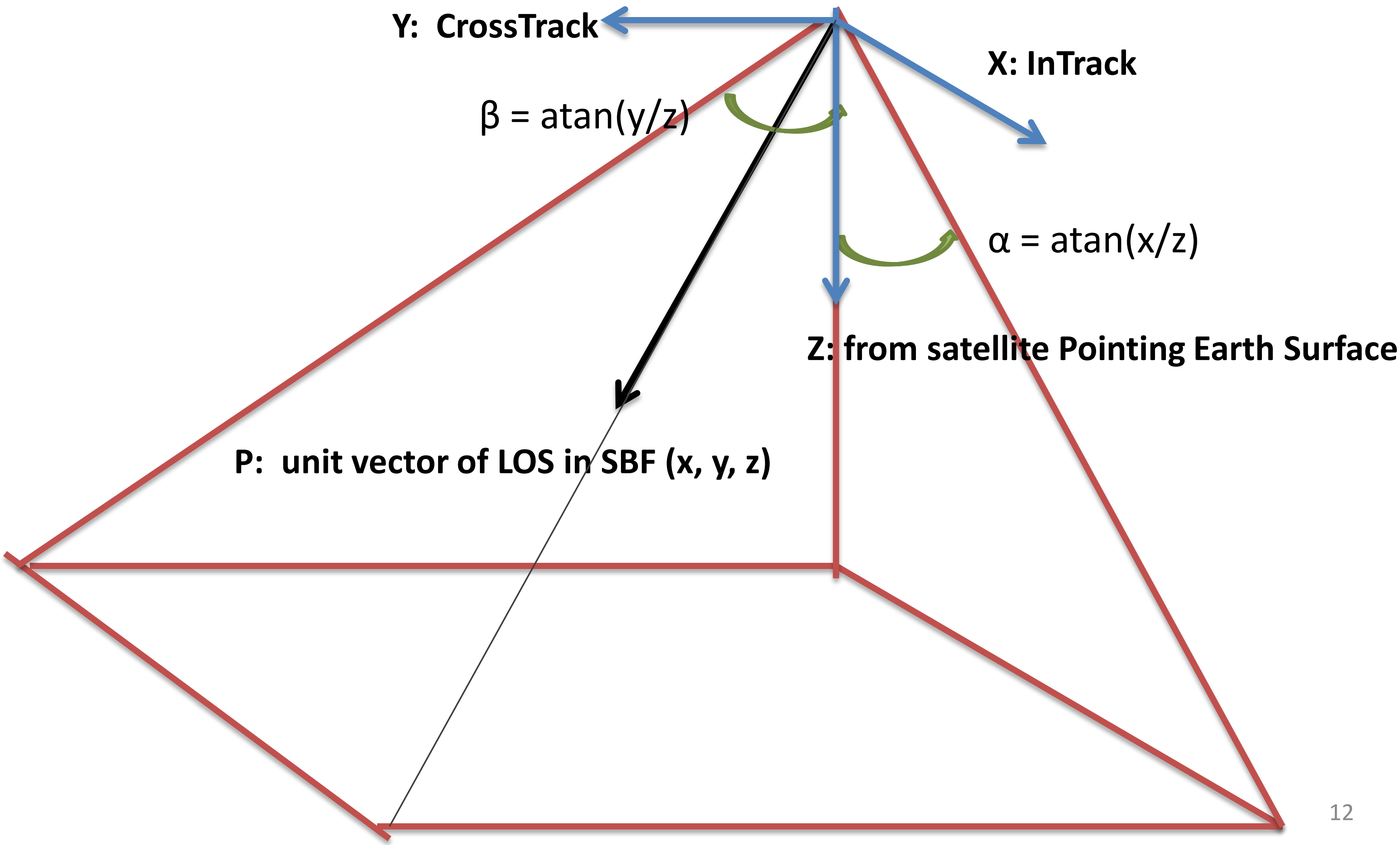

α and β Angles varying with Scan Position (FOV5)

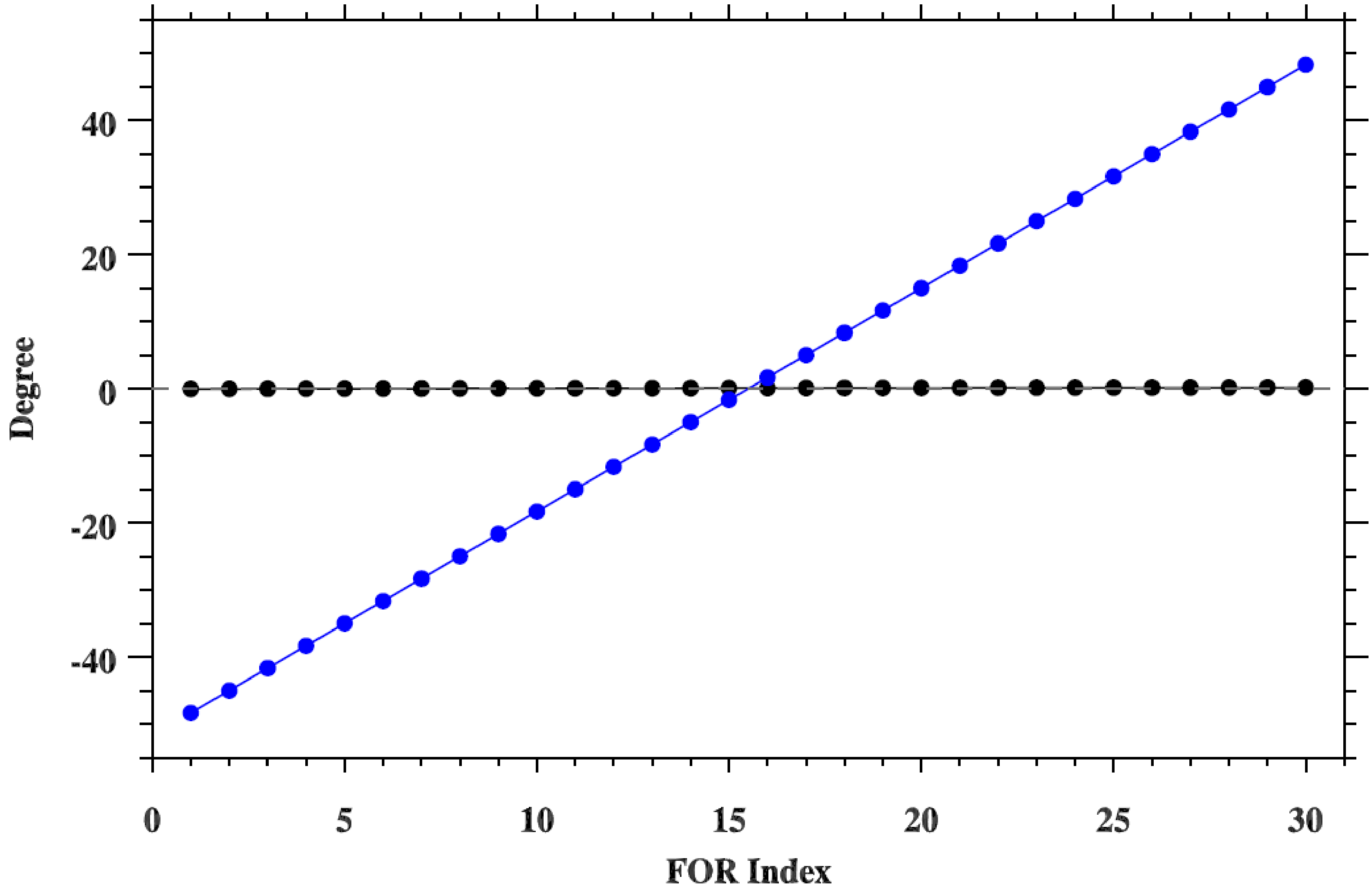

α and β angles are step-by-step perturbed by 21 steps with a angle of 375/833/1000.0

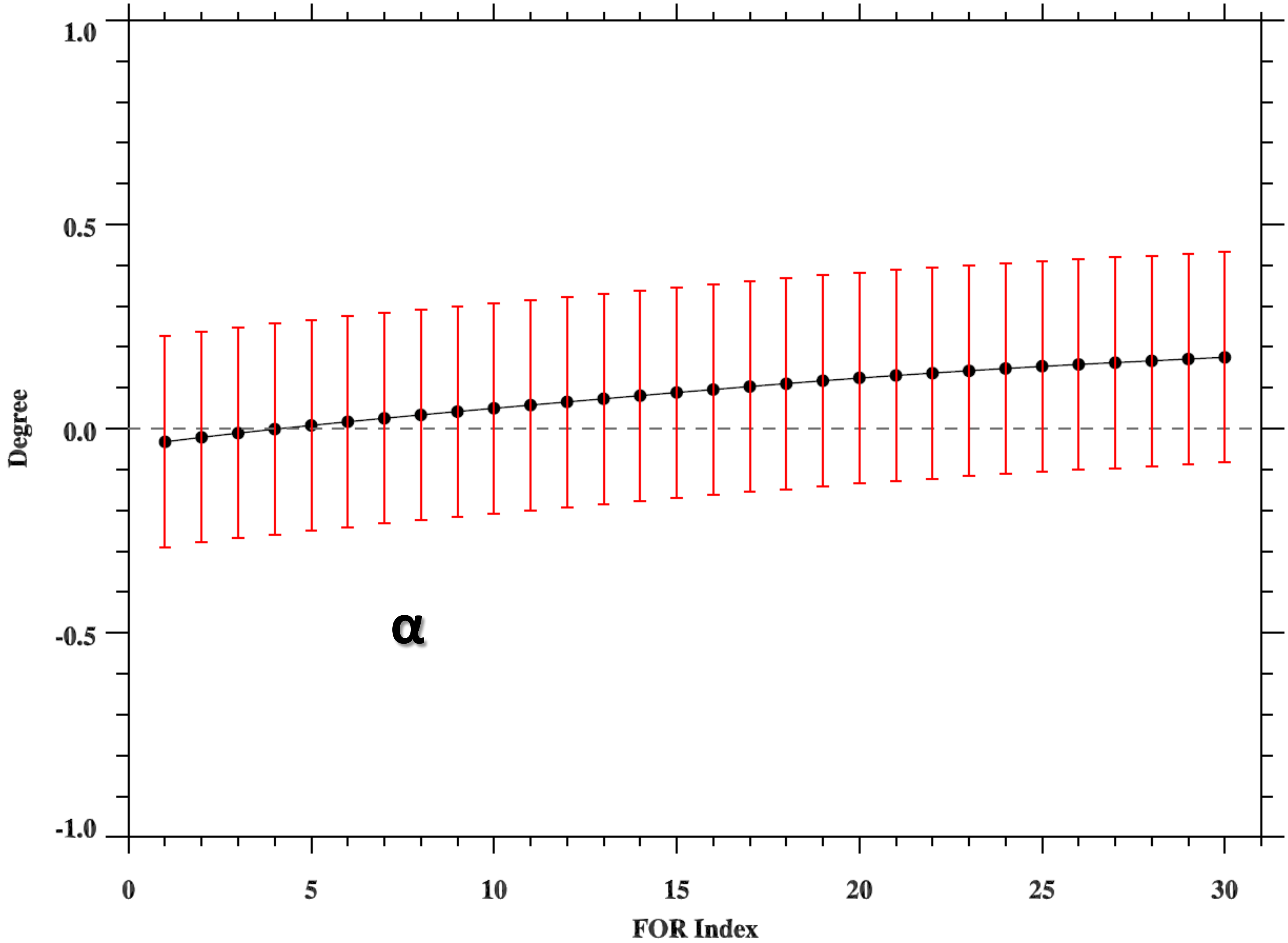

Using VIIRS to find best collocation position

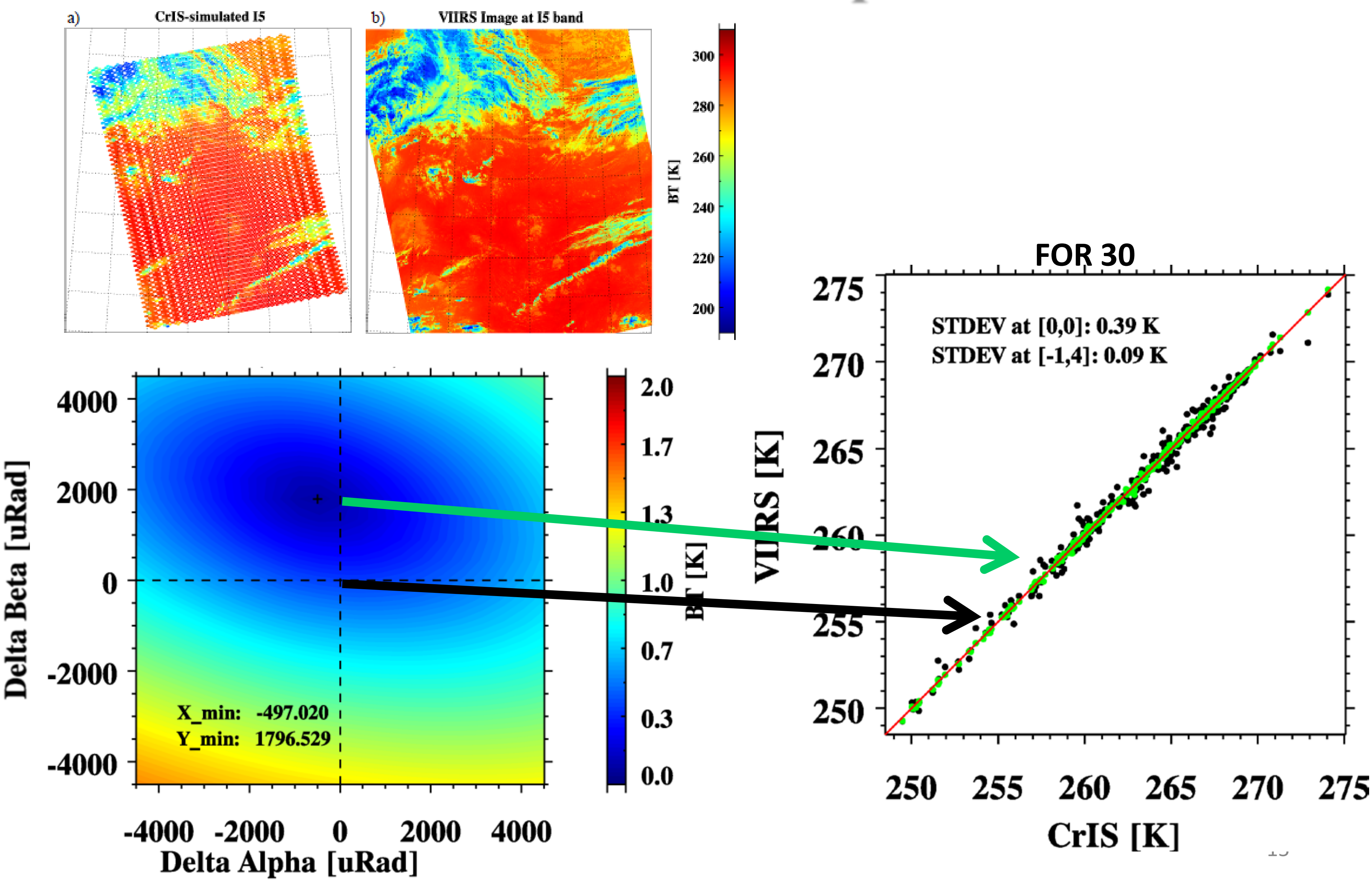

Flowchart for VIIRS-CrIS Alignment Check

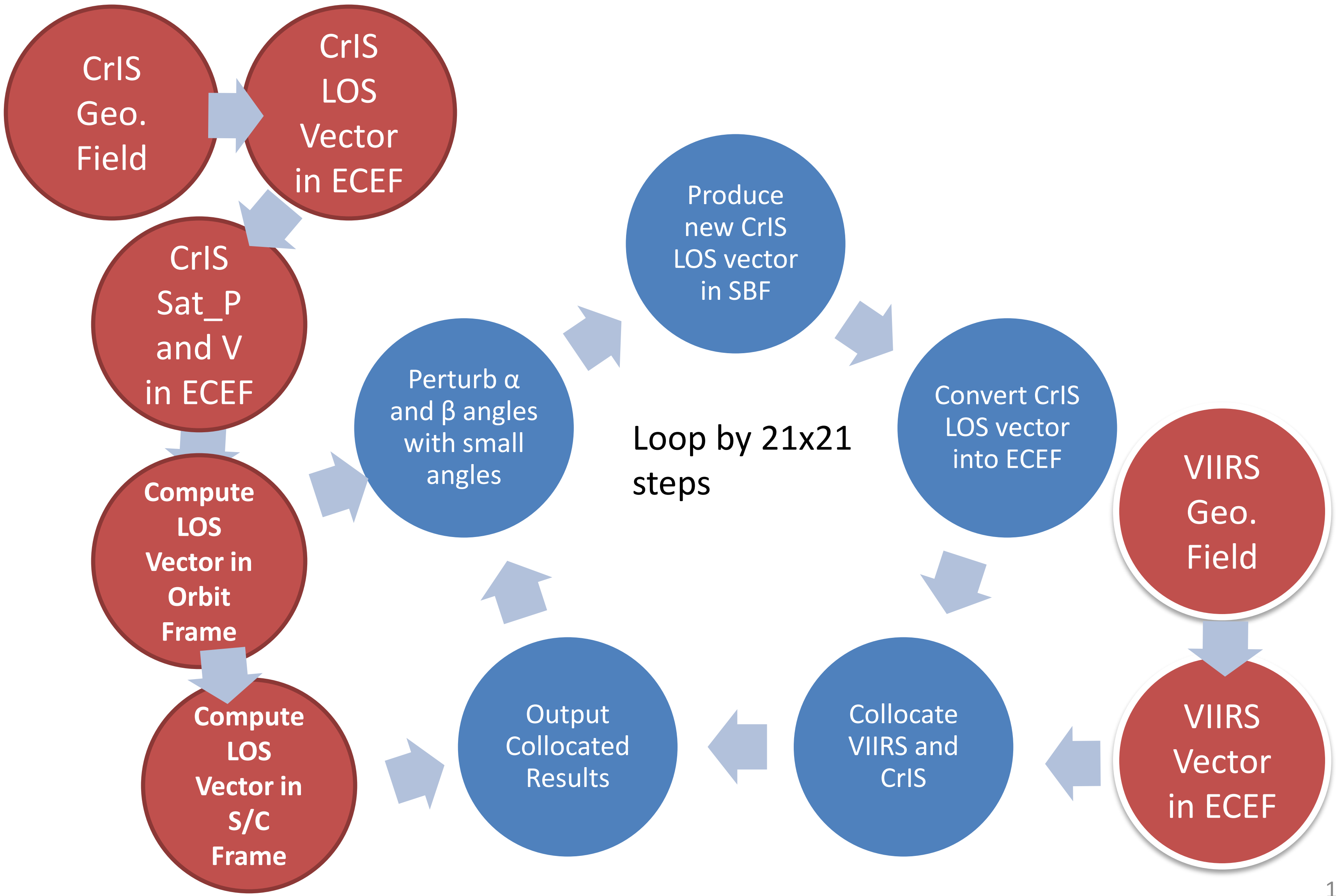

IDPS Data Geolocation Performance

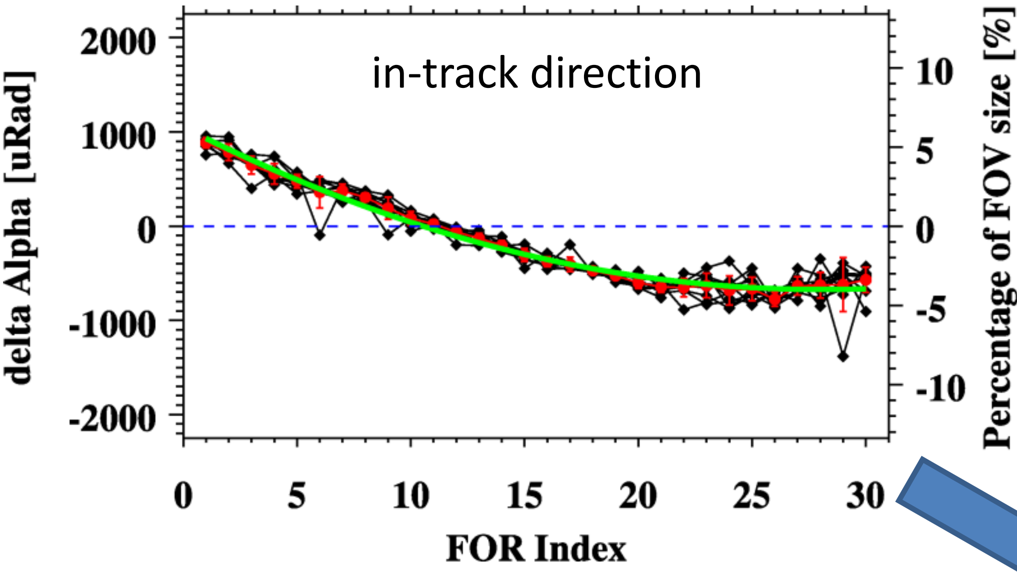

CrIS FOV size in-track and cross-track direction

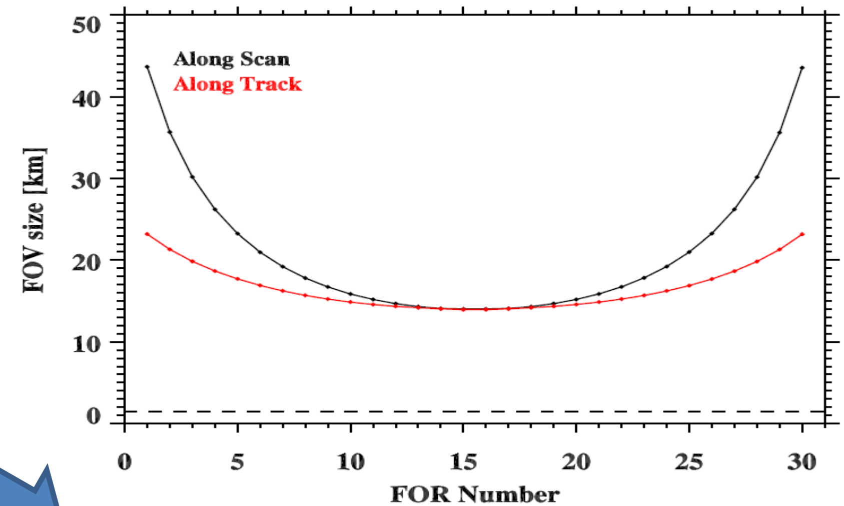

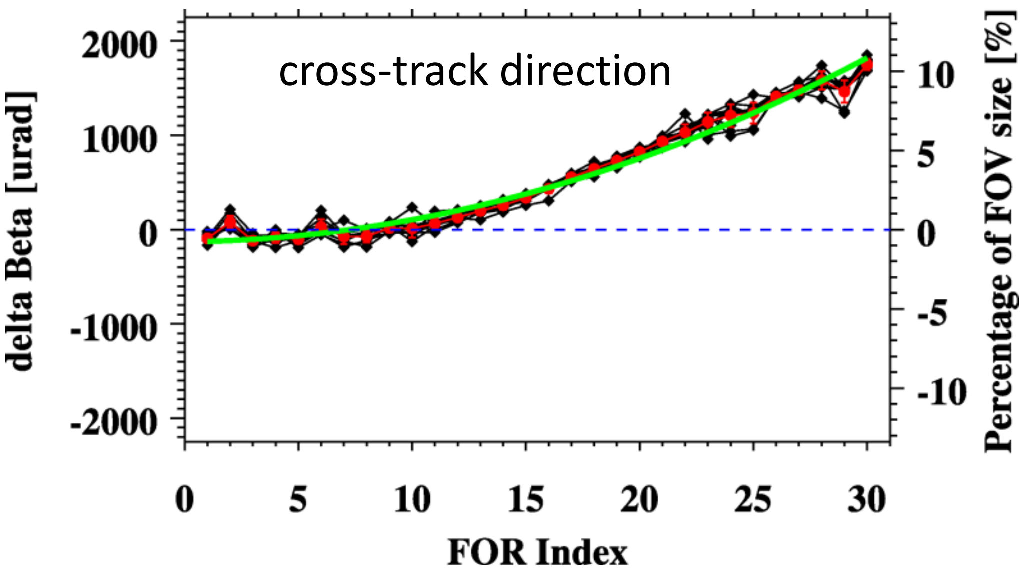

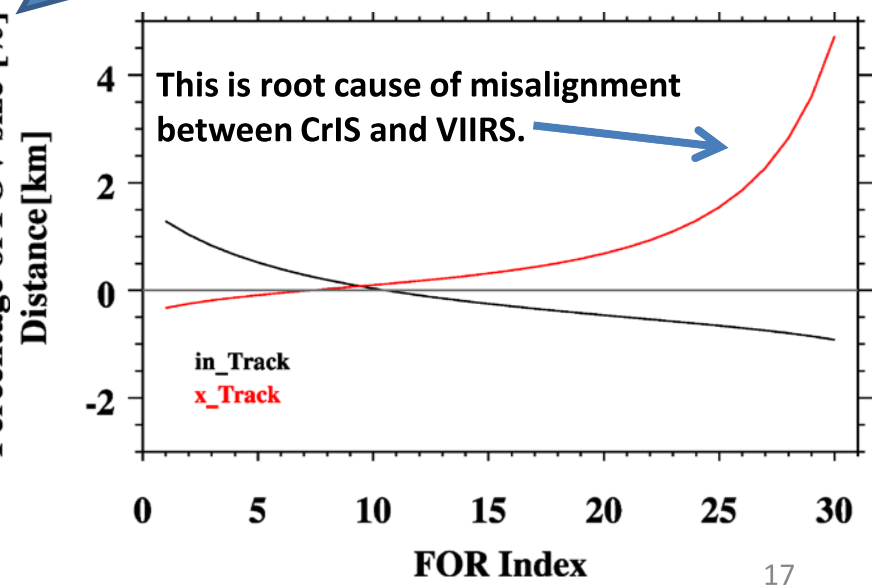

New Geometric Parameters

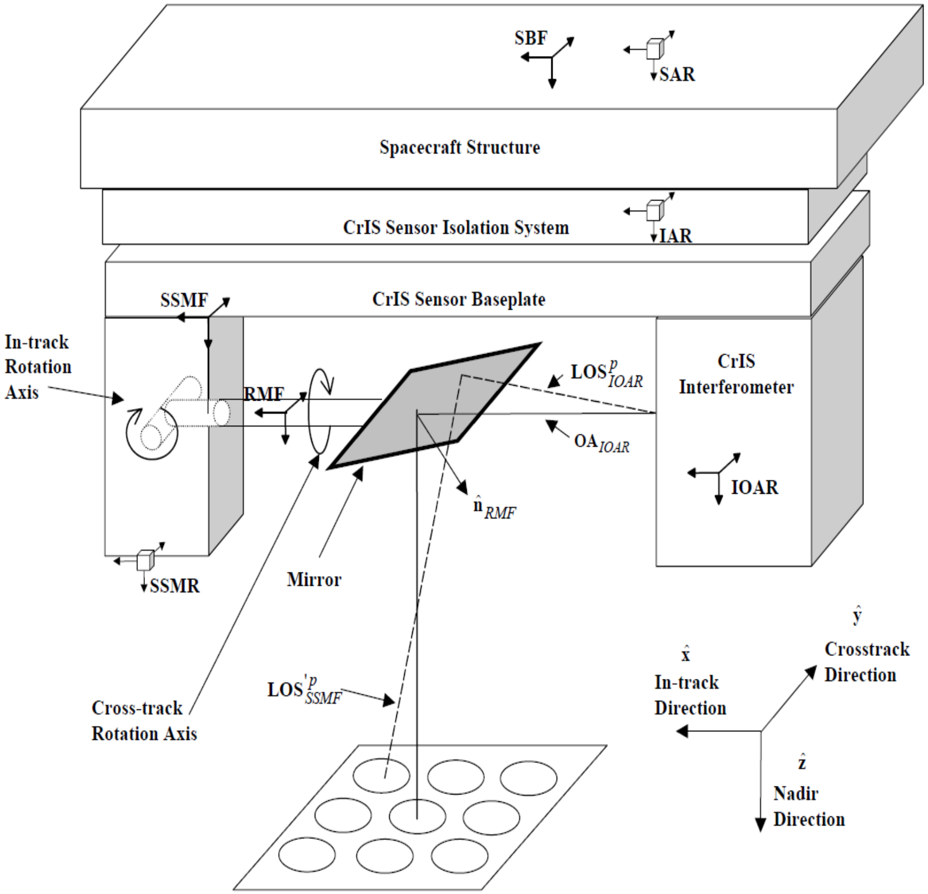

Figure 48: Sensor Algorithm Level Coordinate Systems

Given the assessment results with 60 angles, the best strategy is to retrieve 60 scan mirror rotation angles.

SDR Algorithm Process

1) LOS in IOAR coordinate = ILS parameters (3x3)
2) Convert from IOAR to SSMF coordinate **(2 angles)**
3) Compute normal to SSM mirror in SSMF (30 Scan Pos) **(60 angles)**
4) Apply SSM mirror rotation to get LOS in SSMF coordinate
5) Convert from SSMF to SSMR coordinate **(3 angles)**
6) Convert from SSMR to IAR coordinate **(3 angles)**
7) Convert from IAR to SAR **(3 angles)**
8) From SAR=> SBF coordinate **(0 angels)**
9) From SBF=> Spacecraft **(3 angles)**

New SSMF In-track Angles

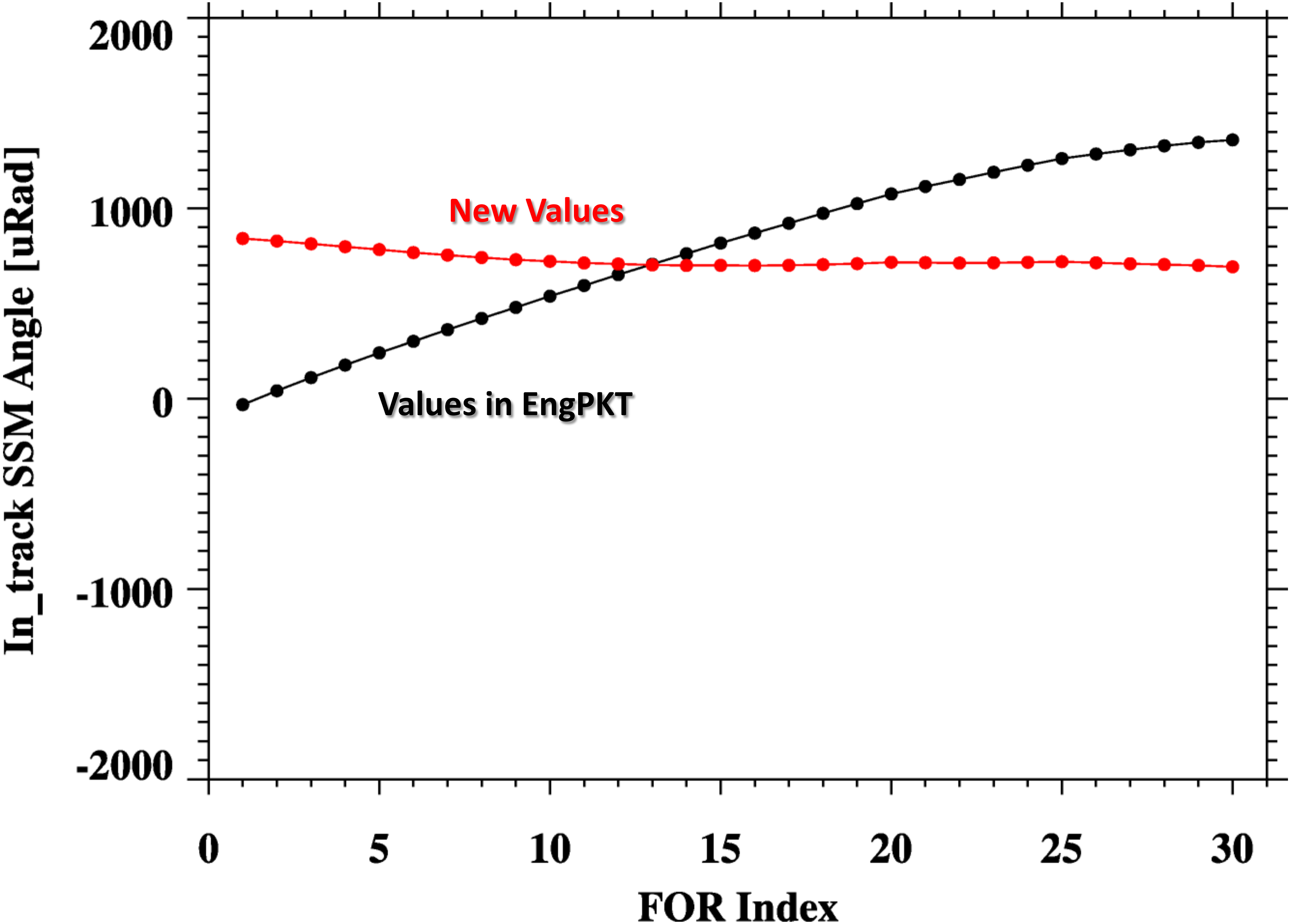

Retrieved SSMF Cross-track Angles

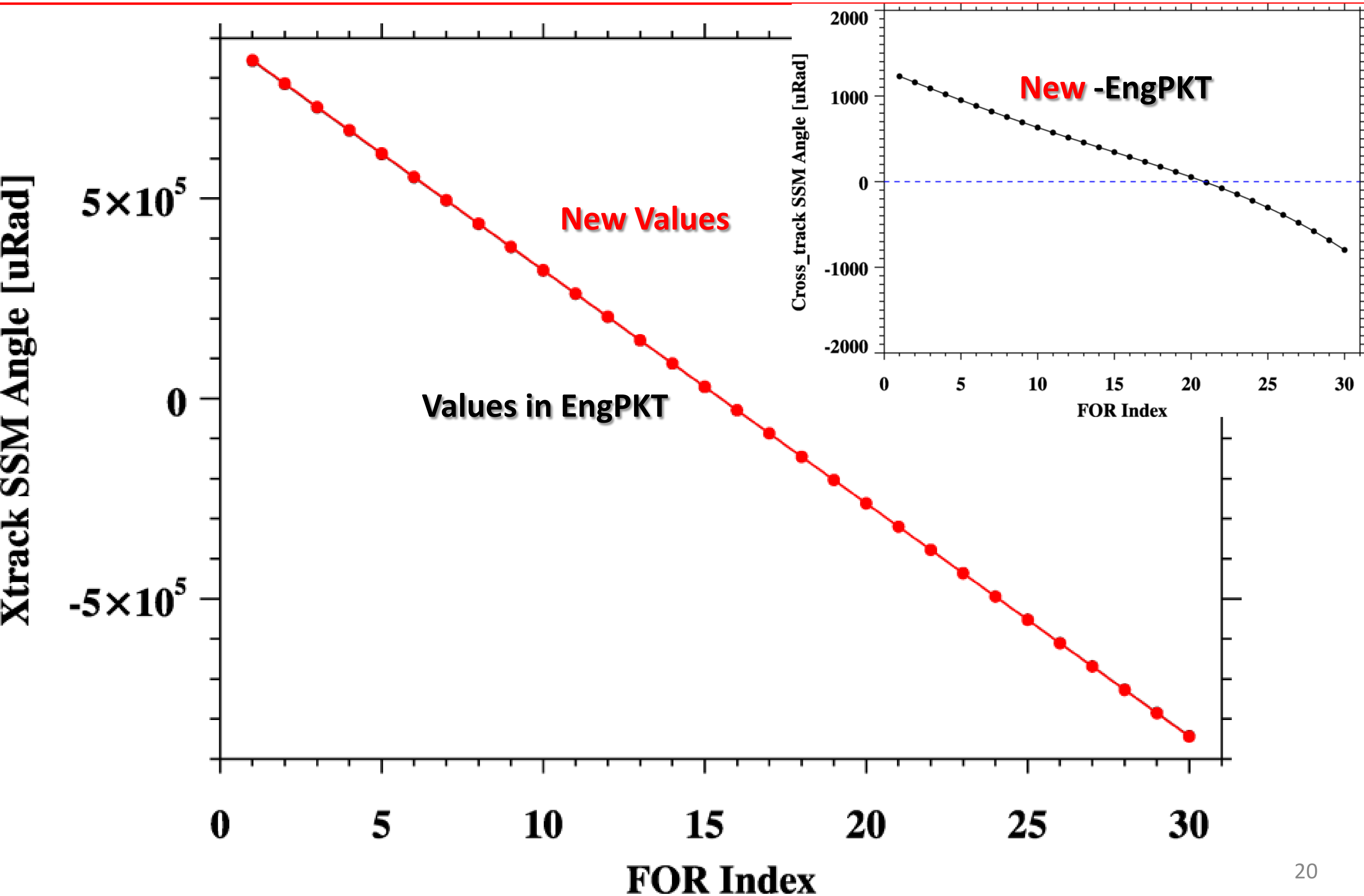

Geolocation Performance (New Parameters)

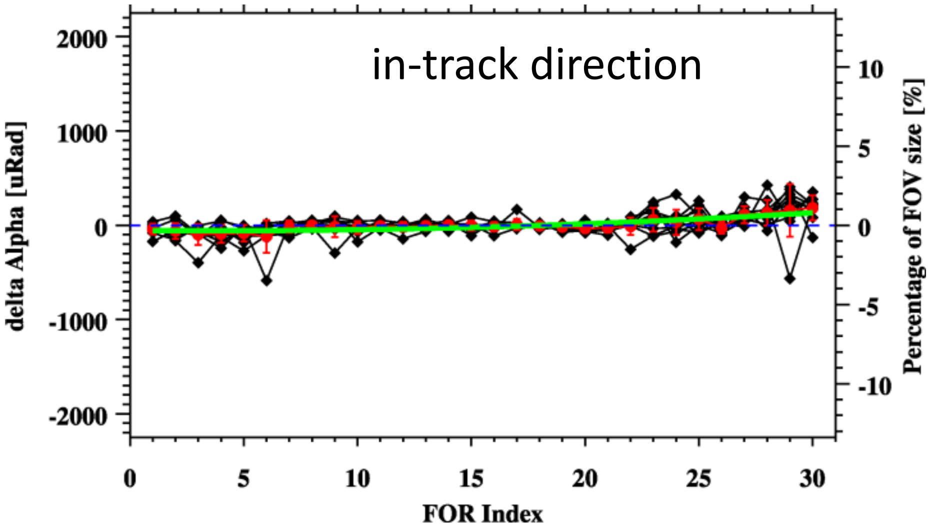

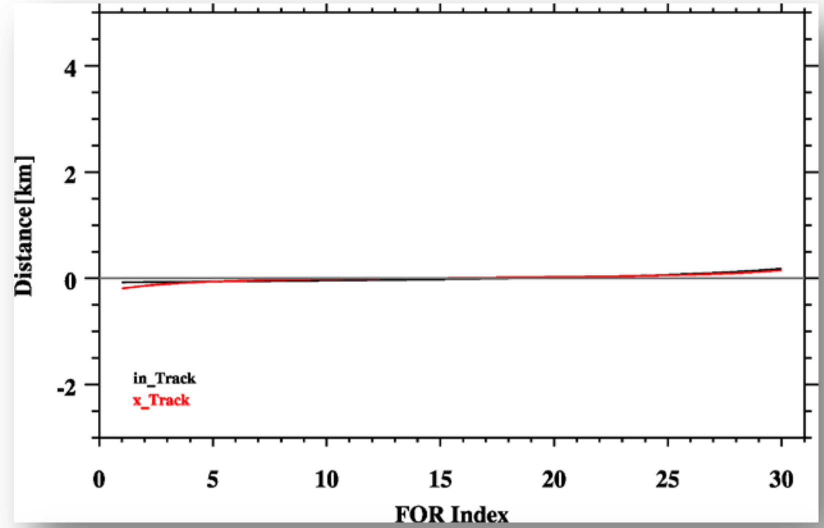

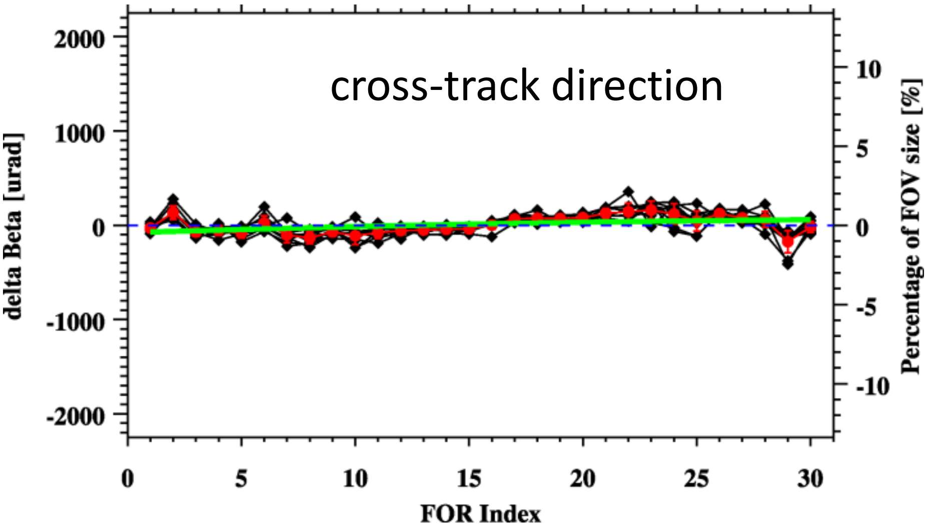

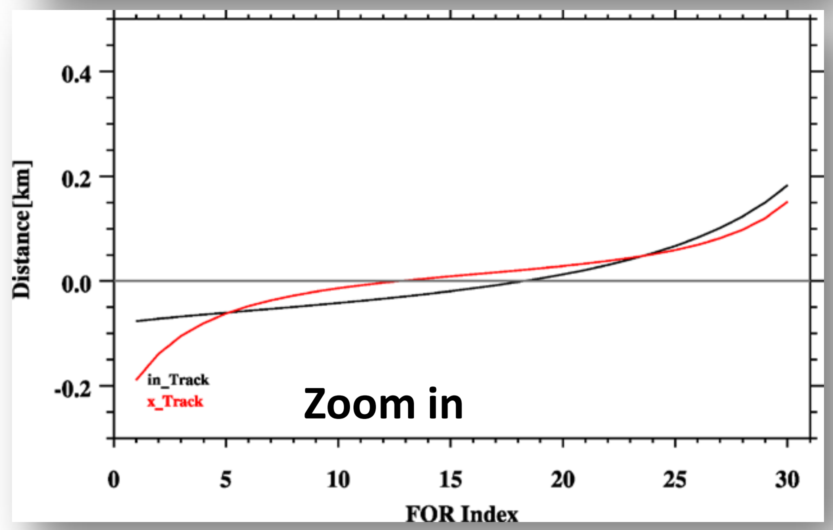

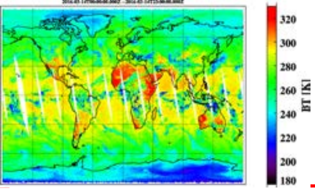

Effects of Geolocation Updates
CrIS-VIIRS (M15)

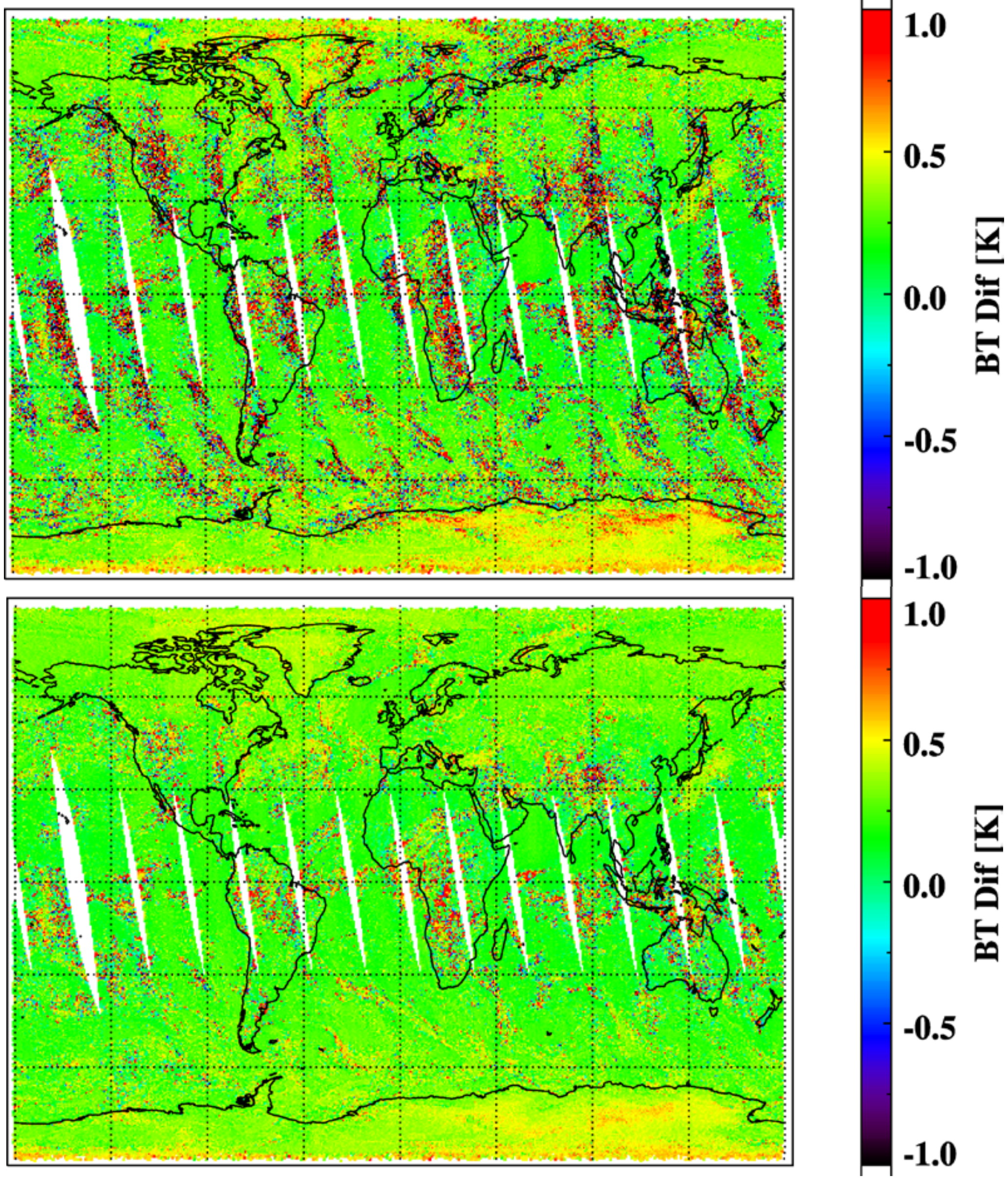

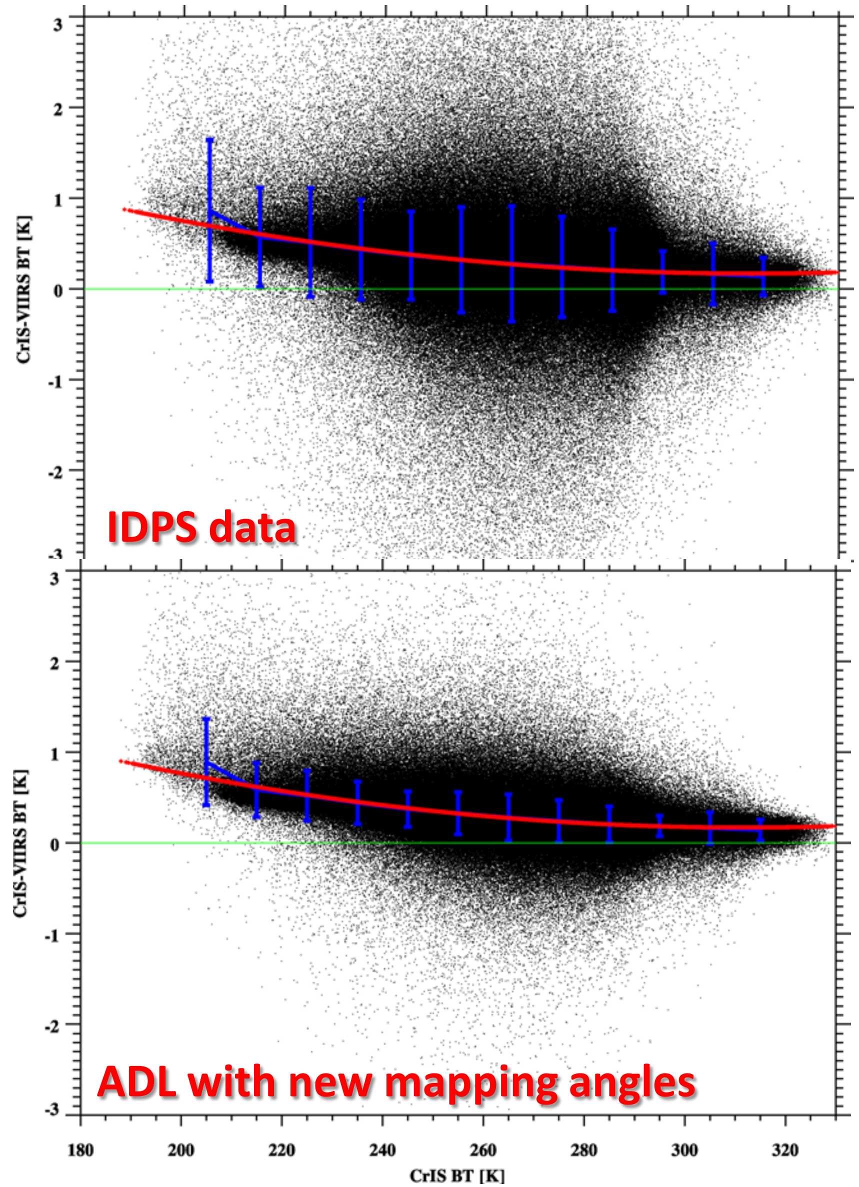

Application (I)
Clear Sky Detection Comparison

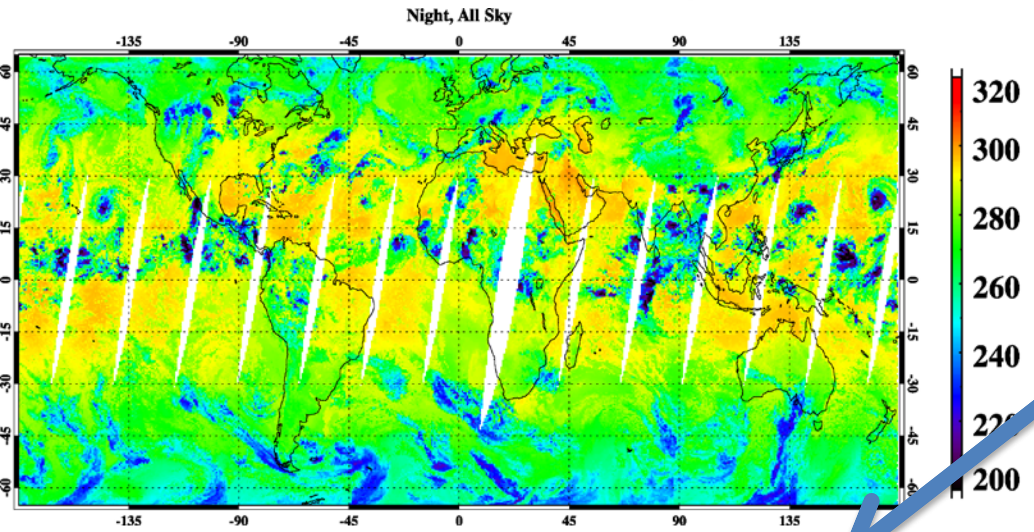

- Compared to NWP method, the VIIRS method represent the most conservative clear sky detection.

- Differences:

1Missed detection of clear sky observations over land by the NWP method

2. More clear sky observations over sea by NWP method

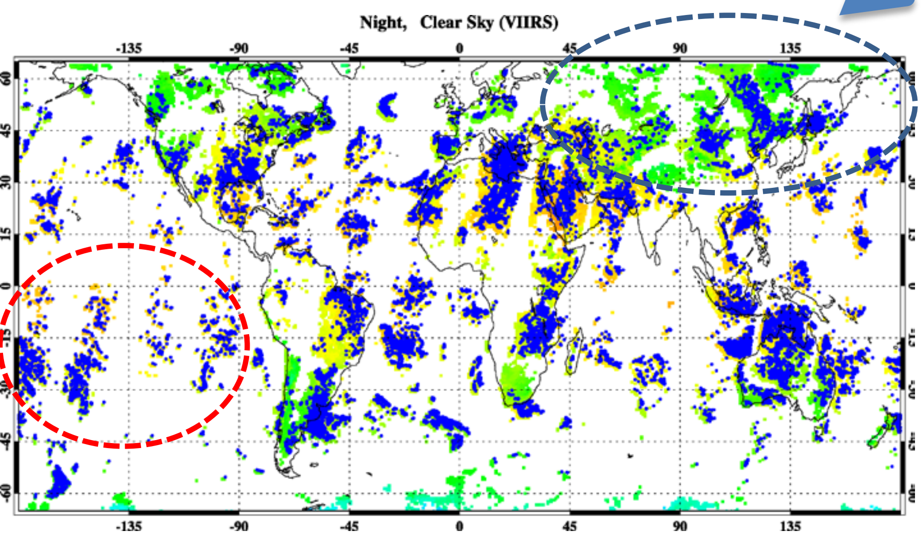

VIIRS method

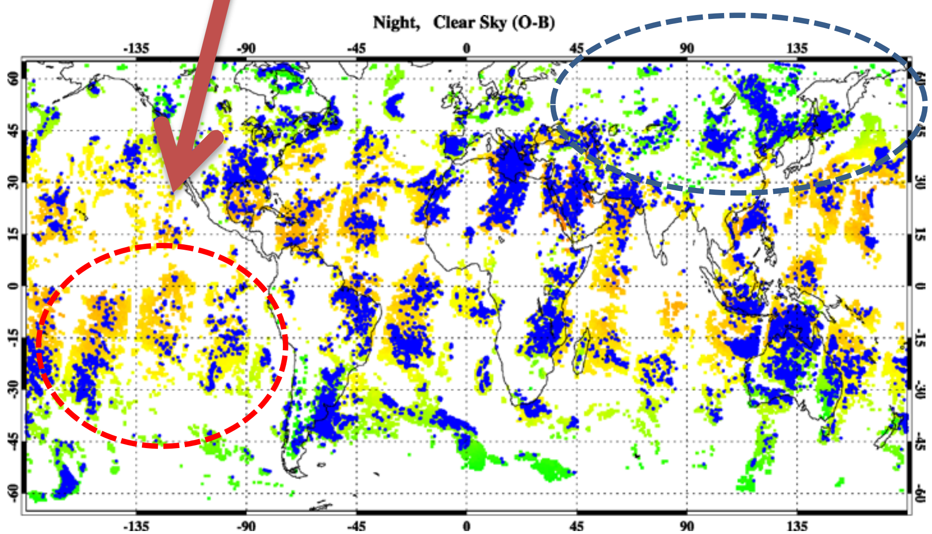

NWP method

Blue dots represents the clear pixels identified by both methods

Application (II)
Clear Sky observations change with FOV size

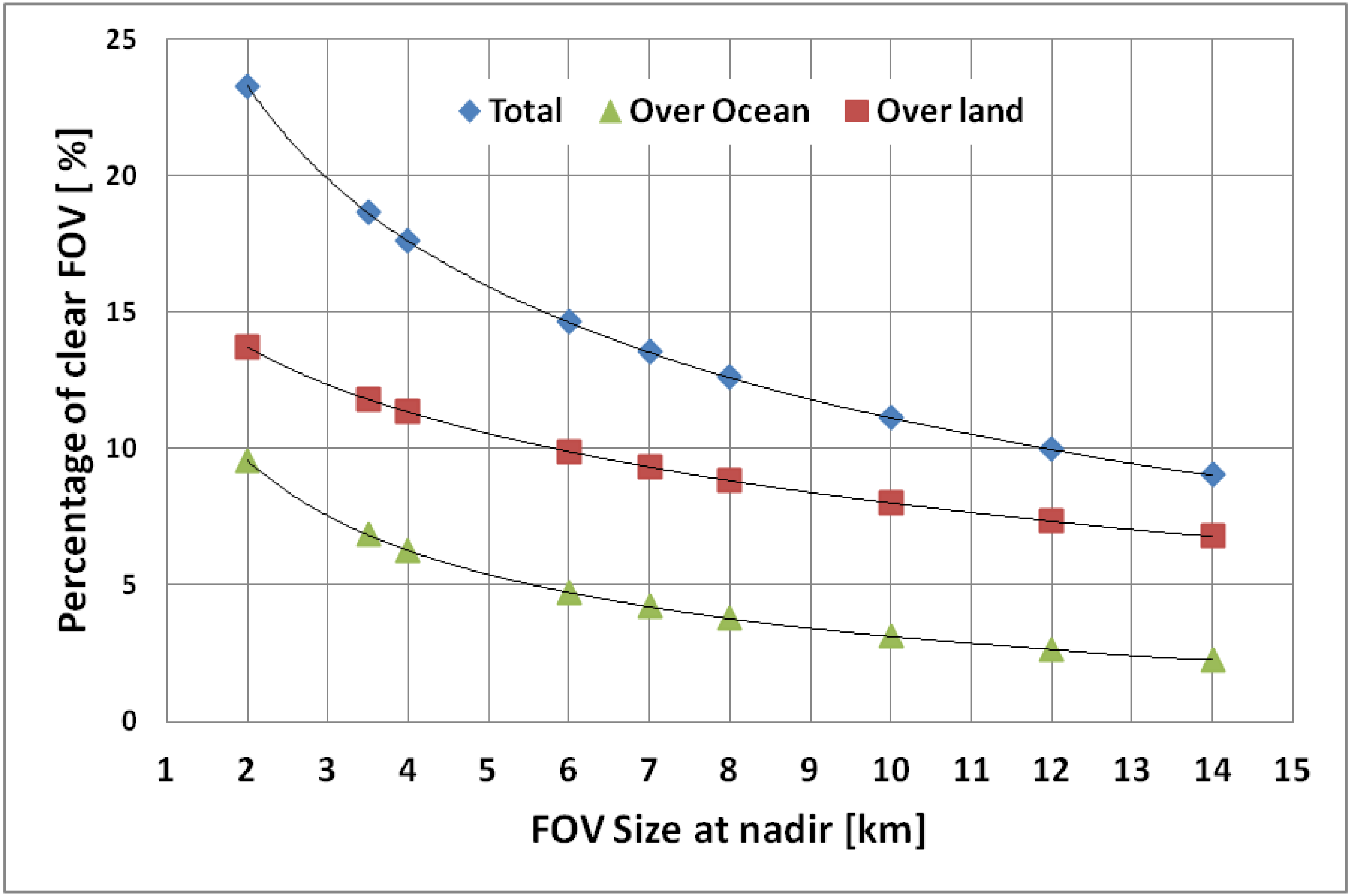

Application (III)

VIIRS radiance cluster analysis under CrIS FOV

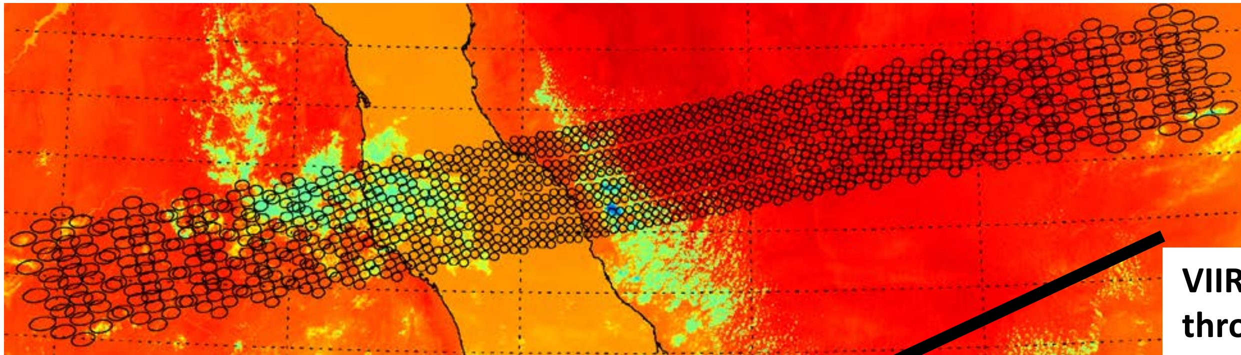

VIIRS can be collocated within CrIS footprint through fast collocation method

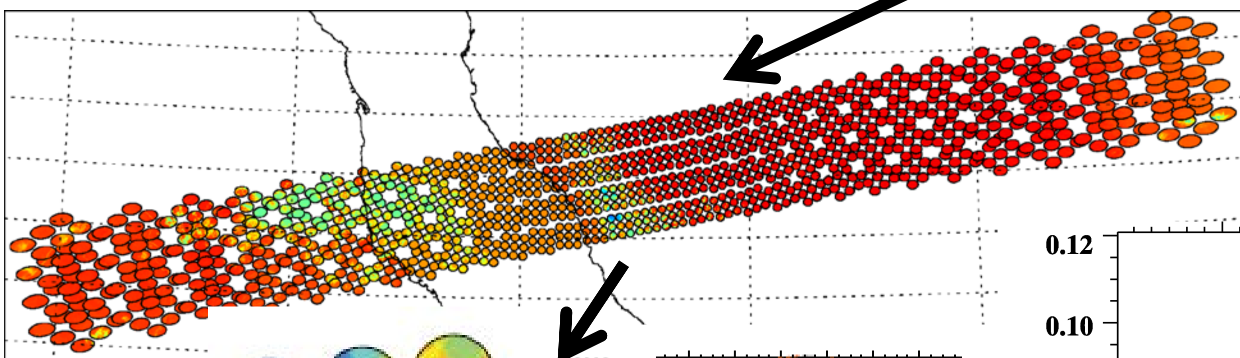

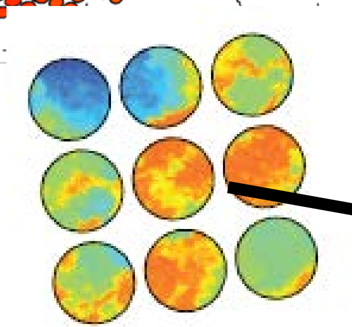

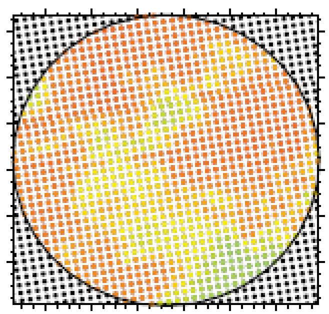

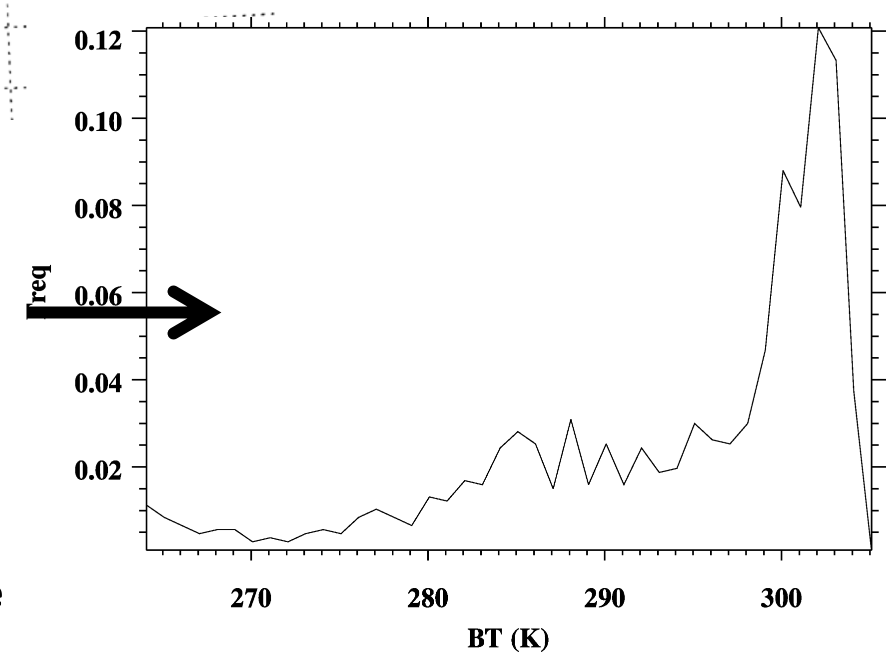

The collocated VIIRS pixels are then separated into several classes (7) based on cluster analysis; for each class, the fraction of CrIS FOV coverage, mean radiance value, standard deviation are provided.

Conclusion

- Fast and accurate collocation method of CrIS and VIIRS has been developed, which is suitable for operational use.

- CrIS geolocation has been adjusted to perfectly align with VIIRS.

- Accurate collocation VIIRS products shows some potentials for data assimilation and geophysical parameter retrivals.

Publication

- **Wang, L.**, D. A. Tremblay, B. Zhang, and Y. Han, 2016: Improved scheme for Cross-track Infrared Sounder geolocation assessment and optimization. Journal of Geophysical Research - Atmosphere (Submitted).

- **Wang, L.**, Y. Chen, and, Y. Han, 2016: Impacts of Field of View Configuration of Crosstrack Infrared Sounder on Clear Sky Observations, Applied Optics (In Print).

- **Wang, L.**, D. A. Tremblay, B. Zhang, and Y. Han, 2016: Fast and Accurate Collocation of the Visible Infrared Imaging Radiometer Suite Measurements and Cross-track Infrared Sounder Measurements. Remote Sensing, 8, 76; doi:10.3390/rs8010076.

QUESTIONS?

BACKUP SLIDES

Retrieve LOS Vectors

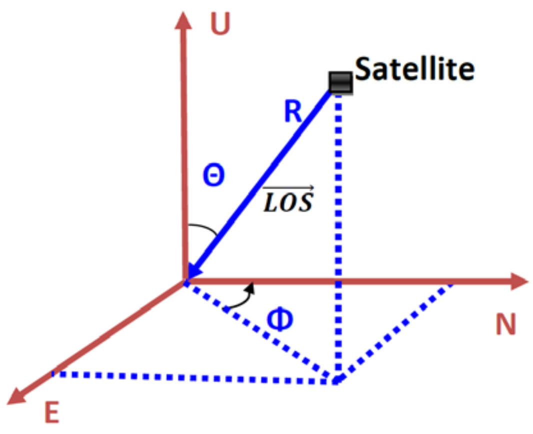

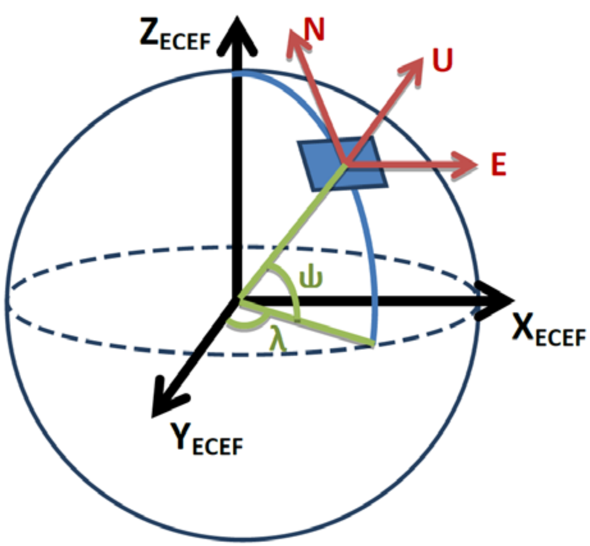

Azimuth, Zenith, Range in Local Spherical Coordinate

↓

(East, North, Up) in meter in Local East, North, Up (ENU) Coordinate

↓

Geodetic Latitude, Longitude, and Altitude (LLA) Coordinate

↓

Earth-centered, earth-fixed (ECEF) Coordinate

CrIS Spatial Response Function

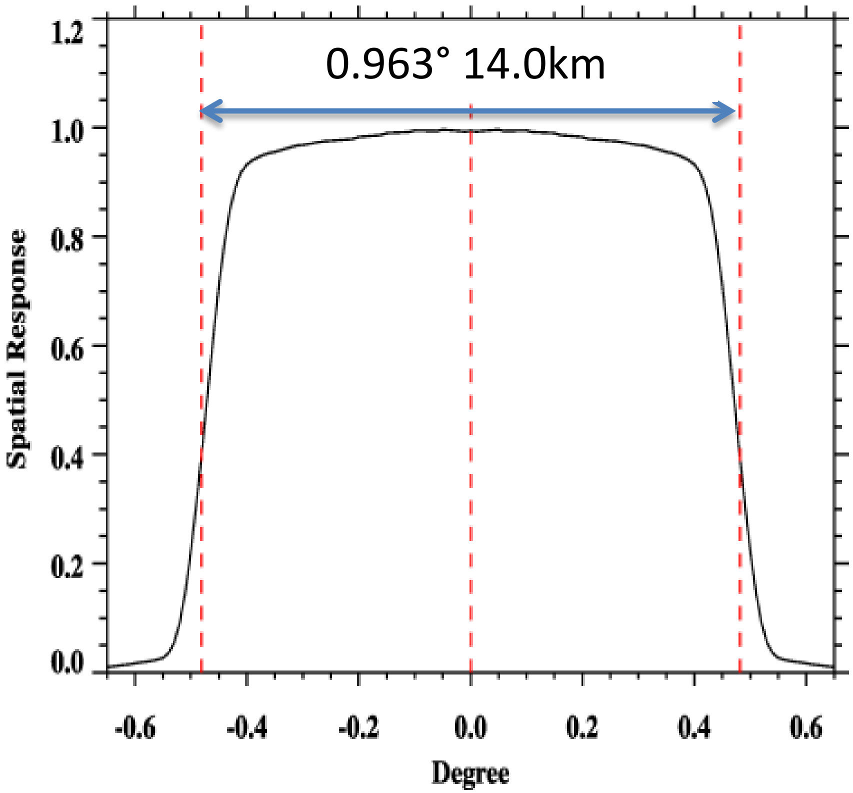

- Ideally, VIIRS images should be convolved with CrIS spatial response function.
- CrIS detector response function: a cutoff value of ±0.963°/2 (14.0 km at nadir) is about 41.19% to its peak value but already collects 98% of total radiation falling on the detector.
- The box-car spatial response is good enough to represent the real CrIS spatial response.

VIIRS (Box Car Average) - (Spatial Response Convolution): ~0.0023K

K-D Tree Search

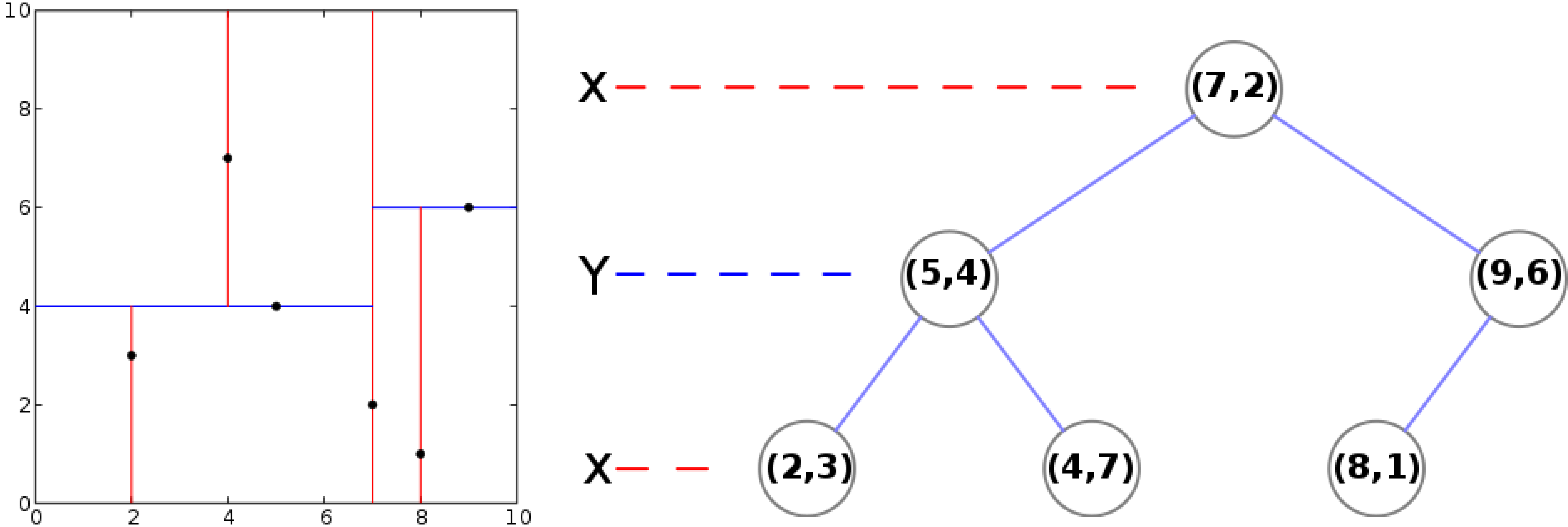

In computer science, a ***k*-d tree** (short for *k-dimensional tree*) is a space-partitioning data structure for organizing points in a *k*-dimensional space.

	Average	Worst case
Search	**O(log *n*)**	**O(*n*)**

Clear Sky Detection Comparison (Day time)

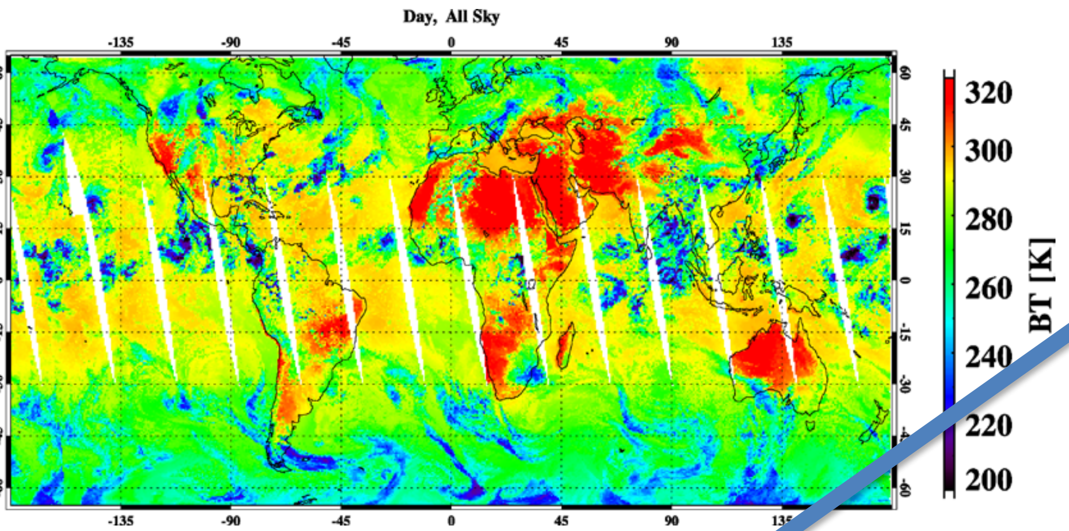

Two issues can be found that:

1) Land Surface temperate errors during day time make the RTM difficulty to simulate observations over land;

2) NWP method found more clear sky pixels over ocean. It seem warm clouds.

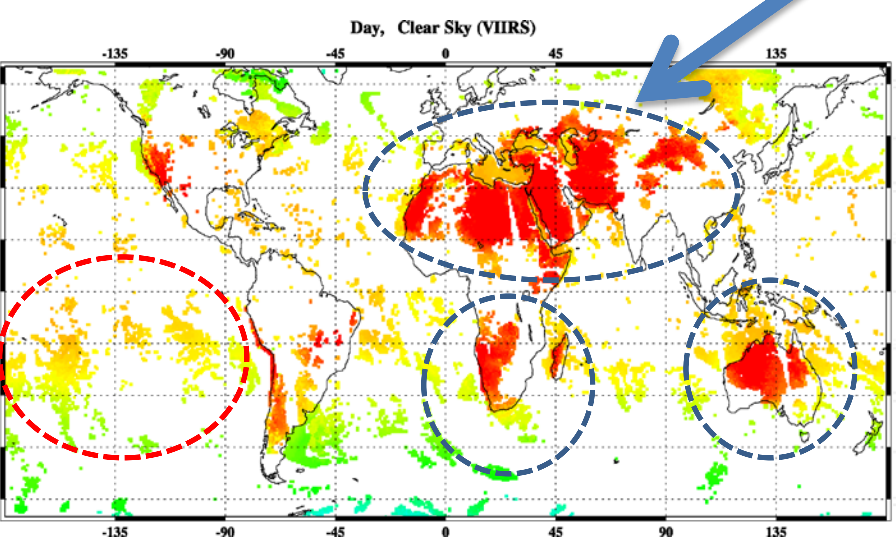

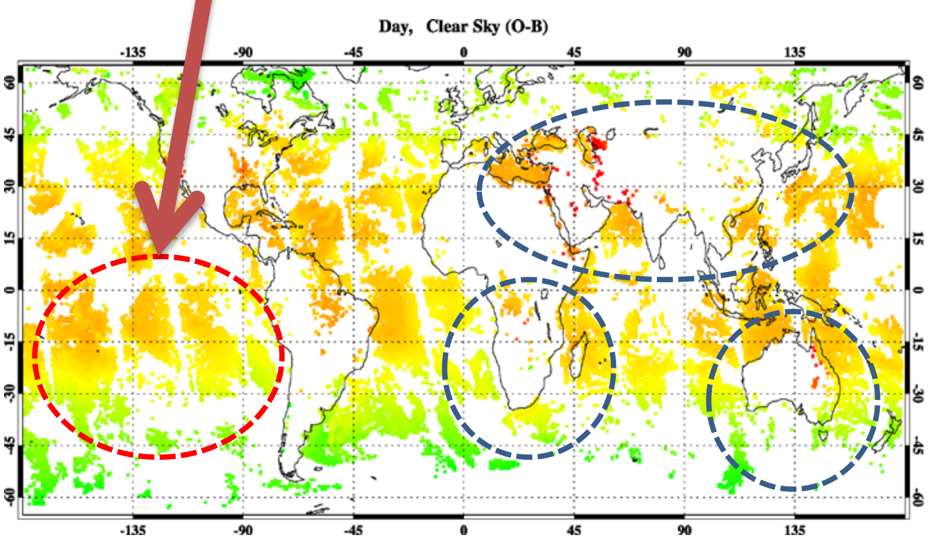

VIIRS method

NWP method

Another Validation Case

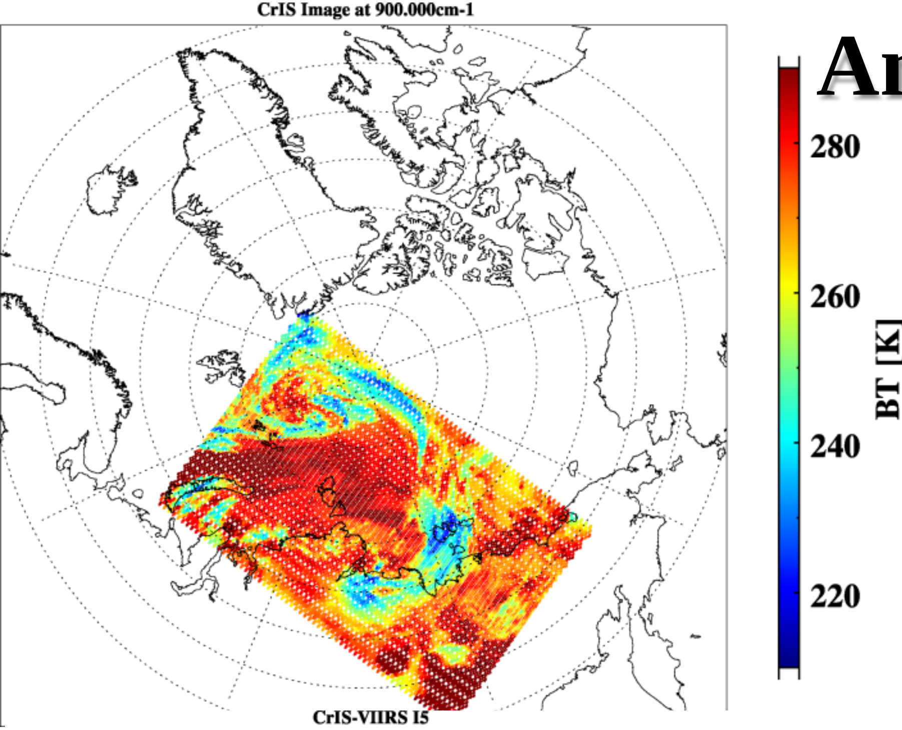

Polar Region

CrIS-VIIRS I5 image

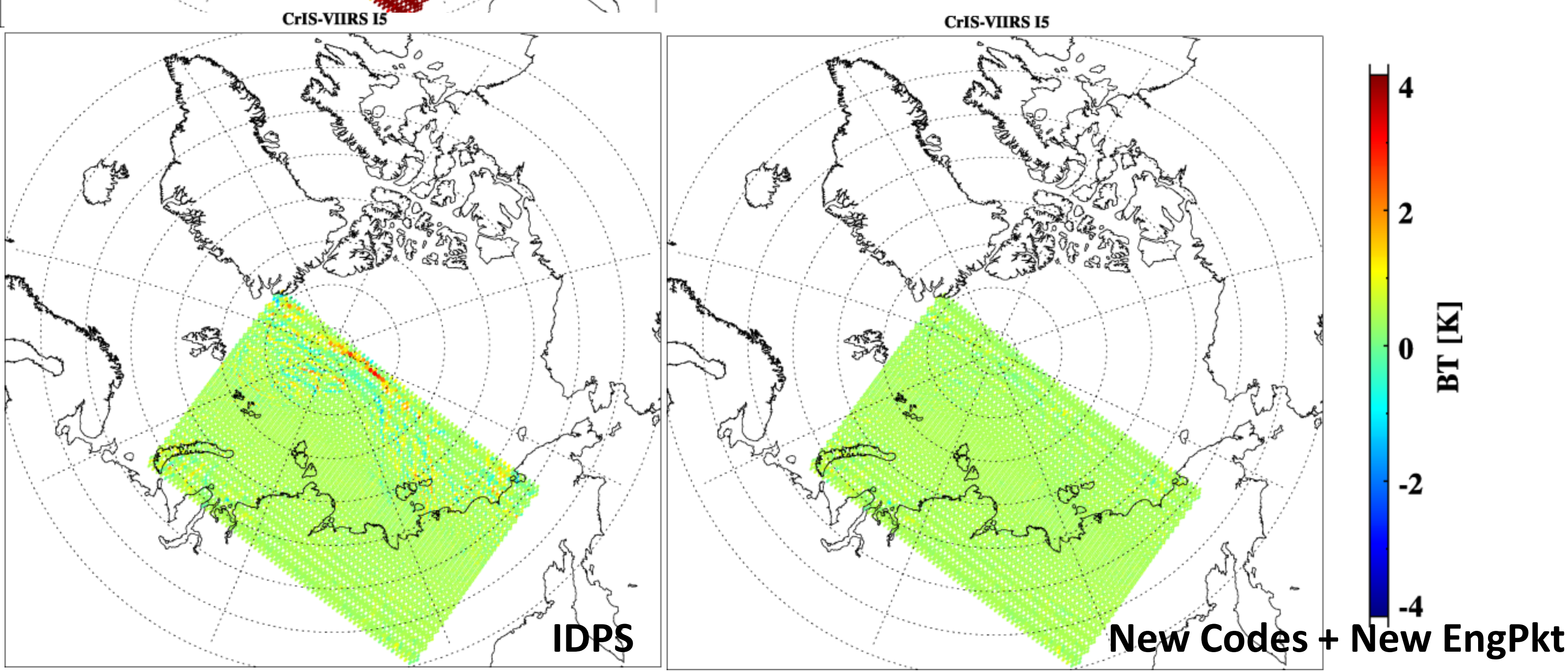

Zoom-in warm clouds

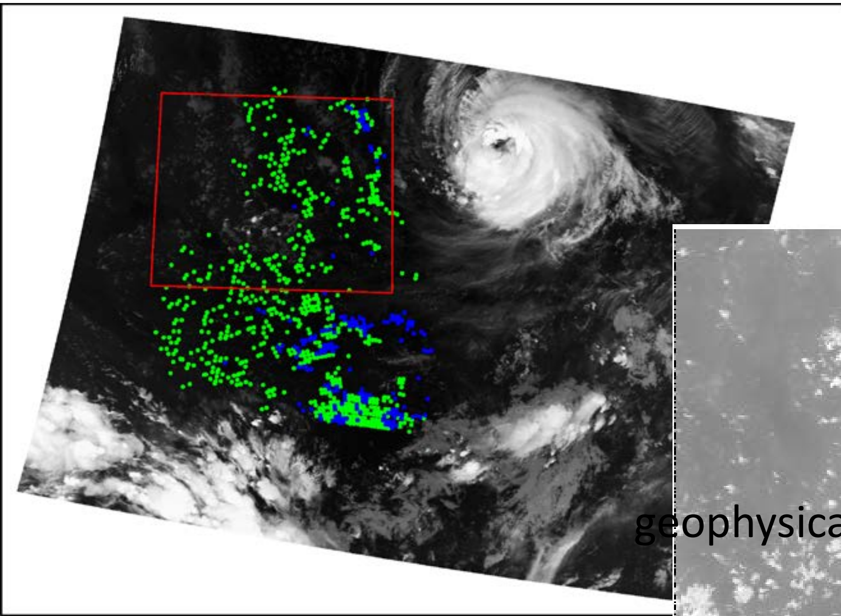

Some cloud contaminated observations are missed by NWP method.

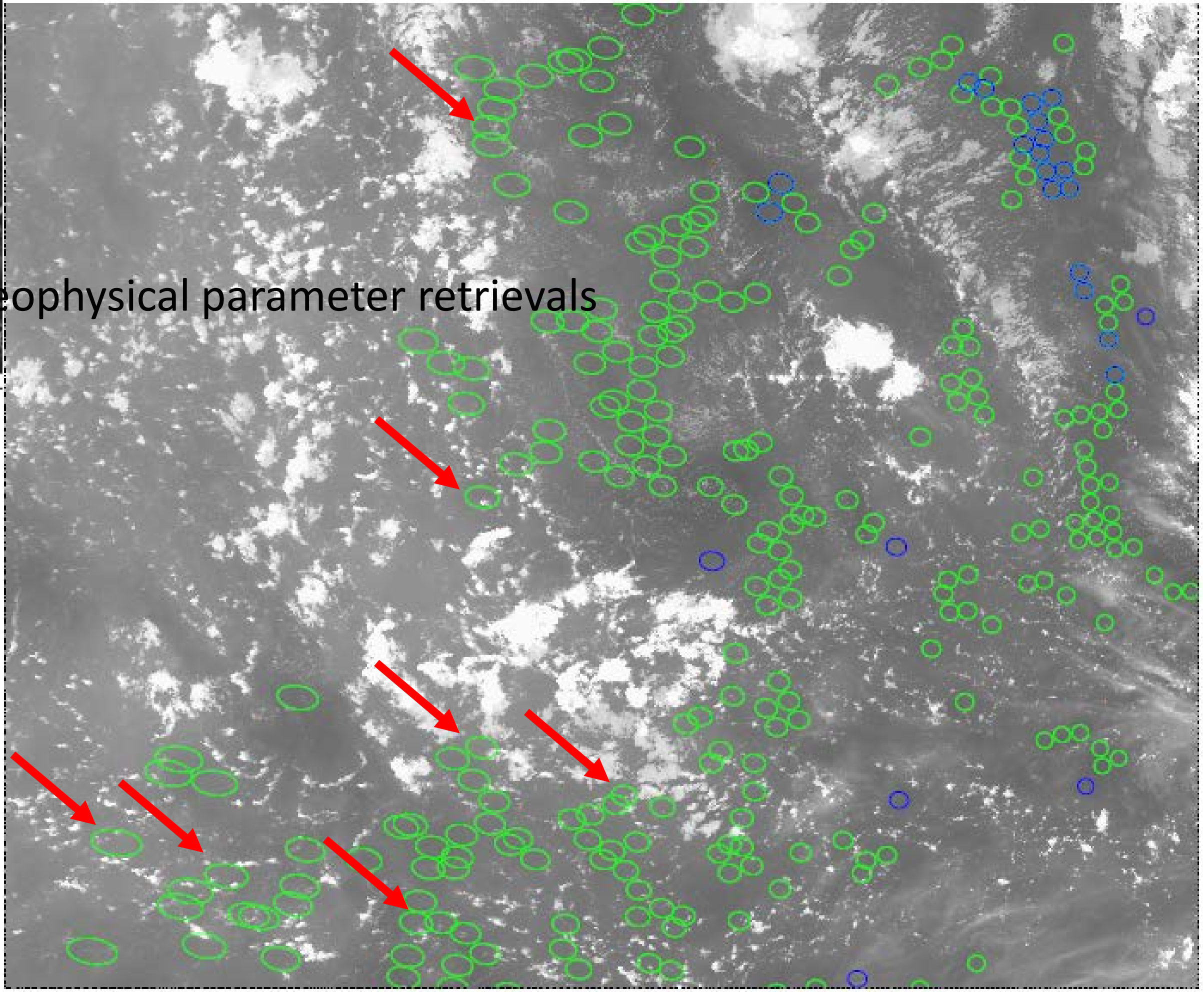

NWP method
VIIRS method

Closed-loop operational calibration checks

Full closed loop CrIS simulation

STAR JPSS Annual Science Team Meeting

Session 4: CrIS & ATMS SDRs

D. L. Mooney, MIT/LL

8/16/2014

Motivation

- **CrIS calibration algorithms are complicated**
  - **Measured interferogram for off-axis extended FOV**
  - **Delivery of equivalent on-axis interferogram on different wavenumber scale**
- **Checking the performance of the algorithm has been difficult with operational data because the "truth" is not known exactly**
- **Operational A4 algorithm requires h5 files**
- **A simulation technique was developed to**
  - **Use NOAA88b atmospheres (T, P, water vapor)**
  - **LBLRTM to produce high resolution LBL spectra**
  - **Operational like long interferograms were computed, FIR filtered, decimated, and packed into binary streams**
- **Code to read operational h5 files and uniquely replace packed interferograms with unique simulated one relatable back to a specific NOAA88b atmospheric**
- **Process h5 files and compare to known input**

The spectra in the LW h5 files are uniquely identified with input spectra with IET time

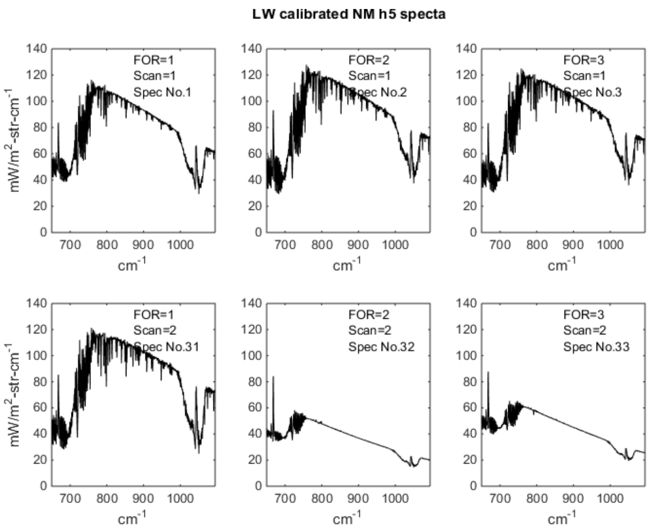

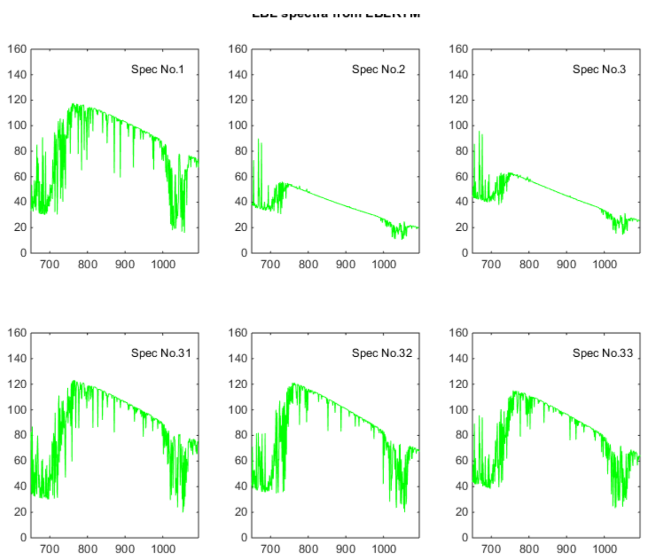

- H5 file cal
- DM matrix cal
- LBL spectra
- NM matrix cal

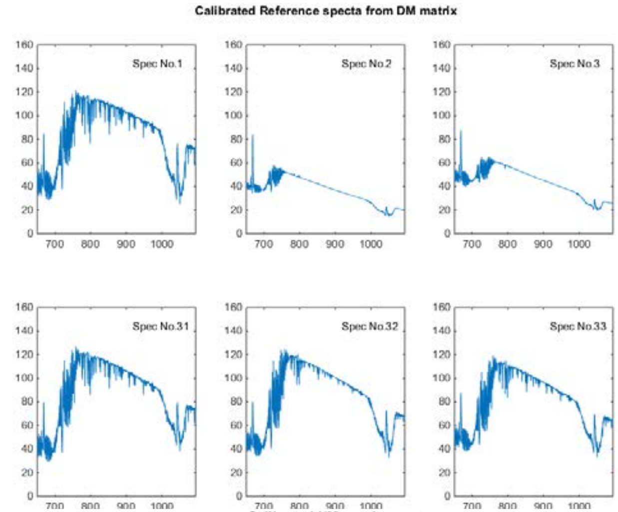

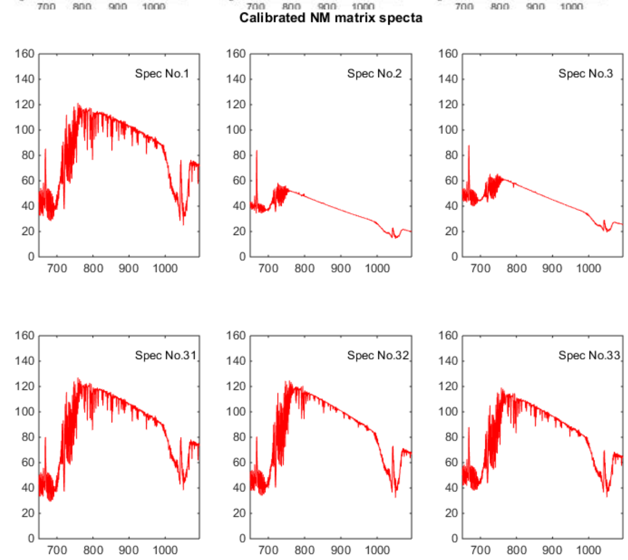

Top level view of closed loop test

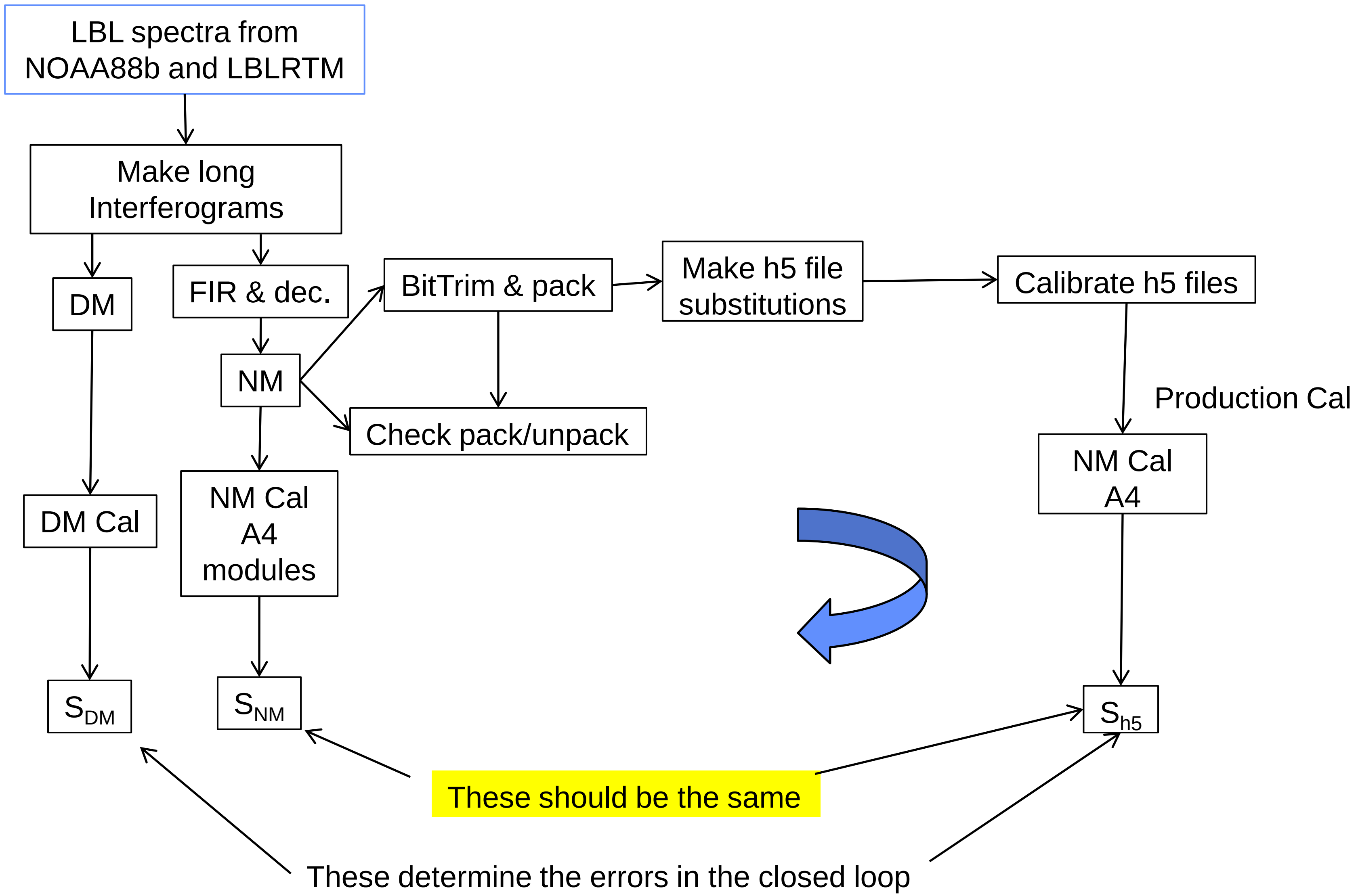

LW h5 file, DM reference, NM reference

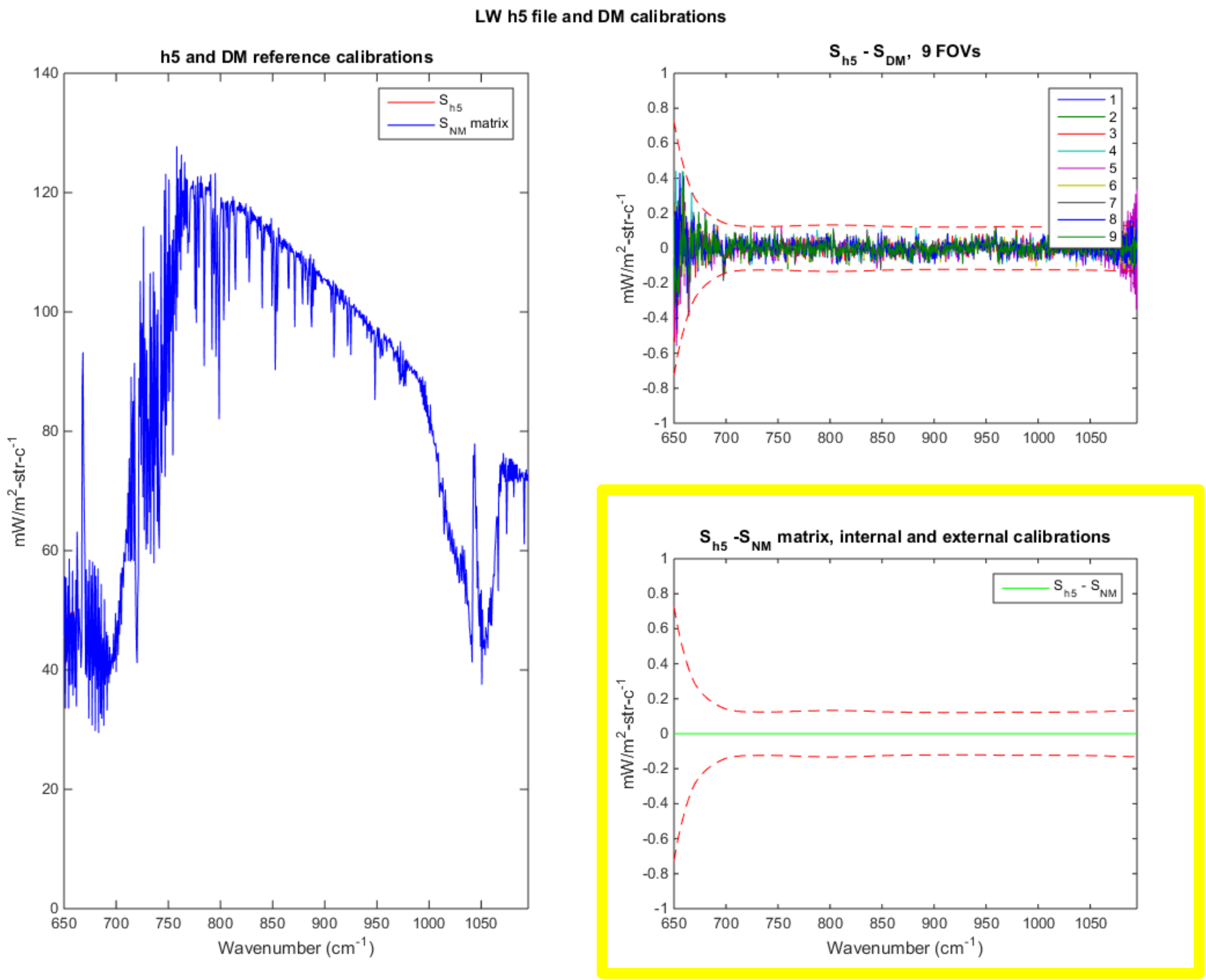

Normal mode calibrations are self consistent

White noise when comparing NM spectra to DM (TRUTH) spectra

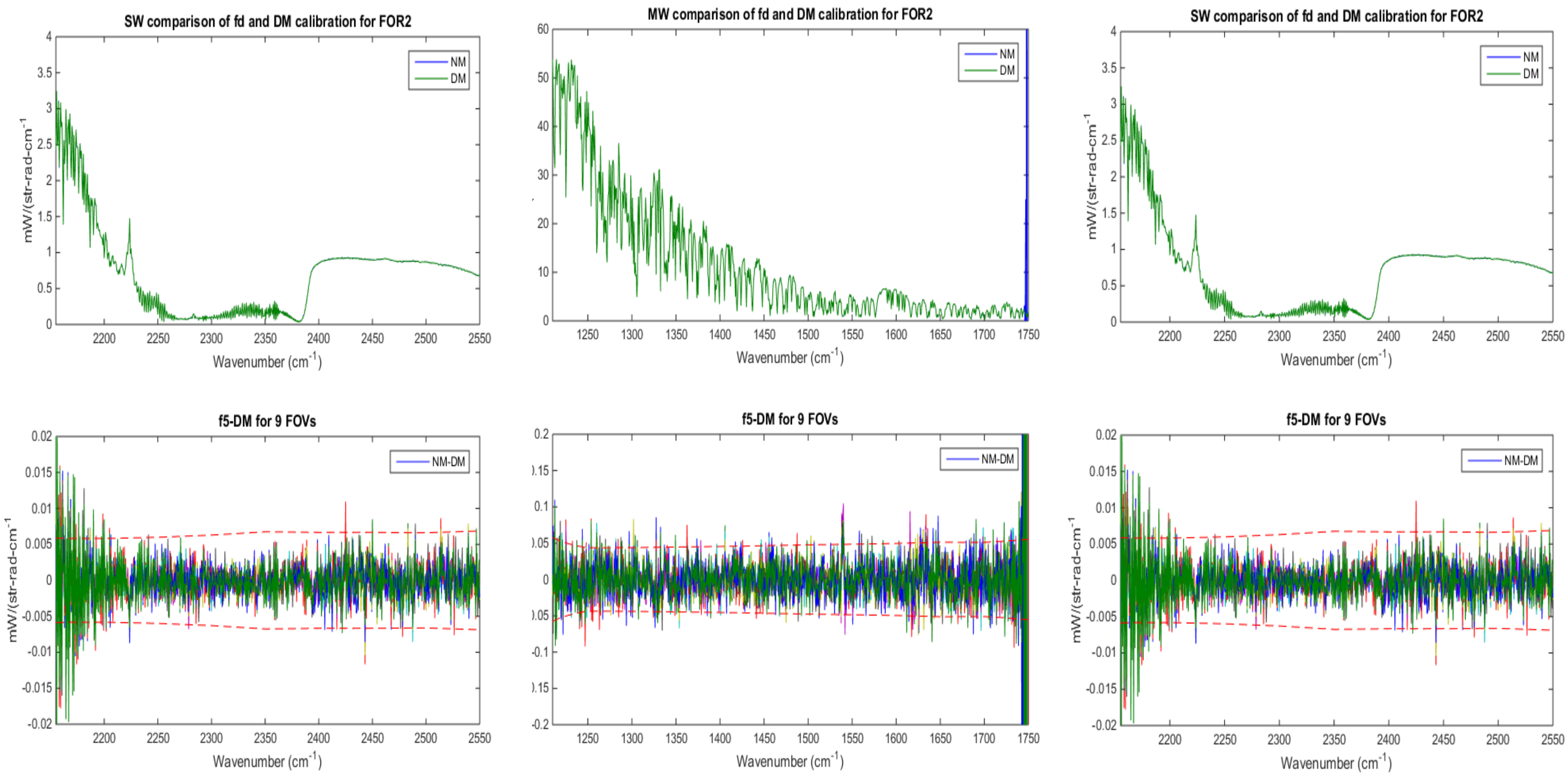

Review of results

- No noise added to simulation
- Gain prior the bit trimming has no error
- Main errors
  - 14 bit A/D error (primary)
  - FIR output trimming error
- Errors mask small algorithm differences

LW NM data is tight within bit trim values as are MW and SW

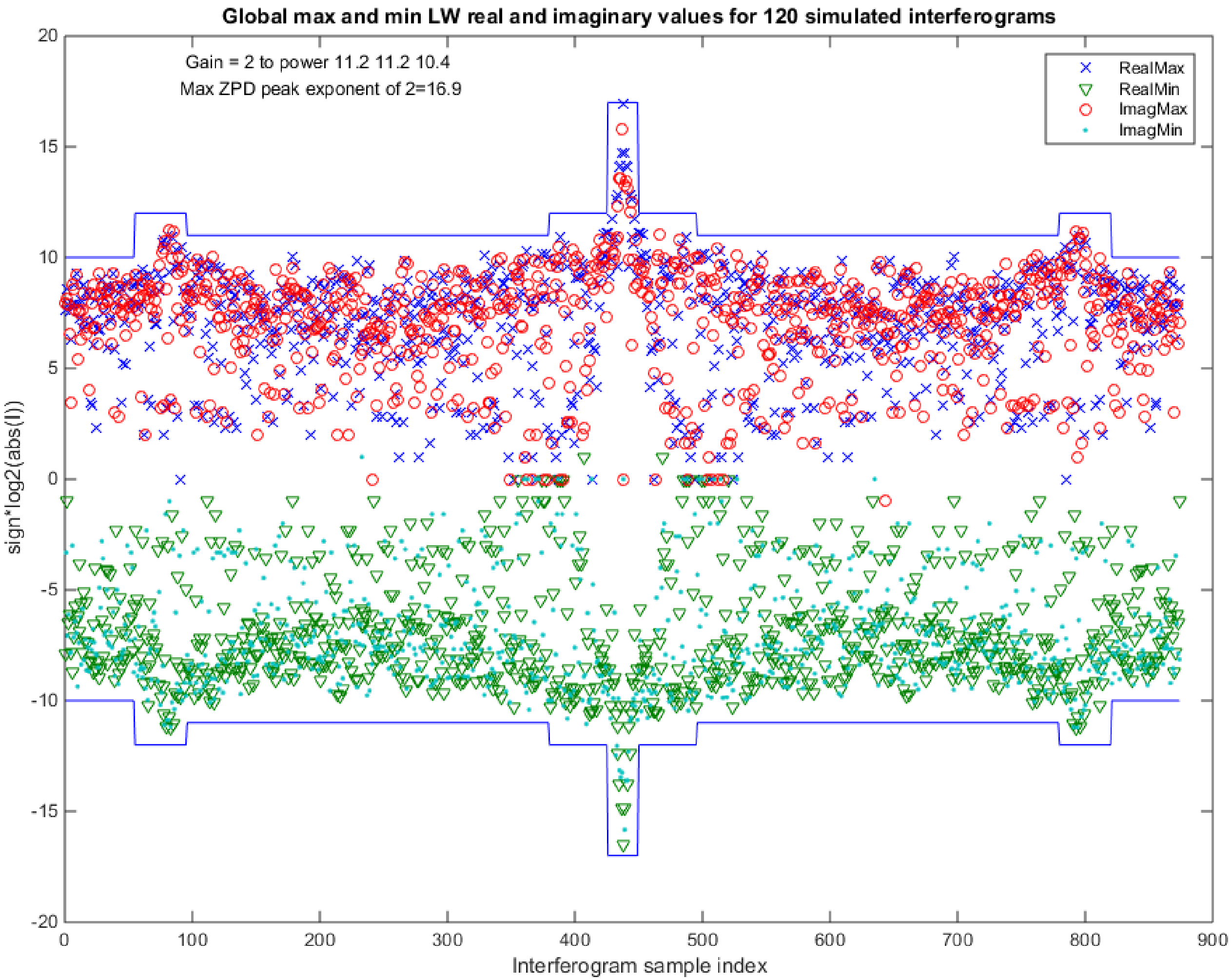

Simple algorithm comparison

- **Three options**
  - Circular filtering (ideal)
  - Non-circular FIR filtering (operational)
  - Extended length interferogram mitigation of non-circular filtering
- **Evaluation of the effects of two non-linear operations**
  - 14 bit A/D truncation
  - FIR filter output truncation
- **ISA and F transformations produce output noise that is uncorrelated with DM (truth) noise**

- **Differences in the algorithms masked by noise**
  - Averaging is required

LW NM cal – DM cal(TRUTH) for A4 algorithm

Simulation

- **Floating point**
- **FIR truncation**
- **14 bit A/D**
- **FIR truncation & 14 bit A/D**

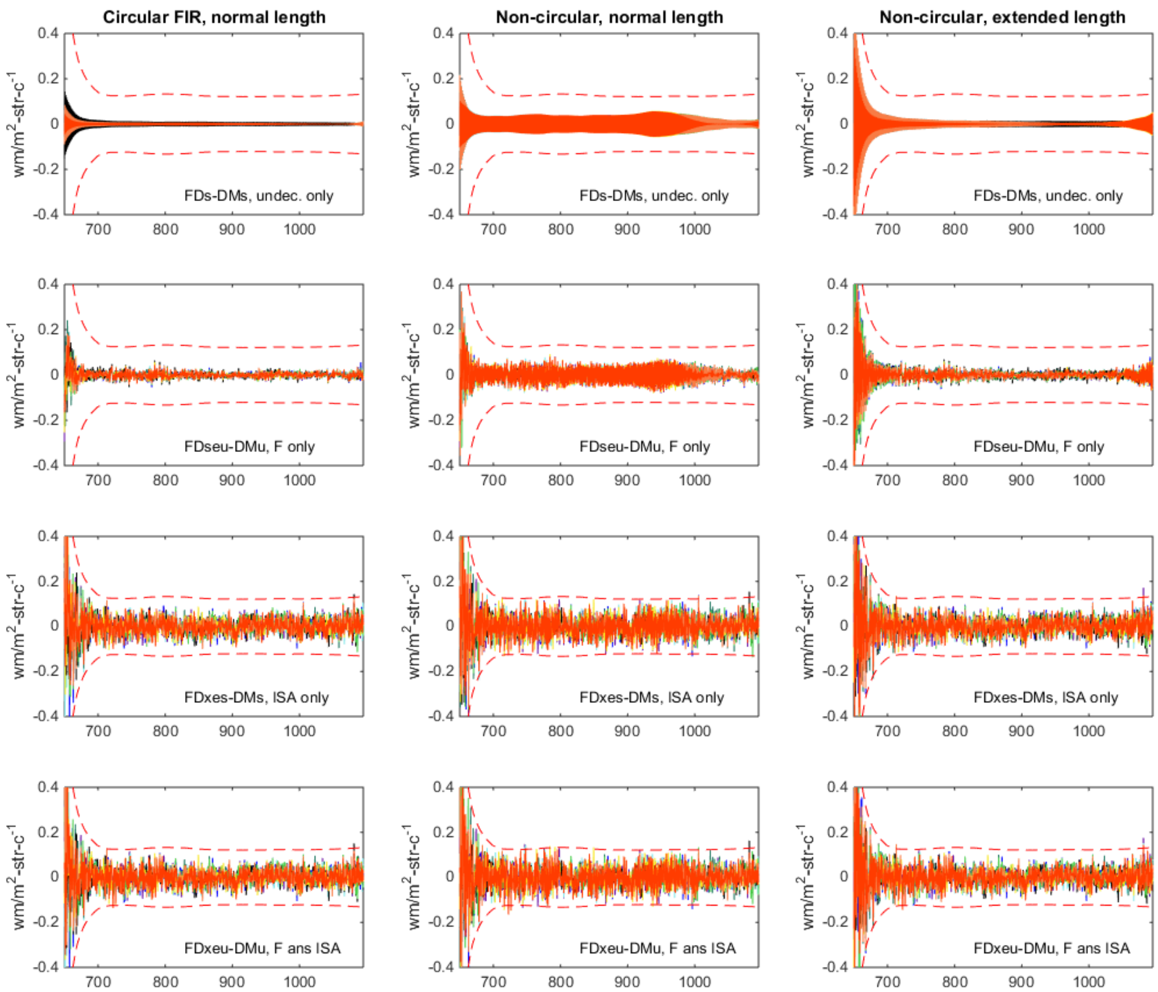

Small algorithm differences masked by truncation noise

MW NM cal – DM cal(TRUTH) for A4 algorithm

Simulation

- **Floating point**
- **FIR truncation**
- **14 bit A/D**
- **FIR truncation & 14 bit A/D**

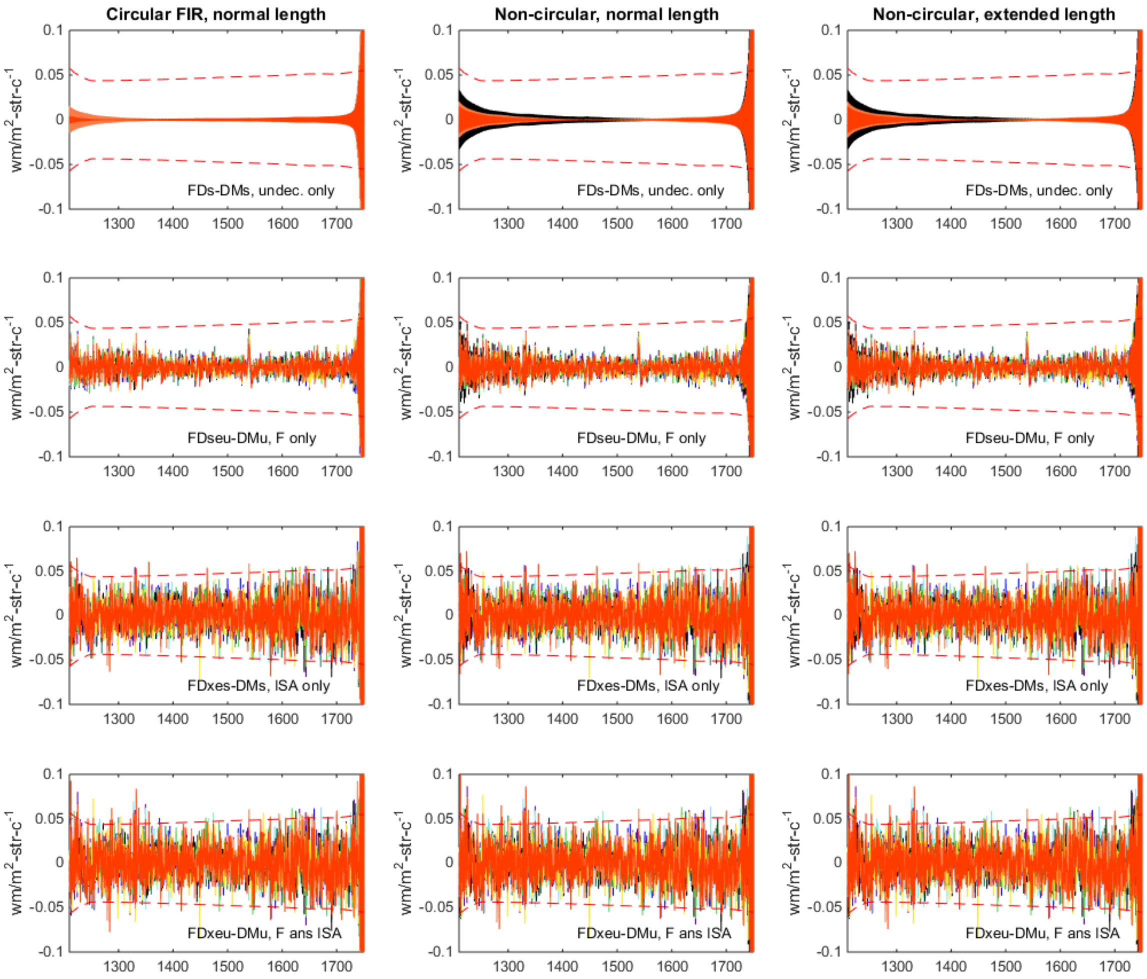

Small algorithm differences masked by truncation noise

SW NM cal – DM cal(TRUTH) for A4 algorithm

Simulation

- **Floating point**
- **FIR truncation**
- **14 bit A/D**
- **FIR truncation & 14 bit A/D**

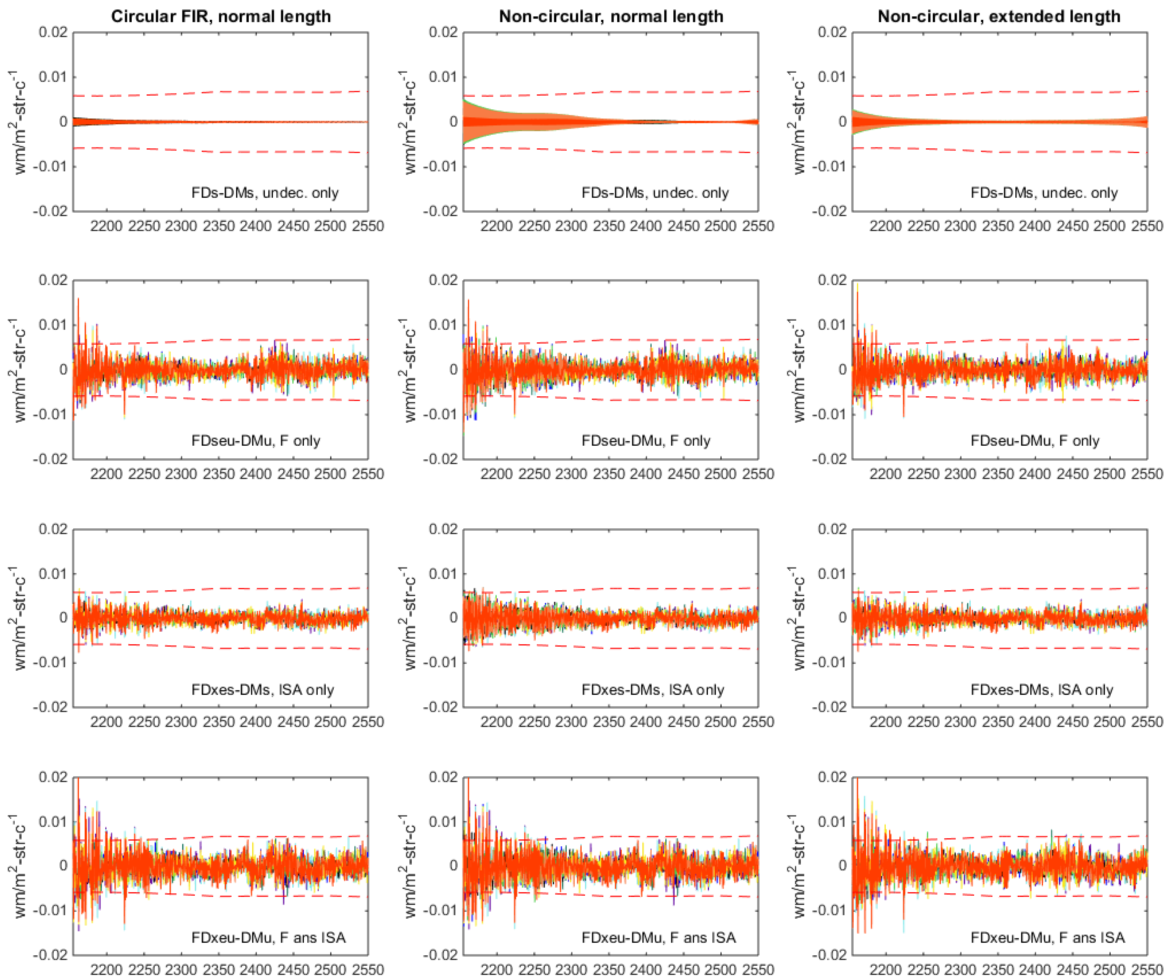

Small algorithm differences masked by truncation noise

Summary

- We can insert simulated interferograms derived from LBL spectra from NOAA88b atmospheres into operational h5 data streams.
- MATLAB code for modifying h5 files is compact and deliverable to NOAA/STAR
- Allows checking of operational algorithms with known inputs
- Various uses are being evaluated
- Algorithm comparisons below the truncation noise require averaging

CrIS on JPSS-2,3,4: Summary of instrument, bus, integration, and test changes

STAR JPSS Annual Meeting
08/09/2016

David Johnson
NASA LaRC
david.g.johnson@nasa.gov
757-864-8580

Overview

- **CrIS on JPSS-2,3,4 are intended to be copies of SNPP/J1 CrIS**
- **However, some minor changes could not be avoided, including:**
  - Vendor changes
  - Part changes due to obsolescence
  - Replacement of aging test equipment
- **Performance requirements have not changed**
  - A robust test program is in place to verify that changes will not impact performance

Instrument Changes

- **Part changes due to obsolescence include:**
  - Neon lamp
  - Metrology laser
  - More details on next slide
- **Vendor changes include:**
  - Beamsplitter coating
    - New vendor means new coating prescription but same performance requirements
  - Power supplies
    - Again, new vendor but same performance requirements
- **Changes to improve manufacturability include:**
  - Detector chip size increased to improve assembly yield
    - No change to active area diameter
  - Chamfer added to lens retainer to avoid contacting singlet
    - Corrective action following discovery of chip on J1 LW singlet

Neon lamp and Metrology laser

- **Neon lamp part obsolescence resulted in search for new supplier**
  - Testing established that new lamp meets glow stability and lifetime requirements

(Generic neon lamp image)

- **Metrology laser part obsolescence resulted in search for new supplier**
  - Testing established that new laser meets requirements for wavelength, beam quality, radiation tolerance, and mission assurance.

Instrument Test Changes

- **Bench test replaced by pre-environmental tvac test**
- **External calibration target (ECT) and control rack**
  - New ECT for reduced thermal gradients
    - Details on following slide
  - New rack for better heater control, more accurate temperature sensor readout, and improved reliability
  - NIST calibration scheduled for January 2017
- **Gas cart being rebuilt**
  - Will correct the gas pressure readout error discovered during J1 testing
- **Improvements to coregistration test setup**
  - More complete FOV mapping in less time
  - Enables early detection of obscurations or defects in detector assembly
- **EMI/EMC testing as well as vibration testing has been moved to Rochester facility**
  - Test equipment has also been consolidated in Rochester
  - Change in location only, not a test change

ECT and ST for Instrument TVAC

- **The Space Target (ST) will be unchanged from J1/SNPP**
- **Issues with current ECT:**
  - Brightness temperature gradients across the ECT aperture exceeding 150 mK were observed during J1 testing;
  - Gradient generally increased with heater power/setpoint temperature;
  - Difference between supplemental sensor temperature readings and brightness temperature also depended on heater power.
- **New ECT design:**
  - Preserves current cavity design and surface treatment;
  - Adds additional temperature sensors that are better integrated with primary plate;
  - Uses temperature-controlled fluid loop rather than LN2 radiative sink to reduce transition time and minimize heater power (and gradients) at each set point.
    - Gradients are predicted to be <10mK at all temperature setpoints.

Satellite Bus and Integration Changes

- **The bus provider for JPSS-2,3,4 has changed from Ball Aerospace to Orbital ATK**
  - The spacecraft orientation during tvac testing will change from vertical (like at launch, as at Ball) to horizontal
  - The Earth target provider for spacecraft tvac testing will also change from Ball to Orbital ATK.
    - The space target will continue to be provided by Harris
    - Requirements for the targets are unchanged
- **The ATMS scan plane will be rotated slightly in yaw relative to CrIS to provide better alignment of the geolocated footprints**
  - Geolocated crosstrack scans are currently misaligned due to the combination of the different crosstrack scan rates and the satellite ground track velocity

Current and Proposed ATMS/CrIS Alignment

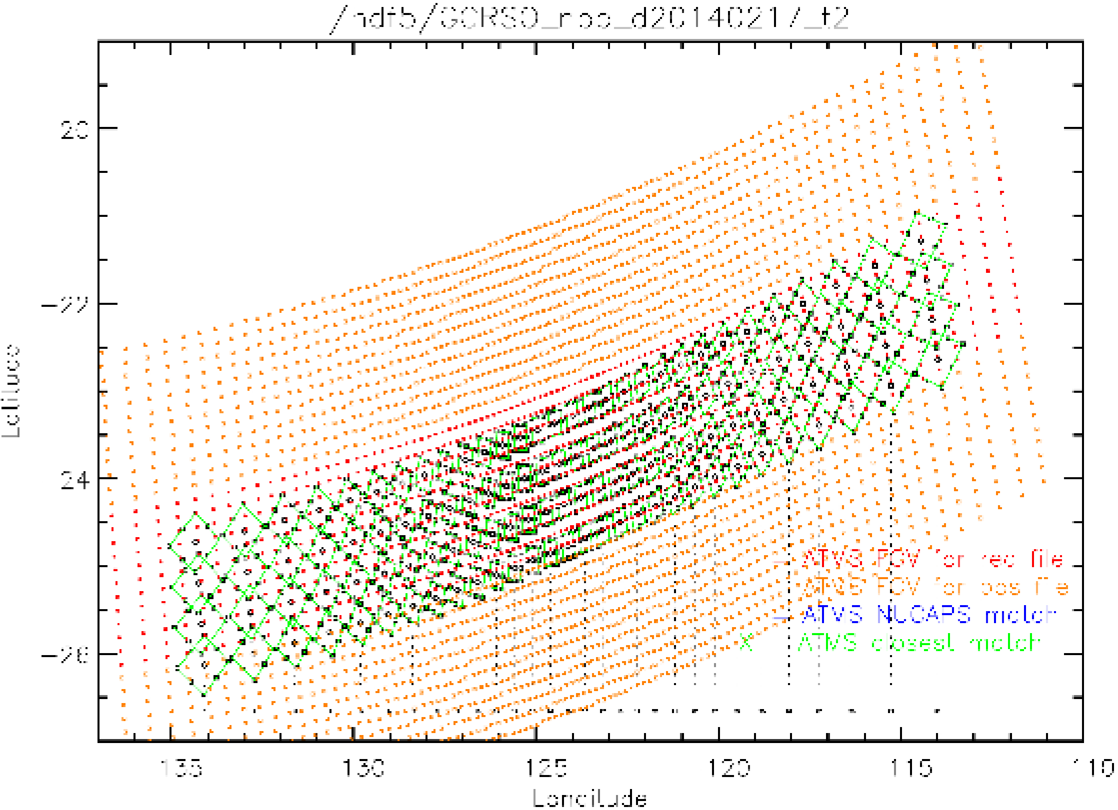

Current S-NPP (from Chris Barnet)

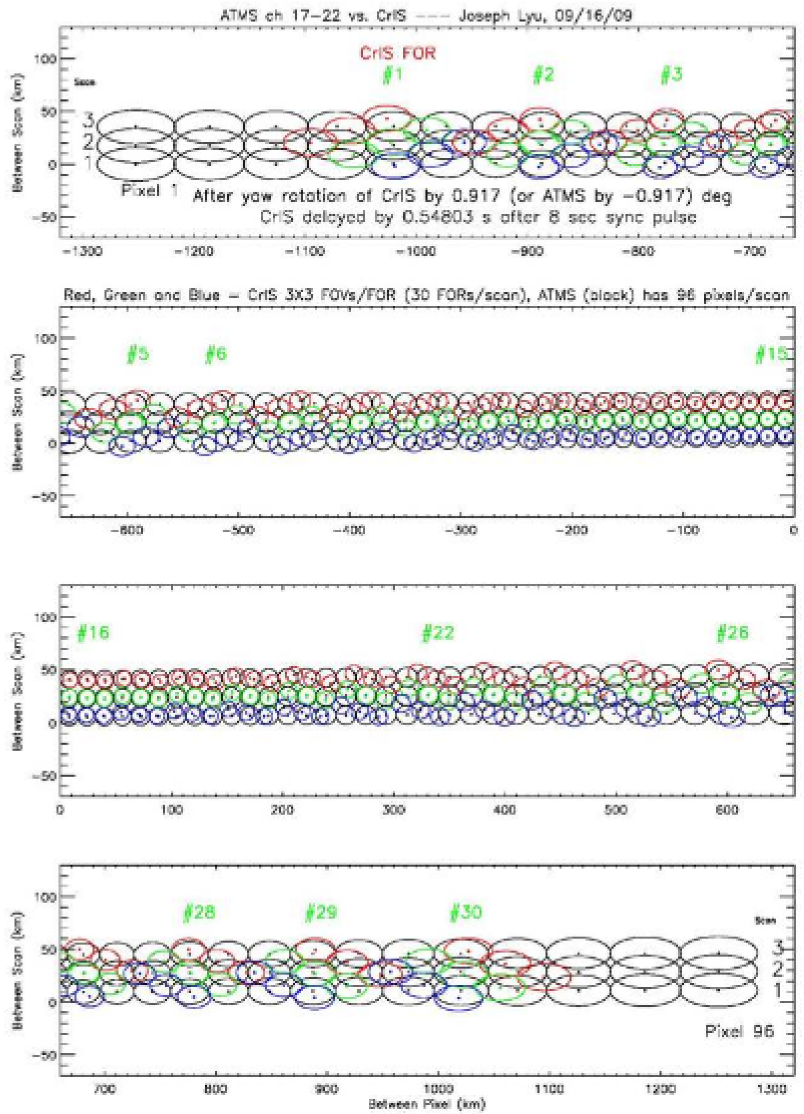

Proposed (from C-H Joseph Lyu)

J1/J2 STATUS UPDATE

JPSS-1 Test Update

- **As of 7/29, the spacecraft-level TVAC test schedule is:**
  - 8/8: Move spacecraft to TVAC chamber (with ATMS EDU unit)
  - 8/13: Start Open Door tests
  - 8/16: Close door and start TVAC
- **TVAC expected to last 50 days**
- **Tests include:**
  - Day-in-the-life testing
  - Jitter tests
  - Diagnostic mode data collection
  - Full spectral resolution diagnostic mode test
- **Two slides describing data access follow:**
  - One slides from Lisa McCormick
  - One from Leland Chemerys

Access to Test Data

- SMD data will be provided on GRAVITE for each instrument
  - Format
    - ATMS: RDR files, HDF5 wrapped CCSDS packets (.h5)
    - CERES: RDR files, HDF5 wrapped CCSDS packets (.h5)
    - CrIS: RDR files, HDF5 wrapped CCSDS packets (.h5)
    - OMPS: RDR files, HDF5 wrapped CCSDS packets (.h5)
    - VIIRS:
      - All test data: raw CCSDS format (.dat)
      - Full Swath Test data: RDR files, HDF5 wrapped CCSDS packets (.h5)
  - Frequency of data arrival
    - End of every shift (time of day not yet known)
    - BATC plans 3 shifts per 24hrs, 7days a week

- Ancillary Data (targets, event logs, etc.) provided on eRooms
  - My eRooms > Flight Integration and Test > JPSS-1 I&T > Satellite Test Ancillary Data
  - Access is Need-to-Know. BATC NDA is not required.

Processing Flow

- BATC pushes all raw SMD and HRD data to the NASA server
- The SMD files will be processed for the science team using the DRL Satellite Telemetry Processing System (STPS) software
  - DRL is the Direct Readout Lab in GSFC building 28
- Arrival of new data triggers processing of each SMD file with the STPS software
  - STPS can generate either HDF-formatted RDRs or raw CCSDS packet files for each instrument
  - An STPS config file controls the output formats
  - An iteration may be required to generate a config file that satisfies each instrument science team
    - This task is complicated a bit by non-flight APID mappings during the ground testing.

JPSS-2 CrIS Status Update

- **Subcontractors working on major subassemblies, including:**
  - Optomechanical assembly (interferometer)
  - Telescope
  - Detectors
  - Electronic Circuit Card Assemblies
- **Major project milestone dates:**
  - 7/18/2017: Pre-environmental TVAC
    - Replaced the bench test on NPP/J1
  - 4/1/2018: Full TVAC performance testing
  - 5/3/2018: Pre-ship review

ATMS SDR SCIENCE REPORT

Fuzhong Weng and Ninghai Sun

NOAAA/STAR

Outline

- Cal/Val Team Members
- Sensor/Algorithm Overview
- S-NPP Product(s) Overview
- JPSS-1 Readiness
- Summary and Path Forward

Cal/Val Team Members

PI	Organization	Team Members	Roles and Responsibilities
Fuzhong Weng	NOAA/STAR	Neal Baker, Lin Lin, Wanchun Chen	ATMS SDR Lead: Budget and execution, strategic science direction, and oversight the SDR team Cal/Val tasks, reprocessing
Ninghai Sun	NOAA/STAR	Khalil Ahmad	ATMS SDR technical lead for science coordination, research to operation transition, ICVS monitoring
Xiaolei Zou	UMD/ESSIC	Yuan Ma, Xiaoxu Tian,	ATMS SDR destripping, RFI interference
Hu Yang	UMD/ESSIC	Jun Zhou,Xu Yang	ATMS SDR calibration algorithm development, improvement, and validation
Ed Kim	NASA/GSFC	Craig Smith, Joseph Lyu	ATMS instrument team for sensor pre- and post-launch characterization
Vince Leslie	MIT/LL		Prelaunch ATMS sensor characterization
Wael Ibrahim	Raytheon		IDPS operational ground processing system
Kent Anderson	NGES		NGES ATMS instrument calibration
Wesley Berg	CSU		ATMMS cross calibration

ATMS Sensor Overview

Ch	Channel Central Freq. (MHz)	Polarization	Bandwidth Max. (MHz)	Frequency Stability (MHz)	Calibration Accuracy (K)	Nonlinearity Max. (K)	NEΔT (K)	3-dB Bandwidth (deg)	Heritage Instrument	Nadir Weighting Function Peak & Primary Applications [1]
1	23800	QV	270	10	1.0	0.3	0.5	5.2	AMSU-A2	Surface & TPW, CLW, Ts, Es[2]
2	31400	QV	180	10	1.0	0.4	0.6	5.2	AMSU-A2	Surface & TPW, CLW, Ts, Es
3	50300	QH	180	10	0.75	0.4	0.7	2.2	AMSU-A1-2	Surface &Ts, Es
4	51760	QH	400	5	0.75	0.4	0.5	2.2		950 mb&Atmos Temp
5	52800	QH	400	5	0.75	0.4	0.5	2.2	AMSU-A1-2	850 mb&Atmos Temp
6	53596±115	QH	170	5	0.75	0.4	0.5	2.2	AMSU-A1-2	700 mb&&Atmos Temp
7	54400	QH	400	5	0.75	0.4	0.5	2.2	AMSU-A1-1	400 mb&&Atmos Temp
8	54940	QH	400	10	0.75	0.4	0.5	2.2	AMSU-A1-1	250 mb&&Atmos Temp
9	55500	QH	330	10	0.75	0.4	0.5	2.2	AMSU-A1-2	180mb&Atmos Temp
10	57290.344(f_o)	QH	330	0.5	0.75	0.4	0.75	2.2	AMSU-A1-1	90 mb&Atmos Temp
11	f_o± 217	QH	78	0.5	0.75	0.4	1.0	2.2	AMSU-A1-1	50 mb&Atmos Temp
12	f_o±322.2±48	QH	36	1.2	0.75	0.4	1.0	2.2	AMSU-A1-1	25 mb&Atmos Temp
13	f_o±322.2±22	QH	16	1.6	0.75	0.4	1.5	2.2	AMSU-A1-1	10 mb&Atmos Temp
14	f_o±322.2±10	QH	8	0.5	0.75	0.4	2.2	2.2	AMSU-A1-1	6 mb&Atmos Temp
15	f_o±322.2±4.5	QH	3	0.5	0.75	0.4	3.6	2.2	AMSU-A1-1	3 mb&Atmos Temp
16	88200	QV	2000	200	1.0	0.4	0.3	2.2	89000	Surface &Vapor, Cloud, Precip
17	165500	QH	3000	200	1.0	0.4	0.6	1.1	157000	Surface &Vapor, Cloud, Precip
18	183310±7000	QH	2000	30	1.0	0.4	0.8	1.1	AMSU-B	950mb&Vapor, Cloud, Precip
19	183310±4500	QH	2000	30	1.0	0.4	0.8	1.1		850mb&Atmos Vapor
20	183310±3000	QH	1000	30	1.0	0.4	0.8	1.1	AMSU-B/MHS	500mb&Atmos Vapor
21	183310±1800	QH	1000	30	1.0	0.4	0.8	1.1		400mb&Atmos Vapor
22	183310±1000	QH	500	30	1.0	0.4	0.9	1.1	AMSU-B/MHS	300mb&Atmos Vapor

1. Weighting function peak is computed from the standard atmosphere, 2. TPW: Total Precipitable Water, CLW: Cloud Liquid Water, Ts: Land Surface Temp, Es: Land Surface Emissivity.

ATMS Sensor Overview

- 22 channels measuring from surface to upper atmosphere for temperature and water vapor profiling
- Scan swath: 2700 km
- Earth FOVs per scan: 98
- Scan angle range: 52.3 degree

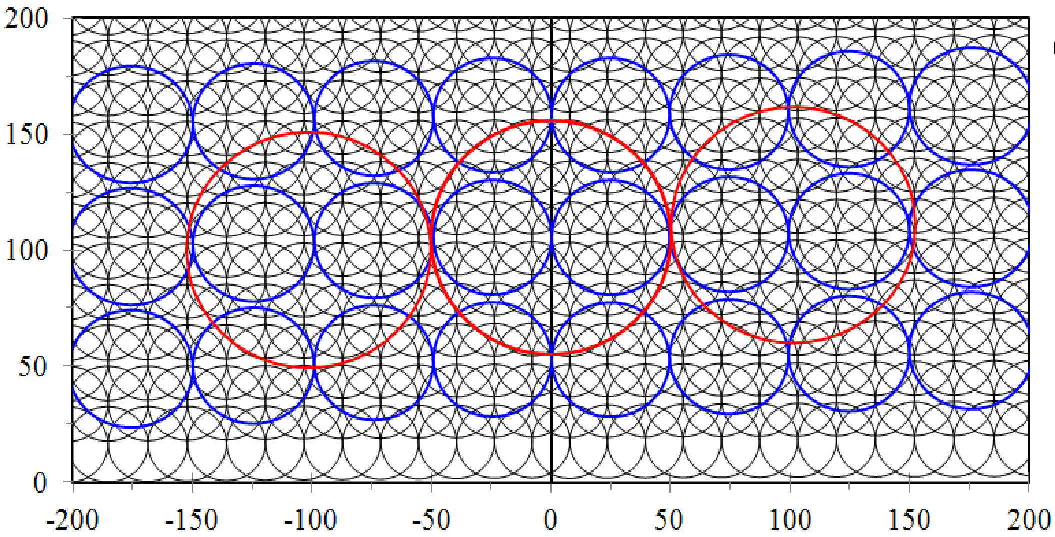

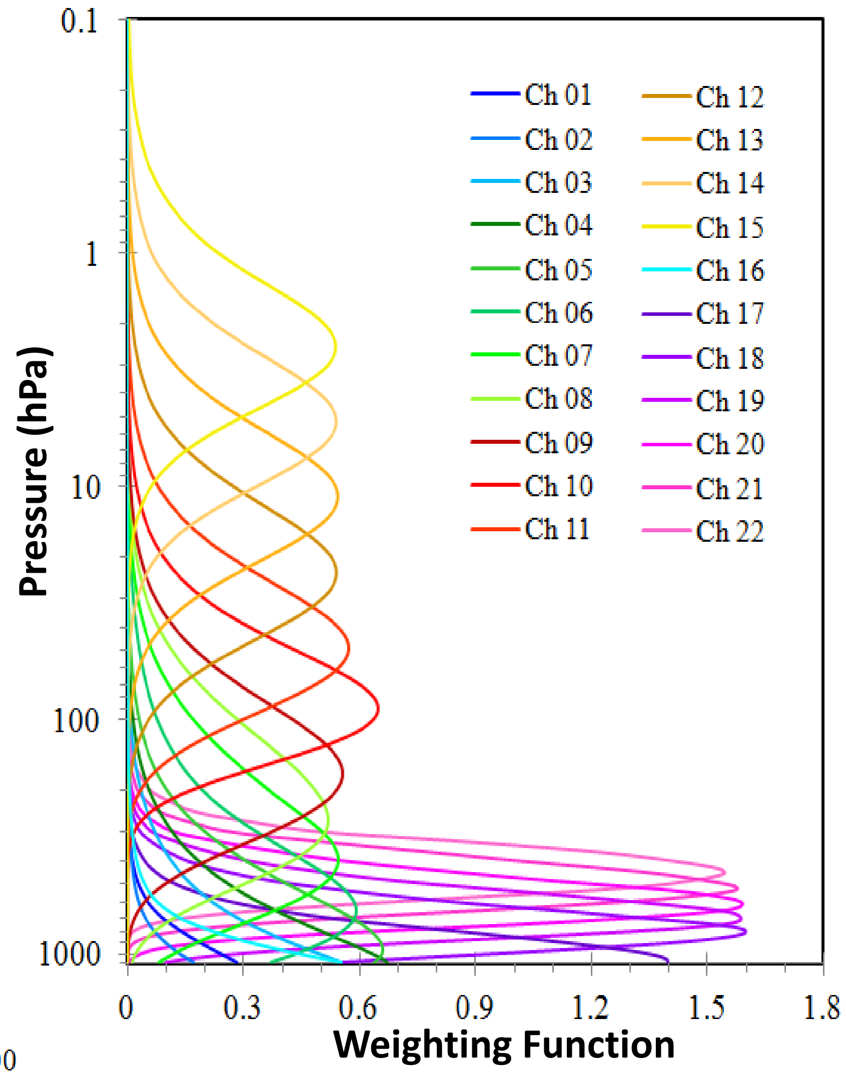

Suomi NPP ATMS On-orbit Performance

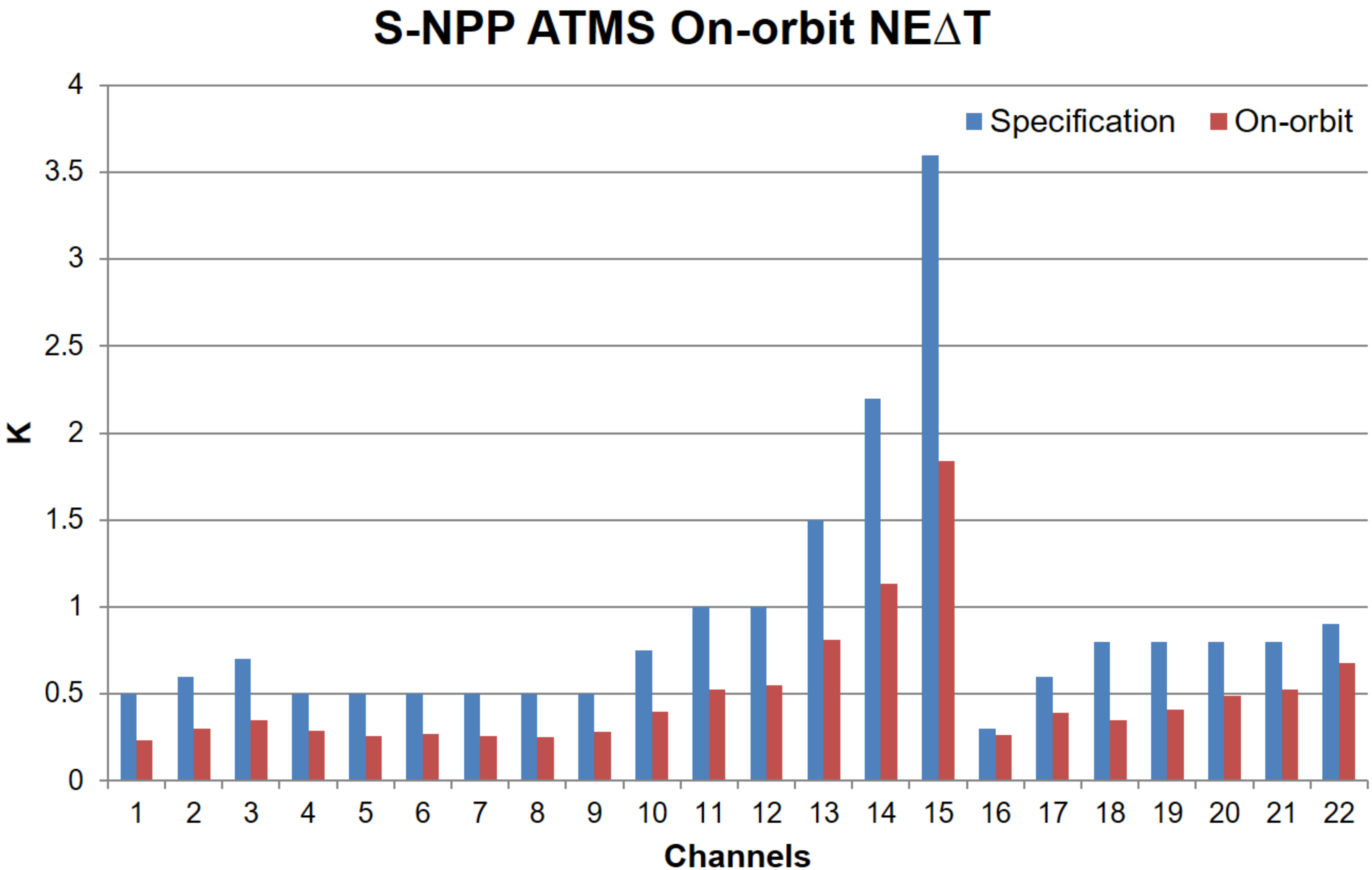

Suomi NPP ATMS all channel noise meets the requirement with margins

Suomi NPP ATMS On-orbit Performance

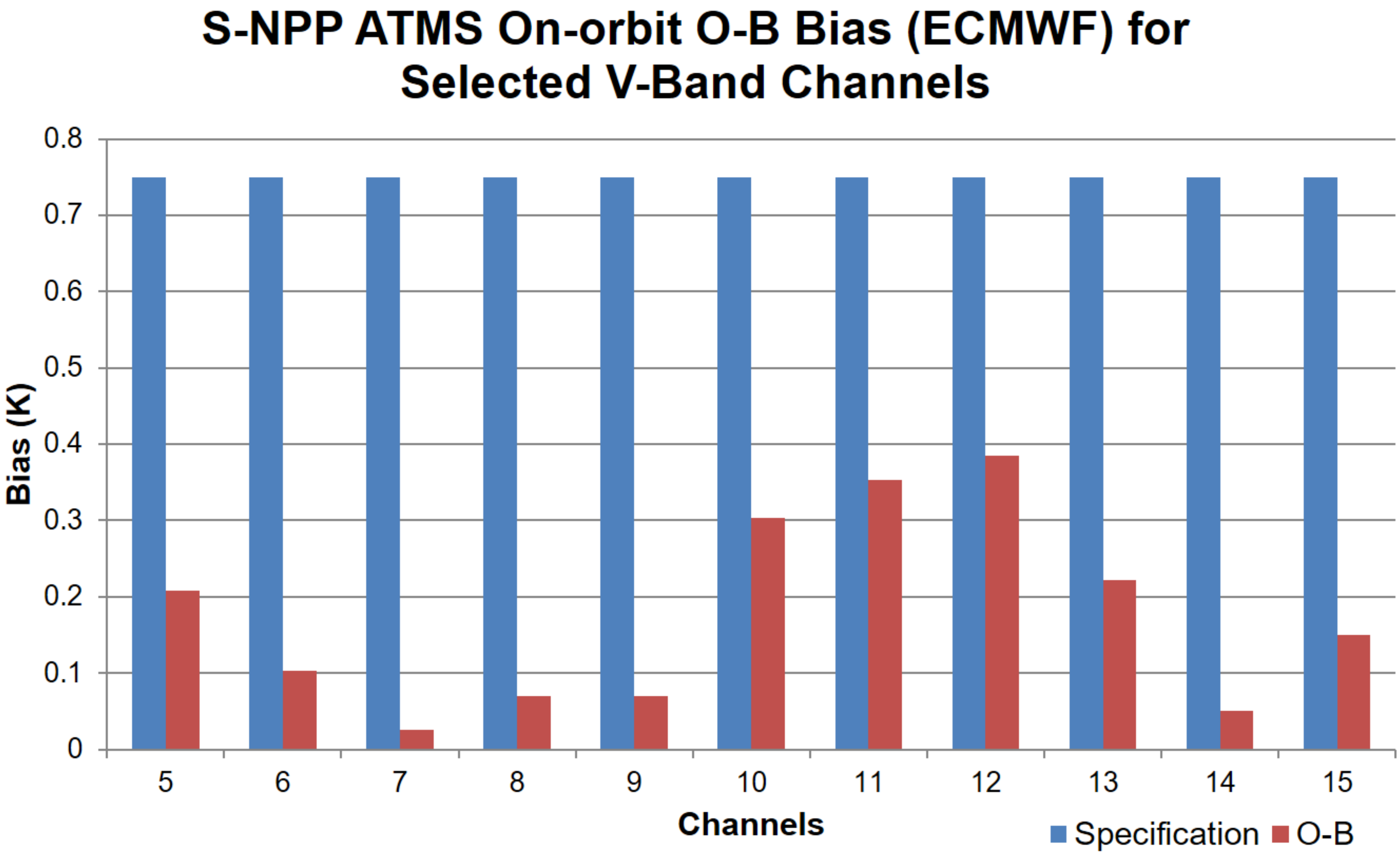

Suomi NPP ATMS on-orbit absolute bias (OBS-RTM) meet the requirement

Suomi NPP ATMS On-orbit Performance

Channel	Euler Angles (degree)			Ground Geolocation Error (km)					
				In-Track			Cross-Track		
	Roll	Pitch	Yaw	FOV Index=1	FOV Index=48	FOV Index=96	FOV Index=1	FOV Index=48	FOV Index=96
1	-0.13	0.21	-0.037	-0.058	-2.8	-5.6	-9.5	-2.3	-8.3
2	0.089	0.29	0.042	-6.9	-4.4	-3.3	2.8	0.76	5.4
3	-0.1	0.098	-0.17	4.0	-1.2	-6.4	-6.0	-1.7	-5.9
16	-0.065	-0.098	0.0053	2.5	1.5	1.2	-3.2	-0.76	-4.0

Ch.1 Ground Geolocation Error

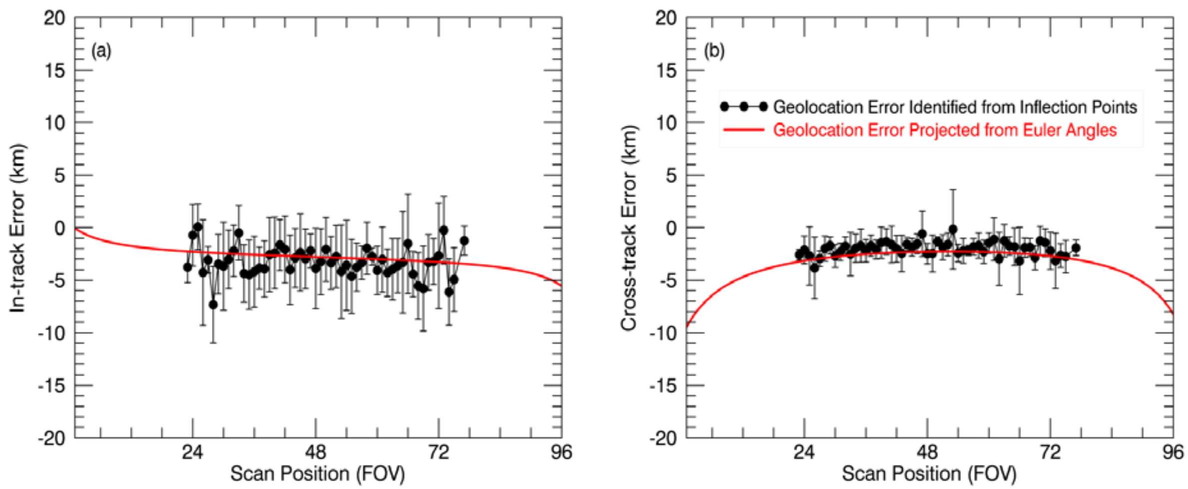

Suomi NPP ATMS On-orbit Performance

ATMS scan drive main motor current major spikes detected

- Instrument temperature increased
- Scan angle shift observed after SD motor current spikes but still well below requirements
- Once per day scan reversal implemented from August 24, 2015
- Once per orbit scan reversal implemented from July 25, 2016 (staggering configuration among consecutive orbits)
- ATMS put in safe mode due to 1553 issue during once per day reversal
- Twice per orbit reversal (staggering configuration near north and south pole) to be implemented soon

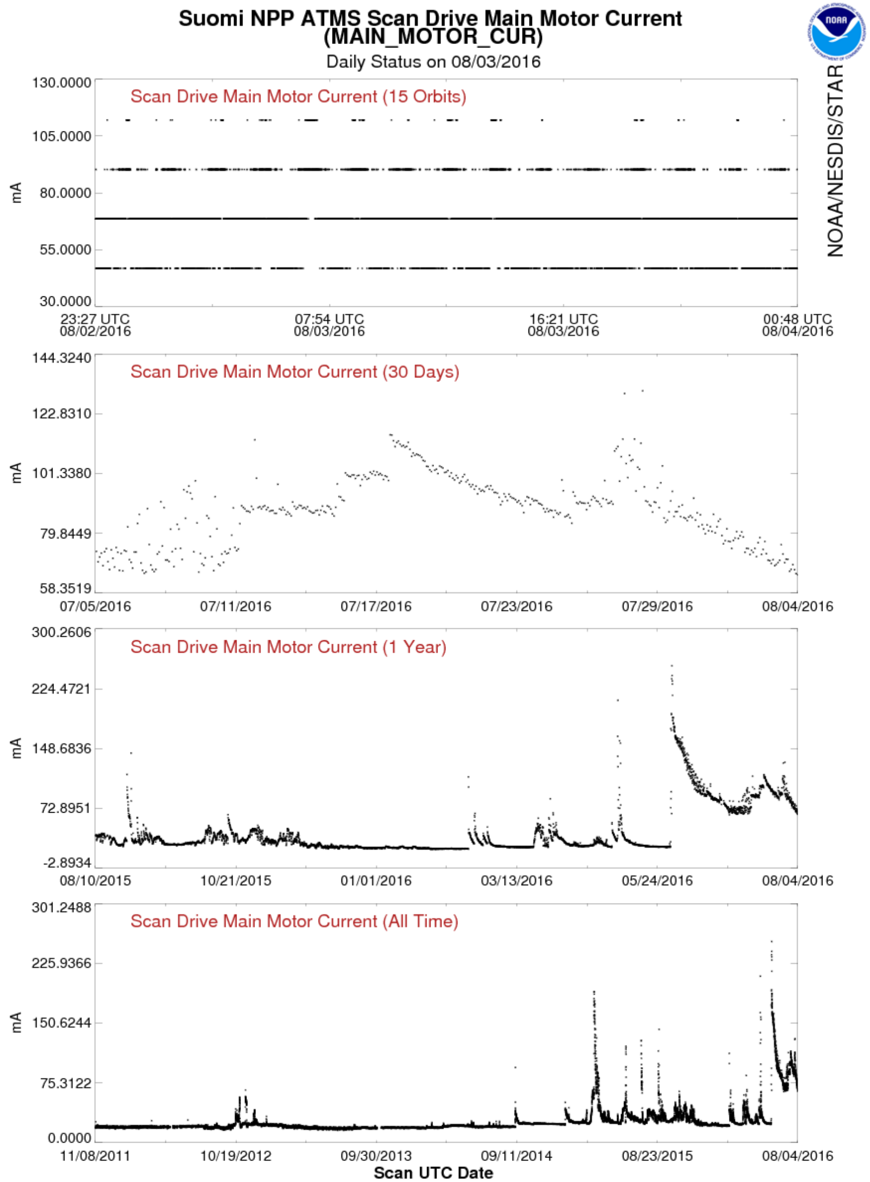

ATMS Scan Reversal Scheme Study

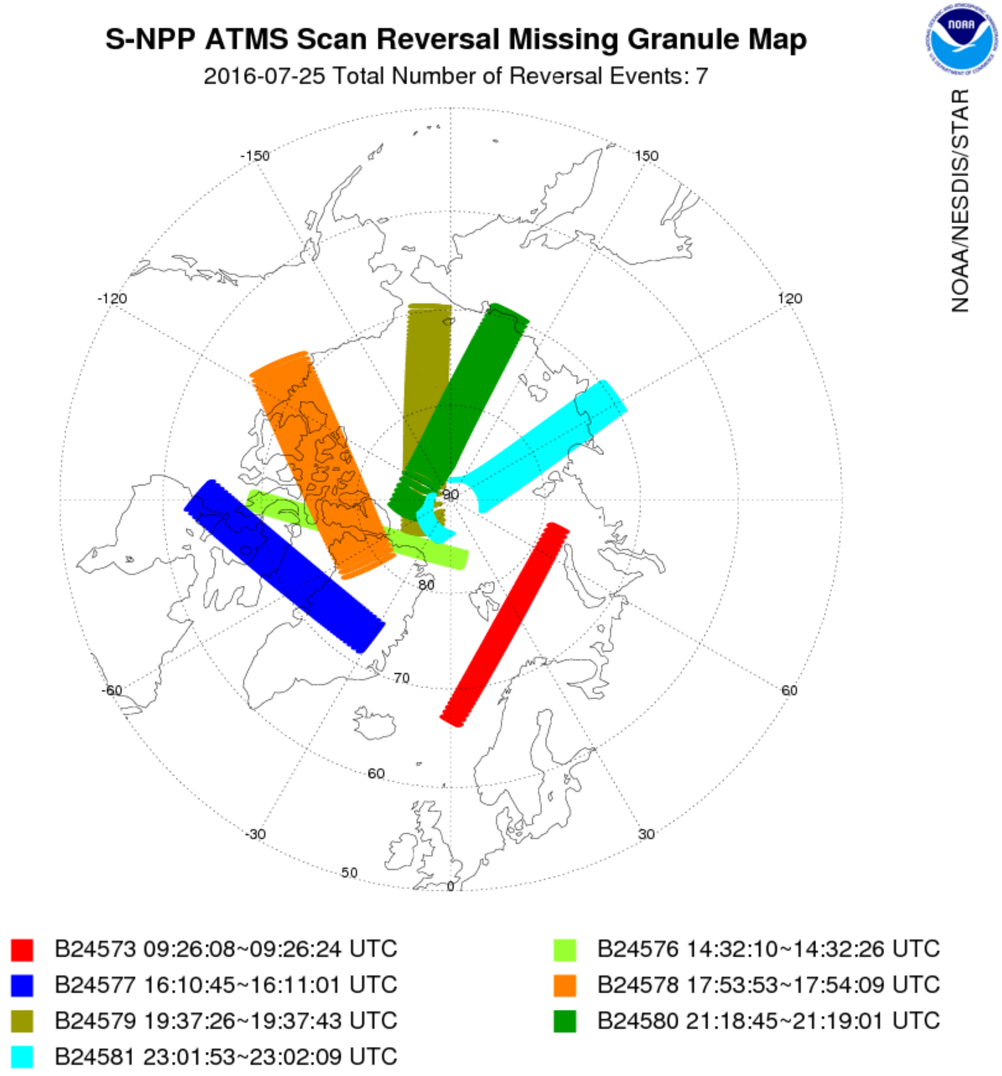

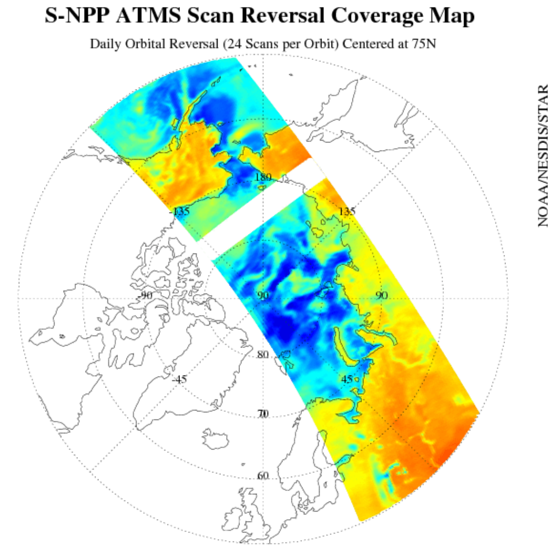

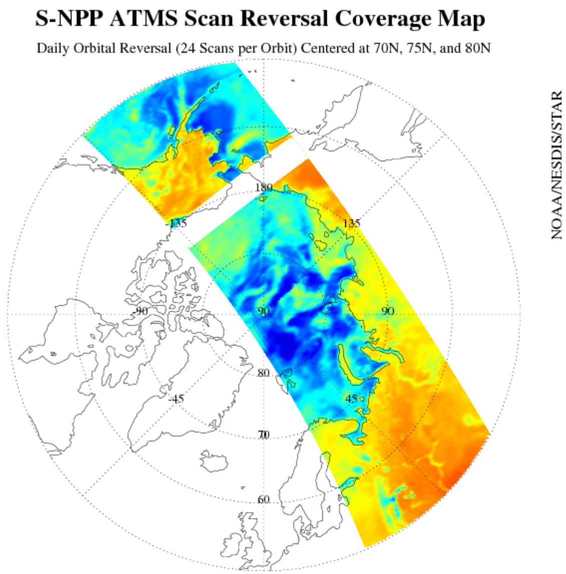

ATMS Algorithm Overview

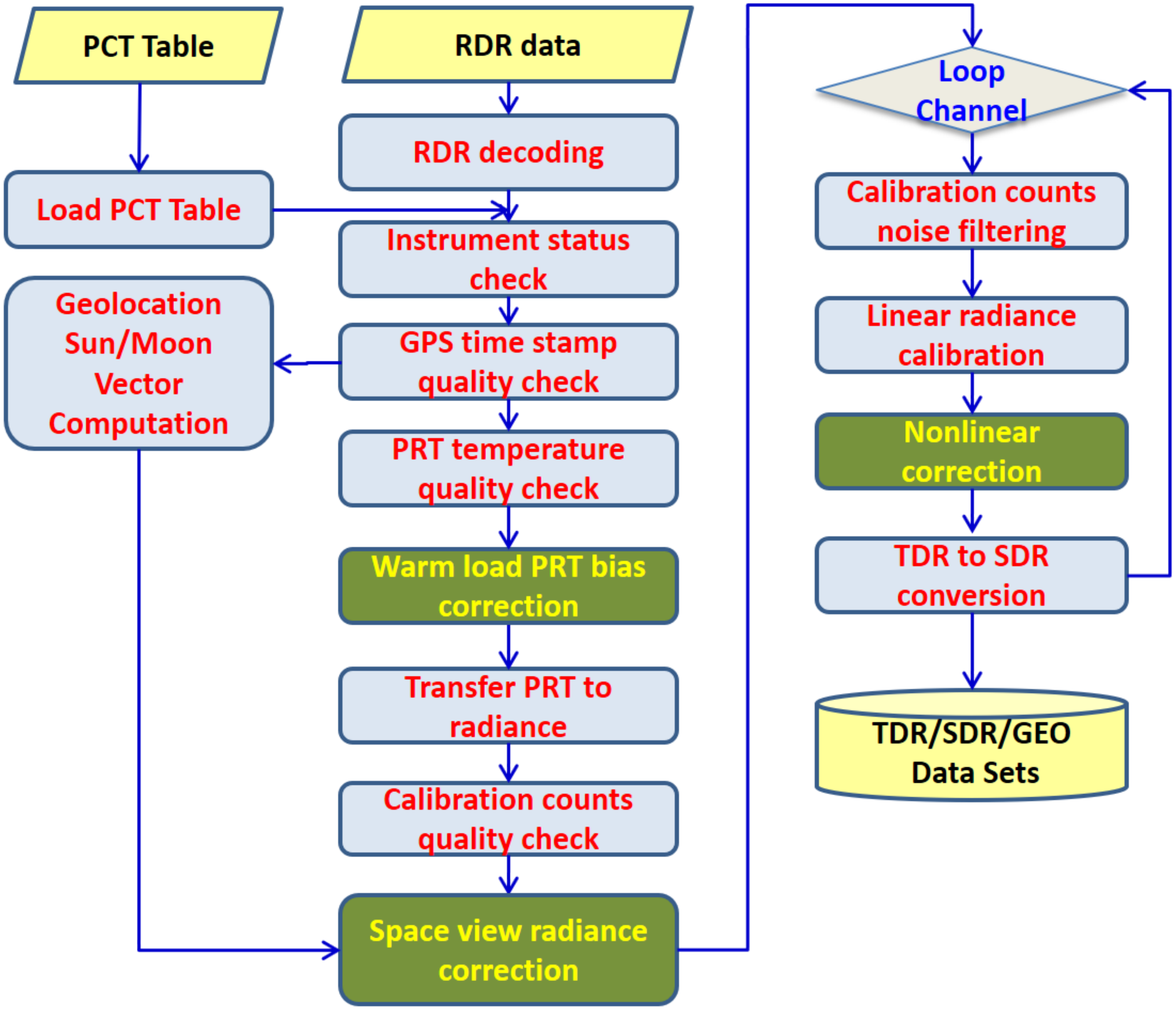

- Radiation from calibration targets are calculated as radiance instead of brightness temperature
- Lunar contamination correction is included in space view radiance correction
- Nonlinearity correction is based on "μ" parameter derived from TVAC
- Brightness temperature is computed from full Planck function in radiance space
- Error budget in calibration are traceable

ATMS Algorithm Overview

SNPP Launch
Since Oct. 28, 2011

- Mx5.0 — 2011-10-28
- Mx5.1 — 2011-12-09
  - Updated ATMS PCT on data range

Beta
Since Apr. 19, 2012

- Mx6.0(6.1/6.2) — 2012-08-09
- Mx6.3(6.4) — 2012-10-15
  - Updated ATMS PCT on TDR to SDR conversion

Provisional
Since Jan. 31, 2013

- Mx6.6 — 2013-02-28
- Mx6.7 — 2013-03-14
- Mx7.0(7.1) — 2013-07-10
- Mx7.2 — 2013-08-20
- Mx8.0 — 2013-11-14

Validated
Since Feb. 20, 2014

- Mx8.1(8.2) — 2014-02-20
  - Fixed 1958 issue
- Mx8.3 — 2014-03-18
  - Updated lunar intrusion correction
- Mx8.4 — 2014-05-22
  - Updated ATMS PCT on warm target range
- Mx8.5 — 2014-08-13
- Mx8.6 — 2014-11-21
  - Updated CMN Geo on lunar intrusion flag
- Mx8.7 — 2014-12-17
- Mx8.8 — 2015-03-06
- Mx8.10 — 2015-06-22
- Mx8.11 — 2015-12-17
  - Updated data gap QF

ATMS Algorithm Overview

- Full radiance process has been tested in Advanced Radiance Transformation System (ARTS)
- FRP code update for IDPS, as well as associated PCT, has been approved for operational implementation

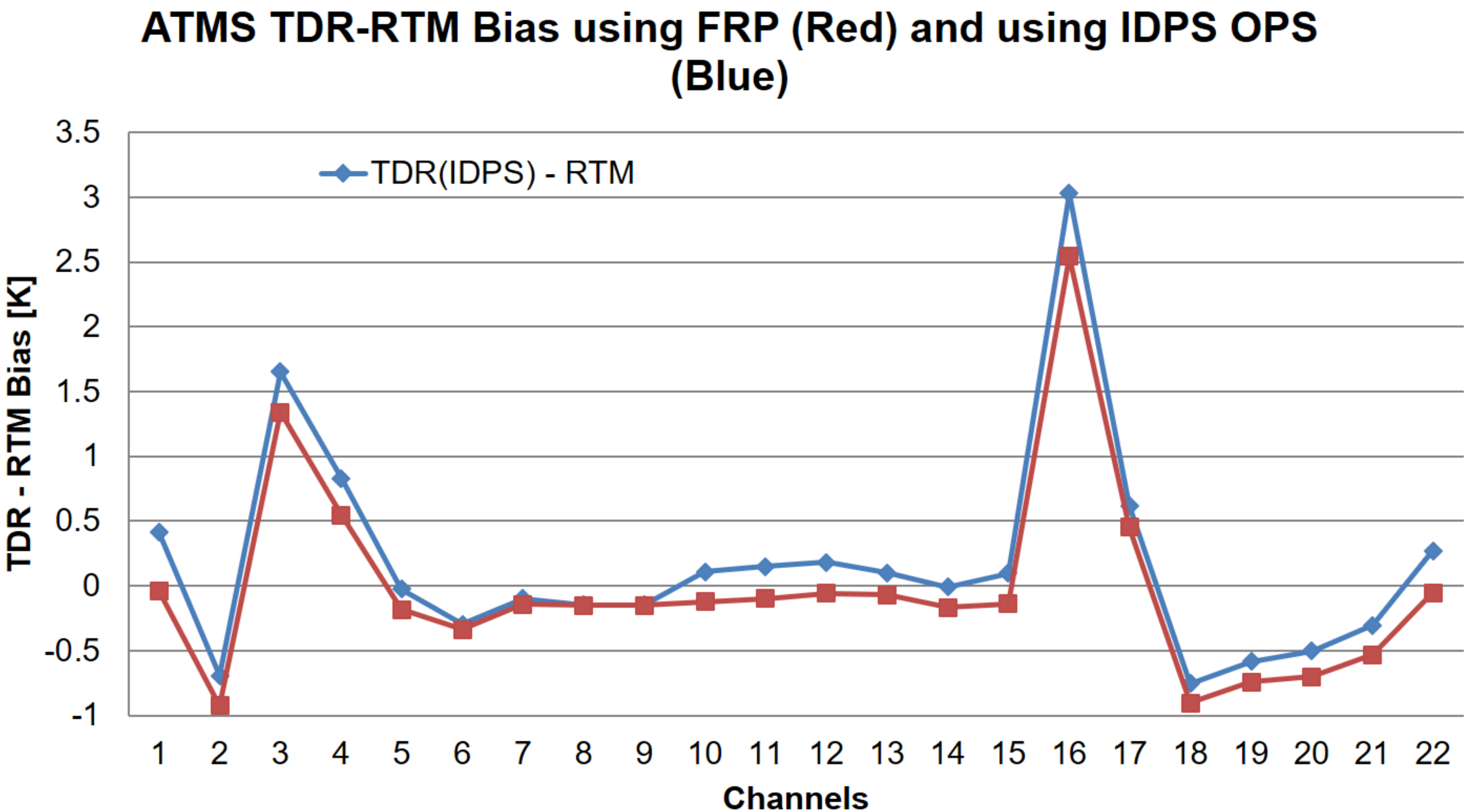

ATMS Algorithm Overview

Channel	NEDT (K)		Allan Deviation (K)	
	Before	After	Before	After
1	0.3490	0.3256	0.2324	0.2171
2	0.3977	0.3593	0.3052	0.2843
3	0.3945	0.3464	0.3473	0.3248
4	0.3279	0.2883	0.2772	0.2581
5	0.3232	0.2871	0.2603	0.2422
6	0.3433	0.3069	0.2714	0.2526
7	0.3518	0.3201	0.2559	0.2382
8	0.3453	0.3138	0.2518	0.2345
9	0.3421	0.3046	0.2816	0.2628
10	0.4542	0.3968	0.3981	0.3716
11	0.5675	0.4900	0.5277	0.4922
12	0.6140	0.5365	0.5534	0.5174
13	0.8718	0.7527	0.8123	0.7593
14	1.1849	1.0179	1.1479	1.0727
15	1.8476	1.5651	1.8319	1.7110
16	0.3914	0.3578	0.2692	0.2501
17	0.9237	0.8865	0.3954	0.3650
18	0.5496	0.5103	0.3479	0.3230
19	0.6637	0.6149	0.4041	0.3740
20	0.7636	0.7039	0.4859	0.4508
21	0.8862	0.8202	0.5239	0.4848
22	1.1194	1.0337	0.6712	0.6217

- Channel noise reduced after applying striping mitigation algorithm
- 45-day de-striping BUFR data generated for NWP impact study

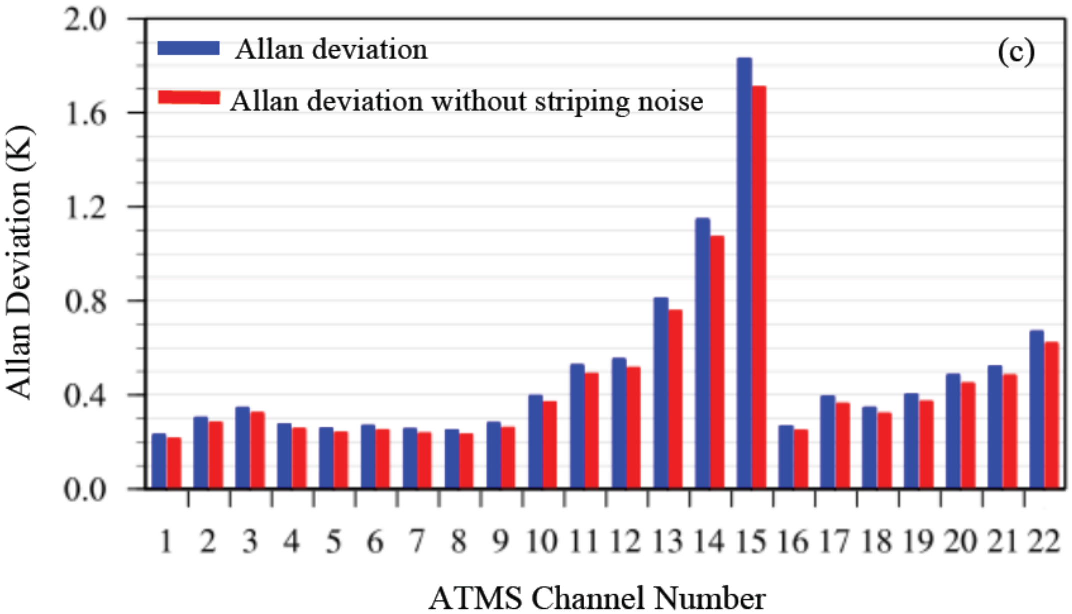

Qin, Z., X. Zou and F. Weng, 2013: Analysis of ATMS and AMSU striping noise from their earth scene observations. *J. Geophy. Res.*, 118, 13,214-13,229, doi: 10.1002/ 2013JD020399

Ma, Y. and X. Zou, 2015: Optimal filters for striping noise mitigation within ATMS calibration counts. *IEEE Trans. Geo. Remote Sensing*, (submitted)

Suomi NPP ATMS Reprocessing

Major updates in S-NPP ATMS Reprocessing

- Calibration algorithm upgraded from R-J approximation based to radiance based
  - Update non-linearity correction coefficients using radiance calibration algorithm
  - Reduce TDR values systematically

- Calibration target smoothing method unified to boxcar
  - Change striping pattern for OPS data using triangular smoothing method prior to October 2012

- Degraded TDR regenerated using updated processing coefficients table

- Lunar intrusion correction applied to life time ATMS TDR
  - Quality flag triggered locations
  - TDR correction updated

Suomi NPP ATMS Reprocessing

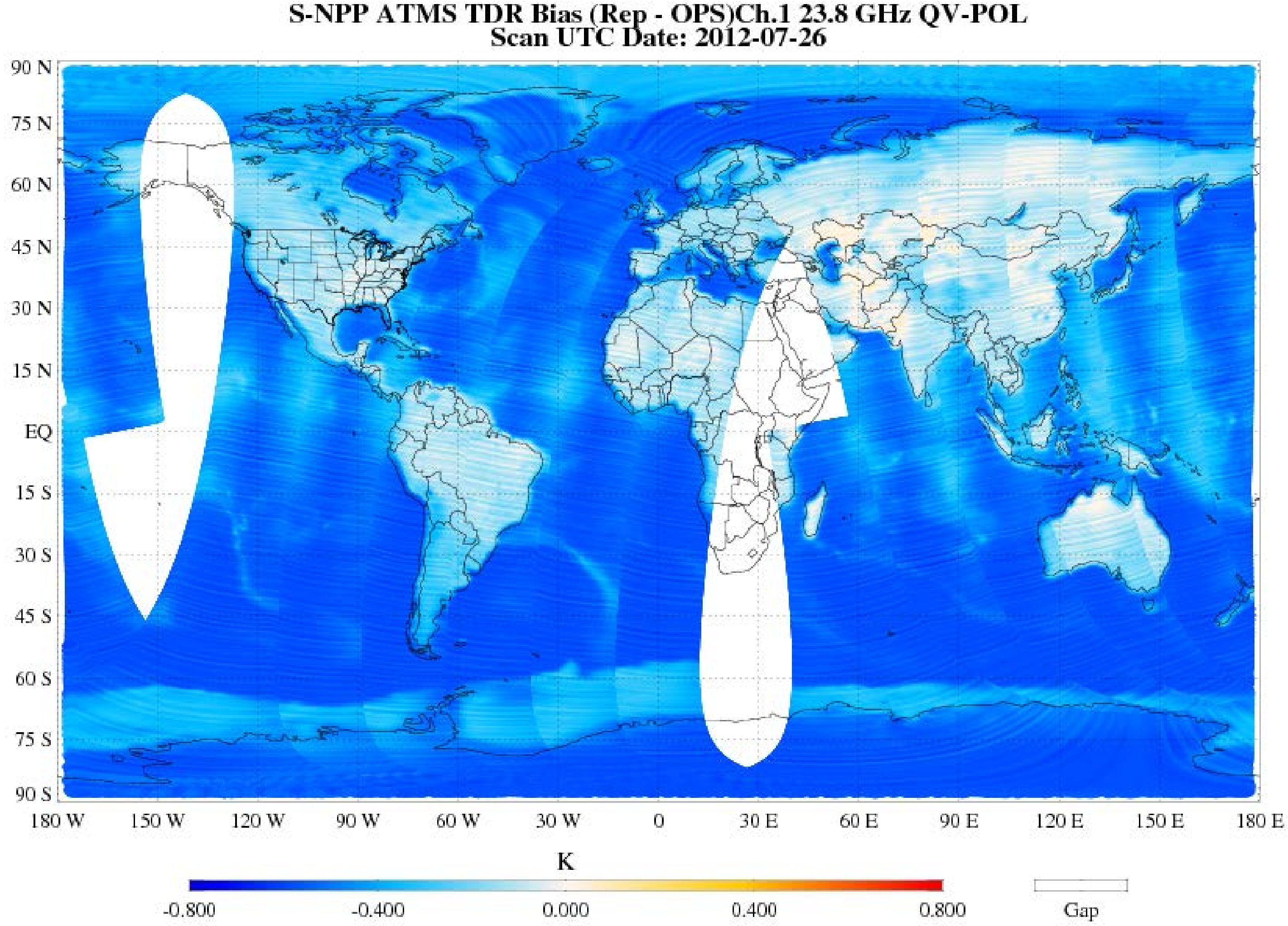

Striping pattern is caused by different smoothing methods, triangular v.s. boxcar

Suomi NPP ATMS Reprocessing

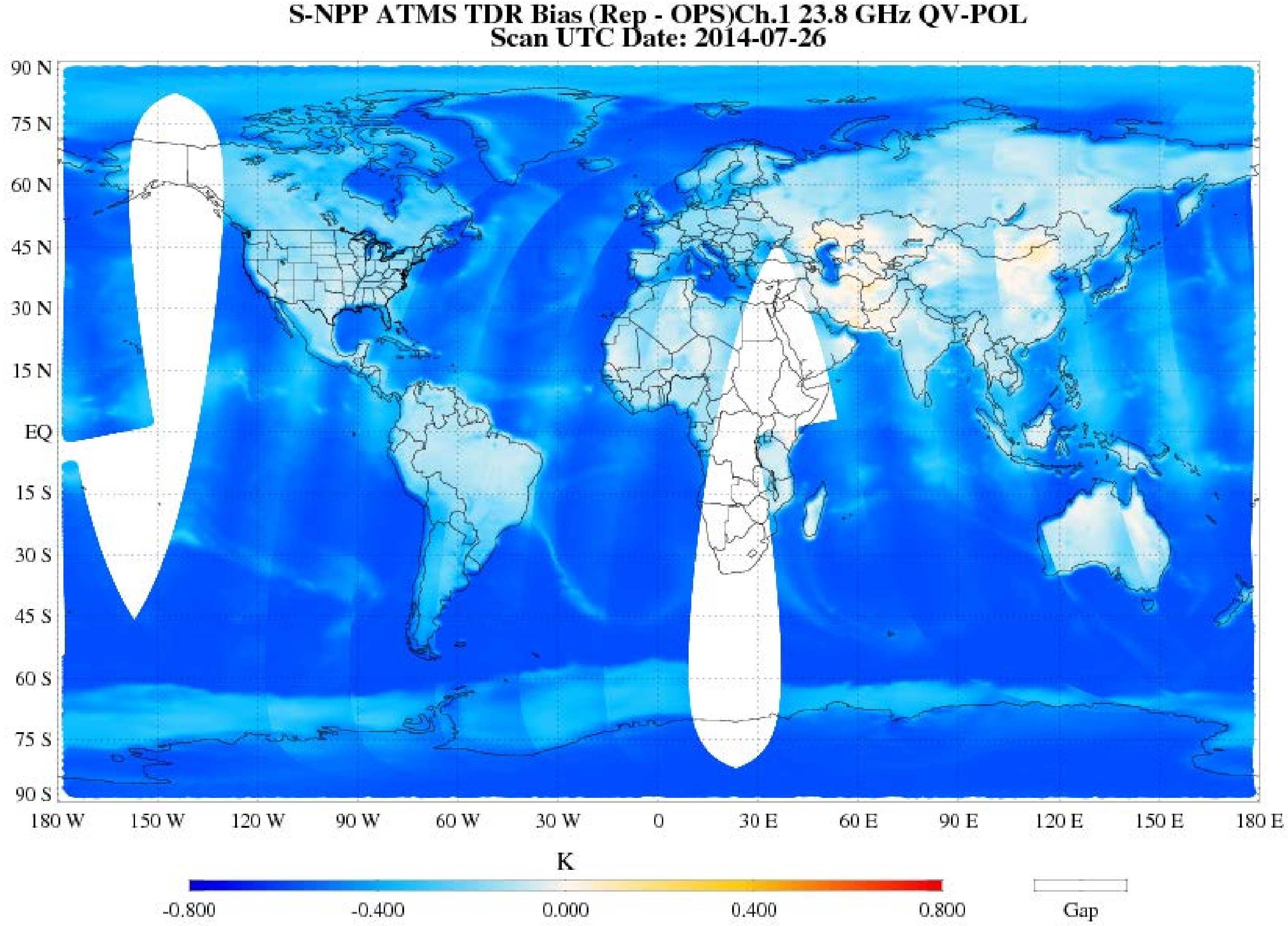

No striping after October 2012 due to the same smoothing method (boxcar) applied

Suomi NPP ATMS Reprocessing

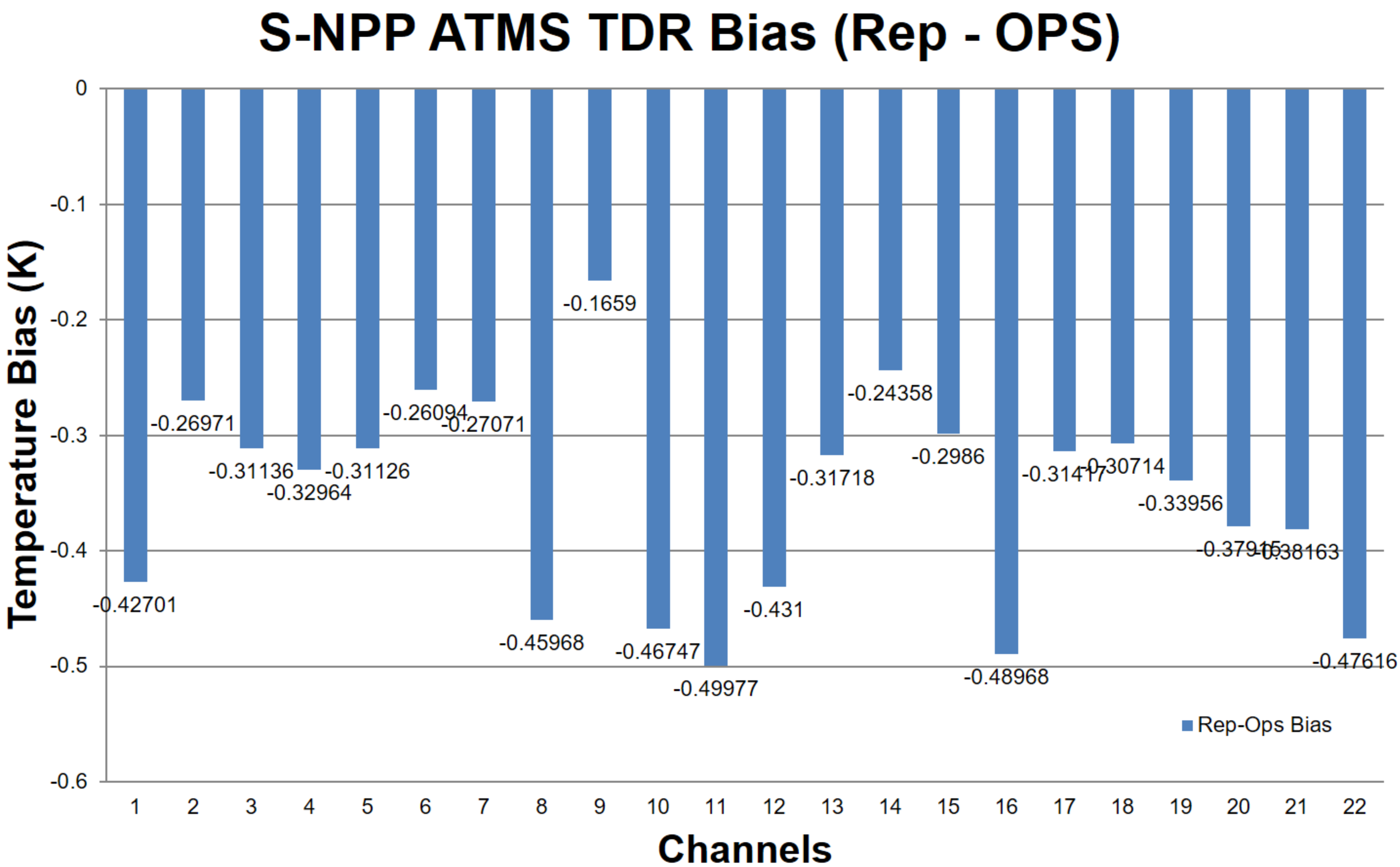

Suomi NPP ATMS Reprocessing

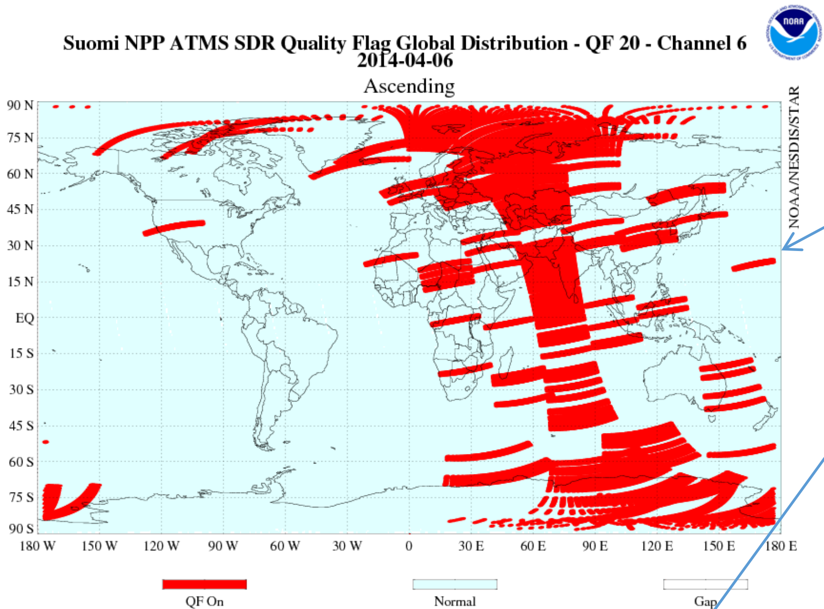

Quality flag triggered before PCT update

Quality flag off after update of PCT

TDR bias before and after PCT update

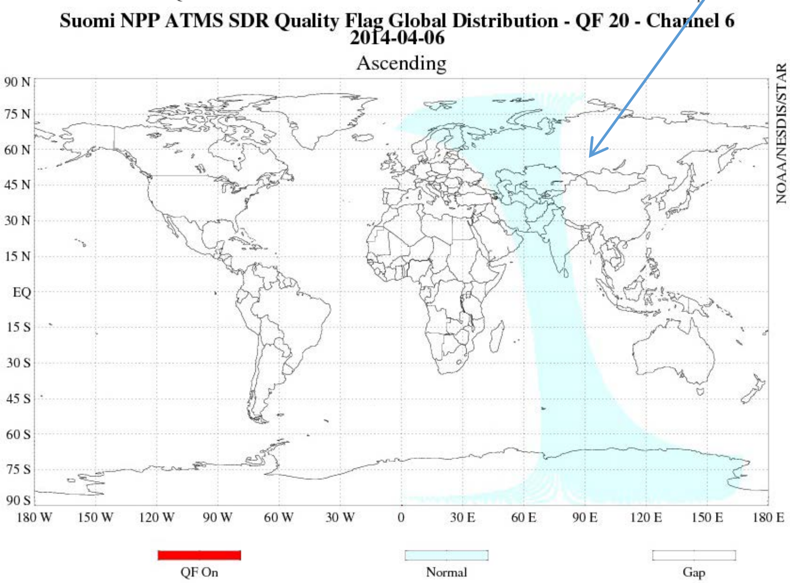

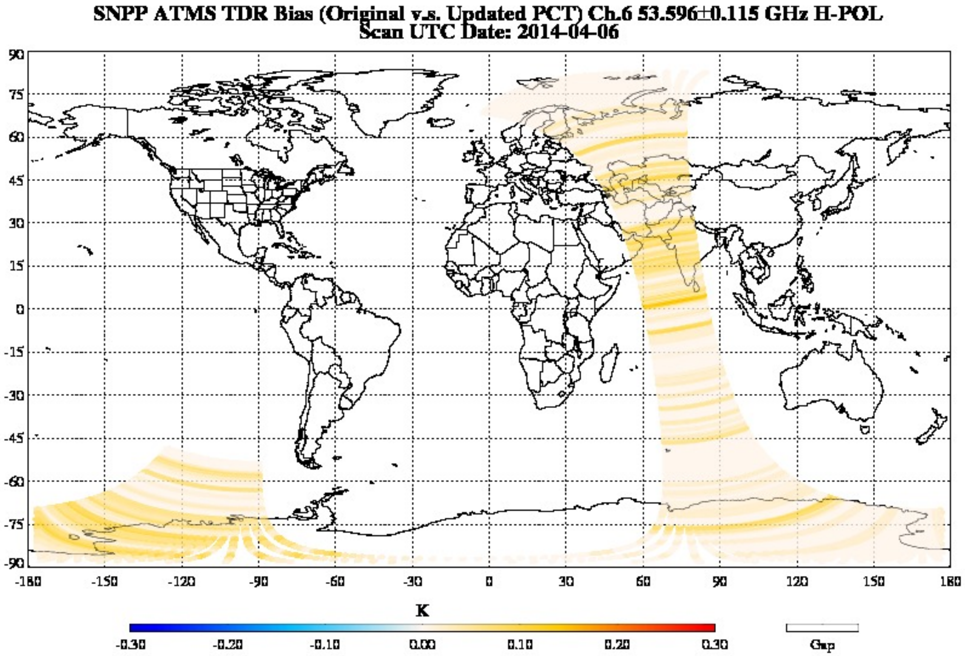

JPSS-1 ATMS Readiness

- Radiance based ATMS SDR calibration algorithm and associated PCT have been approved for operational implementation
- J1 ATMS pre-launch instrument characterization was completed
- J1 ATMS post-rework TVAC data analysis and coefficients generation were performed successfully
- J1 ATMS instrument to spacecraft mounting matrix was generated and updated in J1 PCT
- J1 ATMS channel 17 anomaly in flight unit was observed during EMI testing. Further investigation is ongoing. Now, J1 ATMS EDU is put back to the spacecraft for EMI testing

JPSS-1 ATMS Readiness

- Overall lower channel correlation observed in JPSS-1 ATMS
- Relatively large channel correlation at channel 18 and 19 is possibly due to the shared harmonics

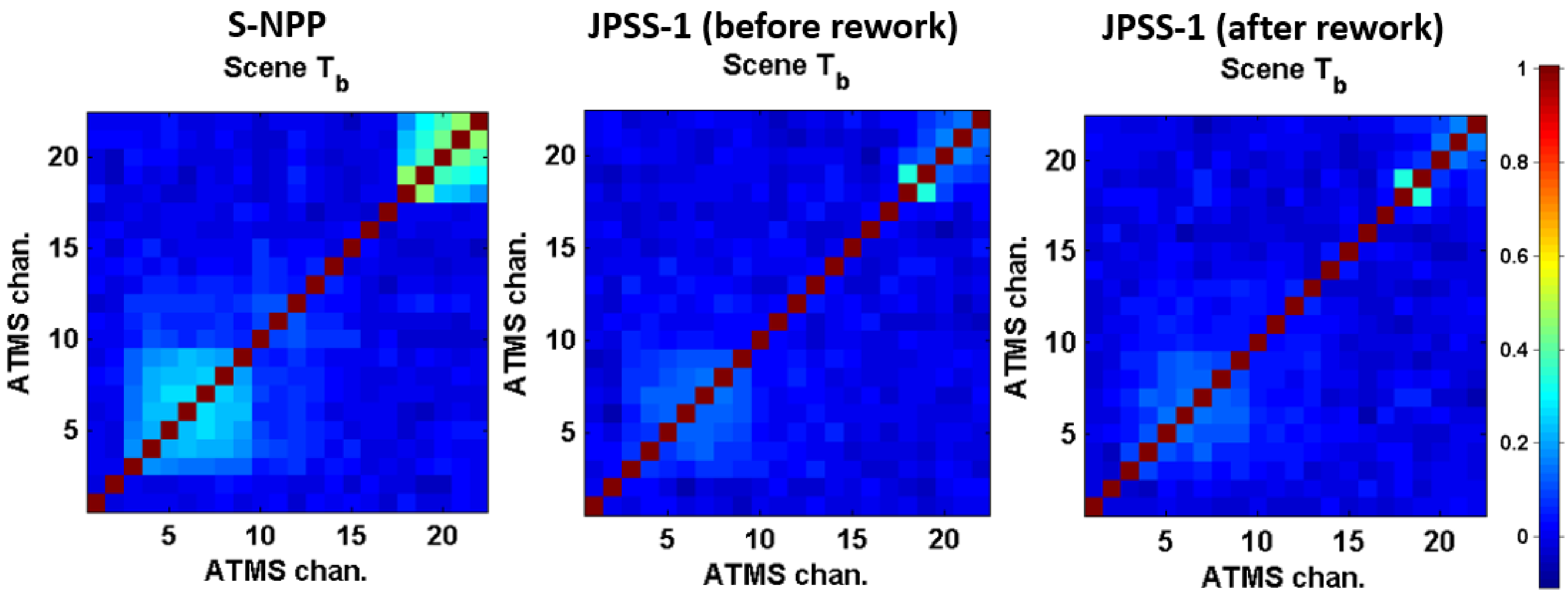

JPSS-1 ATMS Readiness

JPSS-1 ATMS presents lower striping noise

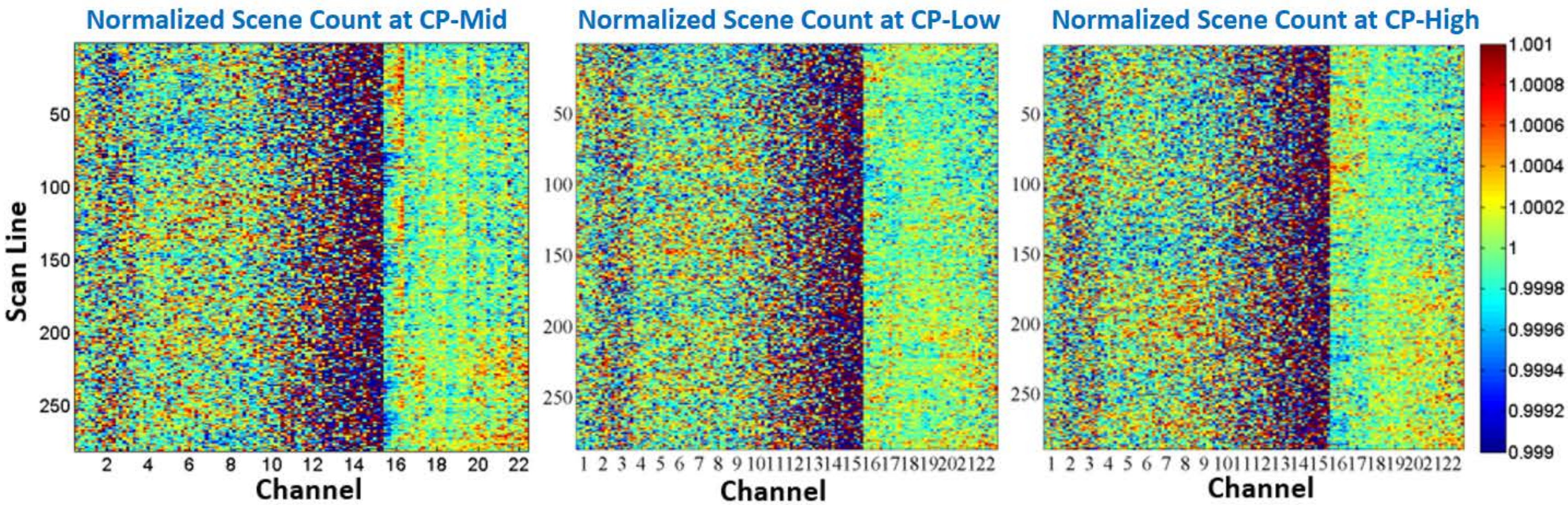

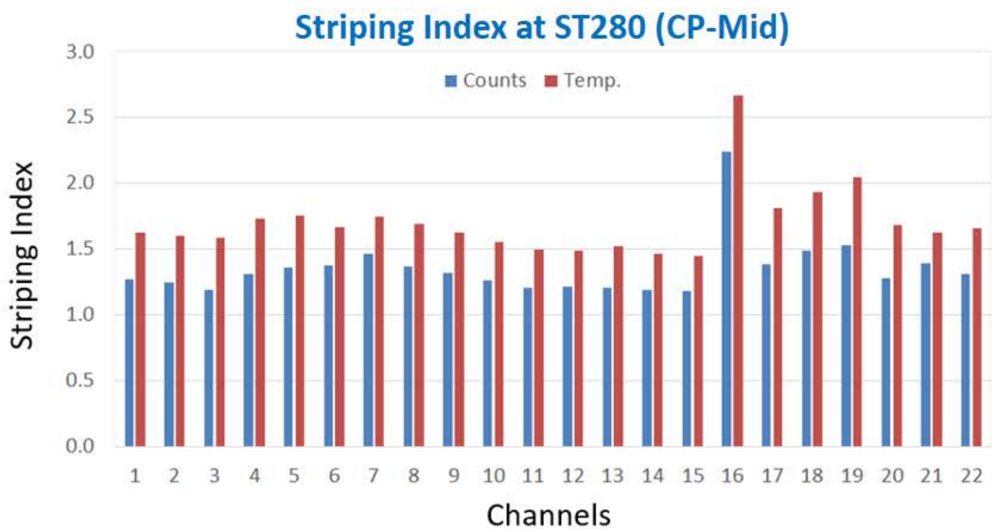

JPSS-1 ATMS Readiness

- ATMS reflector emissivity was retrieved from TVAC test when scene target temperature is close to cold target temperature
- On-orbit emissivity may be changed due to the uncertainty in cold and scene target temperature measurements

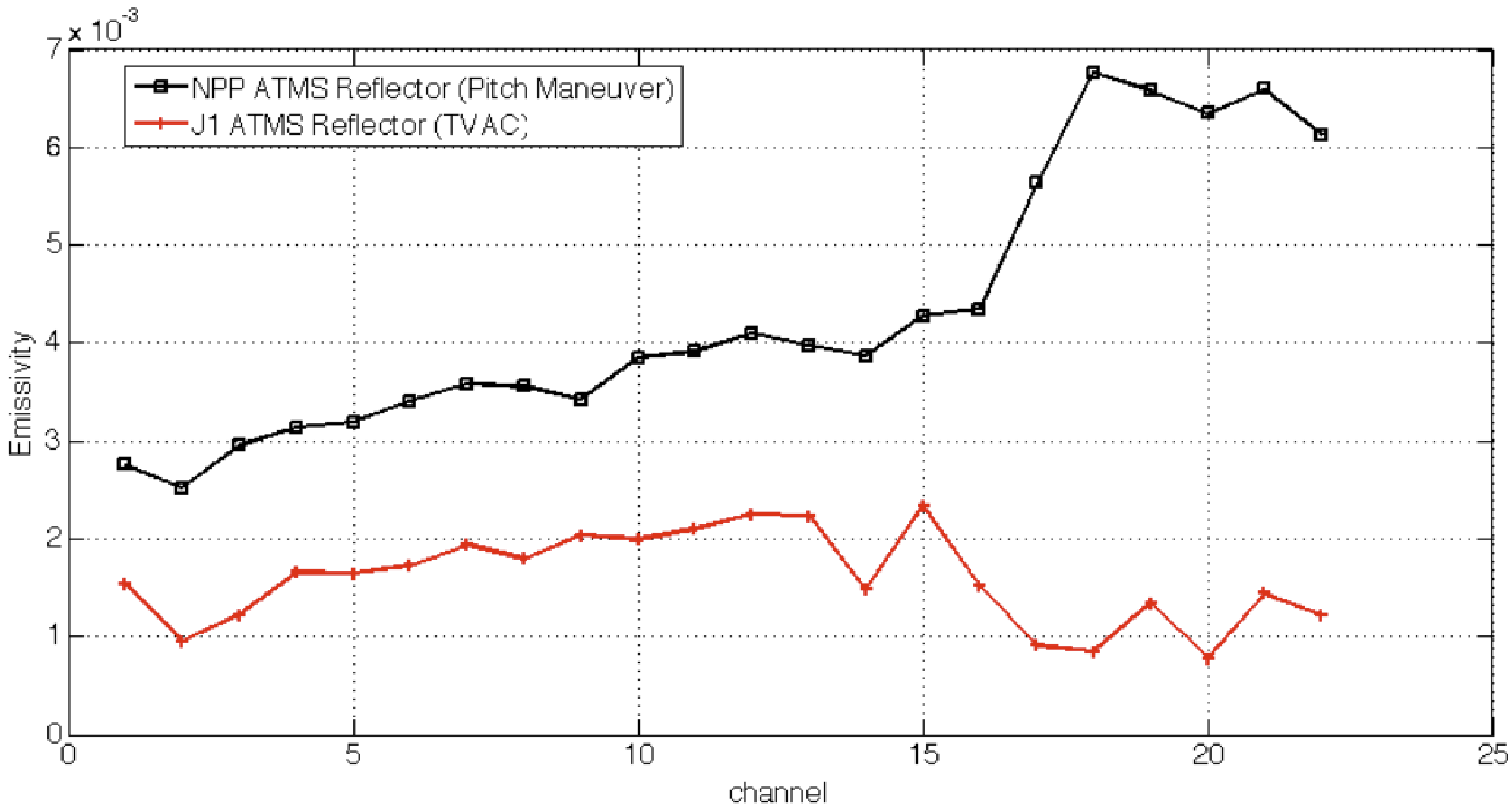

JPSS-1 ATMS Readiness

Channel 18: 183.31 ± 7 GHz

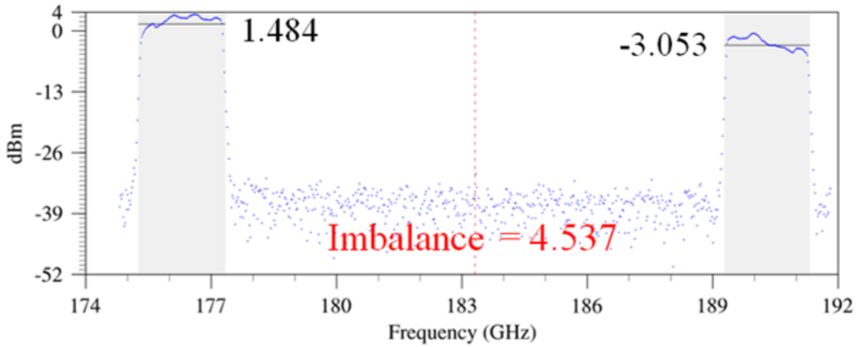

Channel 19: 183.31 ± 4.5 GHz

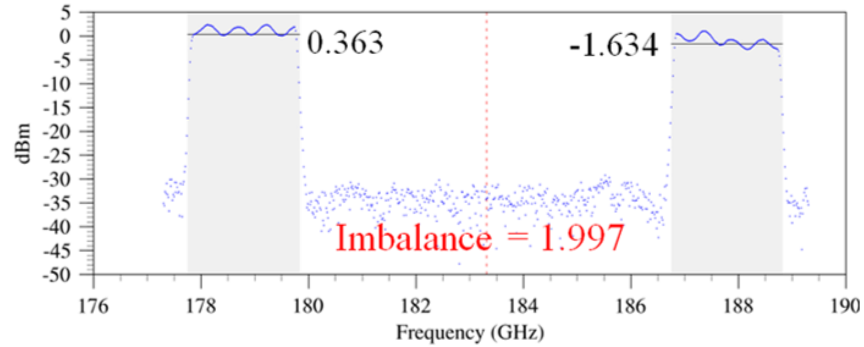

Channel 20: 183.31 ± 3 GHz

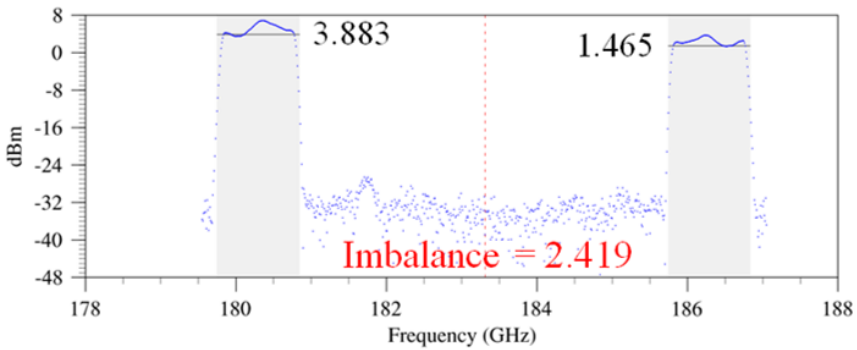

Channel 21: 183.31 ± 1.8 GHz

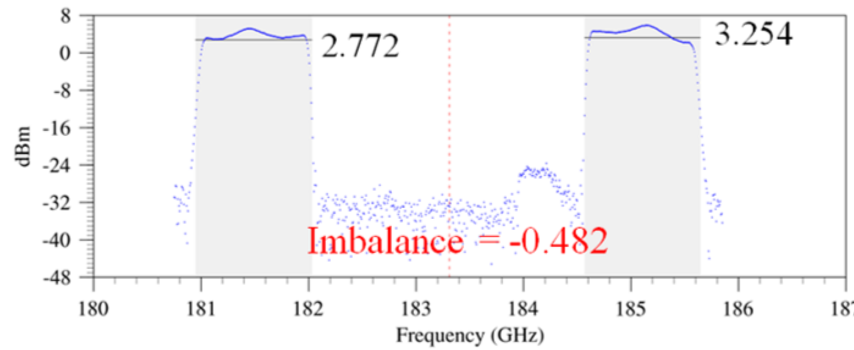

Channel 22: 183.31 ± 1 GHz

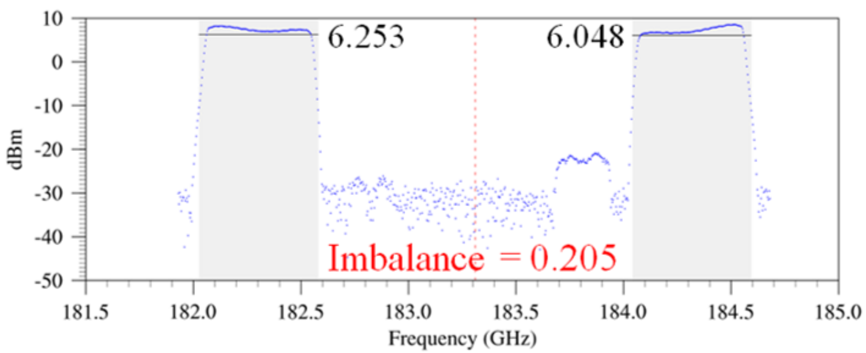

	Channel				
	18	19	20	21	22
STAR	4.537	1.997	2.419	-0.482	0.205
NASA	4.949	2.228	2.625	-0.607	0.263
MIT/LL	4.371	1.958	2.387	-0.017	0.061

STAR's imbalance value is comparable with NASA's result.

Summary & Path Forward

- Summary
  - S-NPP ATMS scan drive motor current increased during the last year. More frequent scan reversal activities can help to reduce motor current
  - S-NPP ATMS on-orbit channel performance meets the requirement with margins
  - JPSSS-1 ATMS post-rework characterization was performed and ground processing system PCT has been updated using newly derived coefficients
  - Radiance based ATMS SDR calibration algorithm has been approved and is waiting for IDPS operational implementation
  - JPSS-1 ATMS flight unit anomalies observed in spacecraft EMI testing are under investigation

Summary & Path Forward

- Path Forward
  - Implement reflector emissivity correction algorithm
  - Revisit JPSS-1 ATMS PCT for launch readiness
  - Work with ATMS SDR team members to support JPSS-1 ATMS post-launch characterization
  - Work with STAR ICVS team for JPSS-1 ATMS health status and performance monitoring
  - Perform additional S-NPP ATMS reverse scan data analysis

Summary & Path Forward

Re-construct normal scan FOVs from reverse scan to minimize impact to data users

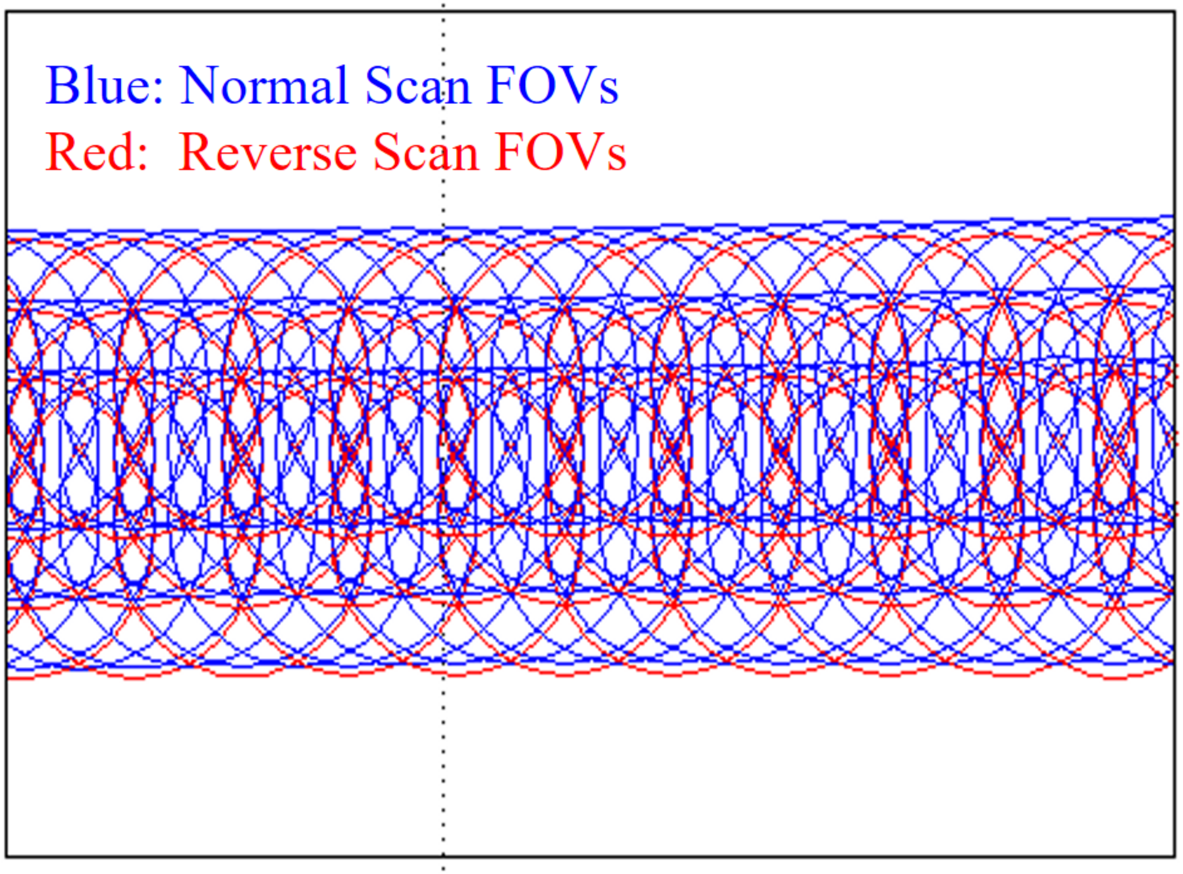

- Current scan profile and reversal scan profile are used for the study
- Reverse scan antenna pattern is used as source and normal scan antenna pattern as target function, calculate coefficients for each channel at every normal scan FOV
- Apply the coefficients to reversal scan observations , reconstruct normal observations with 96 FOVs at target FOV size

SUOMI NPP ATMS INSTRUMENT STATUS REPORT

PRESENTED BY Ninghai Sun
NOAAA/STAR

SESSION 4, AUGUST 9TH, 2016

Outline

- ATMS Instrument Status
- ATMS Data Quality
- ATMS Scan Drive Motor Current Anomaly
- Summary and Path Forward

Suomi NPP ATMS Instrument Status

ICVS Home > ICVS Anomaly History

ICVS Instrument Anomalies

Cumulative Zip file of all MX Releases, (ZIP, 1.57 MB, New: 6/30/2016)

Click column headings to sort; Type in the "Search" box to query table contents.

Updated: 8/8/2016

Show 30 entries — Search: ATMS

Event	Date	Time (UTC)	End (UTC)	Instrument(s)	Retrieved from:	CCR	Notes
ATMS Table and RAM Dumps	08/02/16	16:59	17:02	A	ESPC Ops Report	---	During SVL Contact 24691 SNPP engineers placed the ATMs instrument in safe mode to perform required ATMS table dumps. While in safe mode no scince data was generated resulting in a 2 minute, 40 second ATMS outage.
ATMS Once-per-Orbit Scan Reversals Implemented	07/25/16	-:--	-:--	A	Go-CAM Report, C/V Leads Archive	---	Svalbard Contact 24577, Ground commanded CBM-sequence until 08/04/16, then DAS-commanded at 70N, 75N, 80N, repeat. Expect 14 reversals/day.
ATMS TMon 131 and 132 Activated	07/18/16	-:--	-:--	A	C/V Leads Archive	---	---
ATMS TMon 131 and 132 Load	07/15/16	19:21	-:--	A	Go-CAM Report, C/V Leads Archive	---	On Friday, 15 July 2016, during contact 24437 at 19:21 UTC, OSPO loaded two new TMons (131 & 132) and one new ACBM sequence (100) to ATMS to monitor ATMS Main Motor temperature and DTU-measured ATMS Scan Drive Mechanism temperature. If either temperature exceeds 60C for 24 seconds or 10 seconds, respectively, ATMS will automatically be commanded to safe mode.

Suomi NPP instrument event log is now available in STAR ICVS website provided by Cole Rossiter

Suomi NPP ATMS Instrument Status

Event	Day	Event	Day
ATMS Table and RAM dump	08/02/2016	ATMS Once-per-Orbit Scan Reversals Implemented	07/25/2016
ATMS TMon 131 and 132 Activated	07/18/2016	ATMS TMon 131 and 132 Loaded	07/15/2016
ATMS Manual Command Scan Drive Reversal	05/09/2016 ~ 05/13/2016	ATMS Manual Command Scan Drive Reversal	05/05/2016 ~ 05/06/2016
ATMS Daily Scan Drive Reversals Stopped	04/15/2016	ATMS 1553 Packet Error Counter Alarm	02/01/2016
Commencement of the daily ATMS Scan Reversal	08/24/2015	ATMS Scan Reversal DAS Test Out	08/13/2015
ATMS Scan Reversal Upload Test	07/14/2015		

Suomi NPP ATMS On-orbit Performance

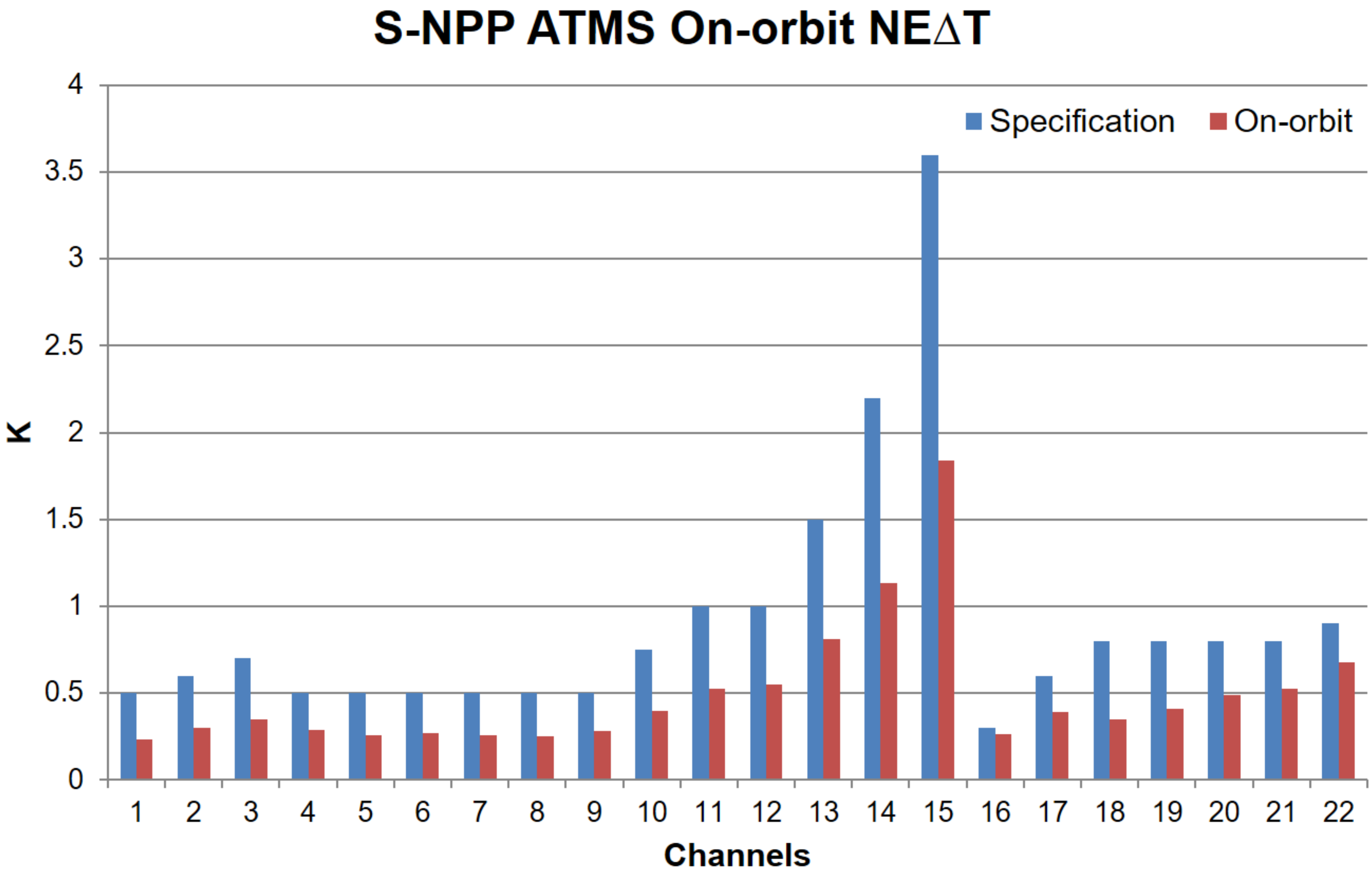

Suomi NPP ATMS all channel noise meets the requirement with margins

Suomi NPP ATMS On-orbit Performance

Suomi NPP ATMS channel calibration gain is stable

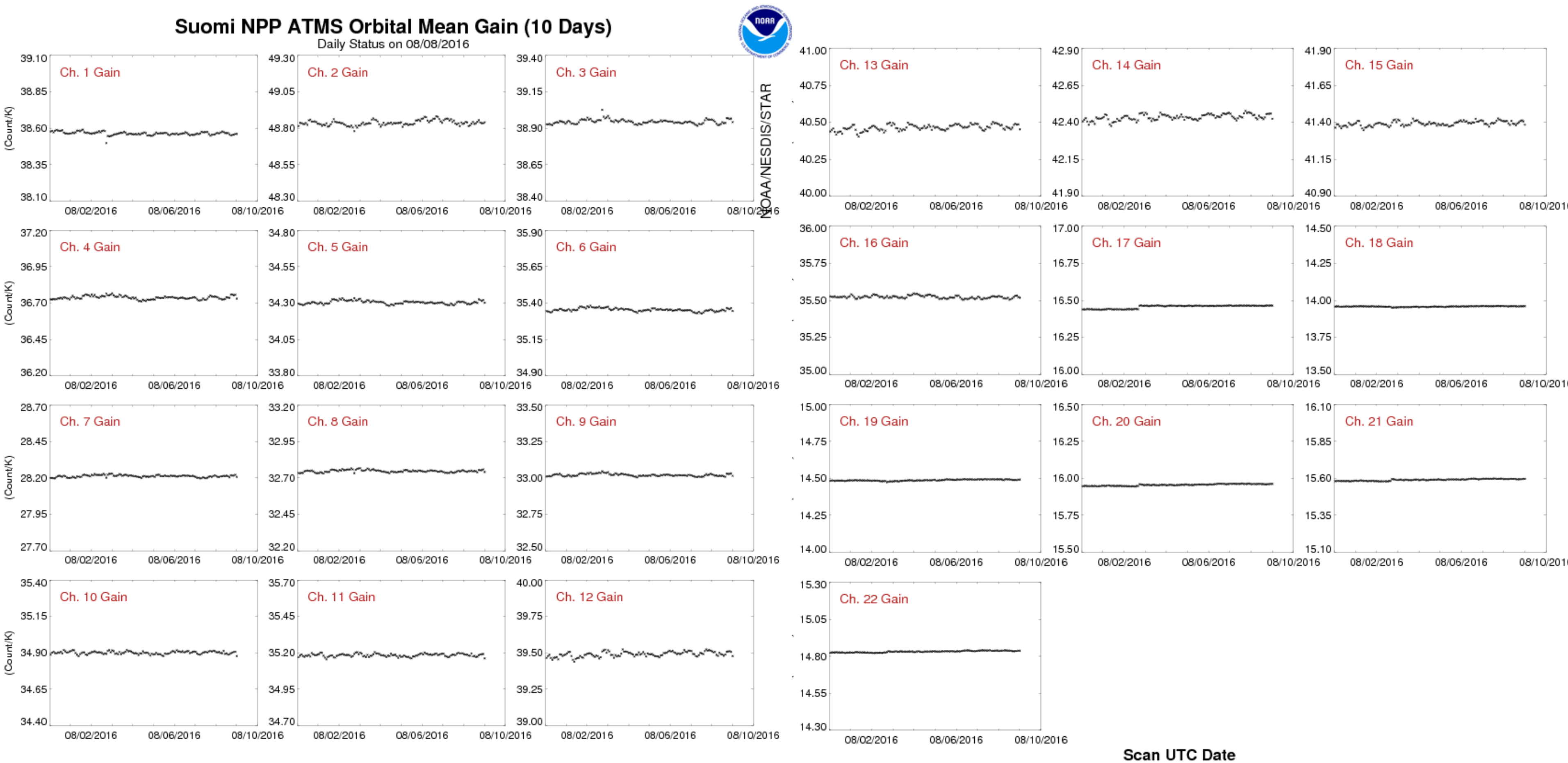

Suomi NPP ATMS On-orbit Status

Suomi NPP ATMS warm load PRT temperature is stable

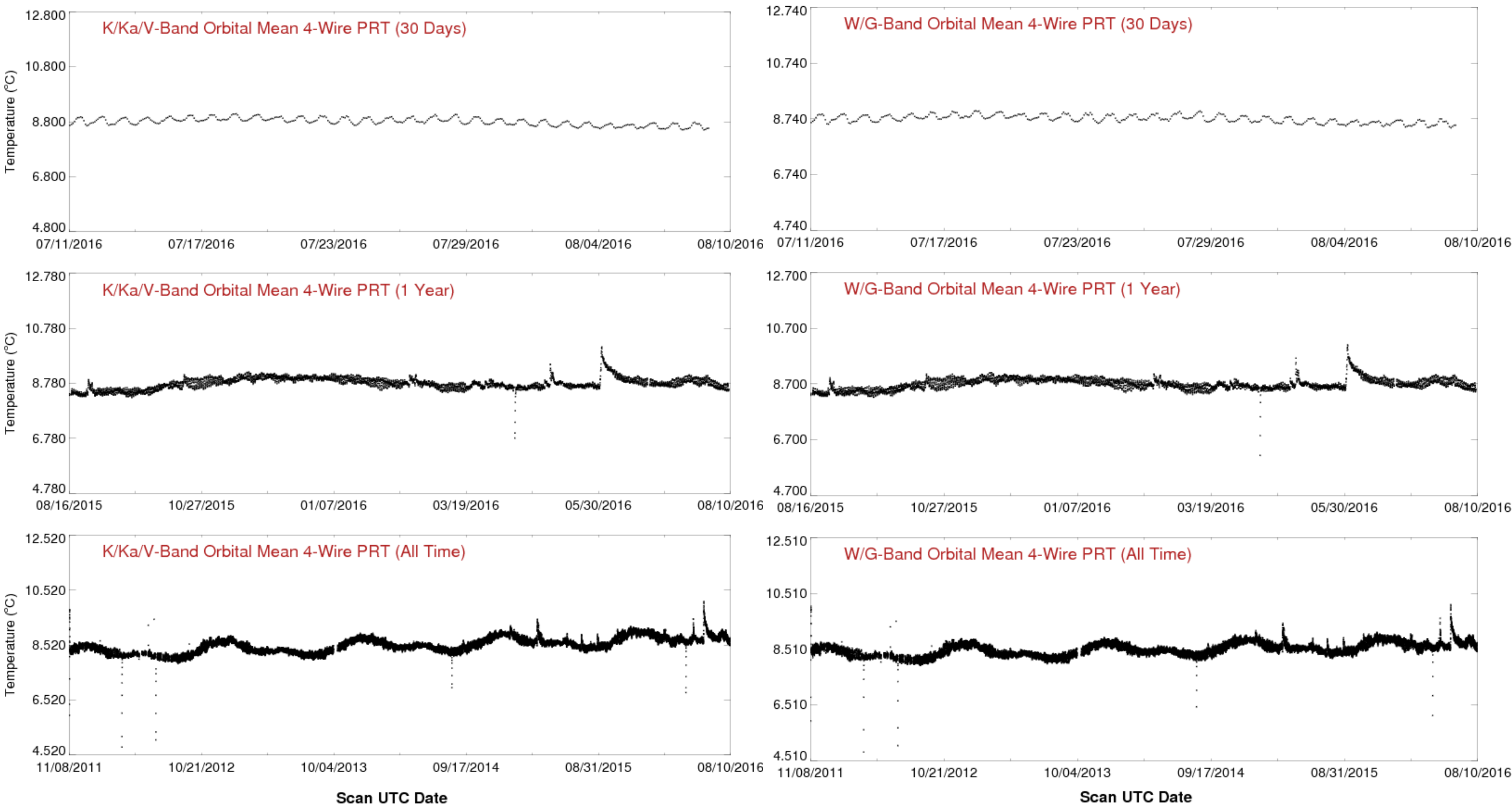

Suomi NPP ATMS On-orbit Status

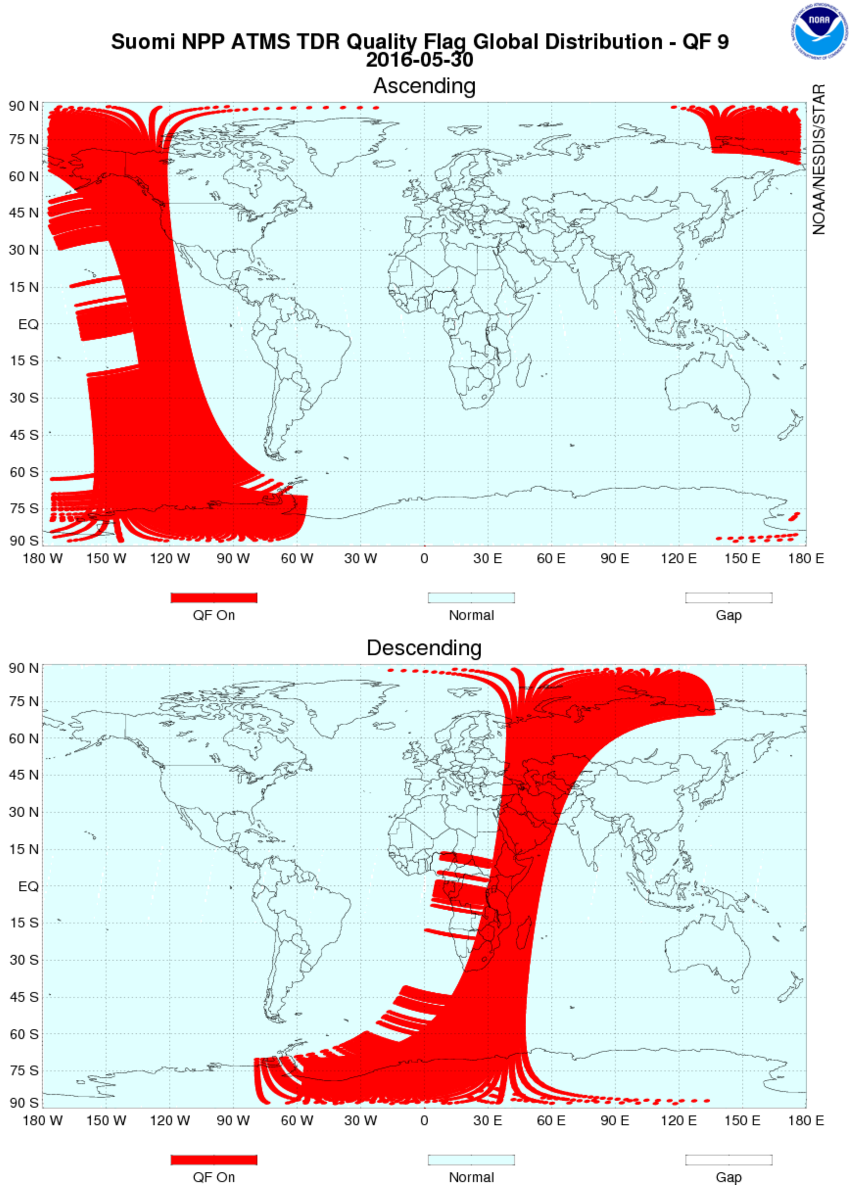

The number of SD Main Loop Integral Error QF scans keeps high orbital percentage since May 30, 2016

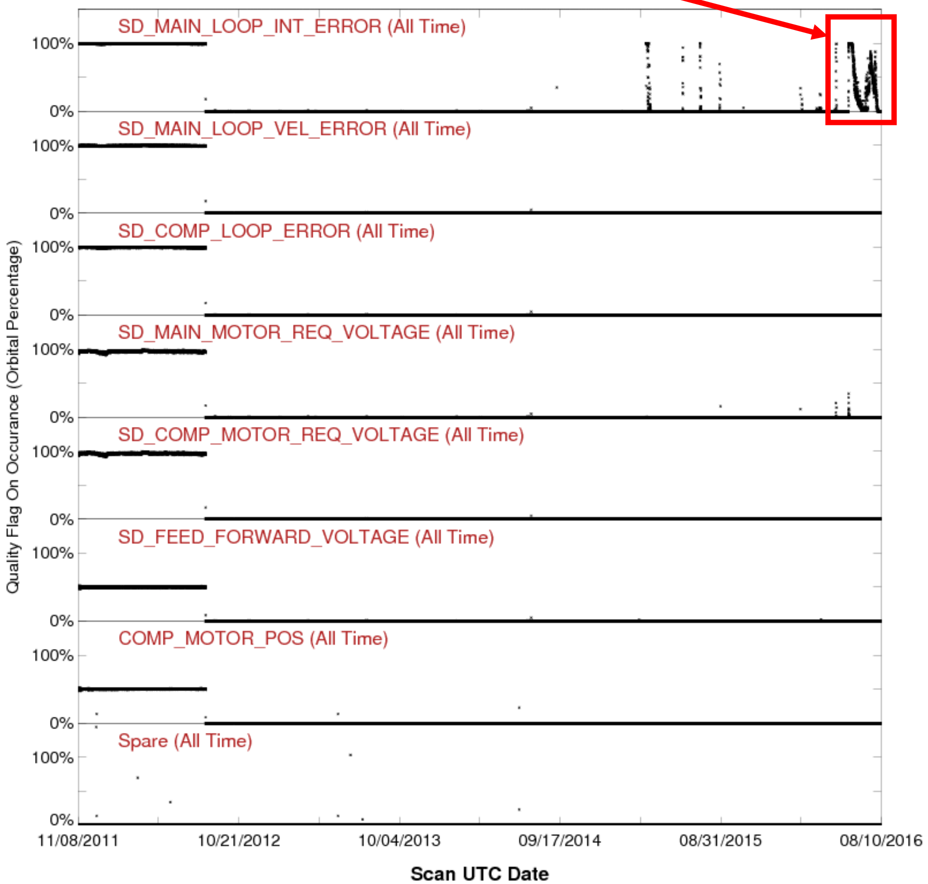

Suomi NPP ATMS On-orbit Performance

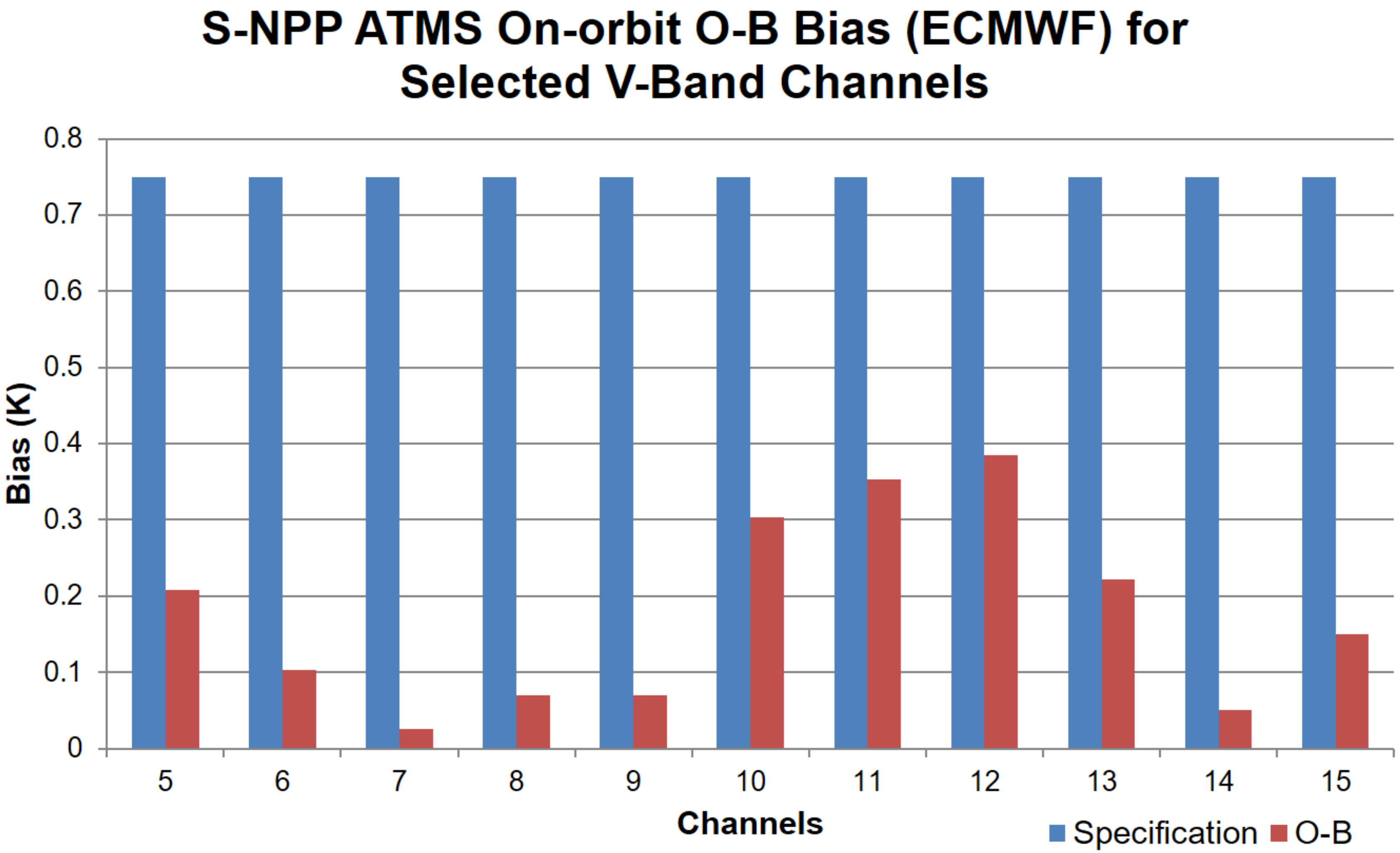

Suomi NPP ATMS on-orbit absolute bias (OBS-RTM) meet the requirement

Suomi NPP ATMS On-orbit Status

ATMS scan drive main motor current major spikes detected

- Instrument temperature increased
- Scan angle shift observed after SD motor current spikes but still well below requirements
- Once per day scan reversal implemented from August 24, 2015
- Once per orbit scan reversal implemented from July 25, 2016 (staggering configuration among consecutive orbits)
- ATMS put in safe mode due to 1553 issue during once per day reversal
- Twice per orbit reversal (staggering configuration near north and south pole) to be implemented soon

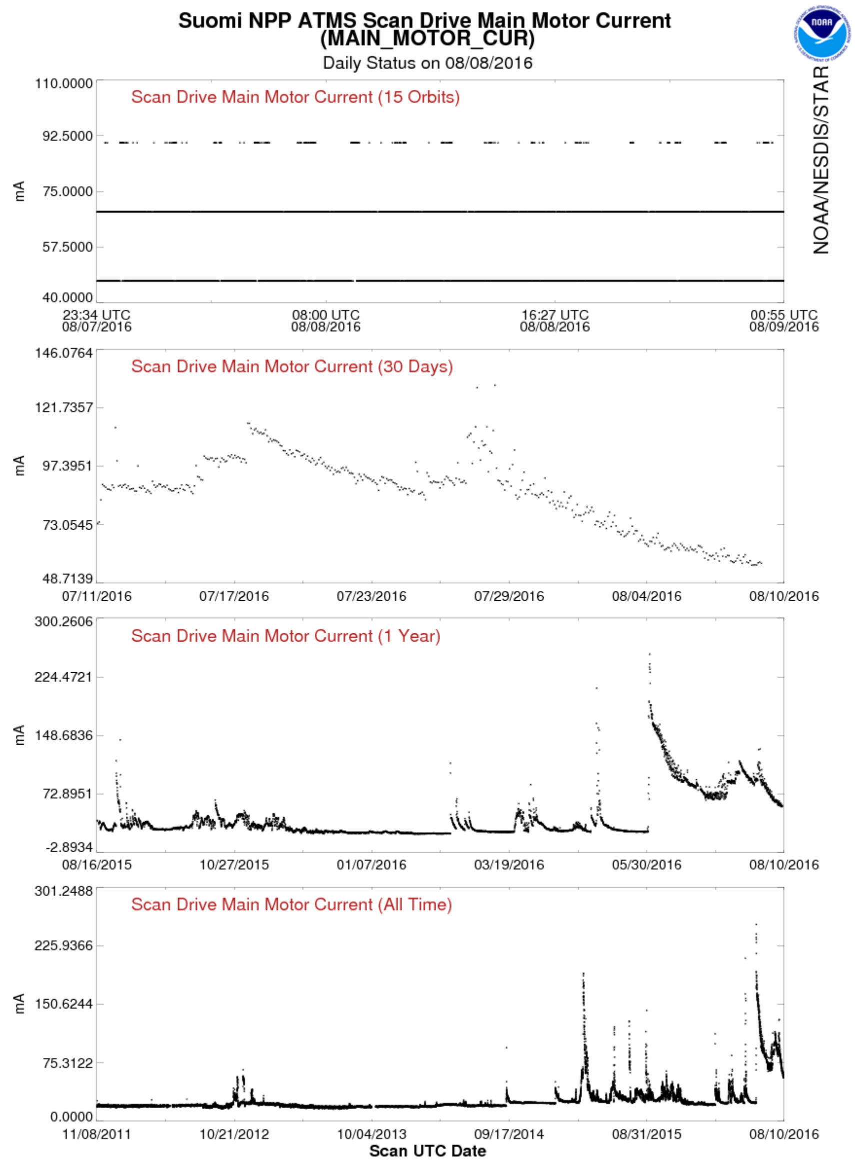

Suomi NPP ATMS On-orbit Status

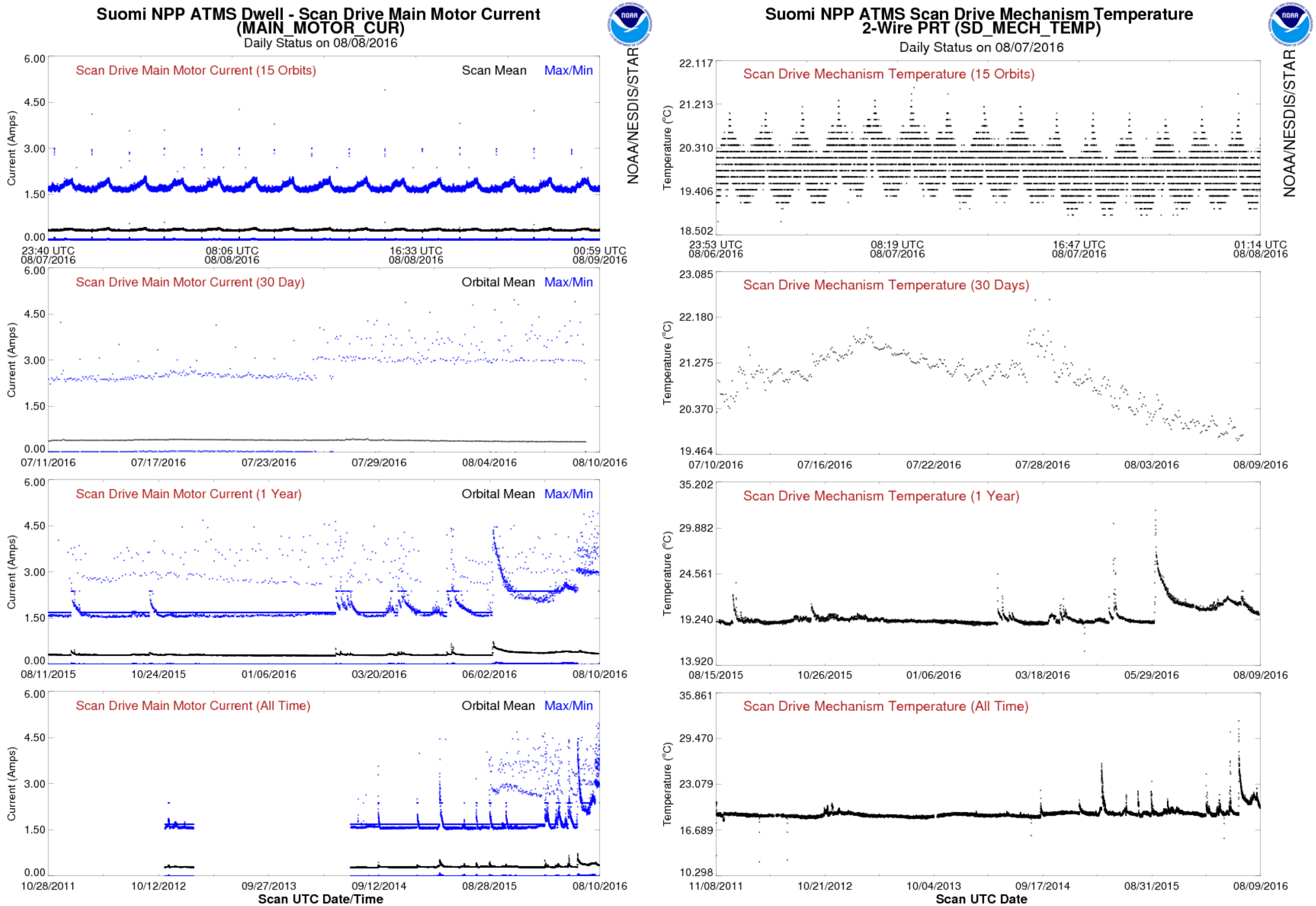

Suomi NPP ATMS On-orbit Status

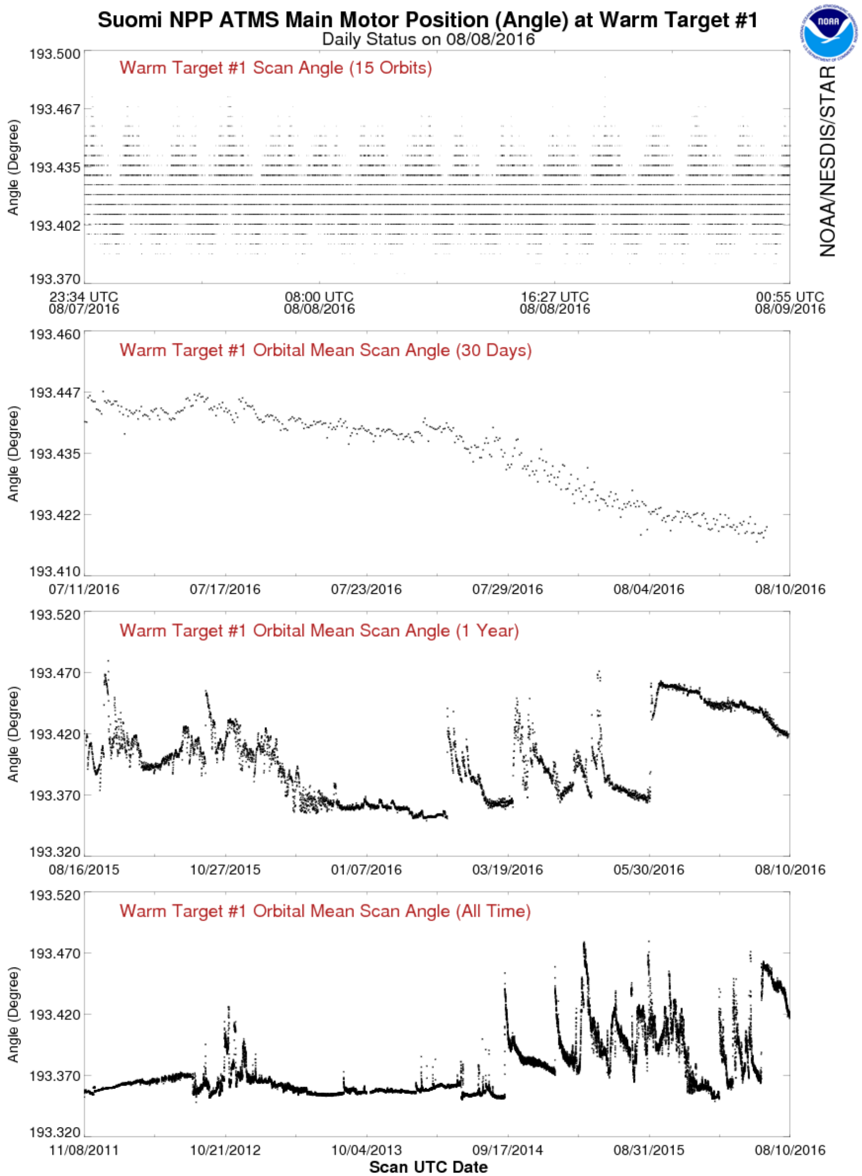

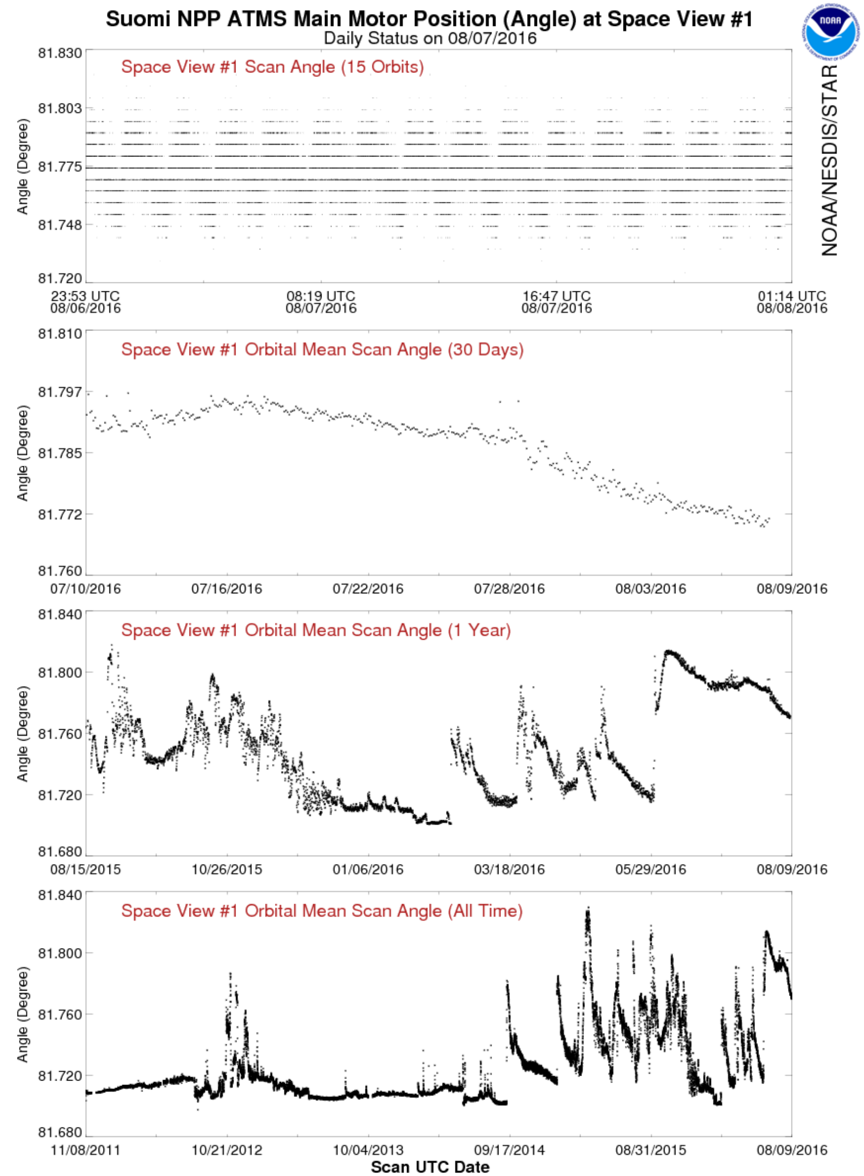

Suomi NPP ATMS On-orbit Status

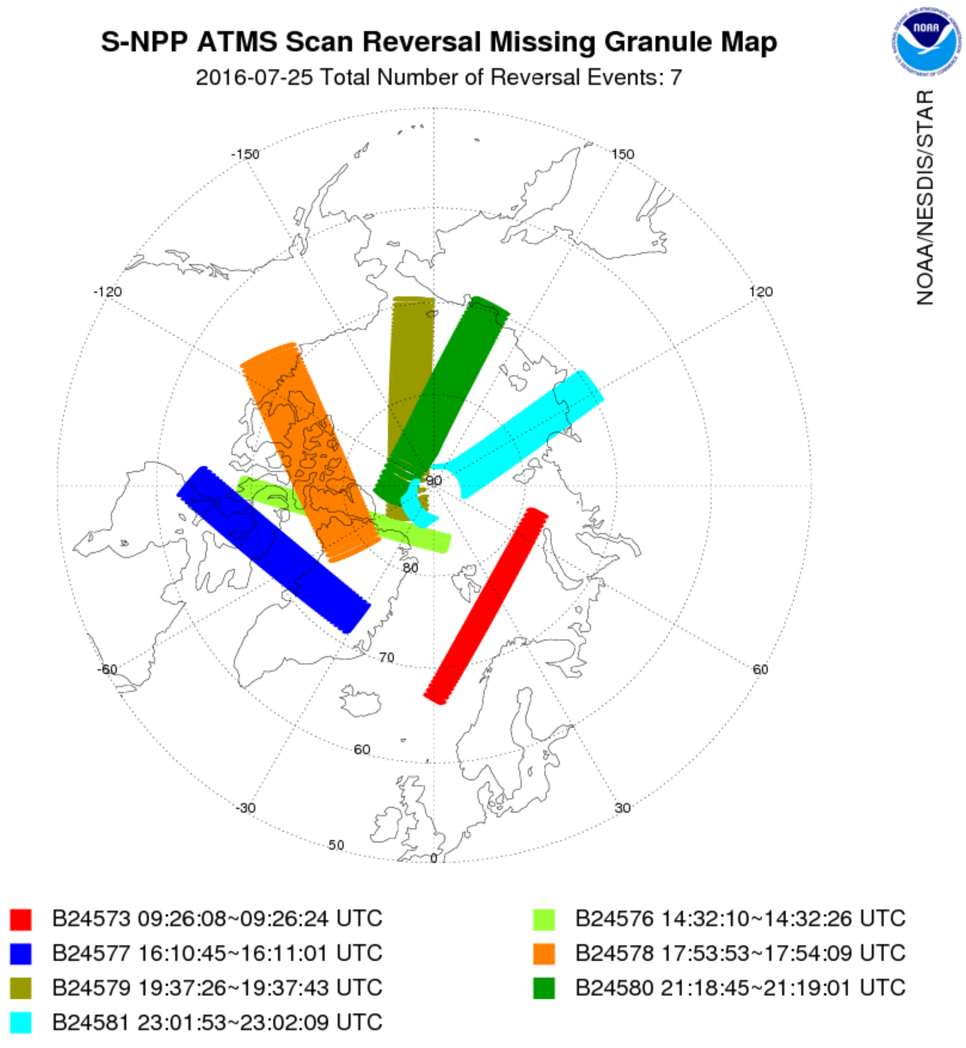

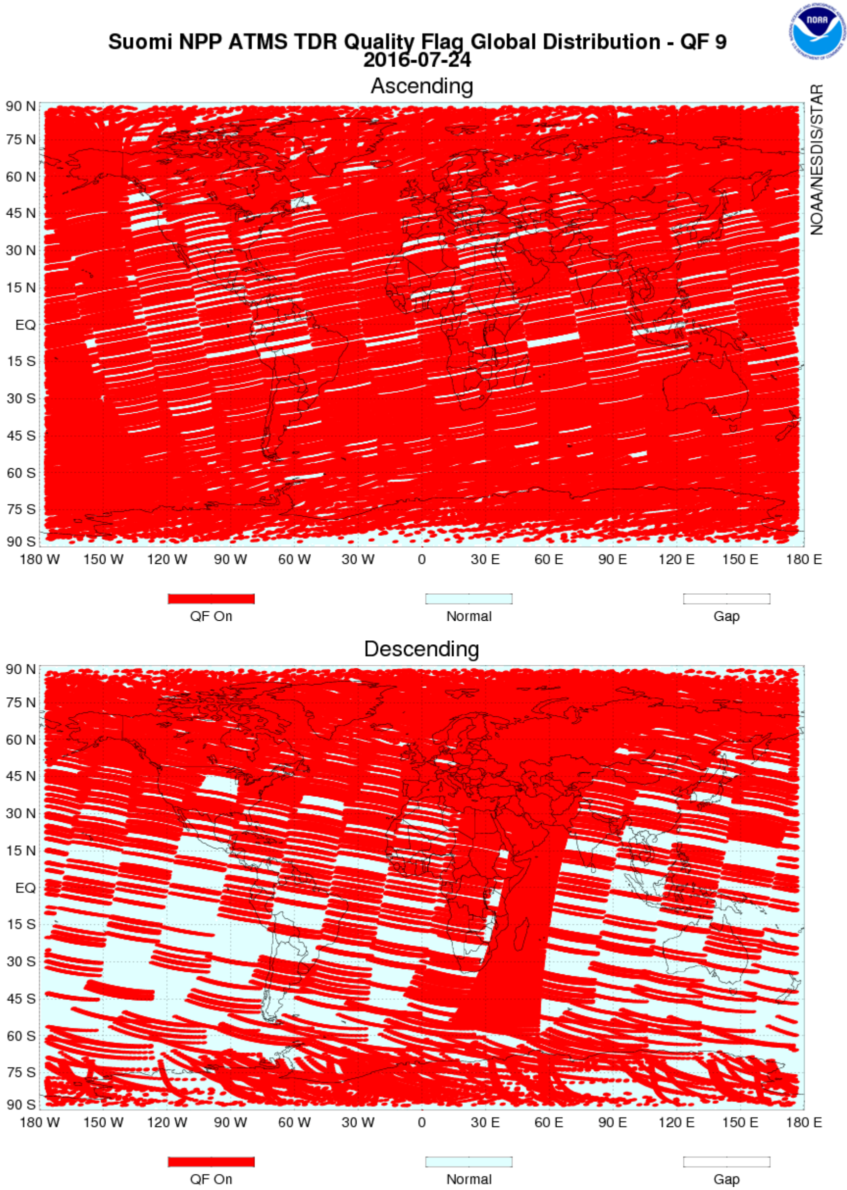

Summary & Path Forward

- Summary
  - S-NPP ATMS on-orbit channel performance meets the requirement with margins
  - S-NPP ATMS scan drive motor current increased during the last year. More frequent scan reversal activities can help to reduce motor current. SD motor current anomaly didn't show apparent impact on channel sensitivity
  - S-NPP ATMS TDR SD loop integral error quality flag was triggered on May 30, 2016 and the affected scans have been reduced since the implementation of once-per-orbit scan reversal
  - S-NPP ATMS reverse scan data are available for additional study from STAR ICVS website
  - ATMS ICVS-LTM packages have been tested successfully and ready for JPSS-1 operations

Summary & Path Forward

- Path Forward
  - Keep watching S-NPP ATMS on-orbit health status, performance, and data quality
  - Enhance ICVS anomaly notification function
  - Implement near real time JPSS-1 ATMS post-launch monitoring to support ATMS SDR team cal/val activities
  - Work with ATMS SDR team to improve current monitoring capability

Colocation of GRUAN

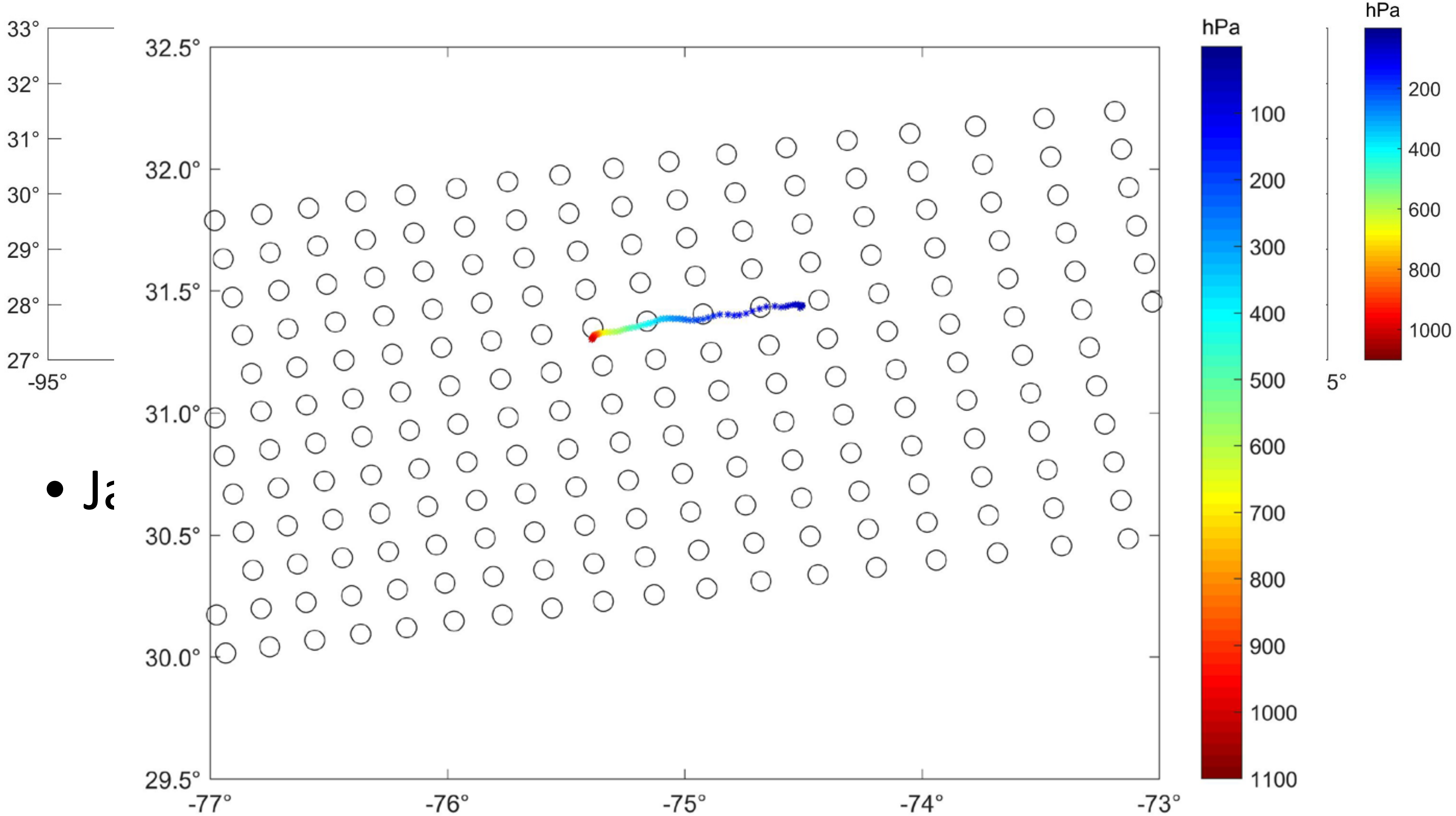

Provide radiosonde based ATMS TDR bias characterization results to support NWP applications

The 2016 STAR JPSS Annual Science Team Meeting, August 8-12, 2016
NOAA Center for Weather and Climate Prediction, College Park, Maryland

Re-evaluation of Suomi NPP ATMS Destriping Algorithm for Surface-Sensitive Channels

Xiaolei Zou, Yuan Ma and Zhengkun Qin

Earth System Science Interdisciplinary Center (ESSIC)
University of Maryland, USA

Fuzhong Weng

Center for Satellite Applications and Research (STAR)
National Oceanic and Atmospheric Administration (NOAA), USA

Outline

- A Recollection of ATMS Striping Noise
- Two Striping Noise Mitigation (SNM) Algorithms
  - — SDR data of ATMS sounding channels
  - — Pitch-over maneuver data of all ATMS channels
- Challenges for Surface-Sensitive Channels
  - — Artifacts are generated by the SNM when scanlines are aligned with coastal lines and edges of heavy precipitation
- Sensitivity Study
  - — Large jumps of TB are aligned with scanelines
  - — Large jumps of TB are aligned in along-track direction
- A potential solution
- Conclusions and Suggestions

A Recollection of ATMS Striping Noise

- SNPP ATMS upper air sounding channels display clear striping noise in NWP model O-B fields (Bormann et al., 2013), which caused discomfort for NWP users who didn't see this in AMSU-A — Finding
- Striping noise are also seen in prelaunch TVAC data and pitch maneuver data. They are characterized by a constant and random variation in ATMS's cross-track and along-track directions, respectively — Confirmed
- An innovative destriping algorithm was developed to eliminate the striping noise in ATMS brightness temperature observations (Qin et al., 2013) — Solution
- At the CGMS 19th International TOVS Study Conference (ITSC) held on Jeju Island, South Korea, March 26-April 1, 2014, NWP users requested the ATMS CalVal team to develop an operational algorithm for an elimination of the striping noise in ATMS radiance measurements — Requirement
- An operational destriping algorithm was developed that for an elimination of the striping noise in ATMS radiance measurements (Ma and Zou, 2015) — Solution
- ATMS CalVal team provided 45 days of ATMS de-striped data for EMC, ECMWF and other NWP centers to test the impacts of striping noise on ATMS data assimilation for NWP — Action

Striping Noise Found in Global O-B Fields for ATMS Temperature Sounding Channels

ATMS channel 12 (25 hPa) on 24 February 2012

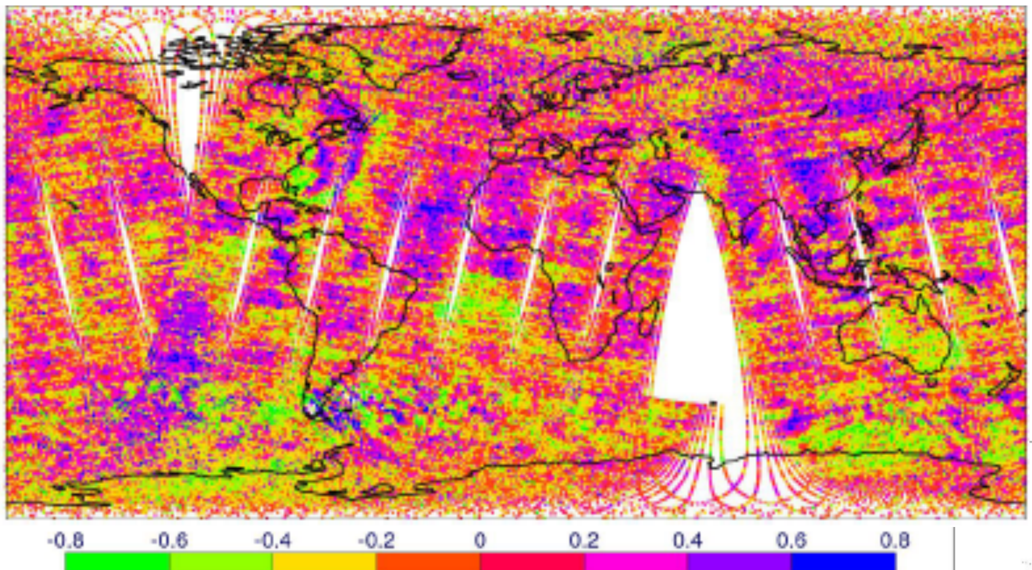

(Bormann et al, 2013, ECMWF)

User Complains !

ATMS channel 8 (250 hPa)

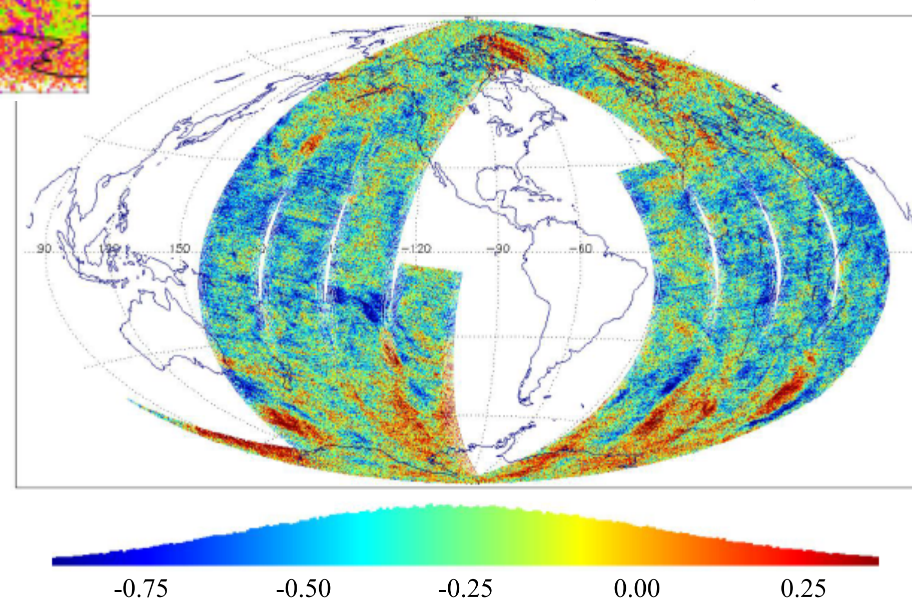

(Swadley et al, NRL)

(2) The Success of the Striping Noise Mitigation

- SDR data of ATMS Temperature Sounding Channels
- Pitch-over Maneuver Data of All ATMS Channels

Qin, Z., X. Zou and F. Weng, 2013: Analysis of ATMS and AMSU striping noise from their earth scene observations. *J. Geophy. Res.*, **118**, 13,214-13,229.

Ma Y. and X. Zou, 2015: Striping noise mitigation in ATMS brightness temperatures and its impact on cloud LWP retrievals. *J. Geophy. Res.*, **120**, 6634-6653.

Power Spectral Density Distributions of Global O-B Fields

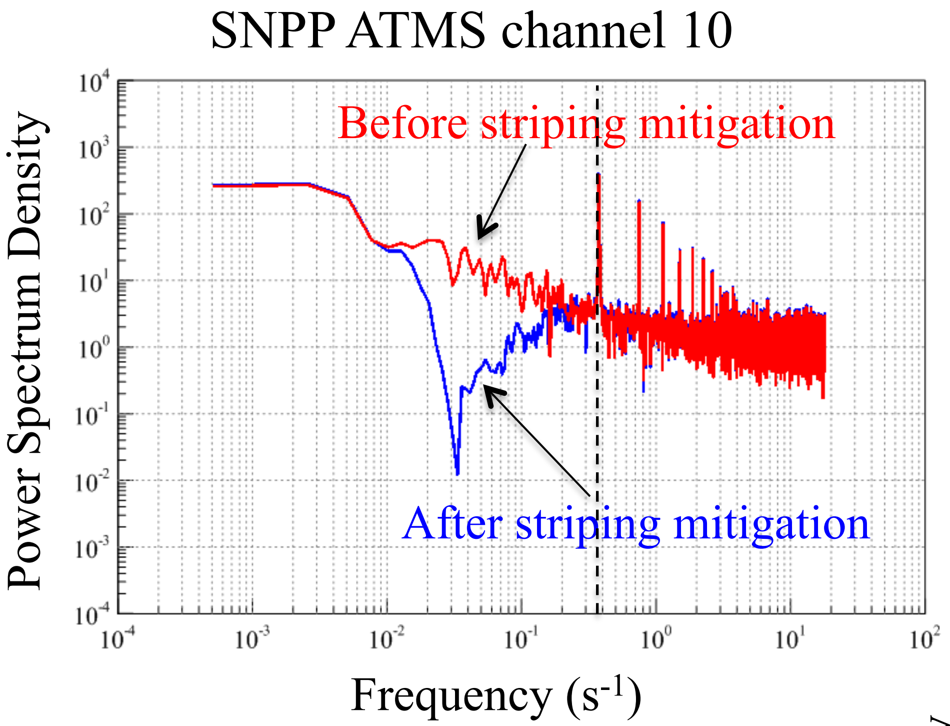

The ATMS power spectrum is significantly modified within frequency range 10^{-2} -0.375 s^{-1} by removing striping noise.

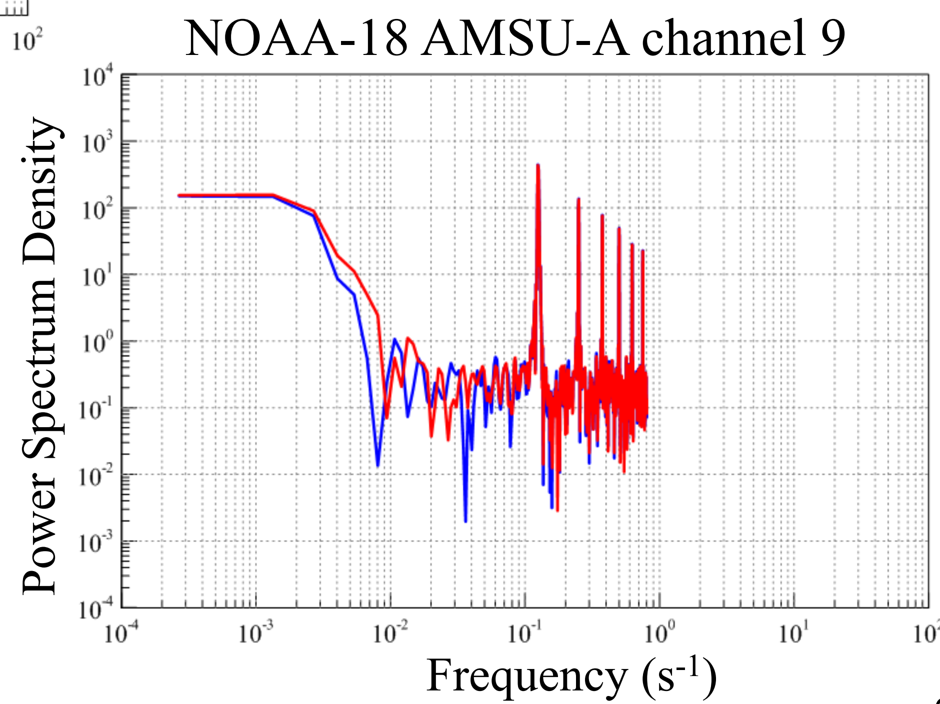

Striping Noise Mitigation for Pitch-Over Maneuver Data

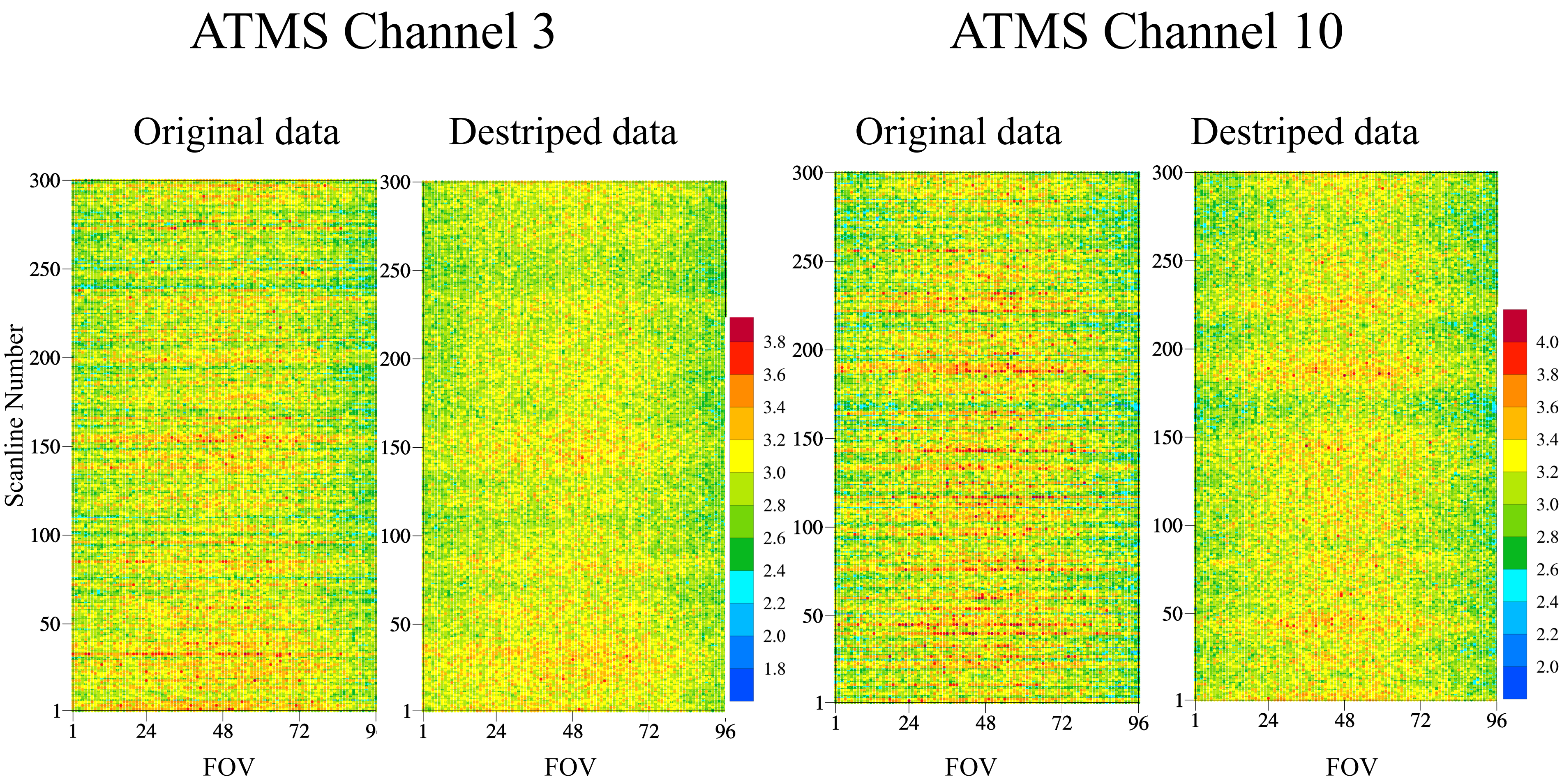

- Striping noise are visible in pitch-over maneuver data of all channels
- Striping noise are successfully eliminated by the mitigation algorithm

Striping Noise for Channel 3 Pitch-Over Maneuver Data

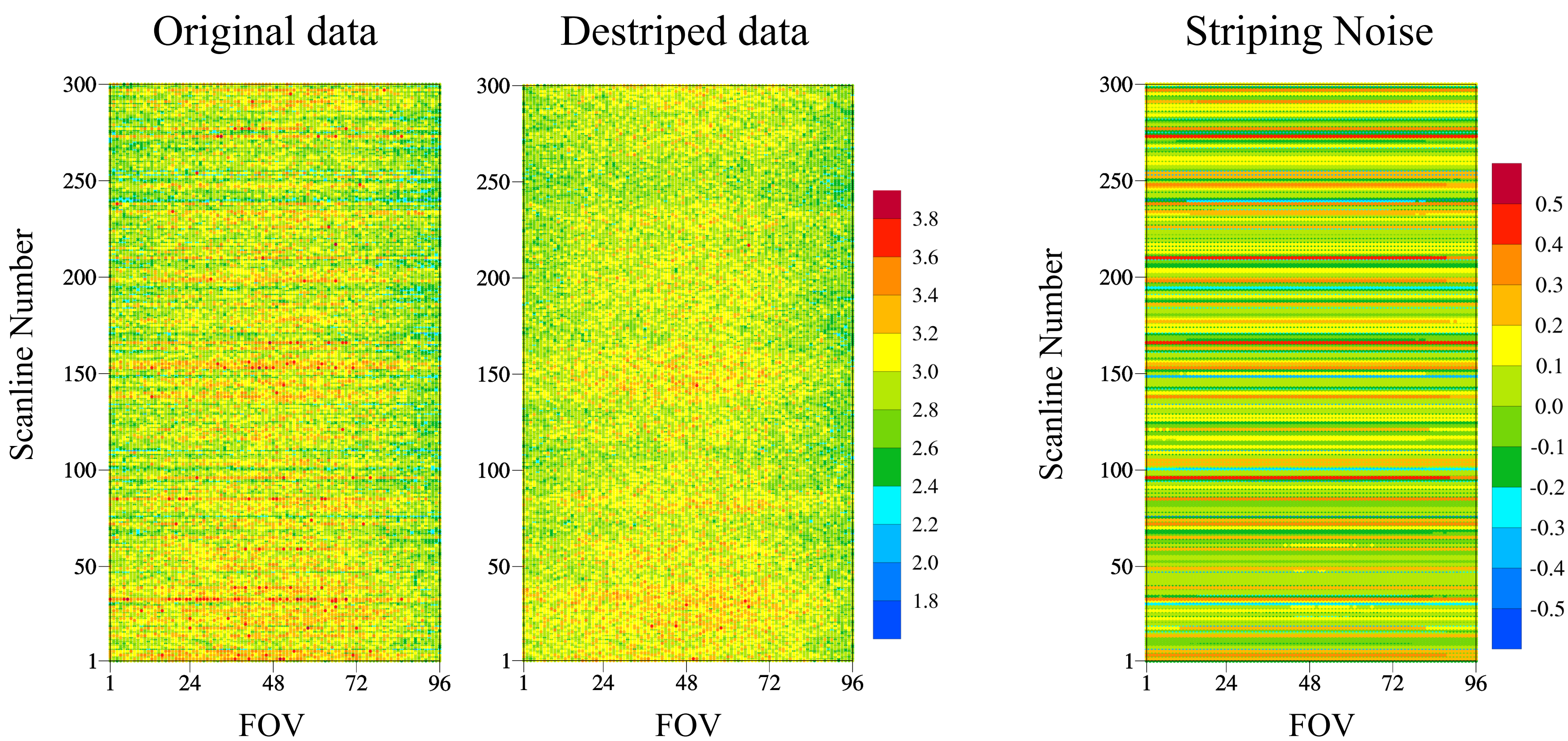

- The striping noise are less than 0.5 K and greater than -0.5 K
- The striping noise vary randomly in the along-track direction

Striping Index: $SI = \frac{\sigma^2_{along-track}}{\sigma^2_{cross-track}}$

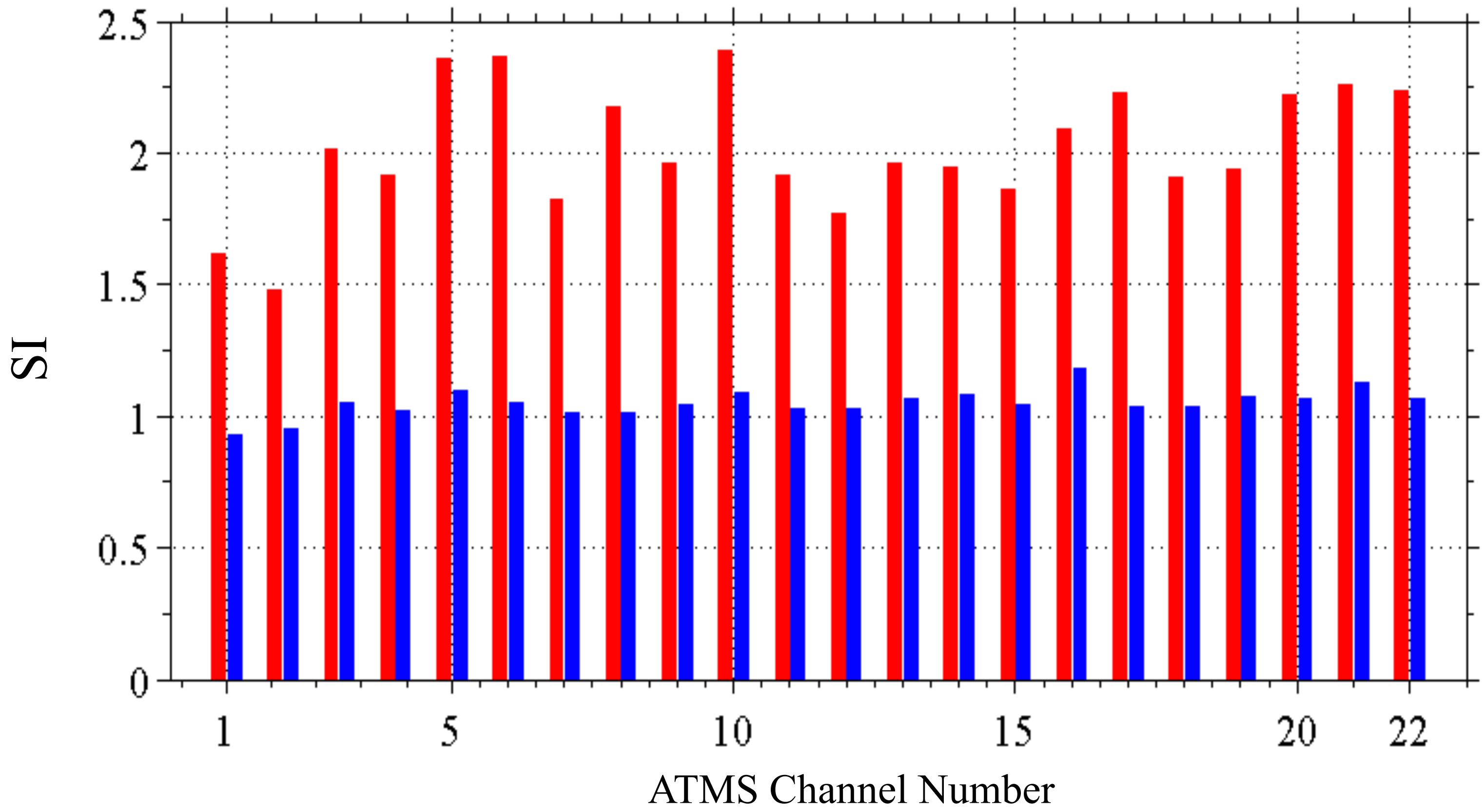

- SIs for pitch-over maneuver data are greater than one
- SIs for destriped pitch-over maneuver data are around one

(3) Problems Encountered by Striping Noise Mitigation for ATMS Surface-Sensitive Channels

— Artefacts in the destriped dataset were found for surface-sensitive channels and reported by ECMWF

— The problems occurred for scanlines that are aligned with coastal curves and edges of heavy precipitation

ECMWF Finding:

Artefacts Are Found in ATMS Destriped Dataset for Window Channels!

An evaluation of the destriped dataset at ECMWF lead to the following conclusions:

- Destriped dataset appears to reduce the striping for temperature-sounding channels
- Evidence of artefacts for window channels and lower humidity sounding channels in regions where there are sharp contrasts of Tb (e.g., terrain, cloud) that are aligned with ATMS scanlines
- The benefits of striping noise removal through post-processing are therefore not clear
- The striping noise should be avoided at source, i.e., at the instrument design level

The content on this slide comes from the talk by Dr. Heather Lawrence at "NOAA Worksop on JPSS Life-Cycle Data Reprocessing to Advance Weather and Climate Applications. May 17-18, 2016. ESSIC, College Park, MD.

O-B$^{clear\text{-}sky}$ (ATMS Channel 3)

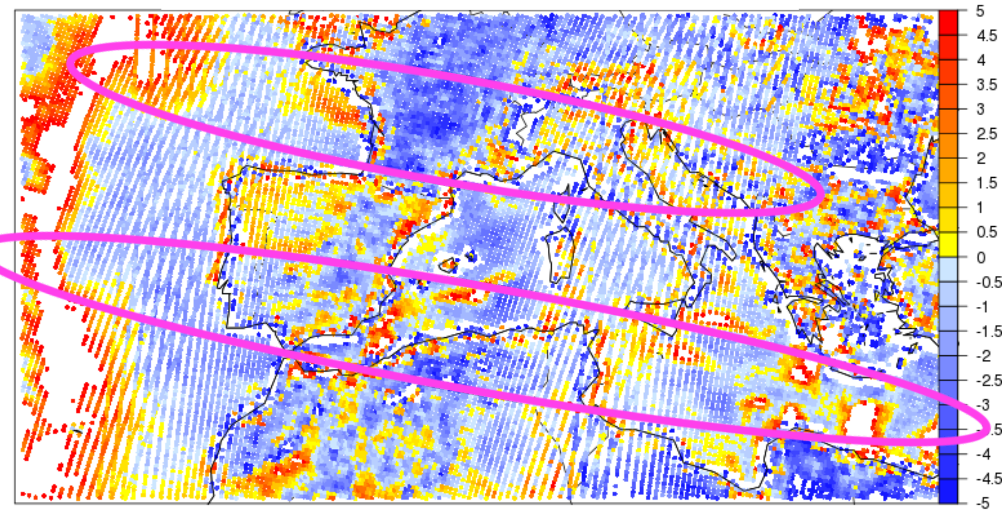

O^{destriped}-B$^{clear\text{-}sky}$ (ATMS Channel 3)

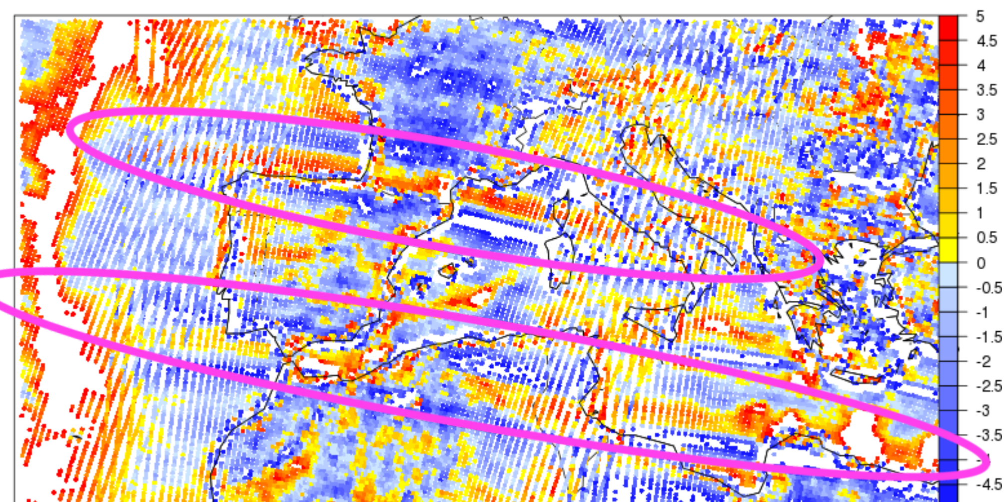

(4) Sensitivity Study

— Large jumps of TB that are aligned with scanelines

— Large jumps of TB that are aligned with a fixed FOV

TB Observations of ATMS Ch9 on 14 June 2016

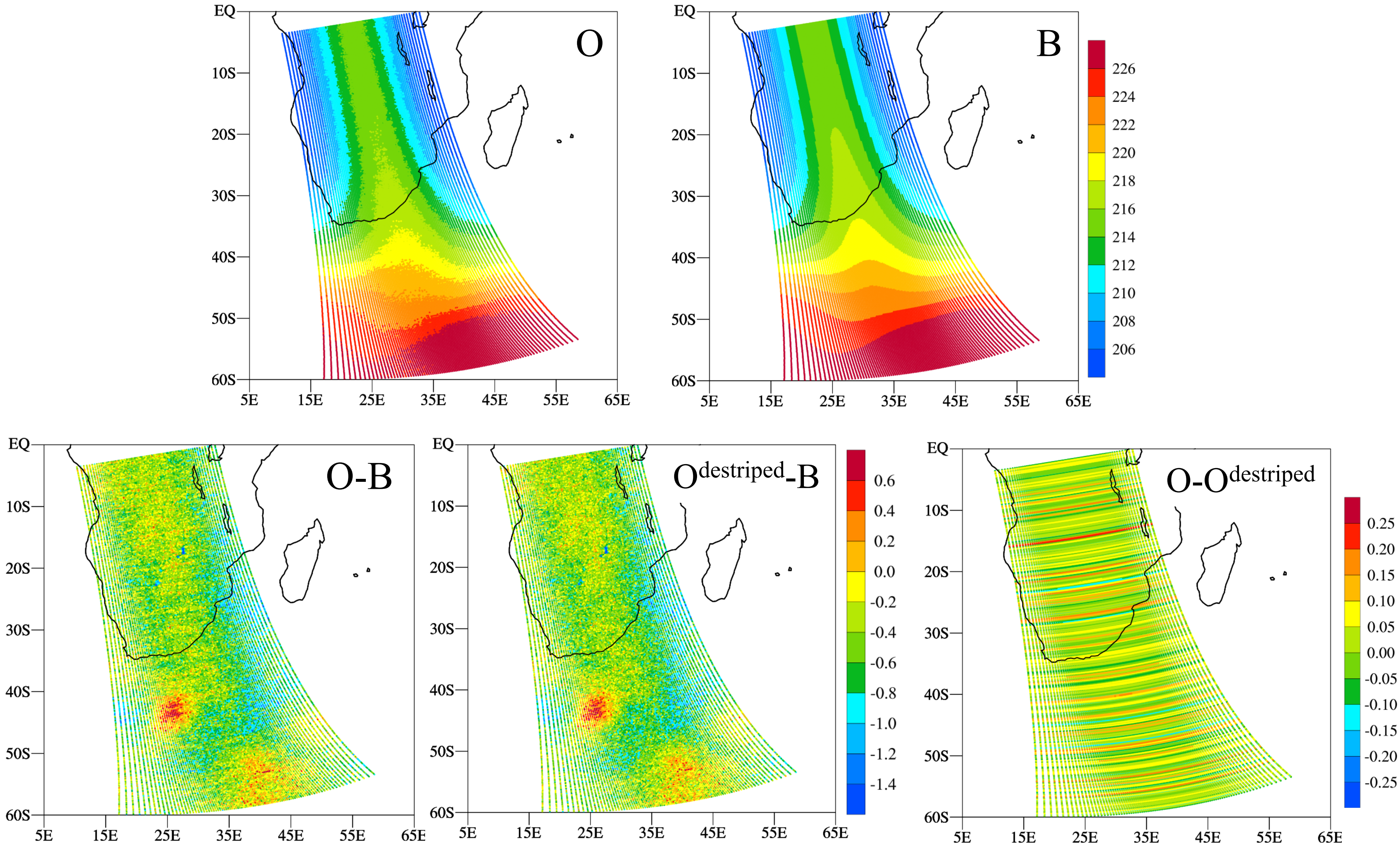

- Striping noise are visible in O and O-B fields
- Striping noise are successfully eliminated by the mitigation algorithm

Impacts of TB Jumps on Striping Noise

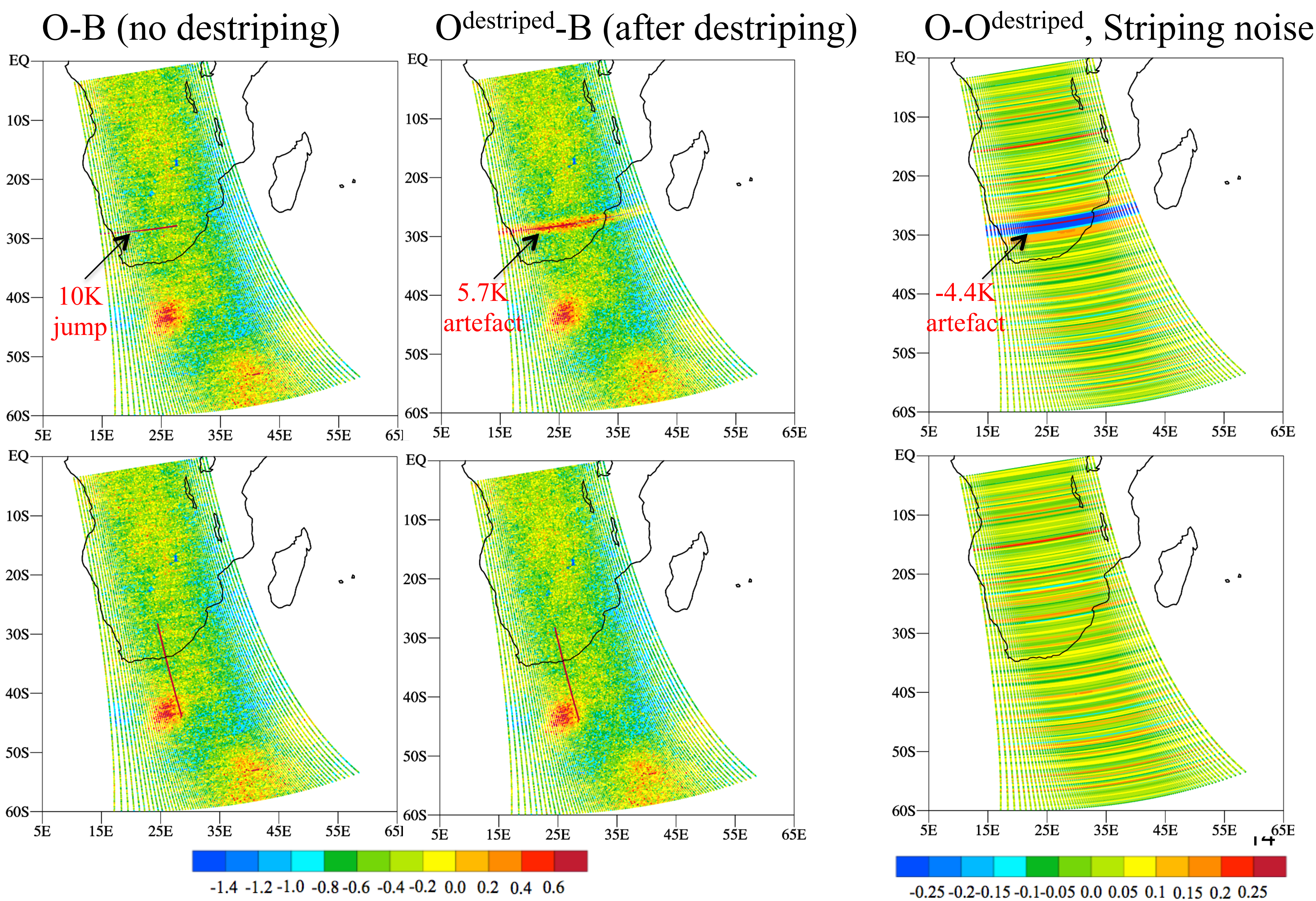

What Happened When TB Experienced a Jump?

ATMS Channel 3 on January 2, 2013

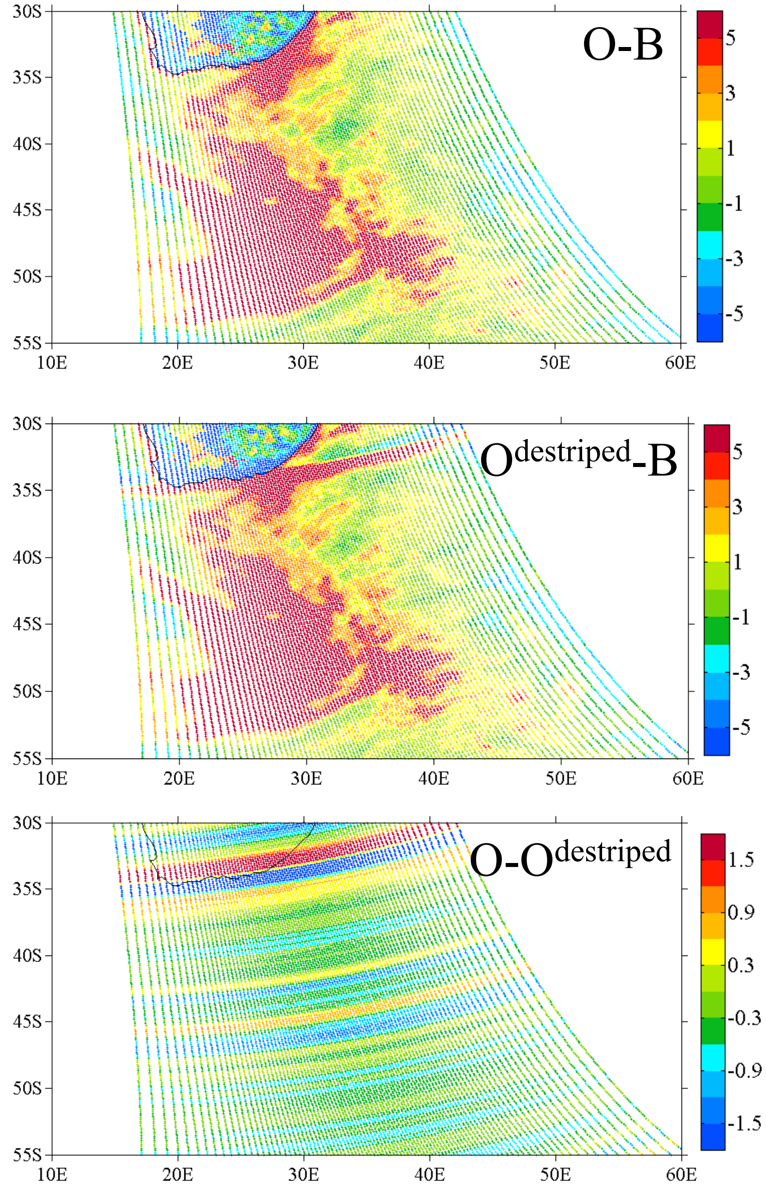

ATMS Observations

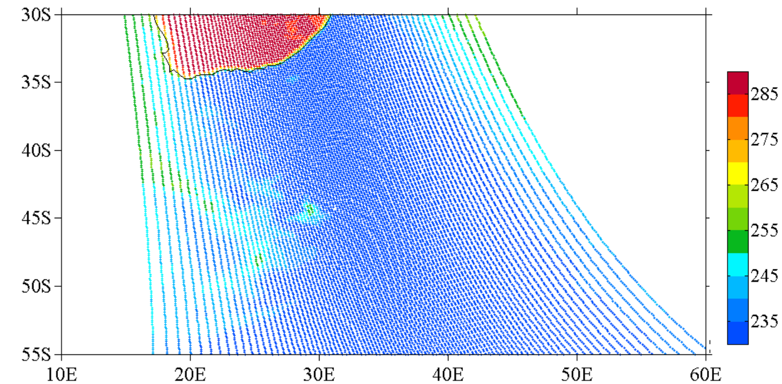

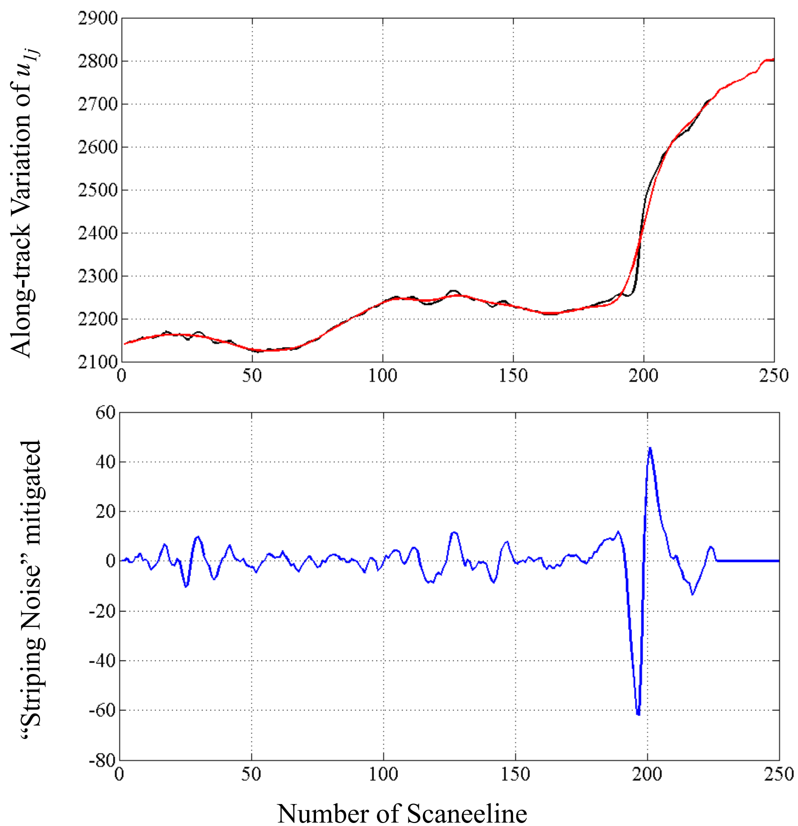

Proposed Modification I

1) An ATMS swath is divided into eight parts. Each narrow swath part consists of 12 continuous FOVs.
2) The striping noise mitigation is applied to each narrow swath.
3) The striping noise of the part with the minimum standard deviation is taken as the striping noise of the entire swath.

Motivation: Often only a portion of the ATMS scanline is aligned with coastal curves or edges of heavy precipitation.

Applications:

- Use pitch-over maneuver data to confirm if the proposed modification works
- Apply the proposed modification to ATMS channel 3 data

Striping Noise in Pitch-Over Maneuver Data for Channel 10

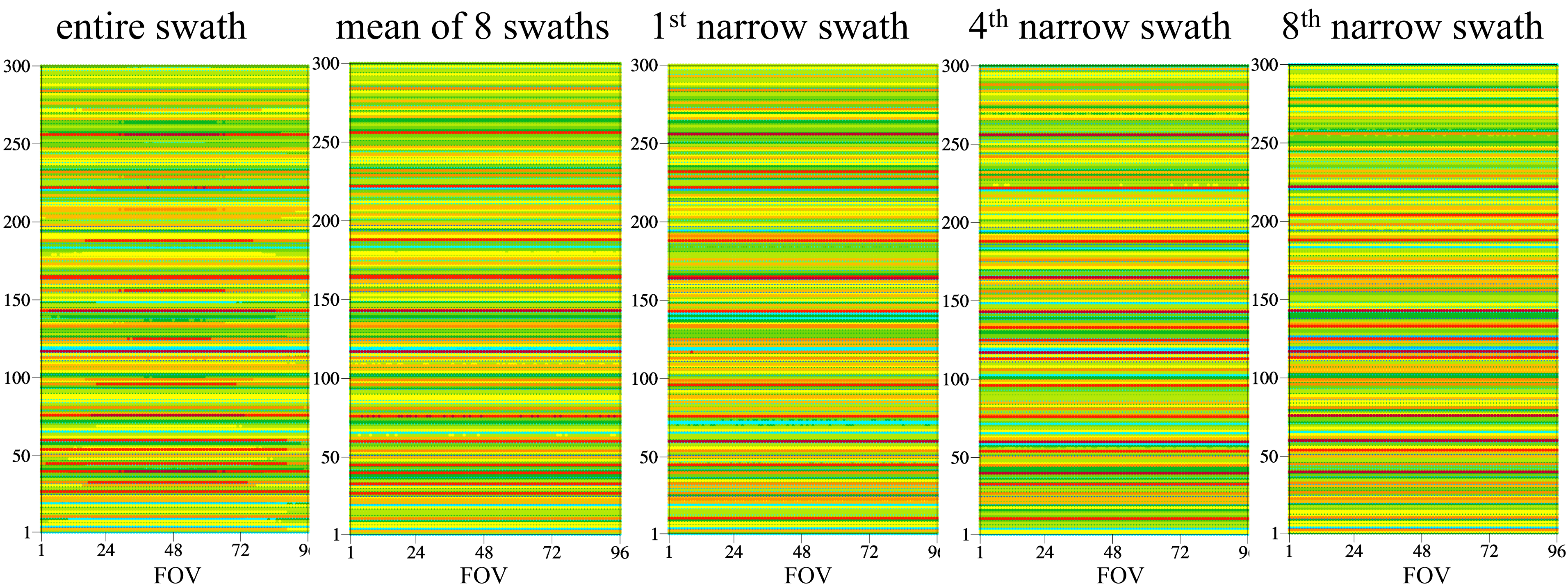

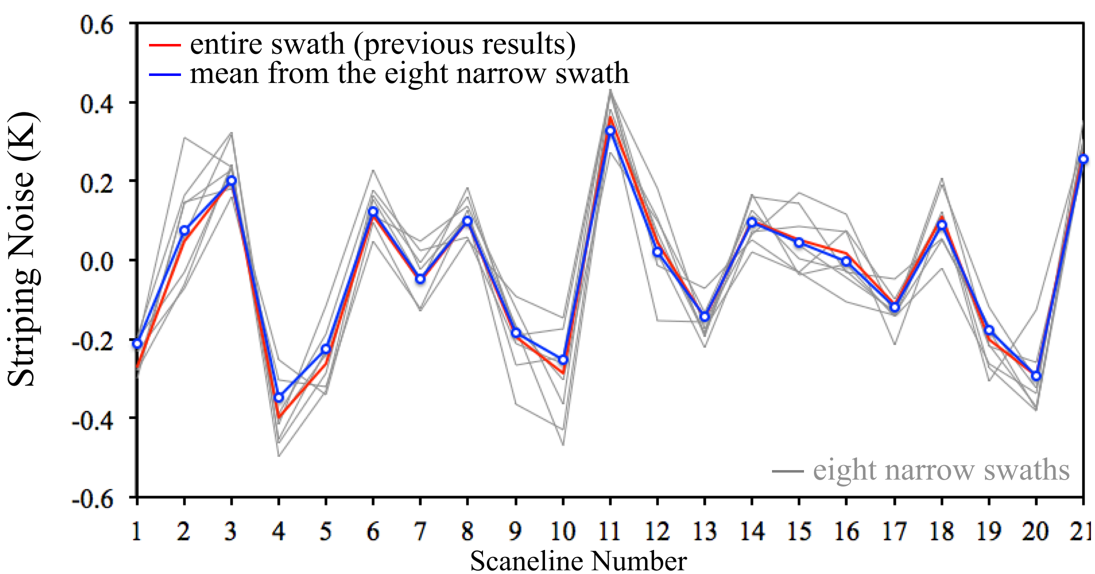

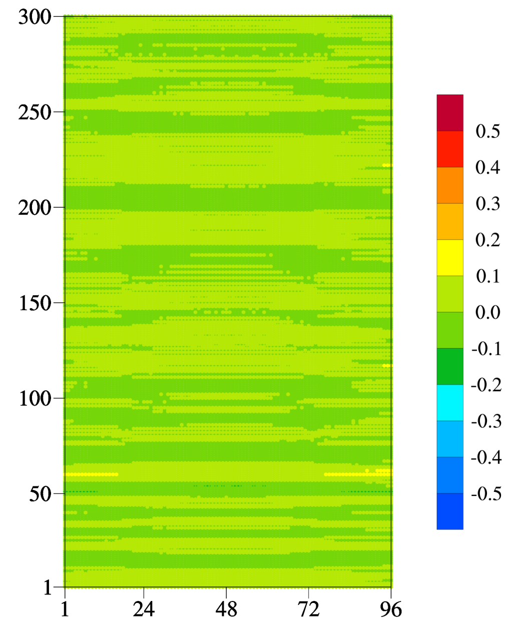

Striping Noise for ATMS Channel 3 on 2 January 2013

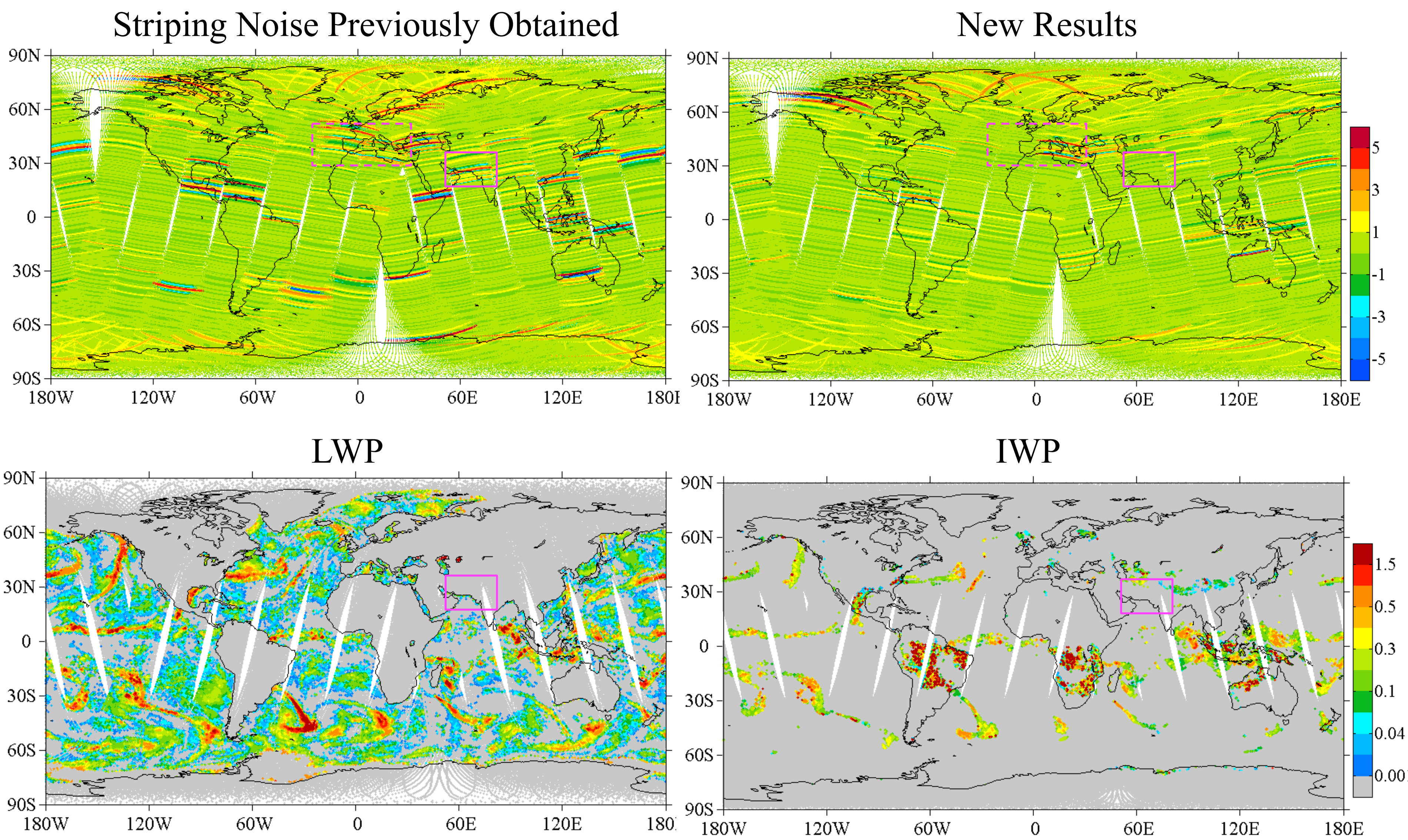

Striping noise of significant magnitudes are mostly eliminated by the proposed modification.

Applications of the Proposed Modification to Channel 3 Observations

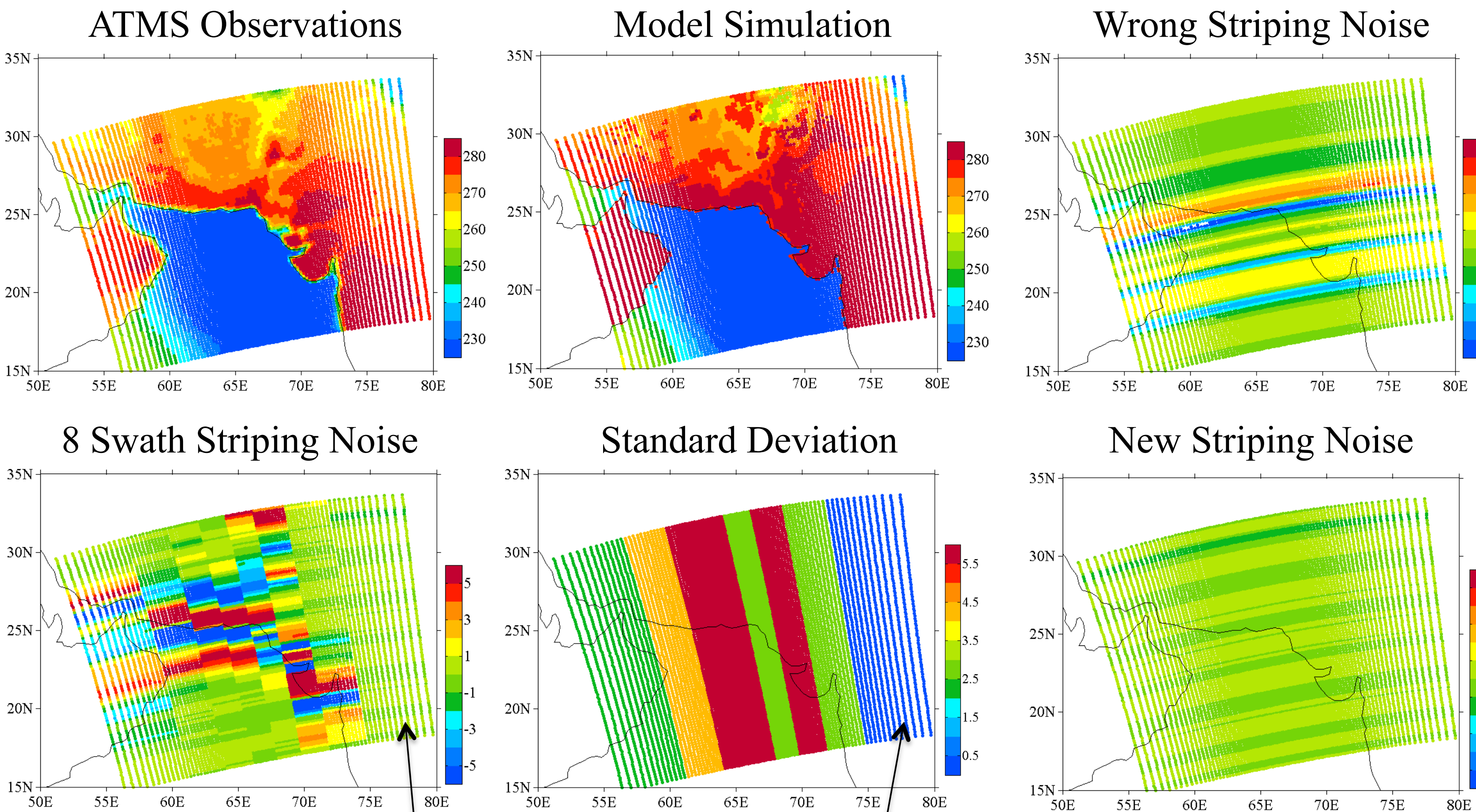

The eighth narrow swath is chosen for striping noise mitigation since it is not affected by a sharp land/ocean contrast and has the smallest standard deviation.

Proposed Modification II

Apply SNM to those scanelines with striping noise being less than 0.5 K.

The "striping noise" in ATMS channel 3 obtained previously

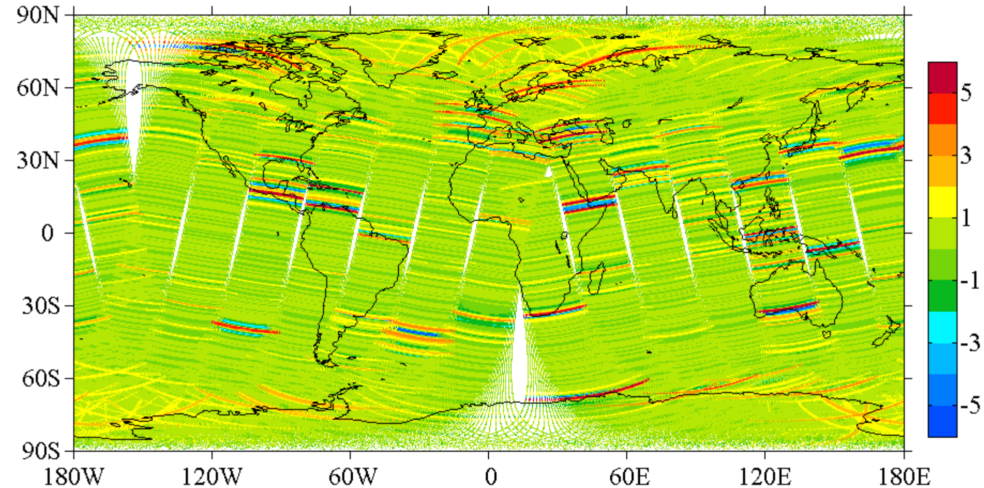

The "striping noise" in ATMS channel 3 obtained by removing those striping noise of magnitudes greater than ±0.5 K

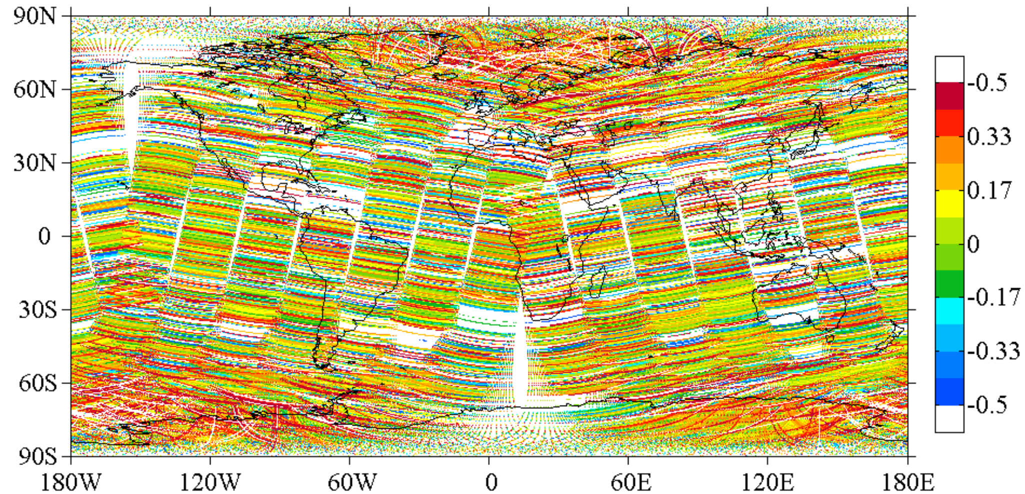

Out of 16300 scanelines, about 6185 (37.9%) have outstanding striping noise.

Summary and Conclusions

- The striping noise mitigation problems found by ECMWF when ATMS channel 3 swaths pass over Europe with complicated land/ocean boundaries were confirmed. Same problems were found in other places over the globe.
- Similar problems of striping noise mitigation were also found over ocean in places with heavy precipitation.
- The causes for the striping noise to be elevated were carefully analyzed by a sensitivity study. It was shown that such problems occur when large jumps of TB are aligned with ATMS scanelines.
- It is suggested that the striping noise mitigation could only be done for those ATMS scanlines for which at least a portion of the scaneline (greater than 1/8) is not aligned with coastal curves or edges of heavy precipitation. Even in this case, a modified implementation of the striping noise mitigation is required to avoid impacts of large jumps in TB for noise mitigation.
- Given the fact that the dynamic ranges of O-B variations are much larger than the striping noise for window channels and lower temperature and humidity sounding channels, striping noise mitigation is not as critical as for upper-level sounding channels and could be avoided.

Acknowledgement

This work was supported by NOAA JPSS Proving Ground Program.

Suomi NPP ATMS Scan Reversal Study

Hu (Tiger) Yang, Ninghai Sun, Fuzhong Weng

NOAA/STAR ATMS SDR Working Group

Summary of Investigation

Scan Drive Current Anomaly

- Scan drive current is kept at a relatively high level after the anomaly happened at May.31,2016
- Scan angle of warm load/space view increased about 0.1^{o}
- Instrument temperature and warm load temperature increased about 2^{o}, temperature gradient is also slightly increased
- There is no calibration accuracy degradation observed in TDR products

Scan Reversal Data Processing Algorithm

- Scan reversal is carried out once every orbit near polar region;
- Two granules science data are lost during scan reversal operation;
- Reversal scan profile was studied from diagnostic data packets;
- Remapping algorithm was developed to minimize the impacts of scan reversal to data user
- Current calibration/geolocation algorithm need to be modified to adapt to reversal scan profile;

Impact of SD Current Abnormal on Science Data

- Scan drive current is kept at a relatively high level after the anomaly happened at May.31,2016
- Instrument performance may be degraded during the process

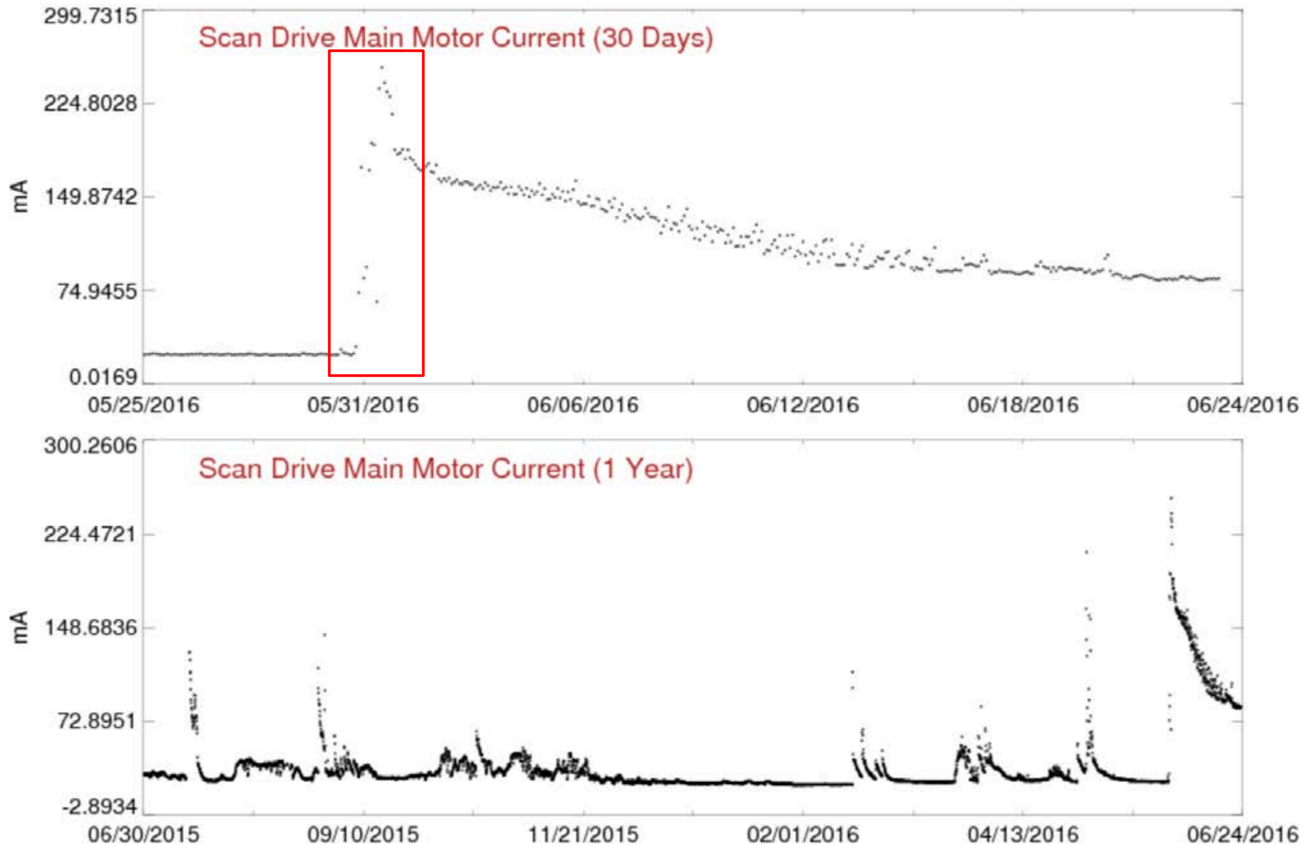

Impact on Warm load/Space view Scan Angle

- Plotted data points start from 05/25/2016 00h to 06/02/2016 23h
- Both scan angles for warm target and space view increased about 0.1 degree after SD current anomaly accident on 05/31/2016

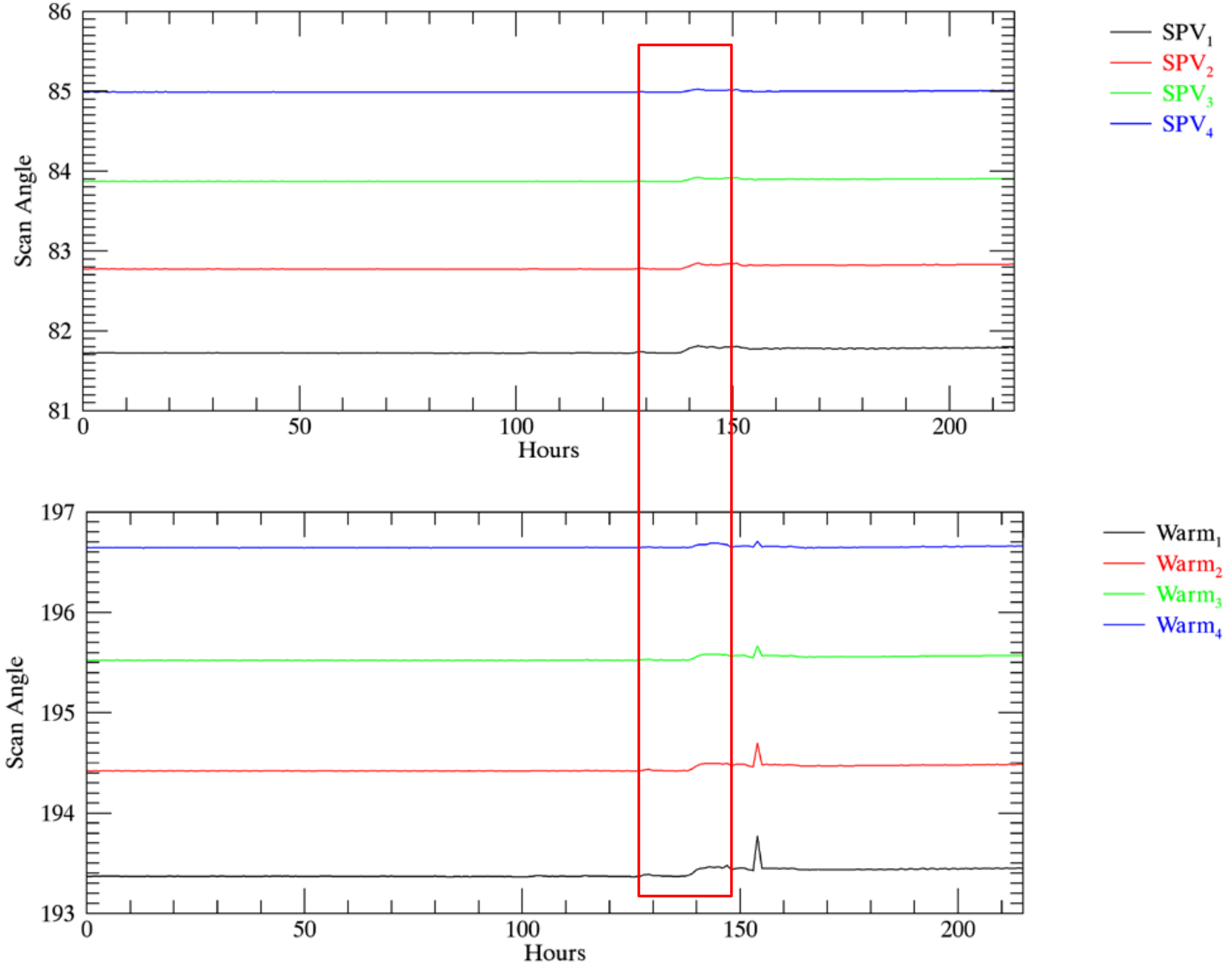

Impact on Instrument/Warm Load Temperature

Temperature Trend

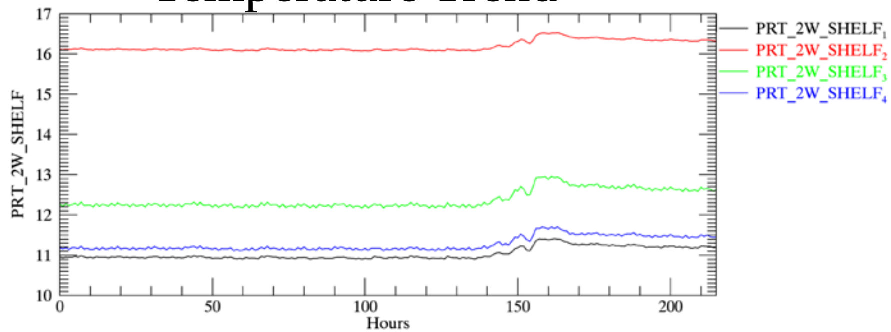

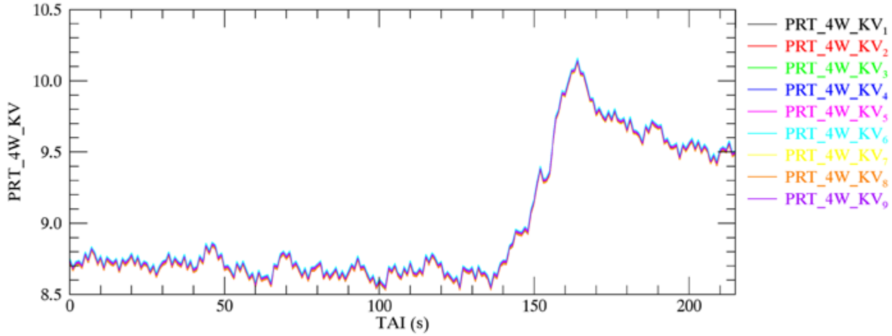

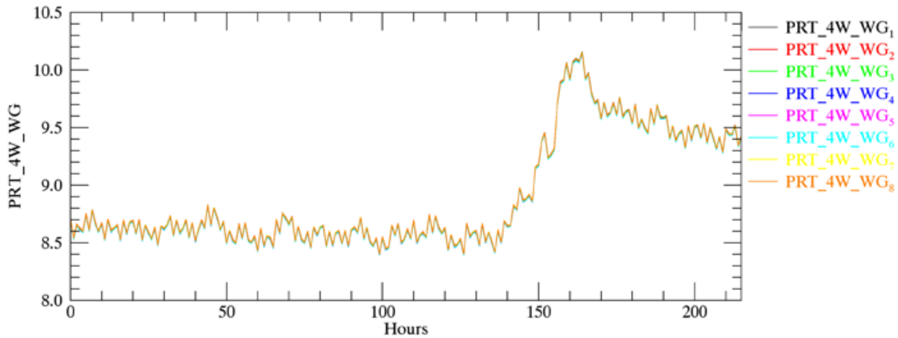

Temperature Gradient

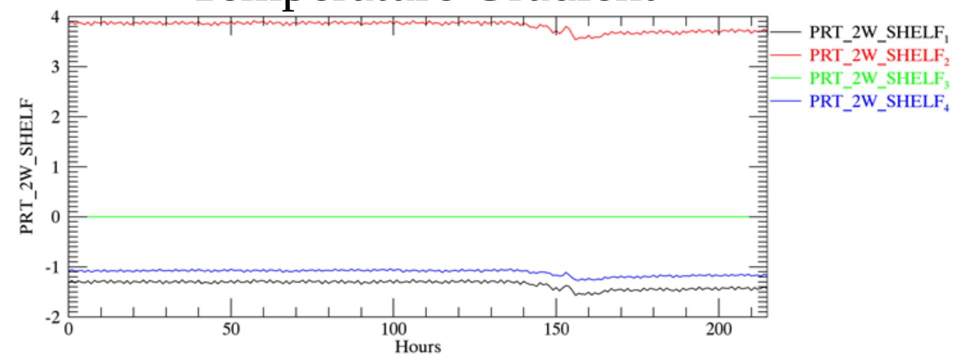

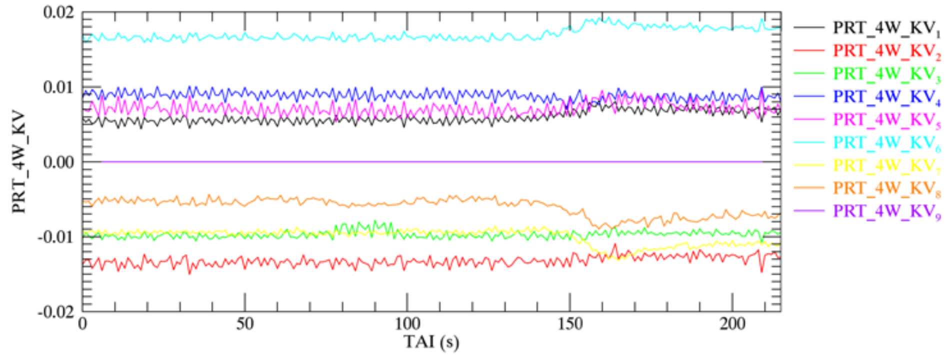

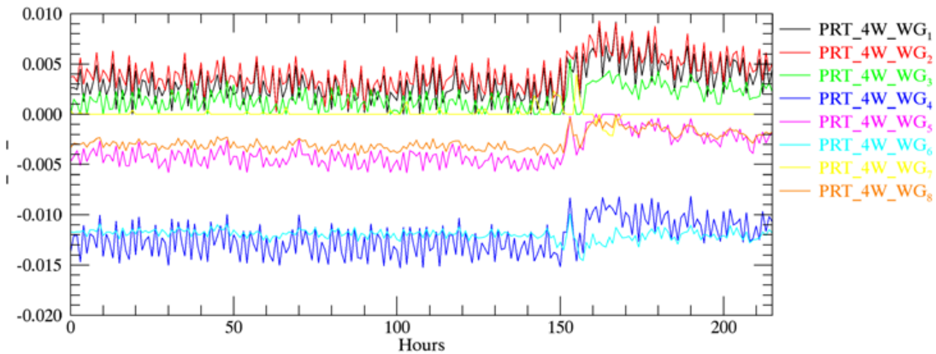

Impact on Calibration Counts

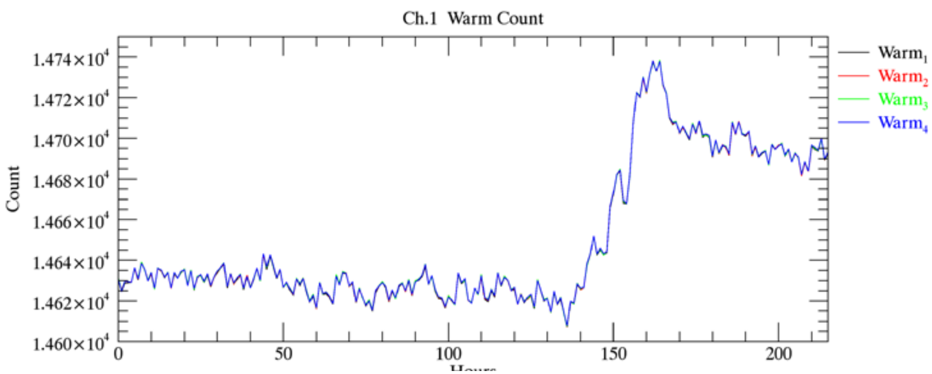

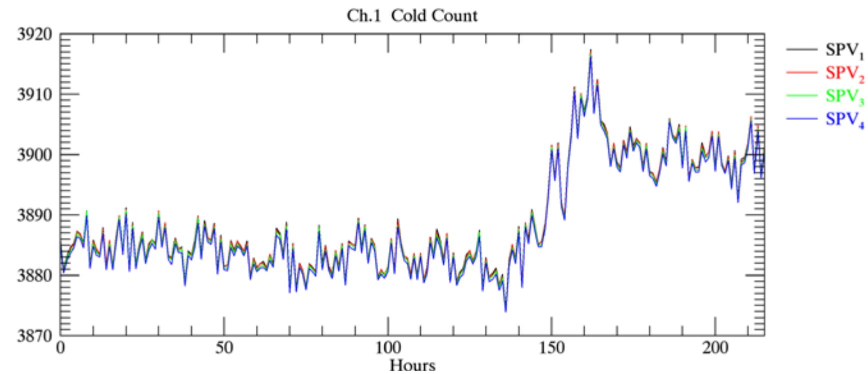

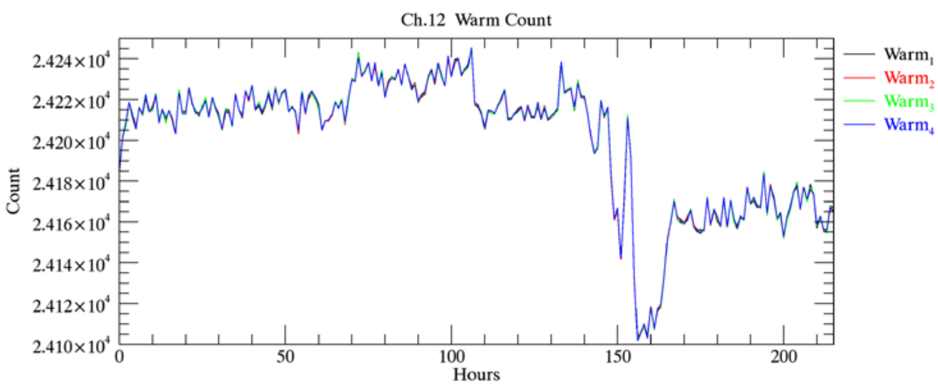

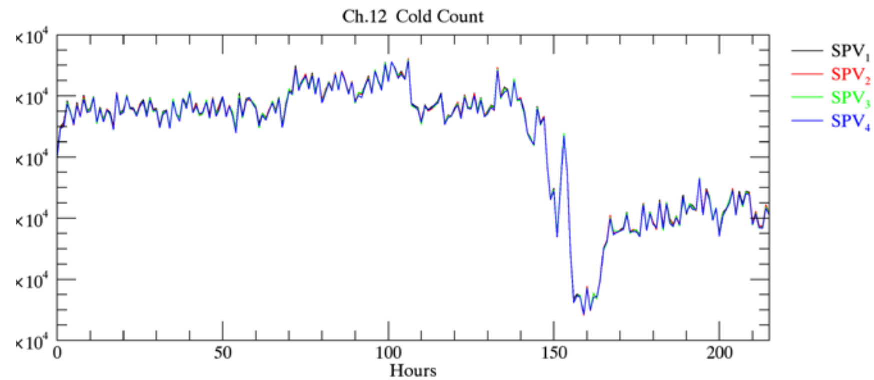

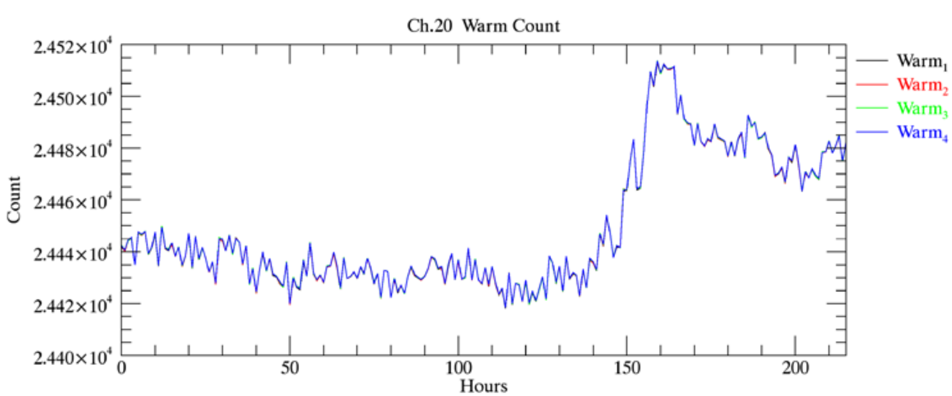

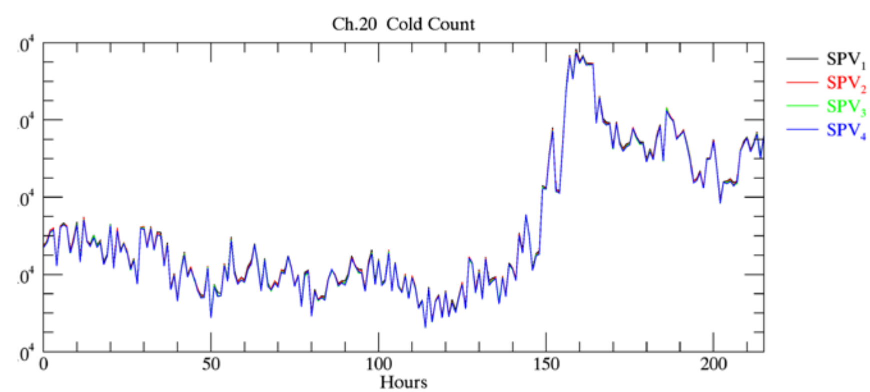

Impact on TDR Calibration Accuracy

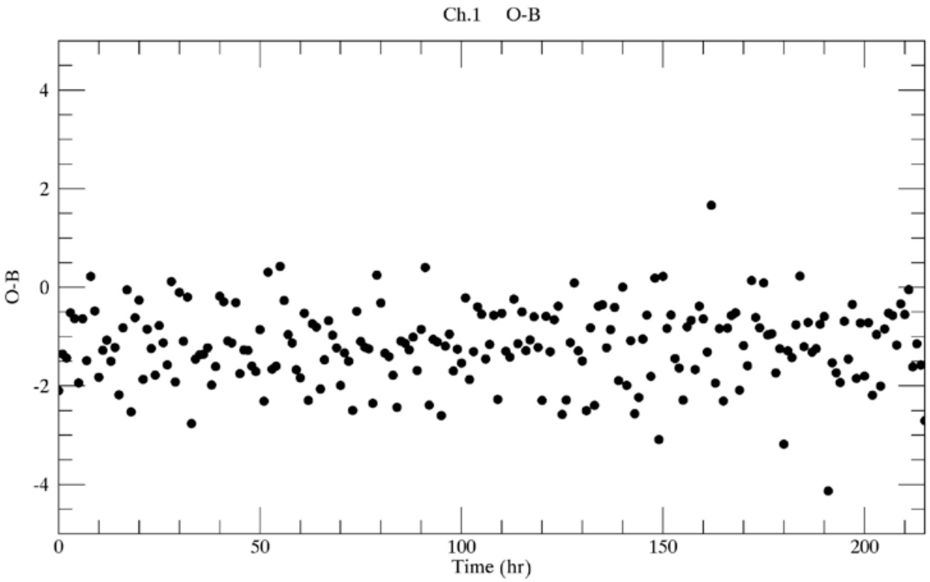

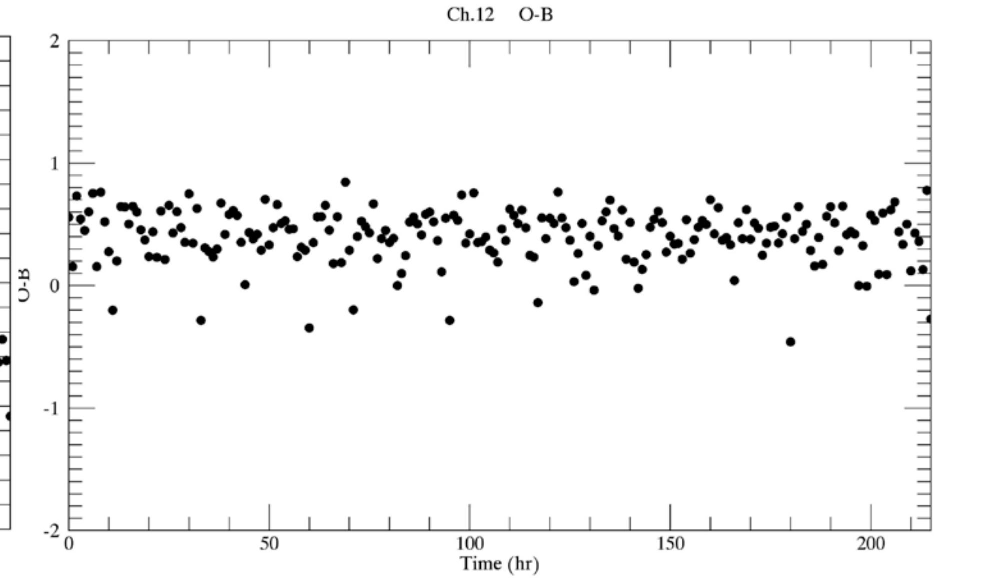

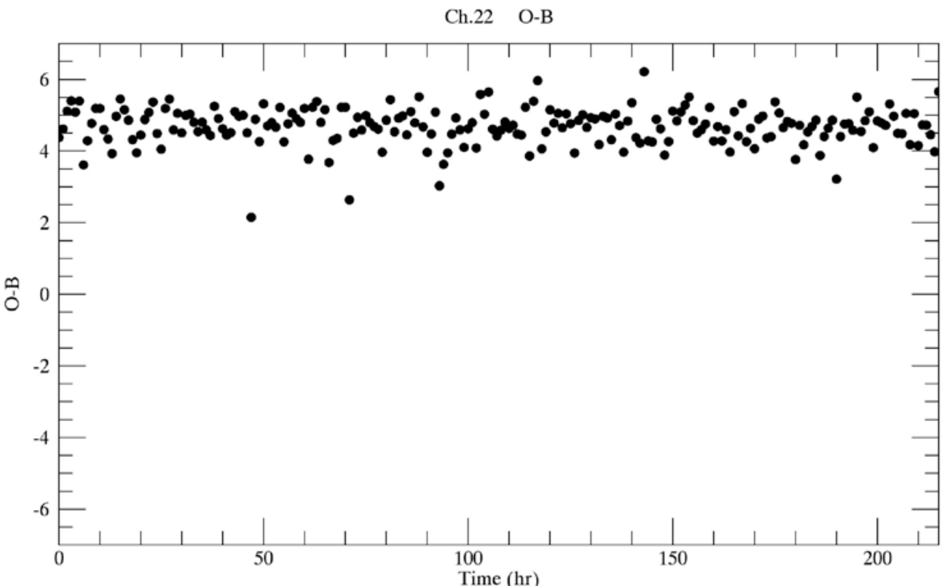

- O: IDPS ATMS TDR products
- B: Model simulation with GDAS forecasts as inputs
- Hourly averaged O-B since May.25 00h, 2016 was calculated
- No significant bias increase was observed

Preliminary Study for Processing Reversal Scan Data

- Evaluated the impact of scan profile change on ATMS data quality
- Developed new remapping algorithm to rebuild normal-scan TDR products from reverse scan datasets with 48 FOVs
- Tested remapping algorithm on simulated reversal scan observations

Impact of Current Scan Reversal on IDPS TDRs

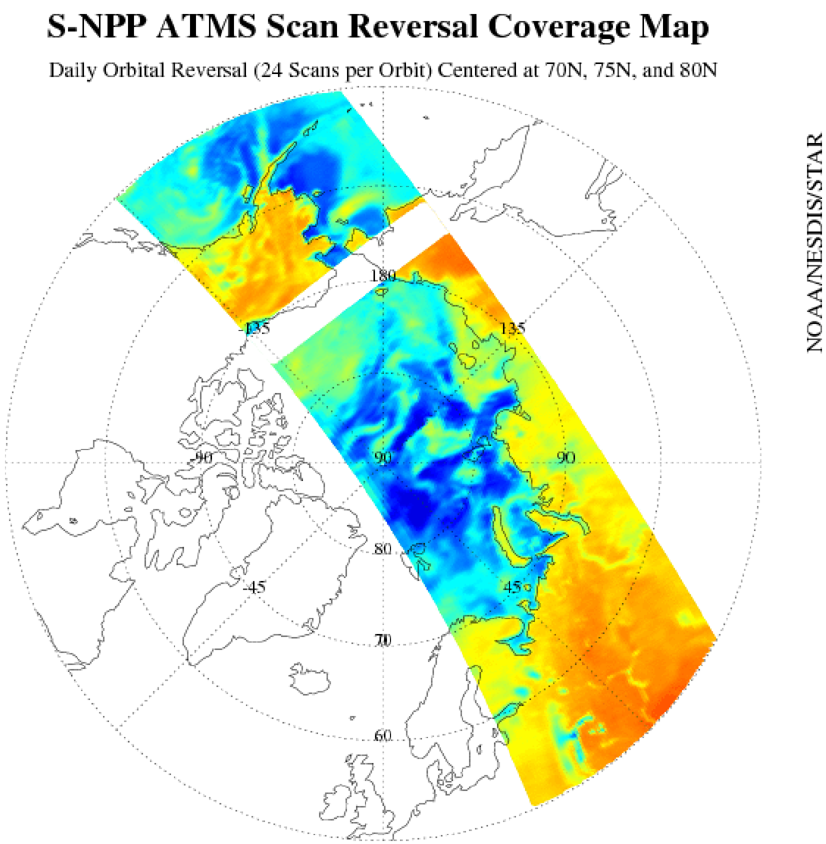

- Frequency of current scan reversal is once every orbit, total of 2 granules are effected and data gap being generated in IDPS TDR products
- Scan reversal operation is carried out at polar region, scan start position is set to random
- Science data can only be found at diagnostic data packet

Comparison of Scan Geometry for Current and Reverse ATMS Scan Profiles

Comparison of Scan Geometry between Current and New Scan Profiles

Scan mode		Current	Reverse
Satellite Altitude (km) and inclination angle		824, sun-synch (i=98.7 deg), 1:30 pm Ascending Node	
Ground Speed (km/s)		7.0	
Scan Period (s)		8/3	
Earth View Scan Rate (degree/s)		60.9	121.8
Earth View Scan Time (s)		1.728	0.864
FOVs/Scan		96	48
Step Angle (degree)		1.1	2.2
Sampling Time (ms)		18.0	18.0
Integration Time (ms)		17.6	17.6
Nadir EFOV Size (Km)	K/Ka	91x75	106x75
	V/W	47x32	63x32
	G Bands	32x16	47x16

Comparison of Sampling/Integration Time between Current and New Scan Profiles

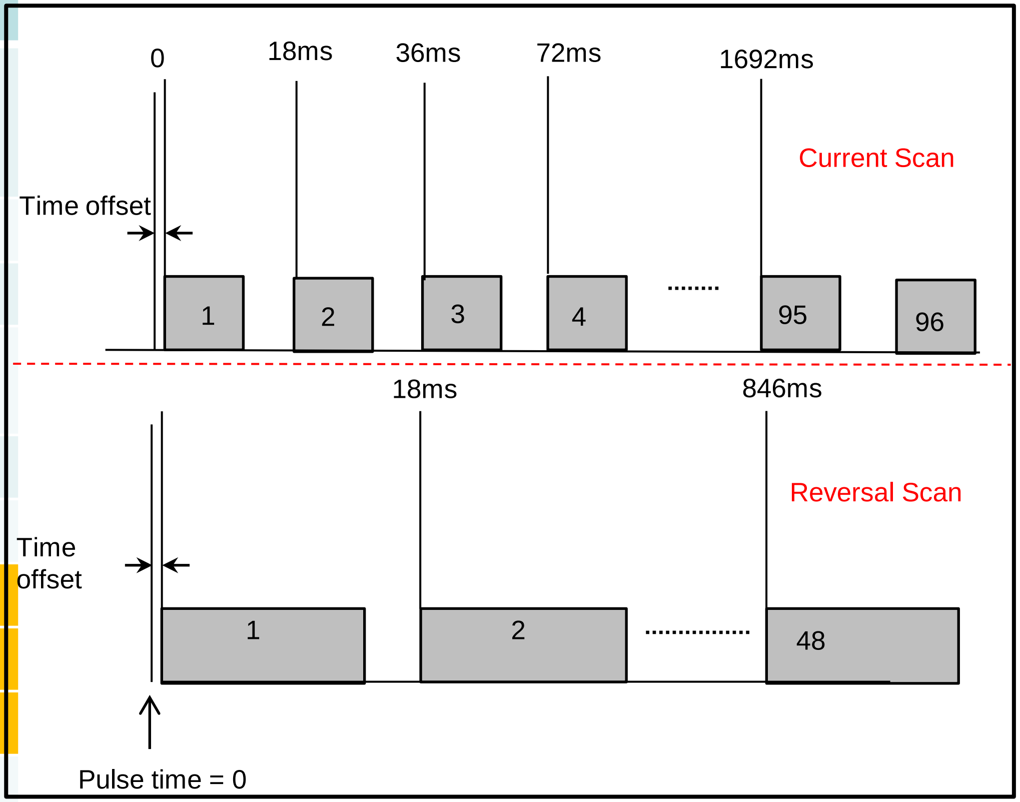

Comparison of ATMS FOVS Between Current and Reversal Scan Profiles

- Field of views at nadir position for both current and new scan profiles are simulated
- Smearing effects are considered in this FOV simulation.
- The reversal scan profile yields larger FOV sizes with less overlapping between FOV

Current Scan Profile

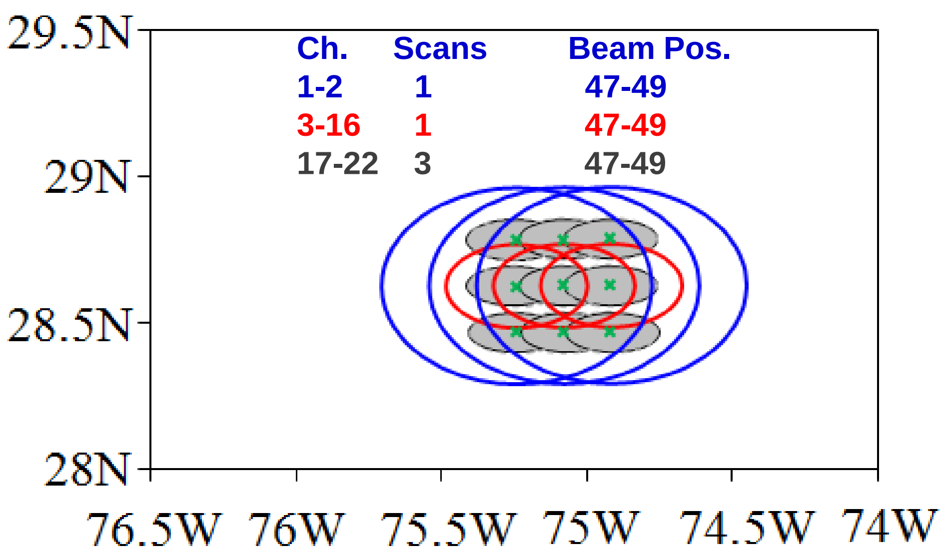

Reverse Scan Profile

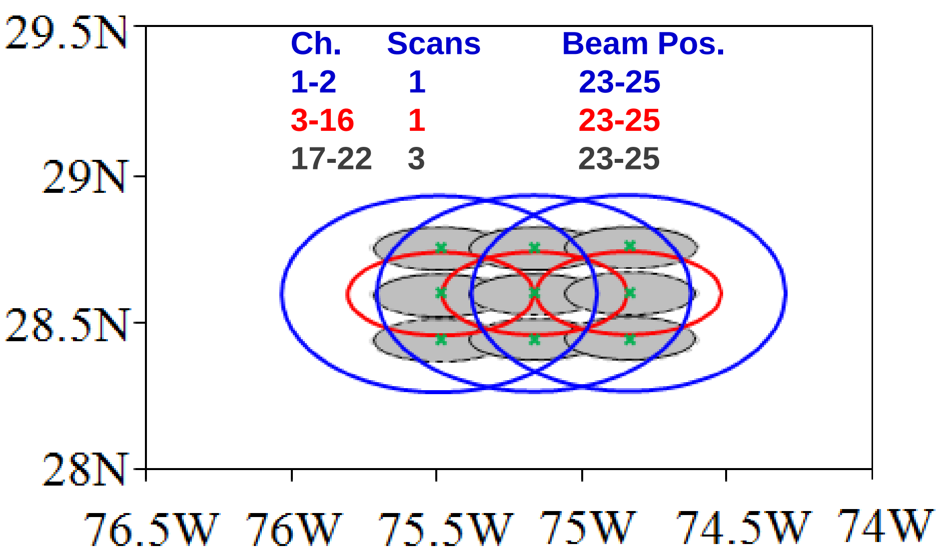

Resolution degradation:

K/V Bands: 17% **V/W Bands: 32%** **G Bands: 48%**

Comparison of ATMS NEDT Between Current and New Scan Profiles

Red : CRIS FOV at nadir
Black: ATMS FOV at nadir

Current
(3x3 looks average)

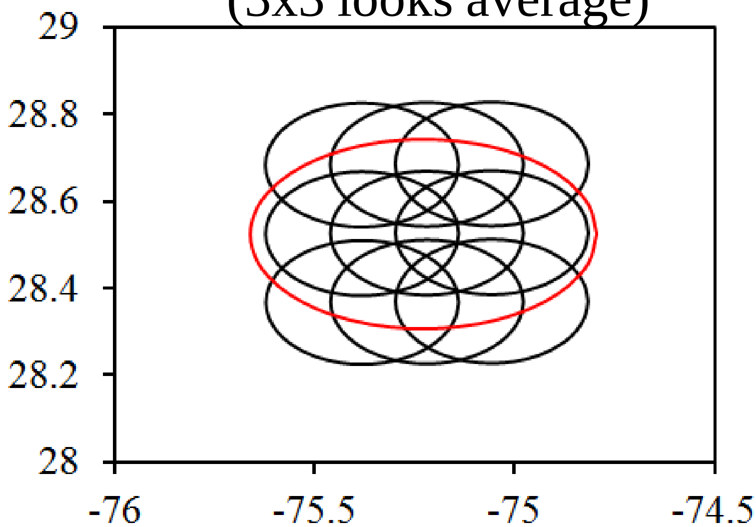

New
2x2 looks average

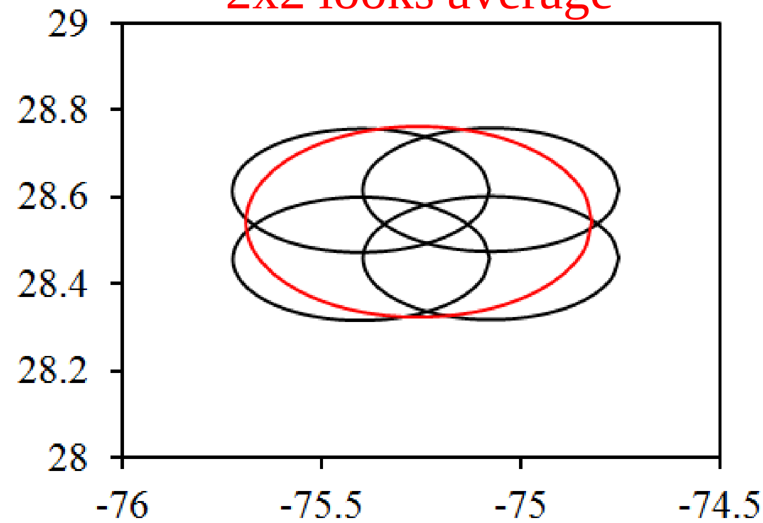

	Noise from Current Scan	Noise from new Scan
Noise for single observation	$NE\Delta T = \frac{T_{sys}}{\sqrt{B \cdot \tau}}$	$NE\Delta T = \frac{T_{sys}}{\sqrt{B \cdot \tau}}$
Noise after average over multiple looks	$NE\Delta T = \frac{T_{sys}}{3 \cdot \sqrt{B \cdot \tau}}$	$NE\Delta T = \frac{T_{sys}}{2 \cdot \sqrt{B \cdot \tau}}$

ATMS Current/New Scan Profile NEDT

Ch.	NEDT (K)				Ch.	NEDT (K)			
	AMSU/ MHS	TDR	RSDR			AMSU/ MHS	TDR	RSDR	
			Current	New				Current	New
1	0.30	0.25	0. 08	0.13	12	0.40	0.62	0.21	0.31
2	0.30	0.34	0. 11	0.17	13	0.60	0.90	0.30	0.45
3	0.40	0.39	0. 13	0.20	14	0.80	1.25	0.42	0.62
4		0.30	0. 10	0.15	15	1.2	2.03	0.68	1.02
5	0.25	0.30	0. 10	0.15	16	0.5	0.30	0.10	0.15
6	0.25	0.30	0. 10	0.15	17		0.47	0.16	0.23
7	0.25	0.30	0. 10	0.15	18	0.84	0.38	0.13	0.19
8	0.25	0.29	0. 10	0.14	19	0.60	0.46	0.15	0.23
9	0.25	0.31	0. 10	0.16	20	0.70	0.54	0.18	0.27
10	0.40	0.44	0. 15	0.22	21	1.06	0.59	0.20	0.29
11	0.40	0.59	0. 20	0.30	22		0.73	0.24	0.37

ATMS Observation Simulation for Different Scan Profile

Scan Geometry

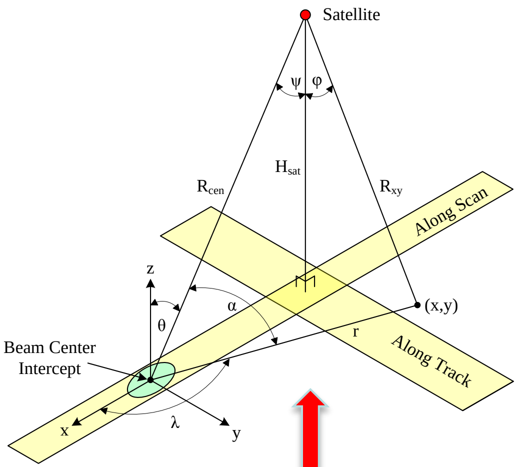

Tb obs. within one single FOV

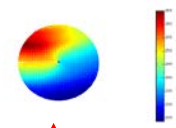

Antenna Pattern within one single FOV

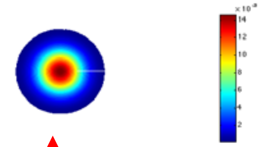

$$Ta = \int T_B(\rho) G_i(\rho) dA$$

Ta is calculated by convoluting Tb with ATMS antenna pattern

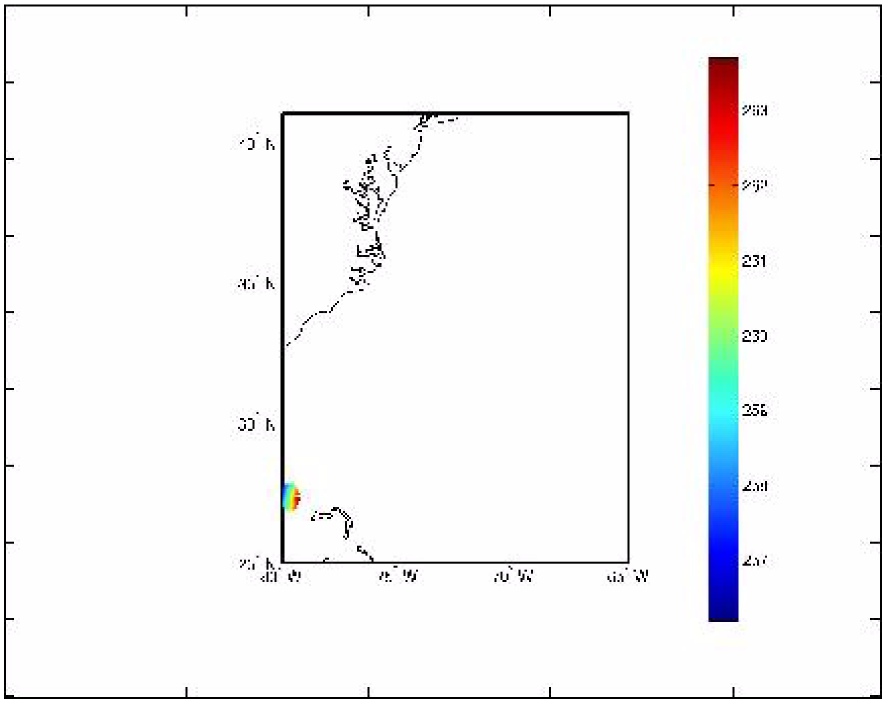

Satellite Orbits

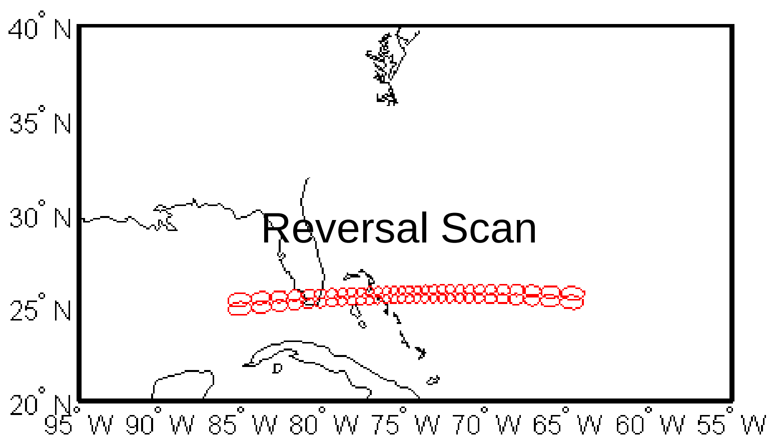

Comparison of ATMS Observations for Different Scan Profile

ATMS observations are simulated for both normal and reverse scan profiles. Simulated case is Hurricane Sandy at 06:00 UTC, Oct. 28, 2012 using CRTM model with the input surface and atmosphere geophysical parameters being provided from the HWRF 9km grid resolution forecasts.

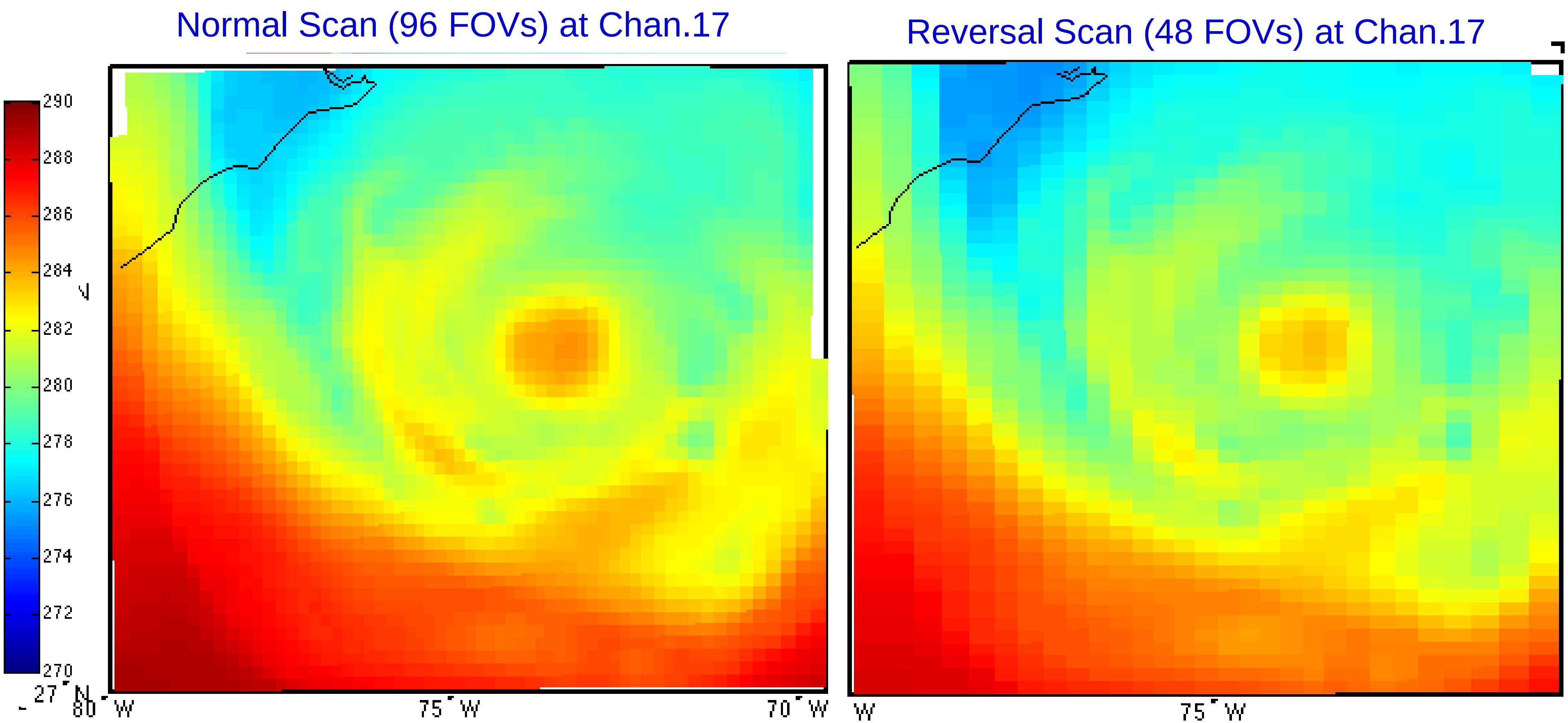

Remapping Algorithm for Reversal Scan Observations

Weighting Coefficients at Edge of Scan for V/W Bands

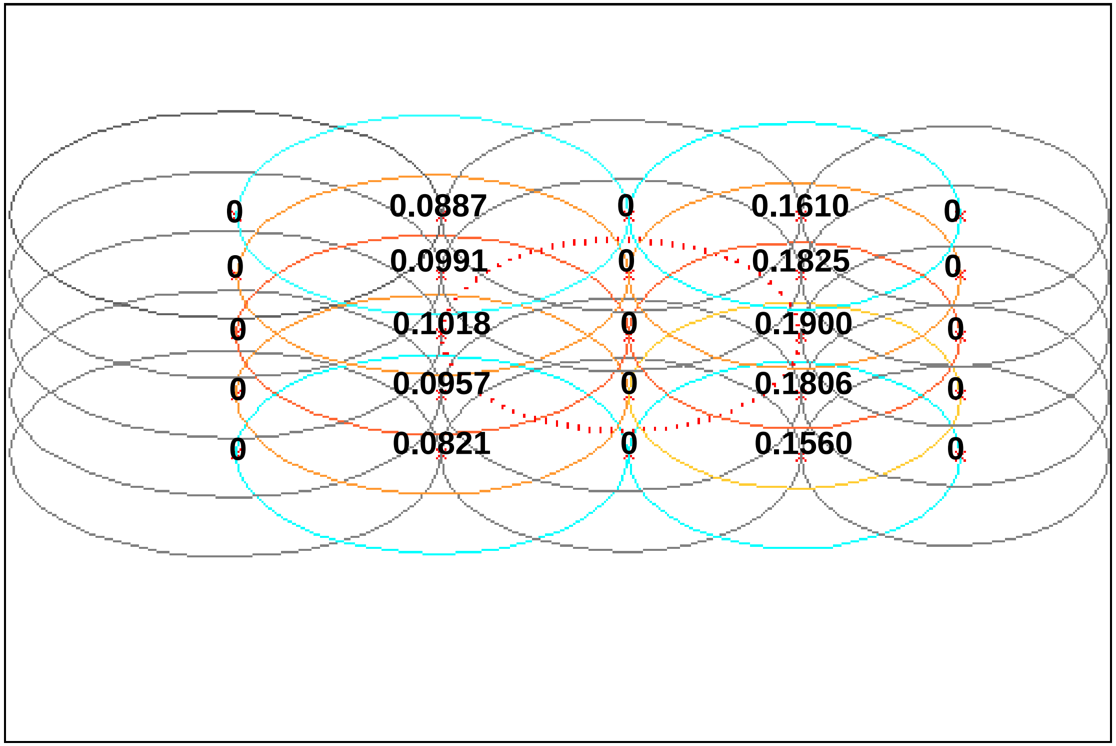

Construct a cost function, in which the antenna pattern being used as source and target function, and should be minimized by a set of optimal remapping coefficients

$$Q_0 = \int \left[\sum_{i=1}^{n} a_i G_i(\rho) - F(\rho) \right]^2 J(\rho) dA$$

Apply the coefficients to source observations

$$\overline{T_{Bi}} = \int T_B(\rho) G_i(\rho) dA$$

Finally reconstruct observations at target FOV size

$$T_B = \sum_{i=1}^{n} a_i \overline{T_{Bi}} = \int T_B(\rho) \sum_{i=1}^{n} a_i G_i(\rho) dA$$

Preliminary Results for Reversal Scan Remapping Results

- ATMS channel 16 antenna temperature was simulated for both reversal and normal scan
- Remapping coefficients was applied to reversal scan simulations to generate normal scan observations with 96 FOVs
- Comparison between rebuilt and original normal scan observations shows data quality improvement

Reverse Scan with 48 FOVs | **Rebuilt Normal Scan with 96 FOVs** | **Normal Scan with 96 FOVs**

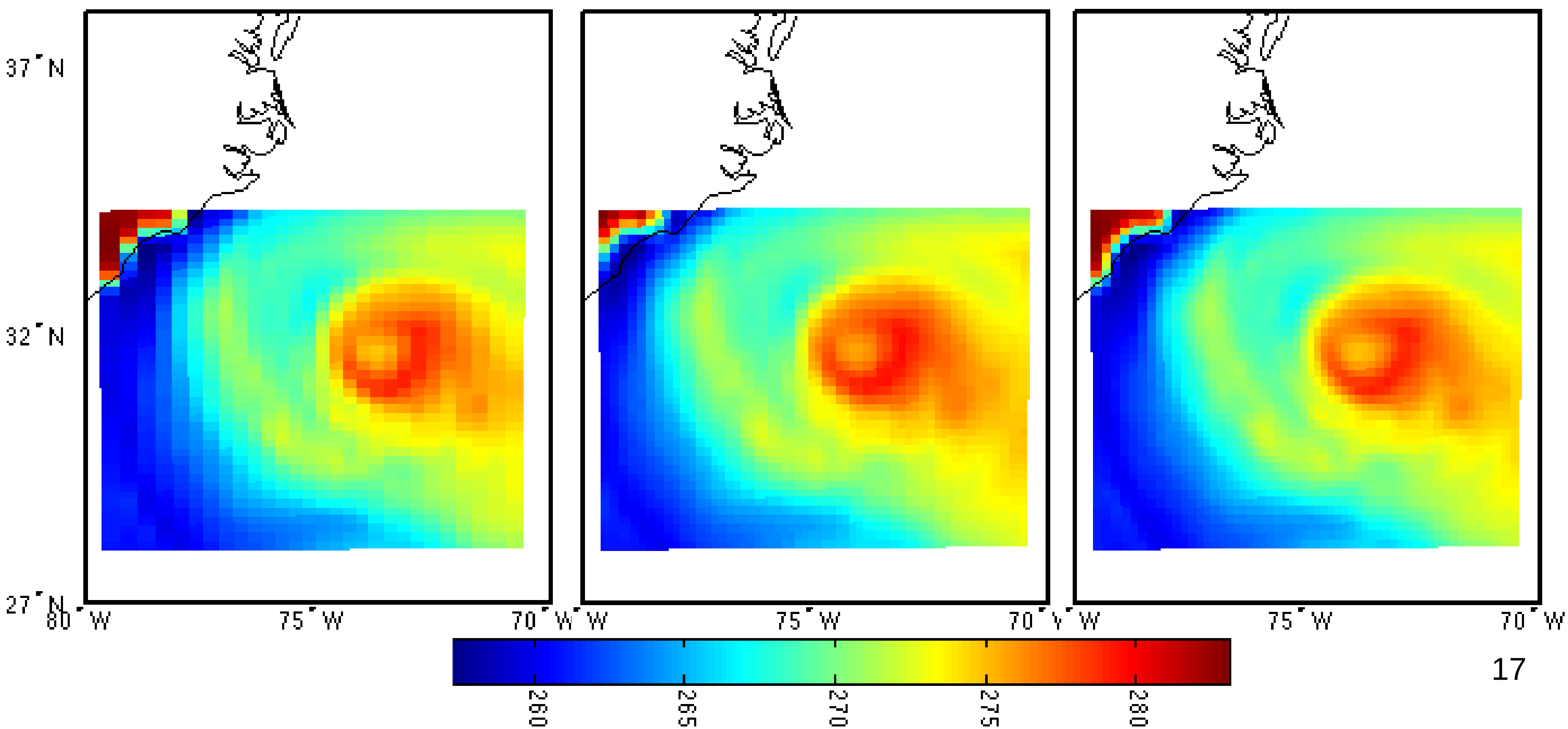

Conclusion and Future Work

- Scan reversal data was studied and remapping algorithm was developed to generate normal-scan-like TDR products from reversal scan observations with only 48 FOVs
- Future work is to implement scan reversal data processing module to current NOAA offline ATMS ground processing software ARTS
- Reprocessing ATMS TDRs to fill the reversal scan data gap by using ARTS if there is such requirements in future

Effects of ATMS SRF Imbalances at G-Band Channels on Brightness Temperature Simulations

Lin Lin[1,2] and Fuzhong Weng[1]

[1]NOAA Center for Satellite Applications and Research
[2]I. M. Systems Group, Inc.

Acknowledgements: Vincent Leslie and William Blackwell (MIT/LL)

2016 STAR JPSS Annual Science Team Meeting
NCWCP, Maryland, August 8-12, 2016

Statement of Problem

- SRF imbalances were found to be present in J1 ATMS double-side water vapor sounding channels (G-band)
- An imbalance in the instrument SRF at side bands could affect the data utilization in NWP if the measured imbalances in SRFs are not taken into account in forward radiative transfer models

Action

- Quantify impacts of such SRF imbalance on brightness temperature simulations

  — Sensitivity study with four scenarios of SRF distributions

  — Comparison of MonoRTM simulations using J1 ATMS measured SRFs with those from using the boxcar SRF

Atmospheric Transmittance and Weighting Functions of ATMS G-band Channels

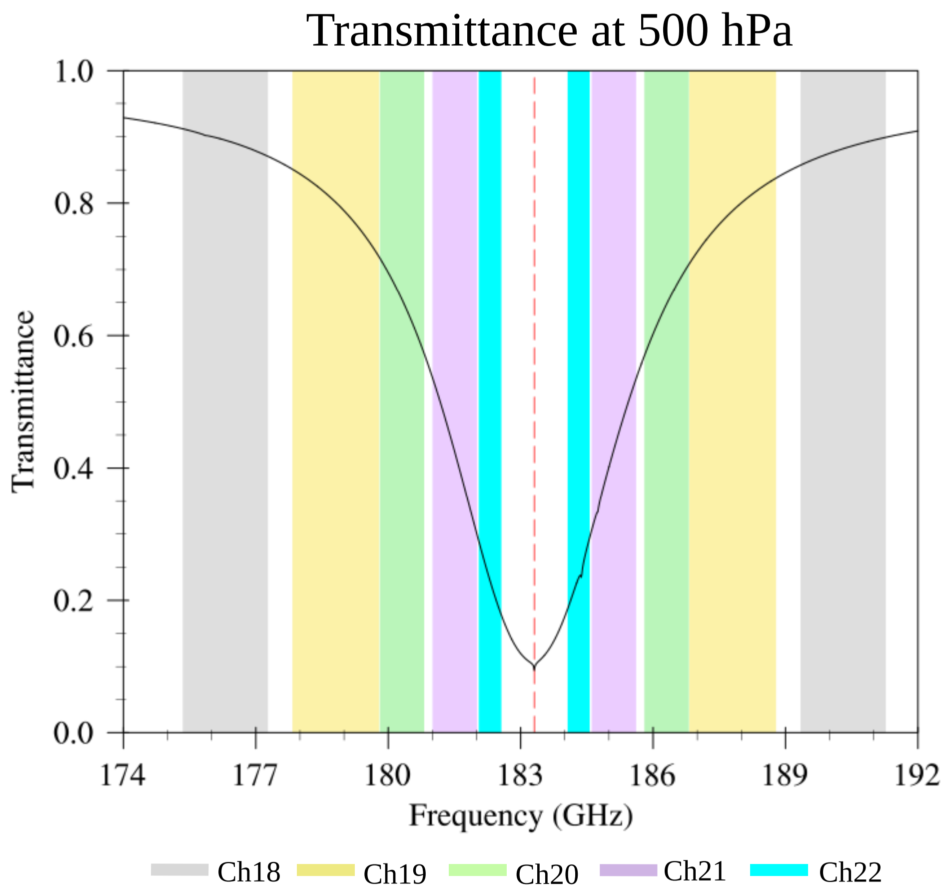

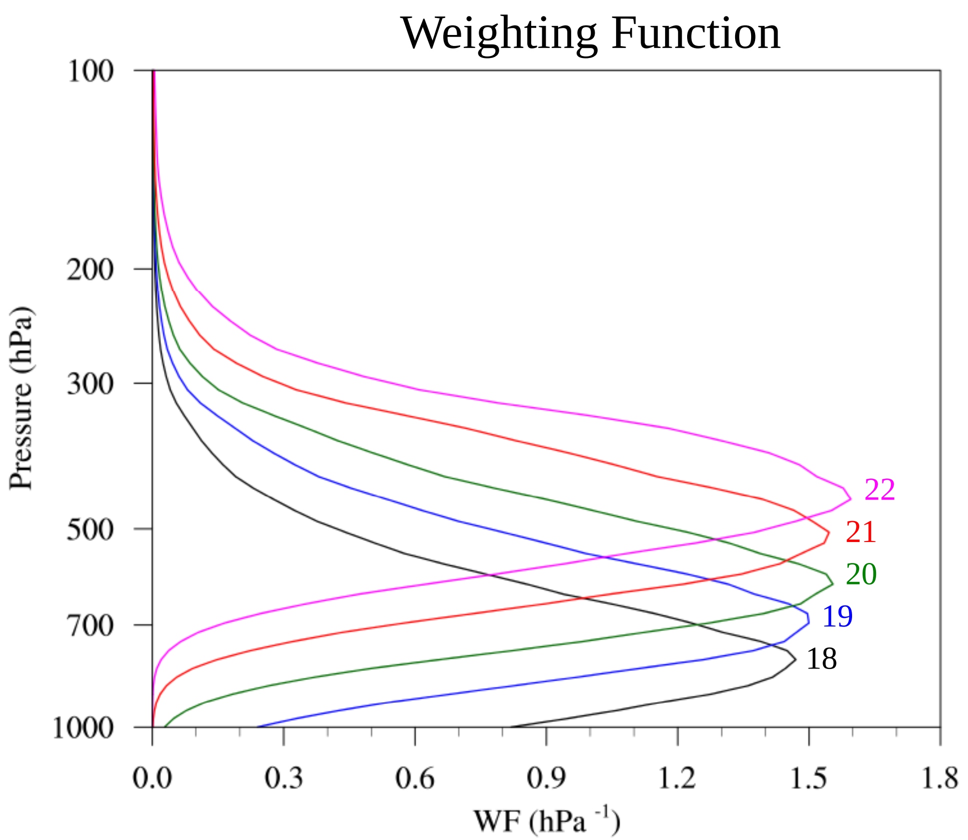

ATMS G-band channels 18-22 are located on a strong H_2O absorption line centered at 183 GHz frequency.

J1 ATMS G-Band SRFs

Channel 18 (183.31± 7 GHz)

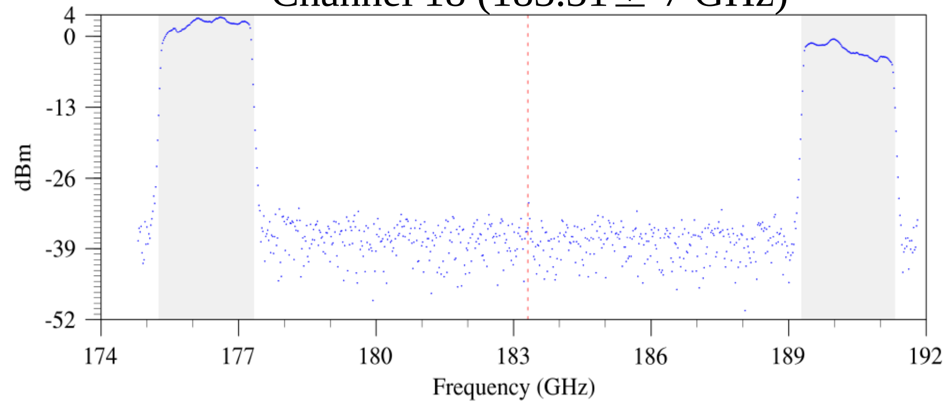

Channel 19 (183.31± 4.5 GHz)

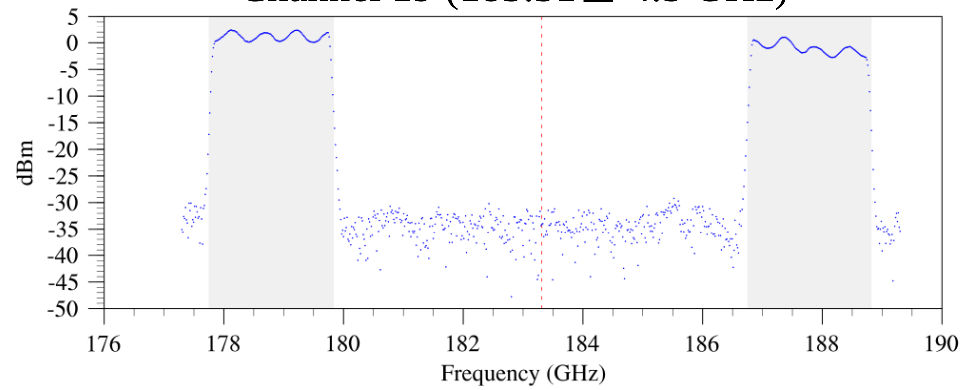

Channel 20 (183.31± 3 GHz)

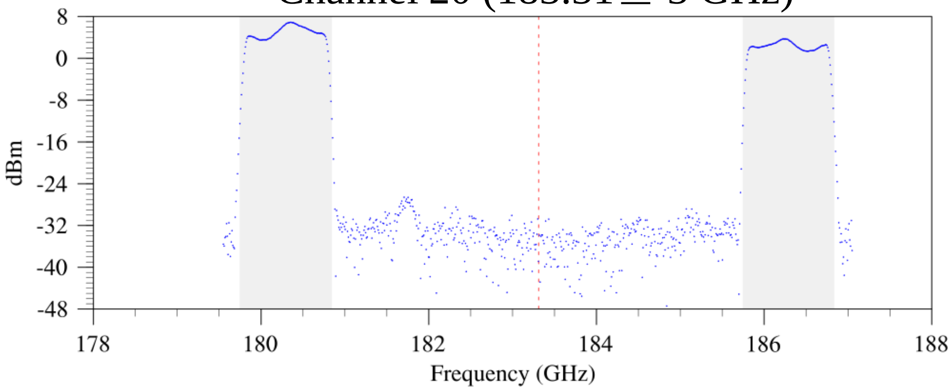

Channel 21 (183.31± 1.8 GHz)

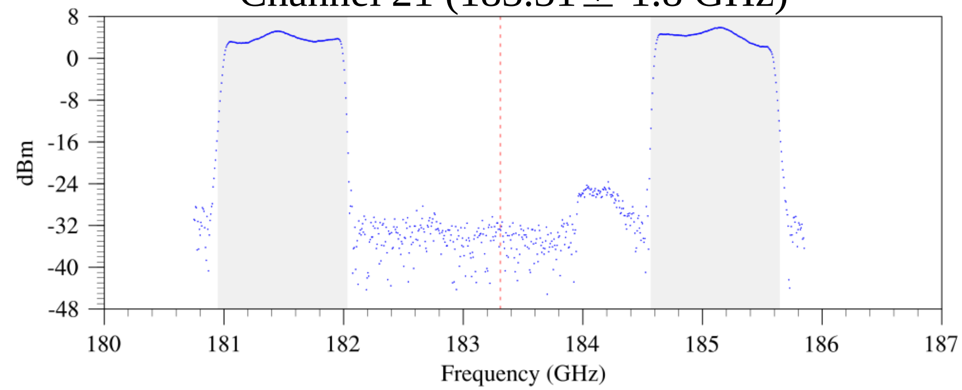

Channel 22 (183.31± 1 GHz)

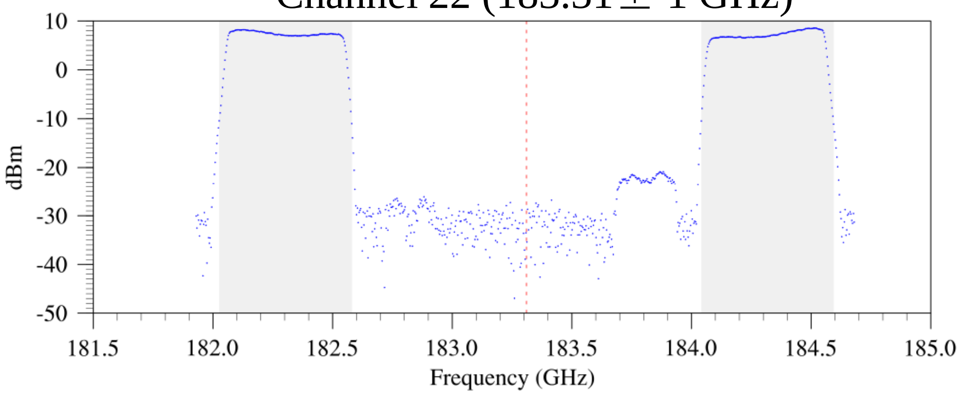

Strong SRF imbalances are found for J1 ATMS channels 18-20.

The requirement of the mean gain ratio for the side-band SRF is less than 2 dB.

SRF data obtained at primary local oscillator with baseplate temperature 20°C

Calculation of SRF Imbalance for J1 ATMS Channel 18

Original lab-measured SRF

↓

Truncate the SRF at -20 dB

↓

Compute average gain at each side band

$$\overline{G}_{low\ band} = \frac{\int_{f_1}^{f_2} G(f)\,df}{f_2 - f_1}$$

$$\overline{G}_{high\ band} = \frac{\int_{f_3}^{f_4} G(f)\,df}{f_4 - f_3}$$

↓

Compute the imbalance (unit: dB)

$$\Delta\overline{G} = \overline{G}_{low\ band} - \overline{G}_{high\ band}$$

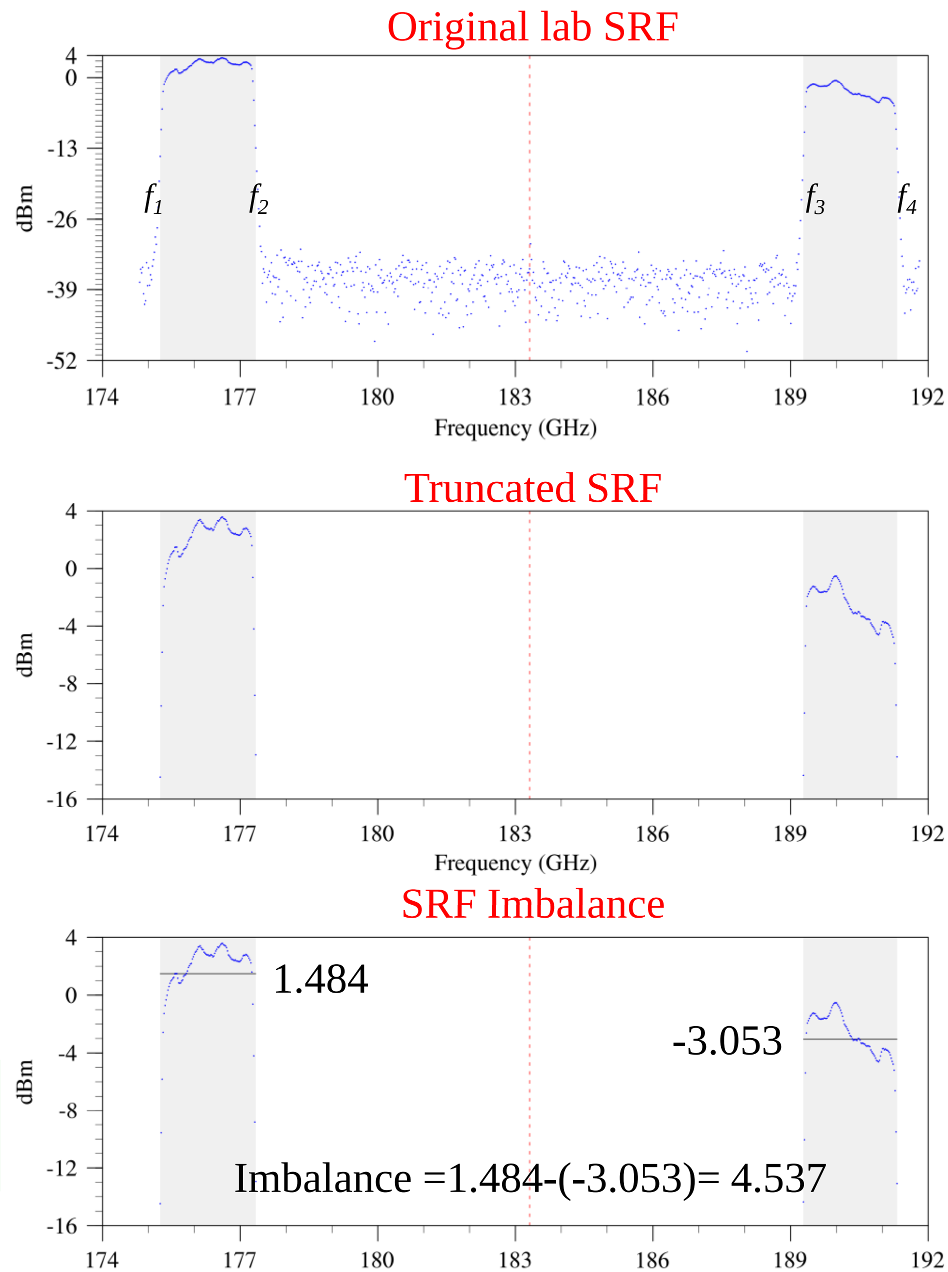

J1 ATMS SRF Imbalances for G-Band Channels

	G-Band Channels				
	18	19	20	21	22
STAR	4.537	1.997	2.419	-0.482	0.205
NG	4.949	2.228	2.625	-0.607	0.263

- STAR’s imbalance values are close to NG’s evaluation
- The SRF imbalances of J1 ATMS channels 18 and 20 are more than 4 dB and 2 dB, respectively. They exceed the specification.

Understanding the Impact of J1 ATMS SRF Imbalances on Brightness Temperature Simulations

Model Simulation:

- Monochromatic Radiative Transfer Model (MonoRTM)
  - — Accurate atmospheric spectroscopy data base
  - — Only gaseous absorption
  - — Vertical stratification
- Input to MonoRTM
  - — ECMWF analysis
- Cloud detection algorithm
  - — Cloud liquid water path (LWP) greater than 0.05 kg m^{-2}

MonoRTM Simulated Optical Depths of H_2O, O_2, O_3 and All Gases

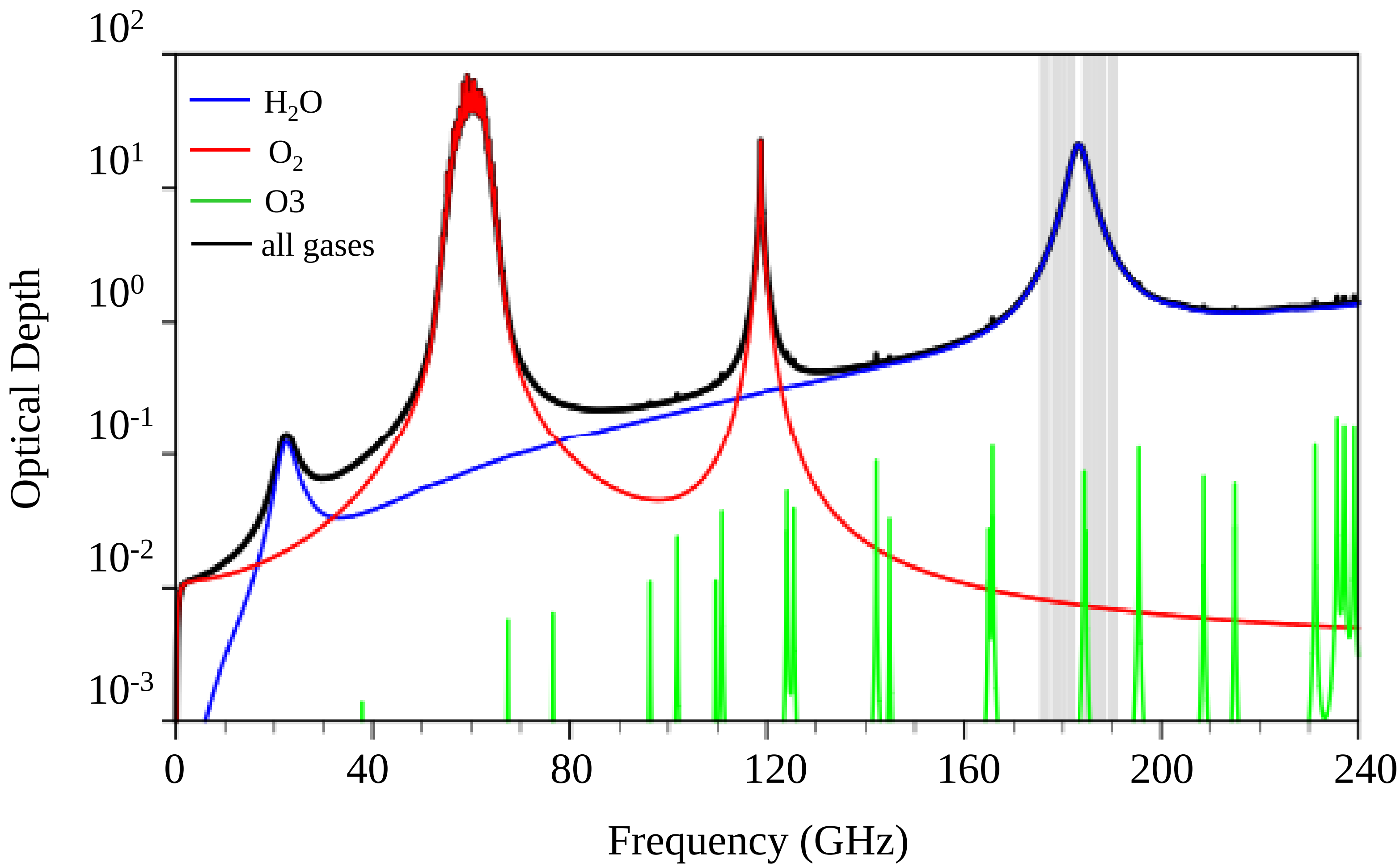

Four Scenarios for Removing SRF Imbalances

Truncated SRF

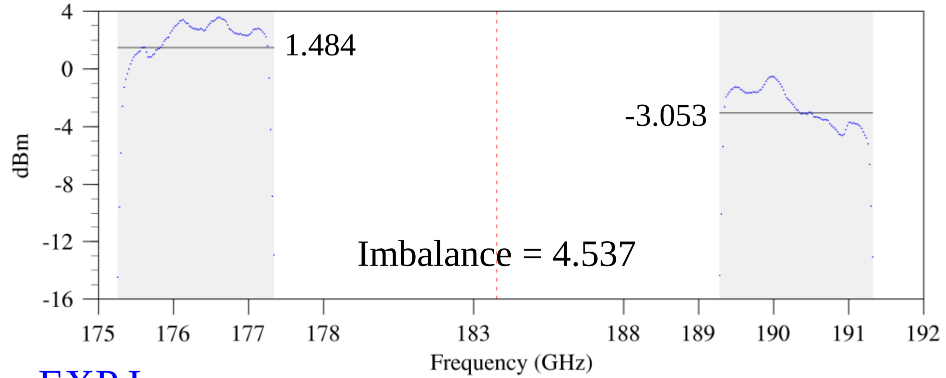

EXP I

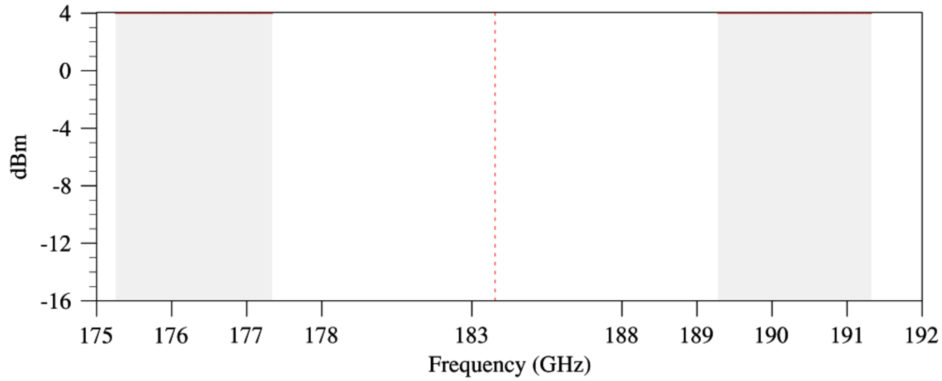

EXP II

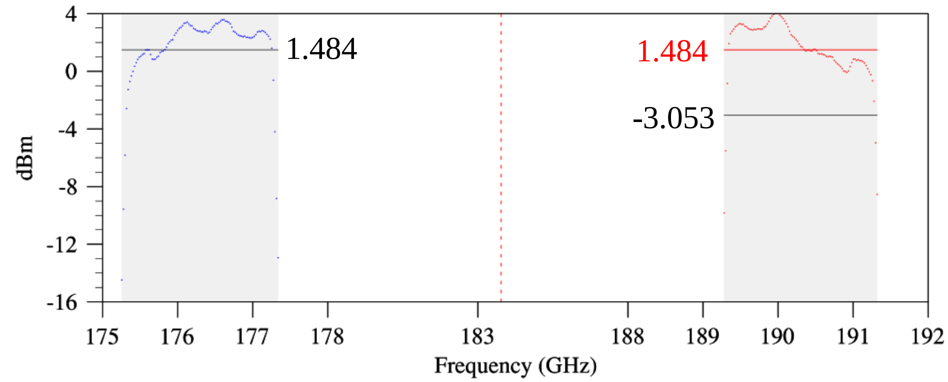

EXP III

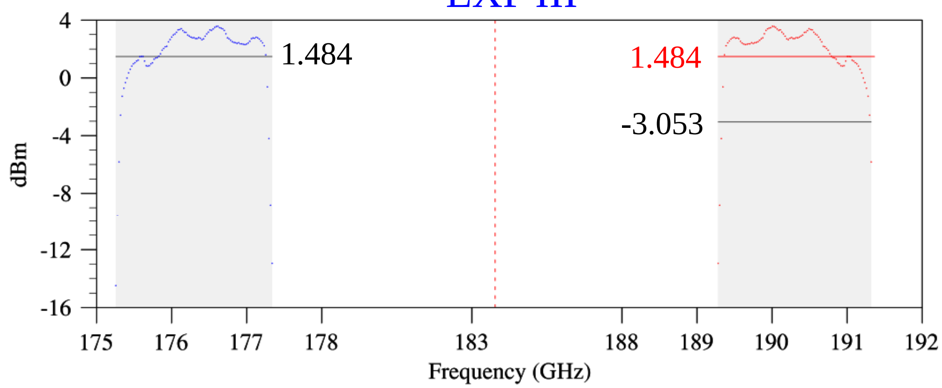

EXP IV

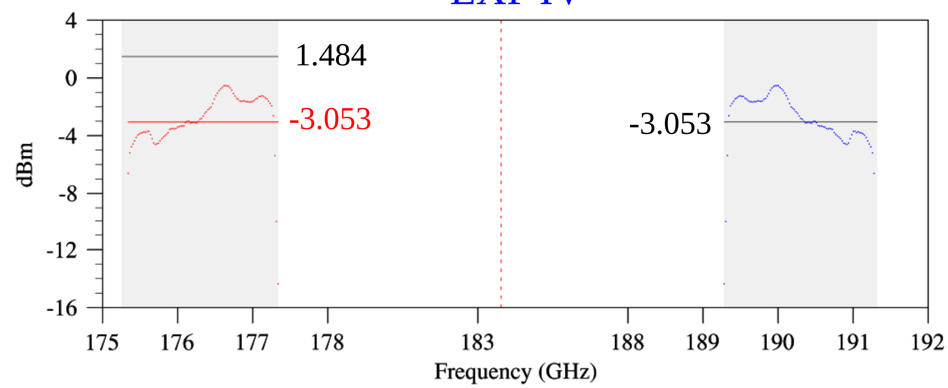

Sensitivity of TB to SRF Imbalances in Four Experiments

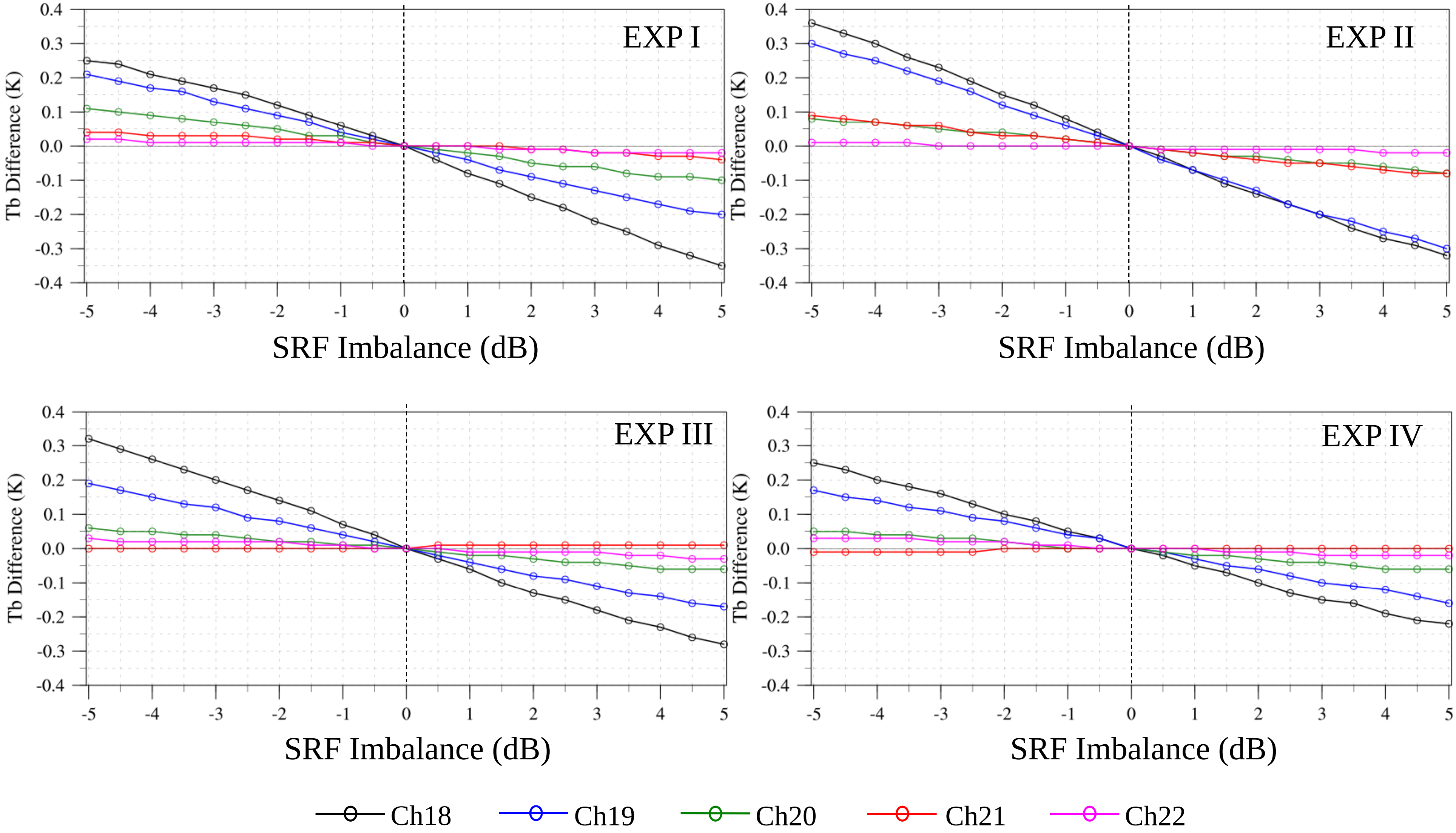

O-B Differences with B Simulated by Using Boxcar or J1 ATMS SRF for Channel 18

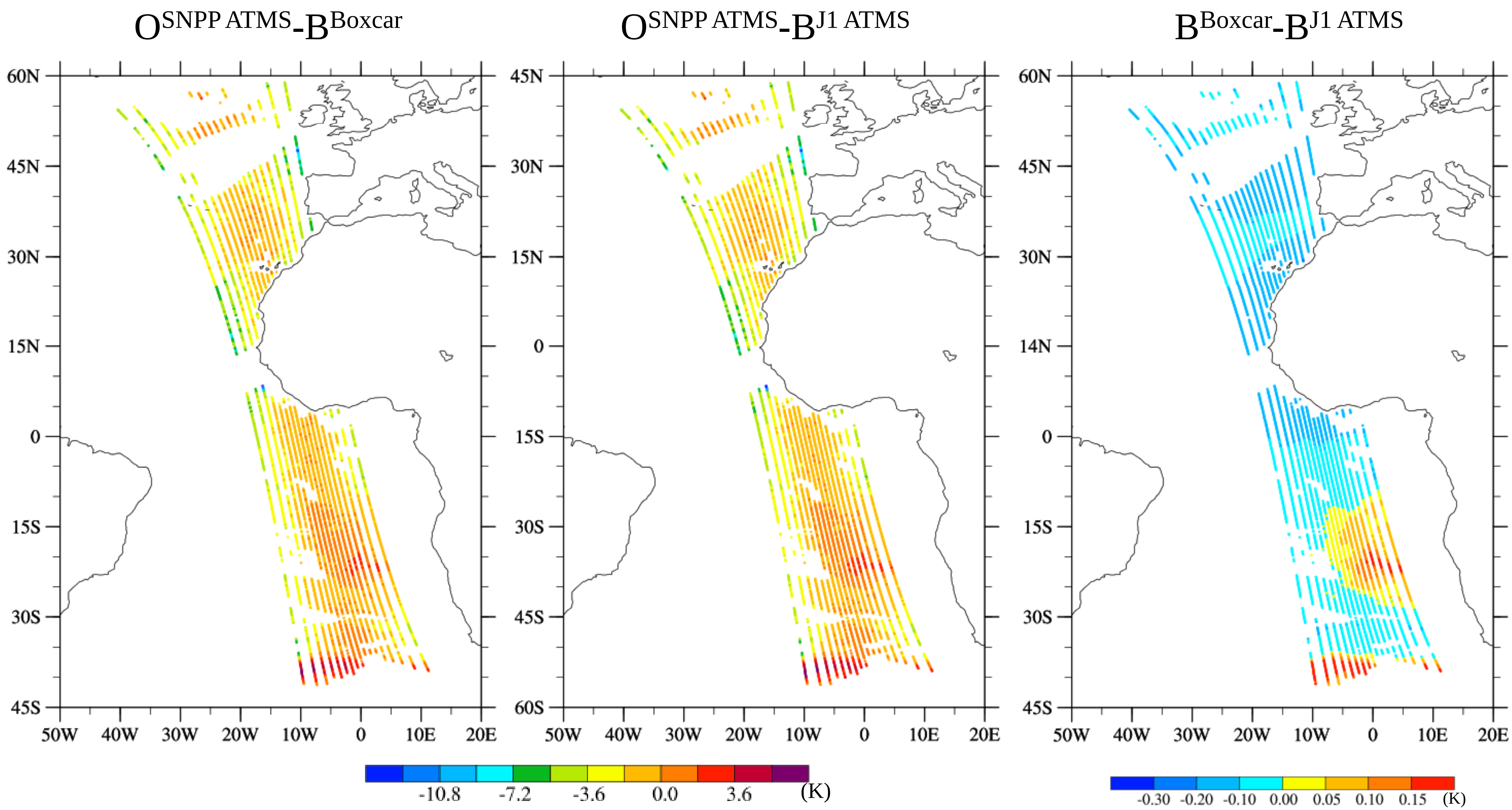

An ATMS swath over ocean in clear-sky conditions at the Suomi NPP ascending node during 1345-1418 UTC 20 July 2016

O-B Differences Obtained by Using Boxcar SRF

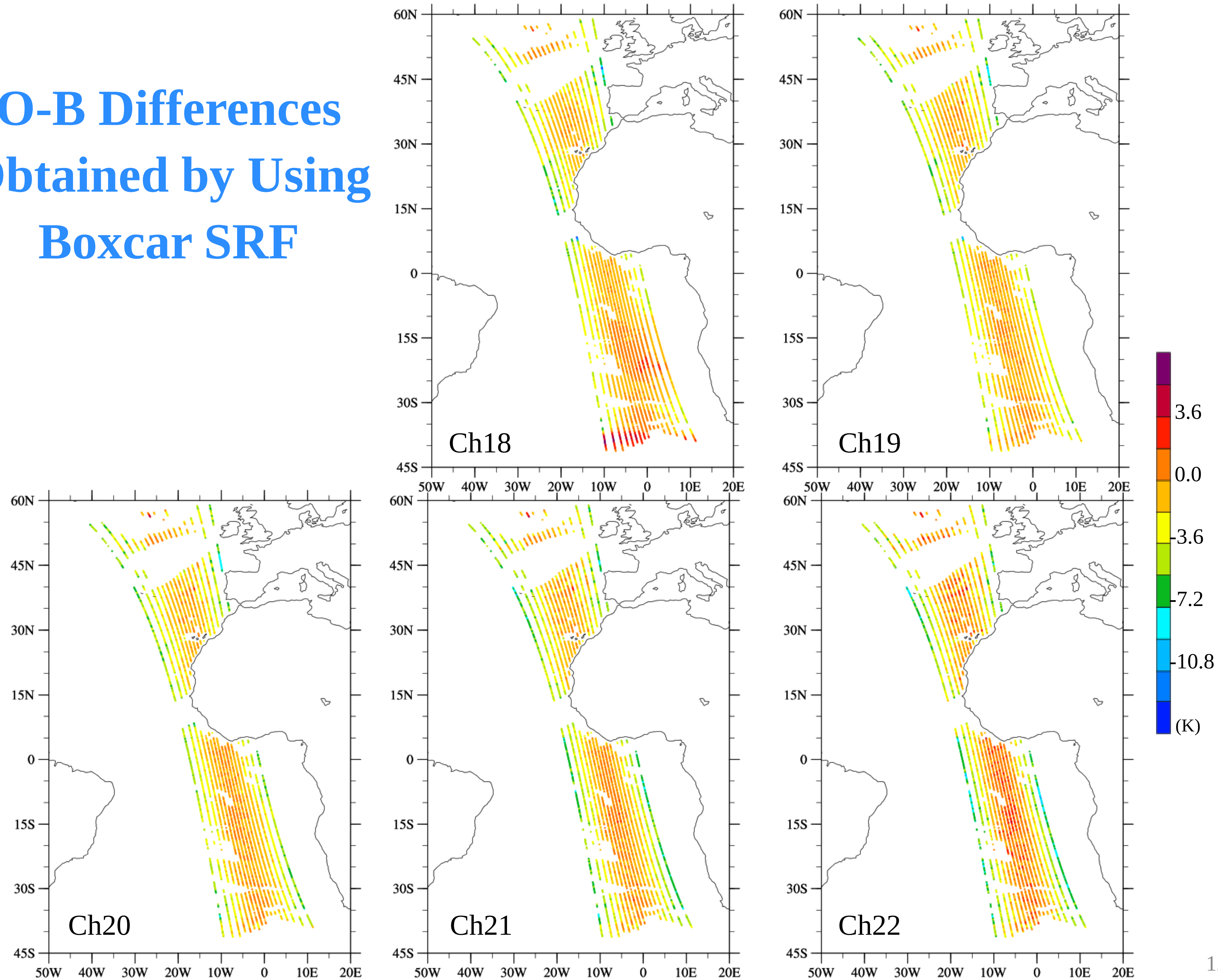

Differences of TB Simulations between Boxcar and J1 ATMS SRF

$B^{Boxcar} - B^{J1\ ATMS}$

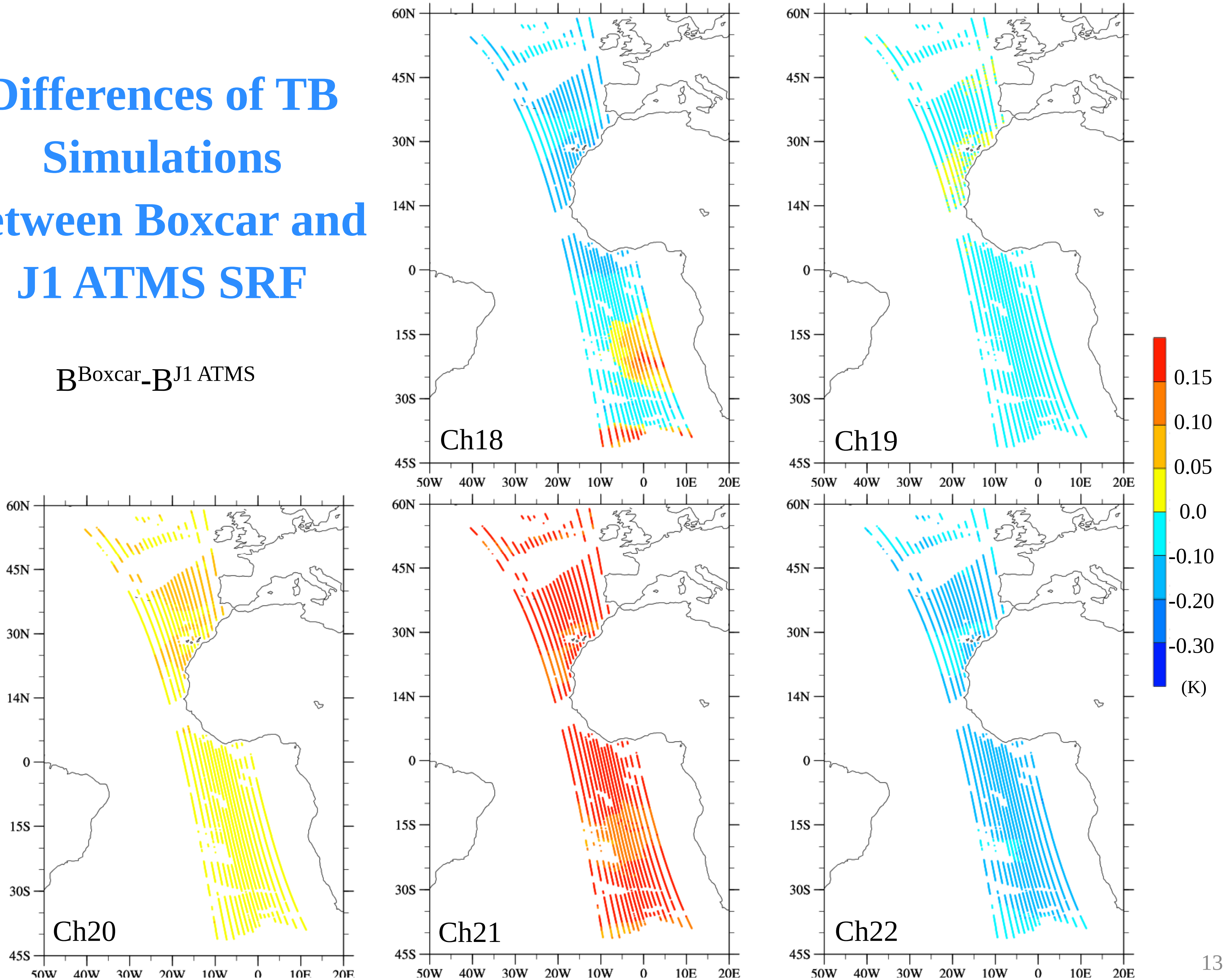

Scan Angle Dependence of O-B Using Boxcar or J1 ATMS SRF

O-B^{Boxcar} (solid), O-B$^{J1\ ATMS}$ (dashed)

B^{Boxcar}-B$^{J1\ ATMS}$

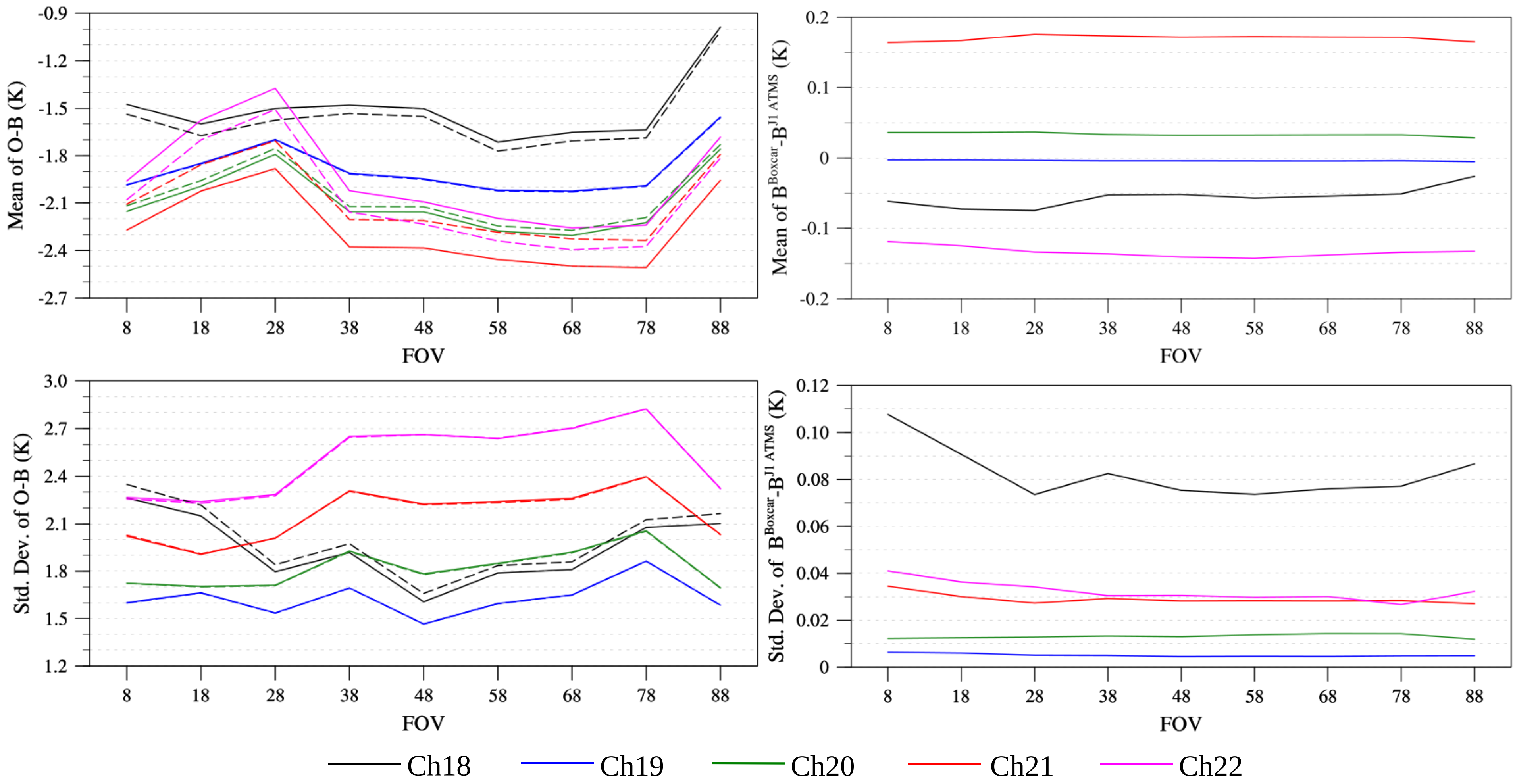

Latitudinal Dependence of O-B Using Boxcar or J1 ATMS SRF

O-B^{Boxcar} (solid), O-B$^{J1\ ATMS}$ (dashed)

B^{Boxcar}-B$^{J1\ ATMS}$

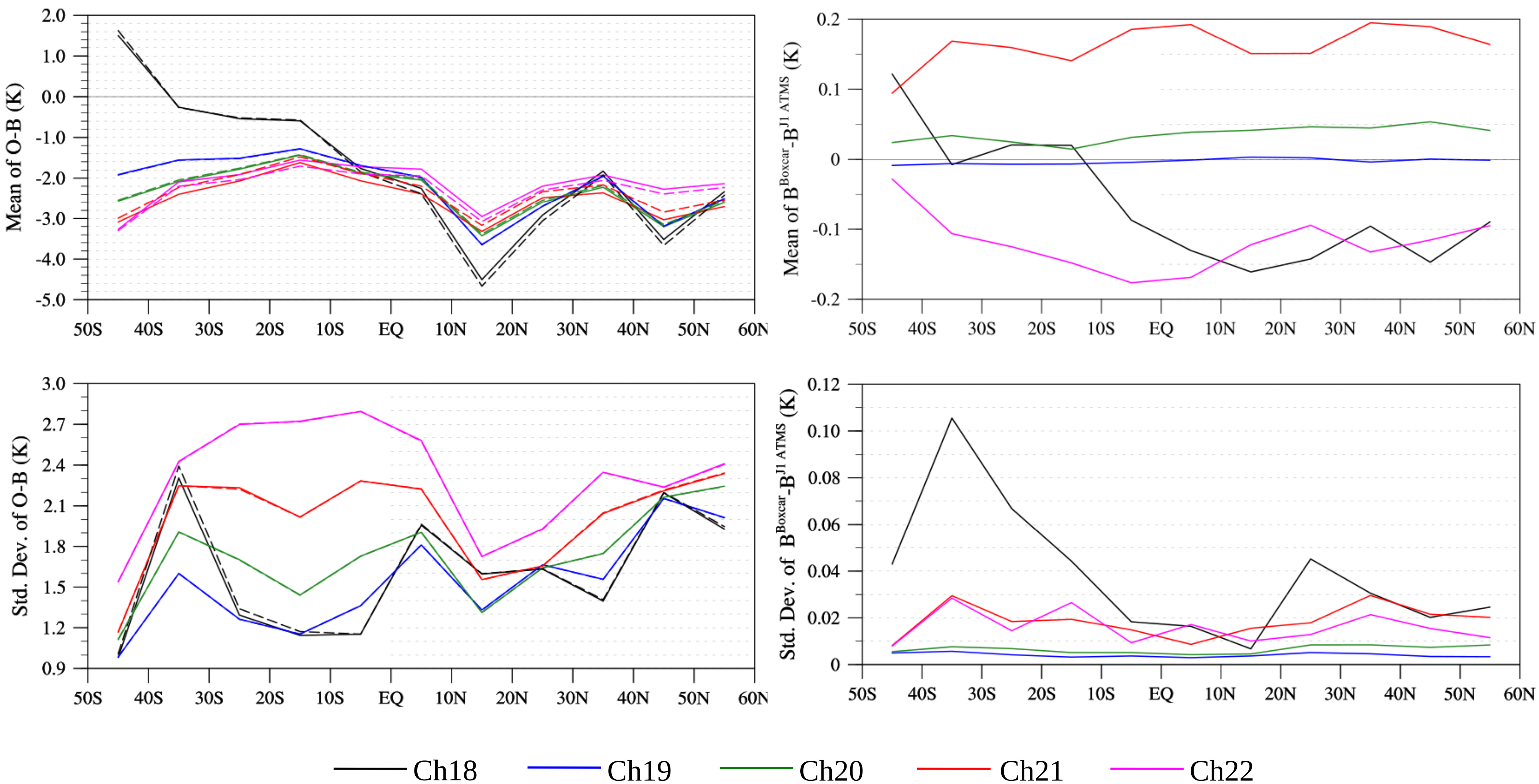

Scene Dependence of O-B Using Boxcar or J1 ATMS SRF

O-B^{Boxcar} (solid), O-B$^{J1\ ATMS}$ (dashed)

B^{Boxcar}-B$^{J1\ ATMS}$

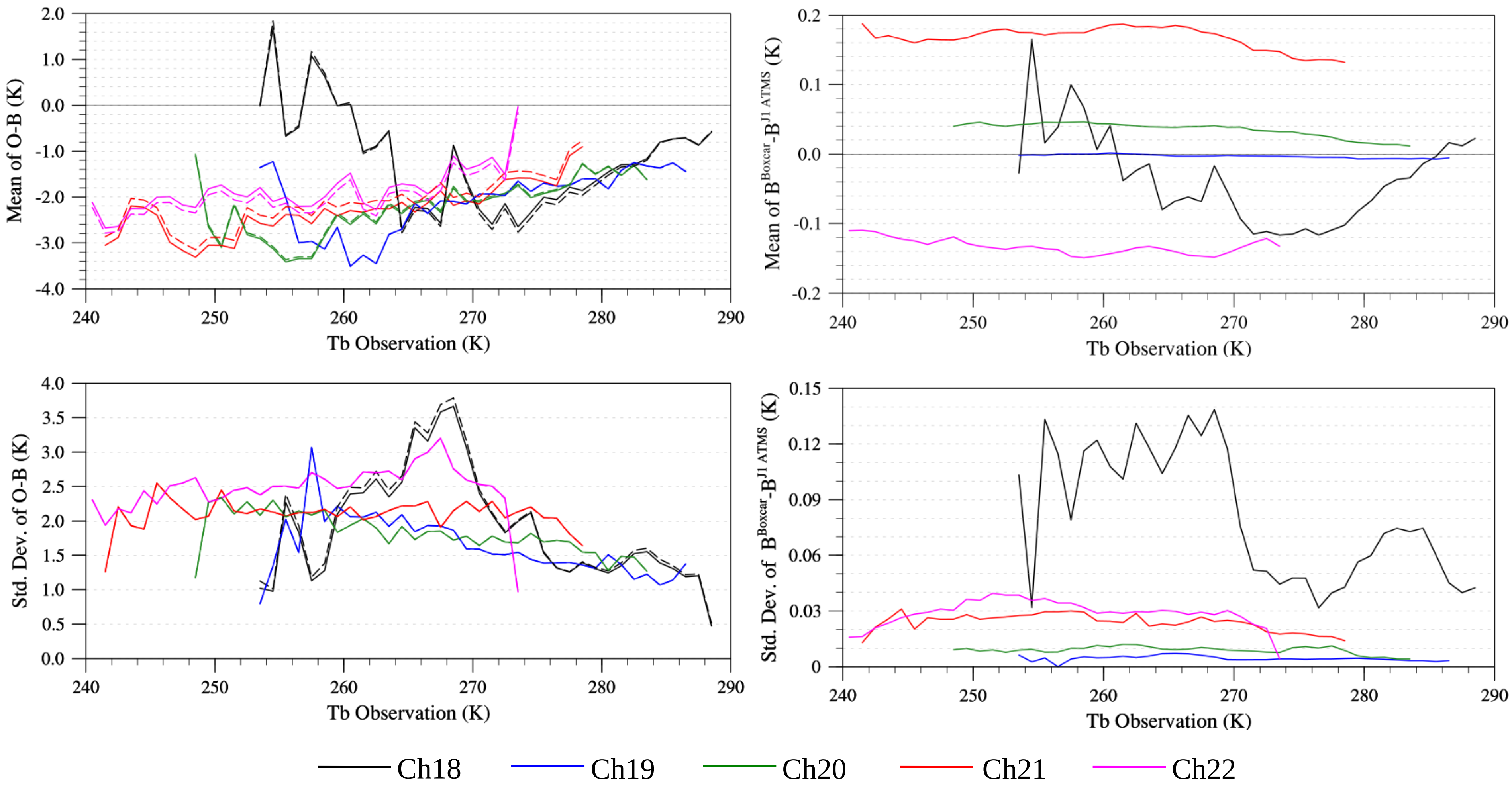

Summary and Conclusions

- The SRF imbalance for J1 ATMS channel 18 and 20 exceed the 2 dB specification for the side-band SRF.
- A sensitivity study showed that the TB can be different by more than 0.1 K when the SRF imbalance varies between 2 dB and 5 dB.
- The impacts of J1 SRF vs. Boxcar on simulations of G-band brightness temperatures were evaluated using MonoRTM. The mean difference is ~ 0.15 K for channels 21 and 22.
- This study suggests a necessity of providing the actual SRFs from all the sidebands carefully measured by the instrument vendor to numerical weather prediction (NWP) users to build an accurate fast RTM for satellite data assimilation in NWP models.

Relevance of GPM XCAL Activities to Suomi NPP/JPSS

Wesley Berg

Colorado State University

GPM -> Global Precipitation Measurement
XCAL -> Precipitation Measurement Missions (i.e. TRMM/GPM) intercalibration working group

Global Precipitation Measurement (GPM) Mission

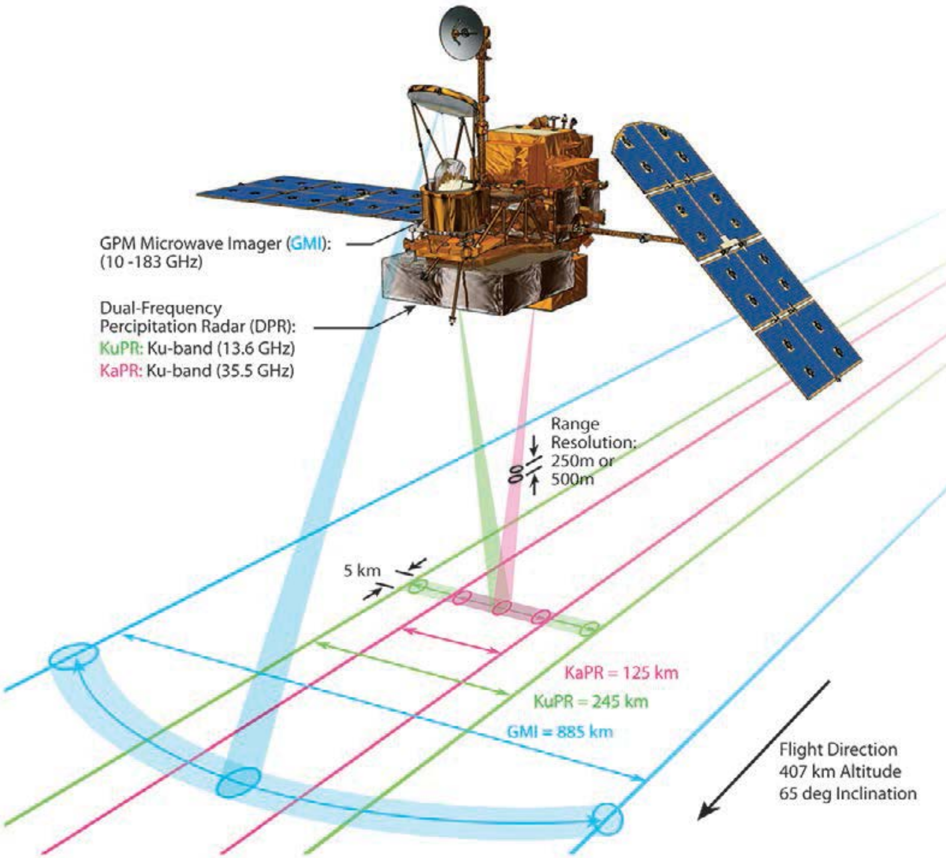

GPM Core Satellite

Dual-Frequency radar (DPR)

- Ku-band (13.6 GHz)
- Ka-band (35.5 GHz)

Microwave Imager (GMI)

- 13 channels
- 10-183 GHz

GPM was designed to provide the next generation of global precipitation products characterized by

1. More accurate instantaneous precipitation estimates, particularly for light rainfall and cold season solid precipitation
2. **Unified precipitation retrievals from a constellation of microwave radiometers through the use of intercalibrated brightness temperatures** and a common observational hydrometeor database consistent with the combined radar/ radiometer measurements obtained by the GPM Core Observatory. Constellation needed to provide 3-hourly global sampling.

GPM Radiometer Constellation

Conical Imagers

Cross-Track Sounders

a) NASA TRMM-TMI and GPM-GMI

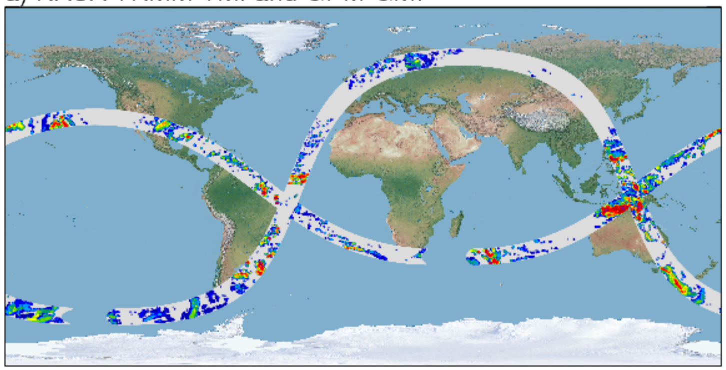

b) CNES Megha-Tropiques SAPHIR

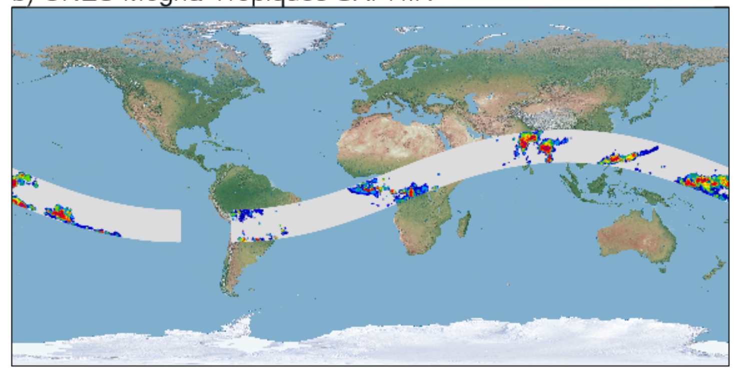

c) JAXA GCOMW-1 AMSR2

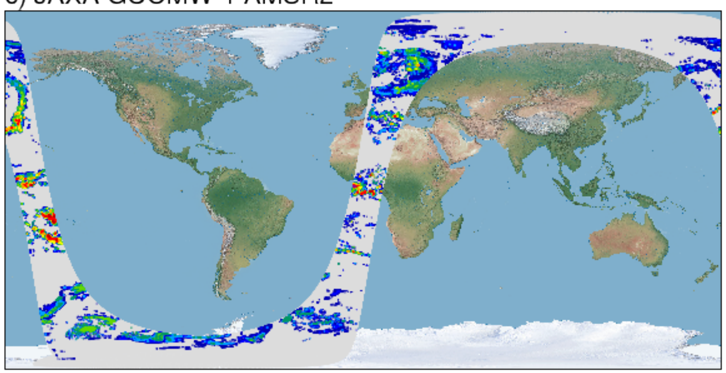

d) NOAA Suomi-NPP ATMS

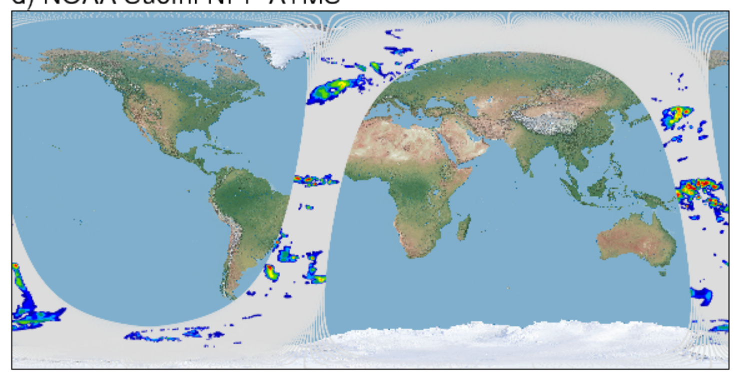

e) DMSP F16, F17, F18 and F19 SSMIS

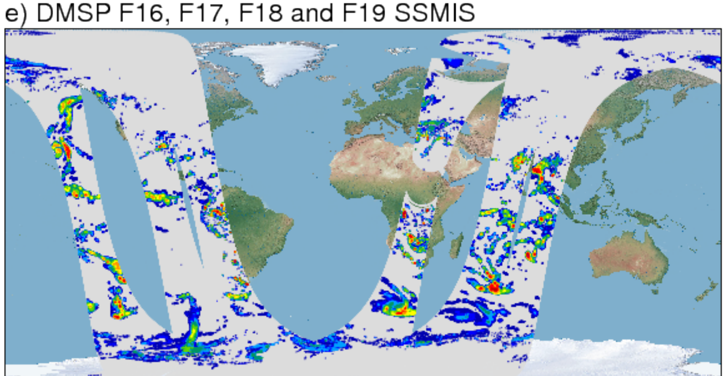

f) NOAA-18/19 & ESA MetOp-A/B MHS

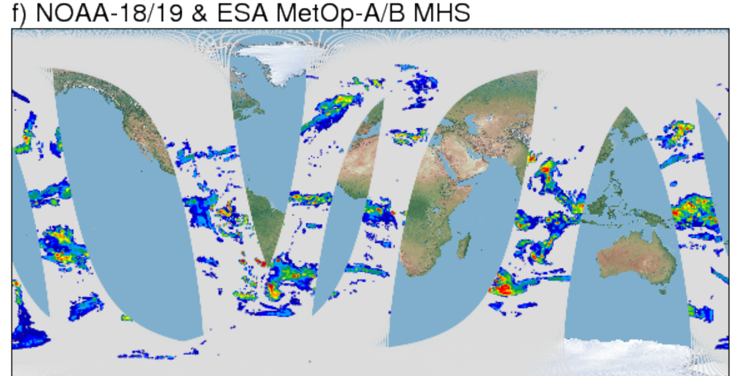

GPM and TRMM Radiometer Constellations

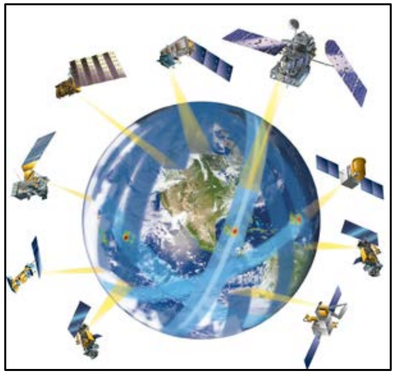

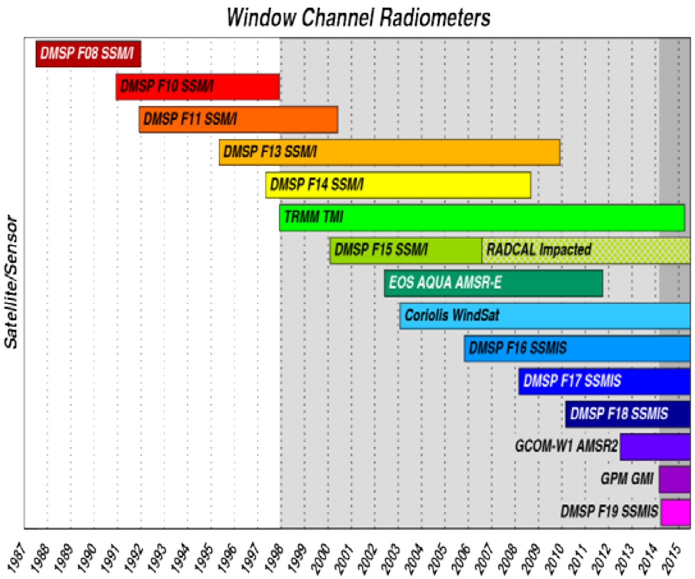

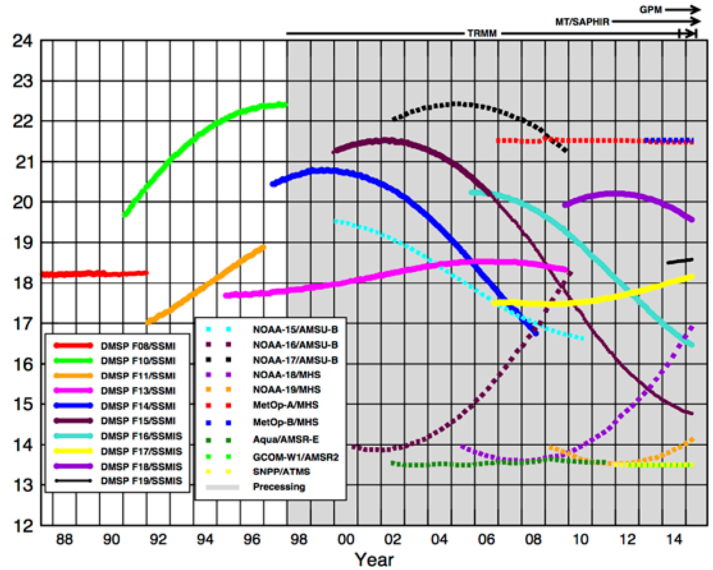

GPM Era (Mar 2014 – Present)

- **GPM Imager Constellation (7)**
  - **GPM GMI (reference sensor)**
  - TRMM TMI
  - GCOM-W1 AMSR2
  - DMSP F16, F17, F18 and F19 SSMIS
  - *Coriolis WindSat
- **GPM Sounders (6)**
  - Metop A and B MHS
  - NOAA 18 and 19 MHS
  - Suomi NPP ATMS
  - Megha-Tropiques SAPHIR

*Not Currently part of GPM constellation

TRMM Era (Dec 1997 – Apr 2015)

- **TRMM Imager Constellation (10)**
  - TRMM TMI
  - EOS-AQUA AMSR-E
  - GCOM-W1 AMSR2
  - DMSP F11, F13, F14 and F15 SSM/I
  - DMSP F16, F17 and F18 SSMIS
  - *Coriolis WindSat
- **TRMM Sounders (6)**
  - NOAA 15, 16 and 17 AMSU-B
  - Metop A, NOAA 18 and 19 MHS
  - Suomi NPP ATMS
  - Megha-Tropiques SAPHIR

XCAL Responsibilities and Goals

The XCAL team was formed to address the issue of radiometer calibration consistency. Primary activities include:

1. Identify sensor issues affecting the calibration and stability of the Tb for each of the constellation radiometers. This involves Investigating calibration errors across scan and/or along orbit (i.e. time-dependent)
2. Develop and apply corrections for sensor calibration issues.
   - Limited to NASA/DMSP instruments
   - Work with instrument teams for other sensors
3. Derive and deliver intercalibration tables to adjust for residual sensor calibration differences in a physically consistent manner.
   - Assess calibration of reference radiometer (GMI)
   - Estimate calibration differences between sensors using multiple approaches (e.g. double differences, vicarious, polar matchups)
   - Investigate both cold and warm-scene differences where applicable

Result is the **Level 1C intercalibrated brightness temperature files** used as input to the operational radiometer precipitation retrieval algorithms.

Additional Tasks include:

1. Assess uncertainties
   - Investigate errors in RTM and geophysical parameters
   - Uncertainties in intercalibration techniques
2. Document results (full transparency)
3. Work to improve intercalibration techniques

GPM Constellation Radiometers

Variations in Channel Frequencies

Satellite (Sensor)	6-7 GHz	10 GHz	19 GHz	23 GHz	31-37 GHz	85-92 GHz	150-166 GHz	183 GHz
GPM (GMI) Conical		10.65v 10.65h	18.7v 18.7h	23.8v	36.64v 36.64h	89.0v 89.0h	166v 166h	183.31±3v 183.31±7v
*TRMM (TMI) Conical		10.65v 10.65h	19.35v 19.35h	21.3v	37.0v 37.0h	85.5v 85.5h		
GCOM-W1 (AMSR-2) Conical	6.925v 6.925 7.3v 7.3h	10.65v 10.65h	18.7v 8.7h	23.8v 23.8h	36.5v 36.5h	89.0v (A) 89.0h (A) 89.0v (B) 89.0h (B)		
DMSP F16, F17, F18, & F19 (SSMIS) Conical			19.35v 19.35h	22.235v	37.0v 37.0h	91.655v 91.655h	150h	183.31±1h 183.31±3h 183.31±6.6h
METOP-A/B, NOAA-18/19 (MHS) Cross-track						89qv	157qv	183.31±1qh 183.31±3qh 190.31qv
Suomi NPP (ATMS) Cross-track				23.8qv	31.4qv	88.2 qv	165.5qh	183.31±1.0qh 183.31±1.8qh 183.31±3.0qh 183.31±4.5qh1 83.31±7.0qh
Megha-Tropiques (SAPHIR) Cross-track								183.31±0.2qh 183.31±1.1qh 183.31±2.8qh 183.31±4.2qh 183.31±6.8qh 183.31±11qh
**Coriolis (WindSat) Conical	6.8v 6.8h	10.7v 10.7h 10.7-3rd 10.7-4th	18.7v 18.7h 18.7-3rd 18.7-4th	23.8v 23.8h	37.0v 37.0h 37.0-3rd 37.0-4th			

Hurricane Arthur Precipitation from GPM Constellation

(Conical Scanners, GPROF 2014v1-3, 3 July 2014)

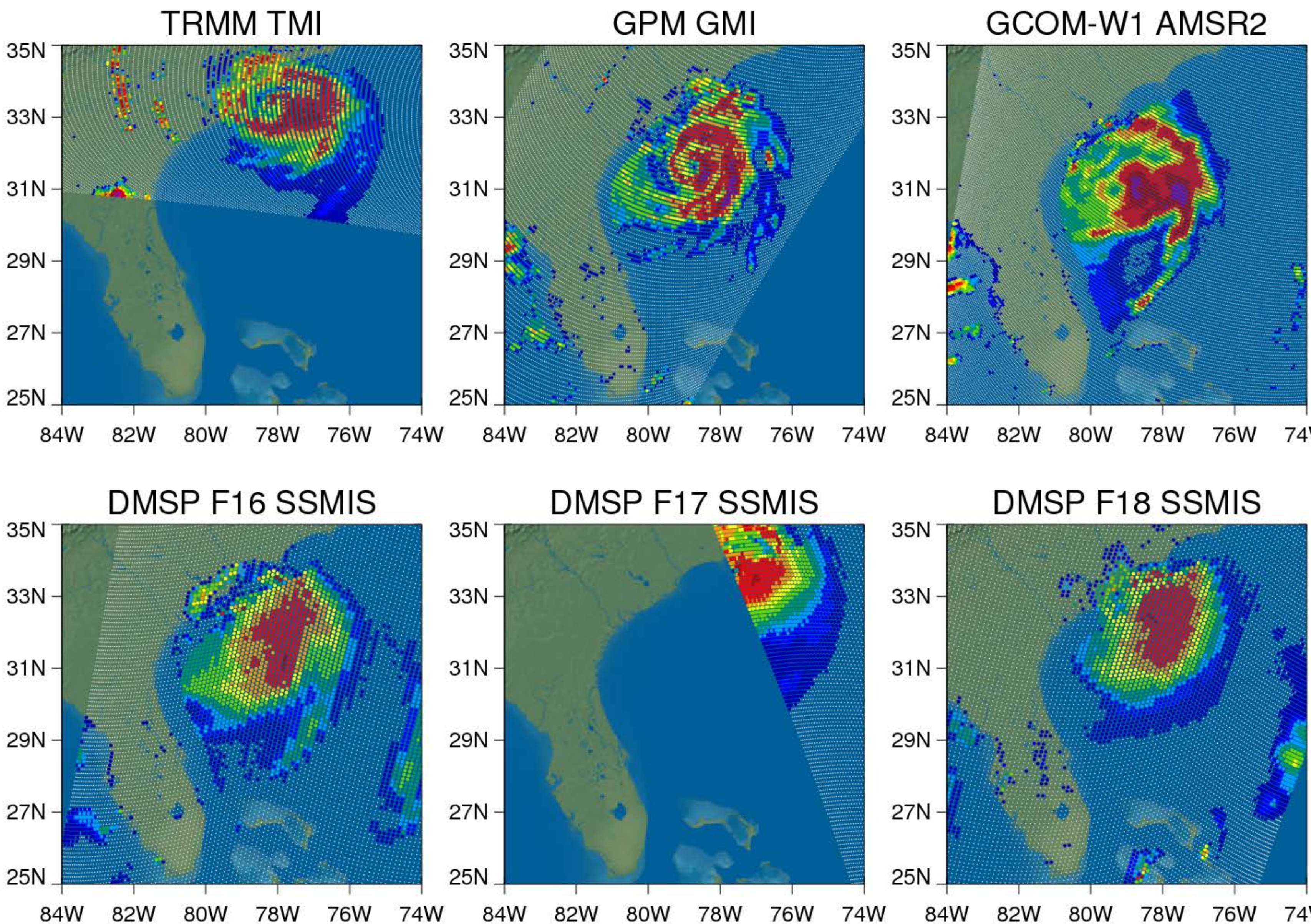

Global Mean Precipitation from GPM Constellation Radiometers

(Microwave Imagers, March – July, 2014)

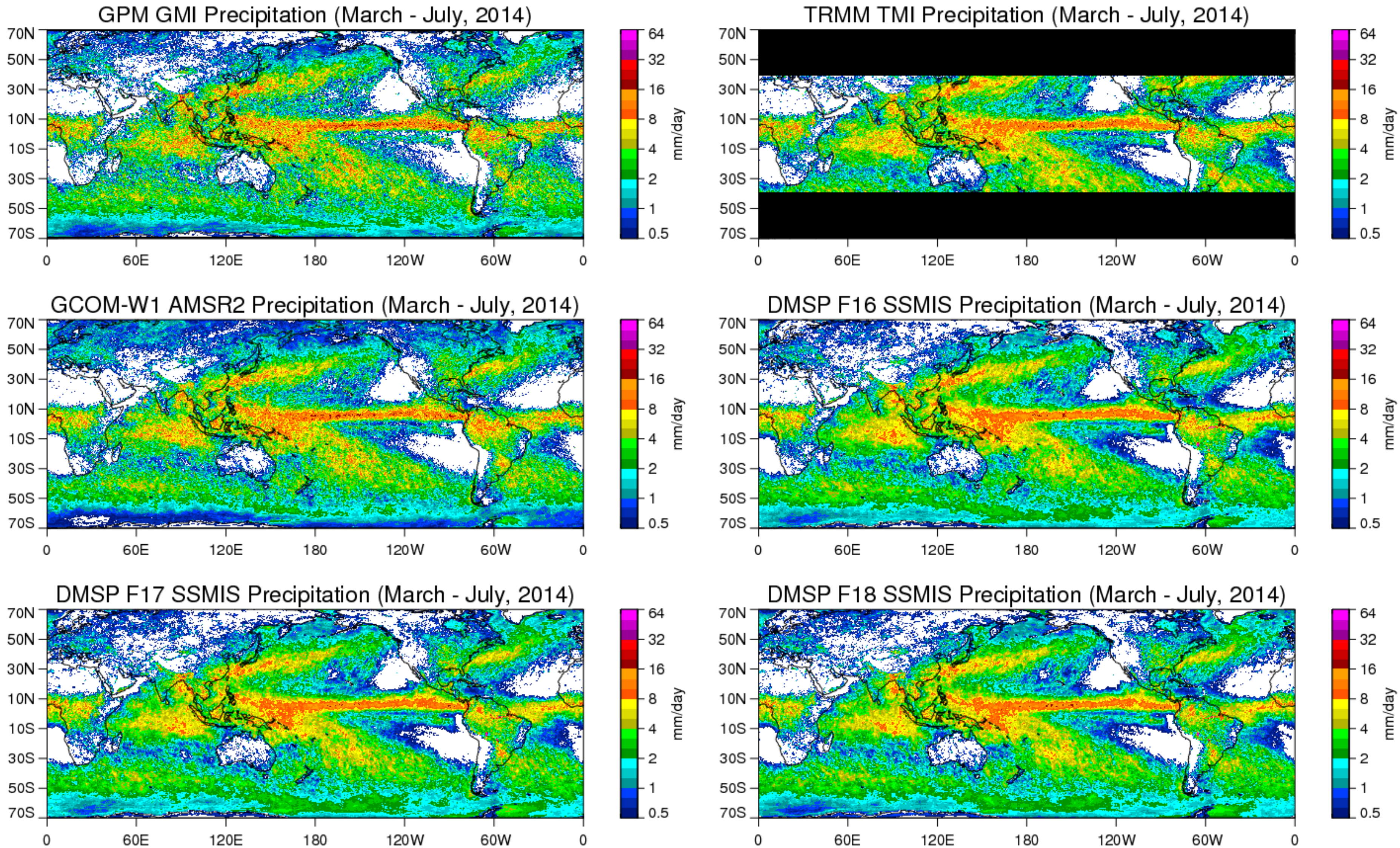

January 2015 Precipitation from GPM Constellation Radiometers

GPM GMI

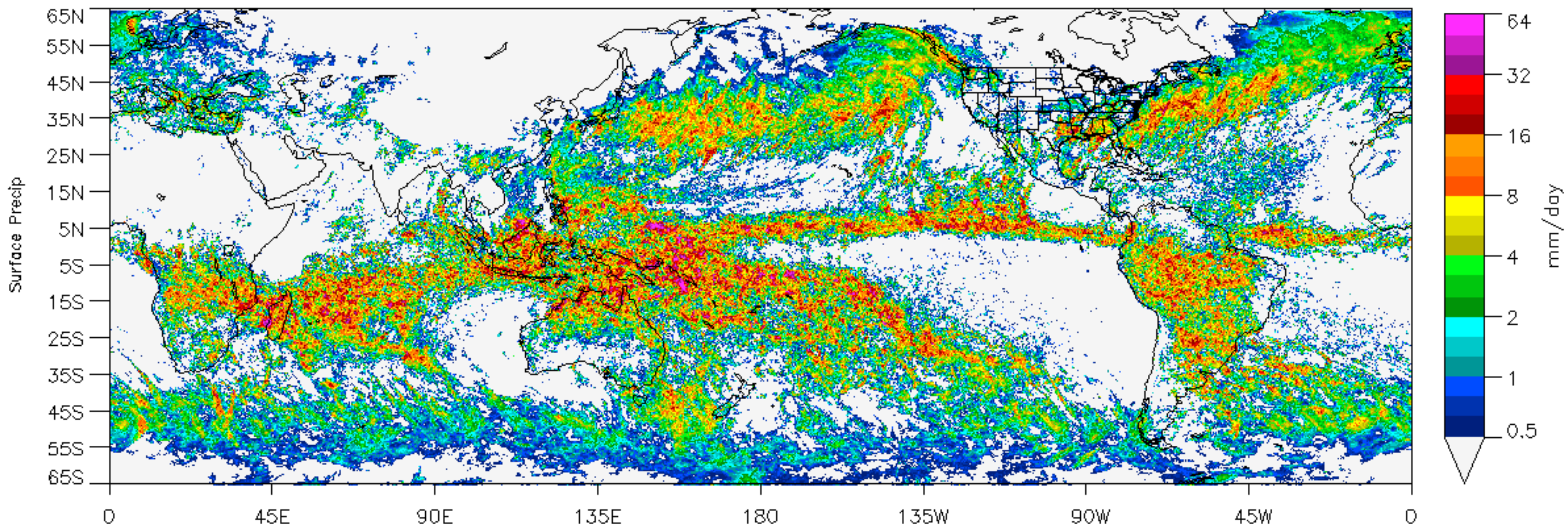

Suomi NPP ATMS

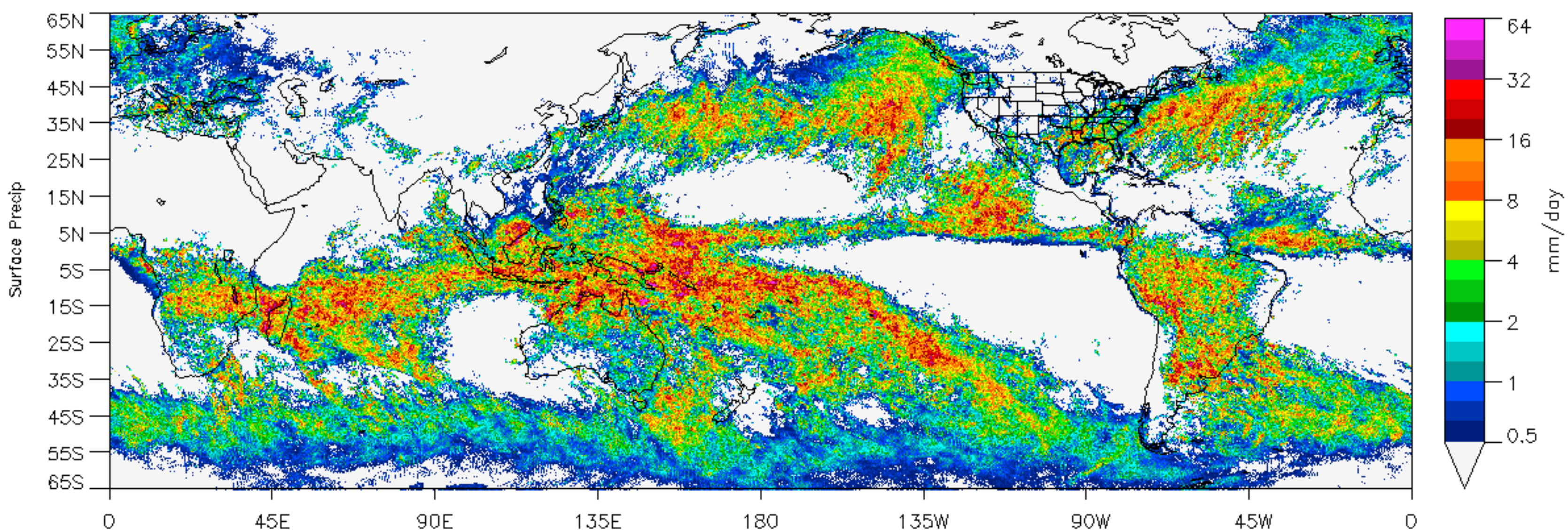

GPM GMI: Calibration Reference Sensor

GMI Specs	10.65v/h	18.7v/h	23.8v	36.64v/h	89.0v/h	165.5v/h	183+3v	183+7v
DT x CT Res in km	32.1x19.4	18.1x10.9	16.0x9.7	15.6x9.4	7.2x4.4	6.3x4.4	5.8x3.8	5.8x3.8
Beamwidth (deg)	1.72	0.98	0.85	0.81	0.38	0.37	0.37	0.37
NEDT (K)	0.96	0.84	1.05	0.65	0.57	1.5	1.5	1.5
Beam Efficiency (%)	91.1	91.2	93.0	97.8	96.8	96.5	95.2	95.2
Uncorr Nonlinearity (K)	0.2 0.2	0.1 0.1	0.1 0.1	0.5 0.5	0.5 0.5	0.5 0.5	0.5	0.5
Band Width (MHz)	100	200	400	1000	6000	4000	3500	4500
Feedhorns	1	1	1	1	1	1	1	1
Integration Time (ms)	3.6	3.6	3.6	3.6	3.6	3.6	3.6	3.6

Satellite/Instrument Characteristics

Nominal EIA	52.8/49.2
Orbit Inclination	65.0 deg
Local Obs. Time	Variable (Precessing)
Altitude	407 km
Reflector Size	1.22 m
Sampling Interval	13.5 km

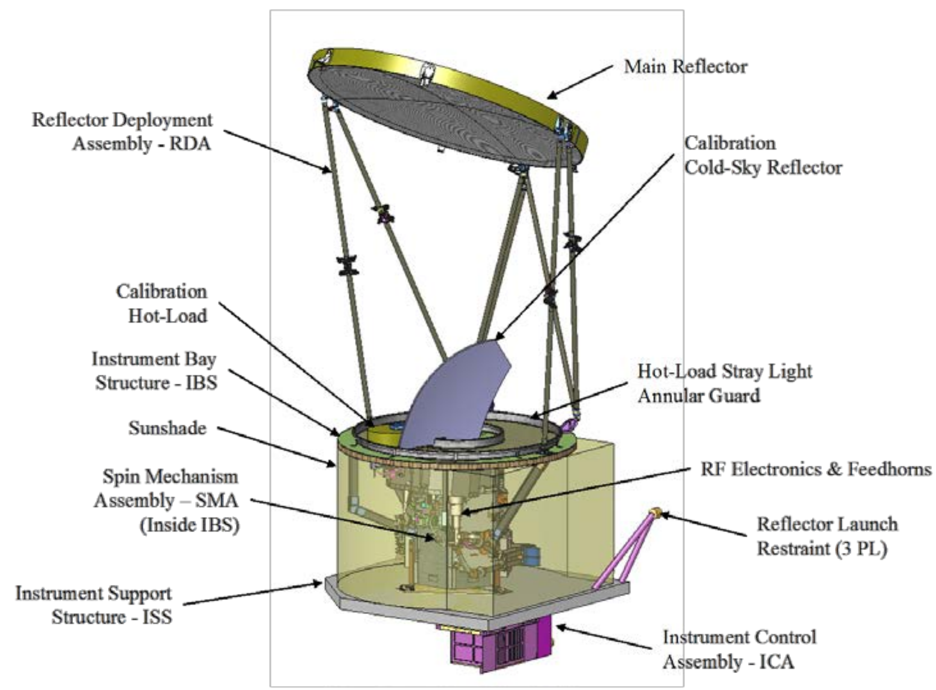

GMI Calibration Summary

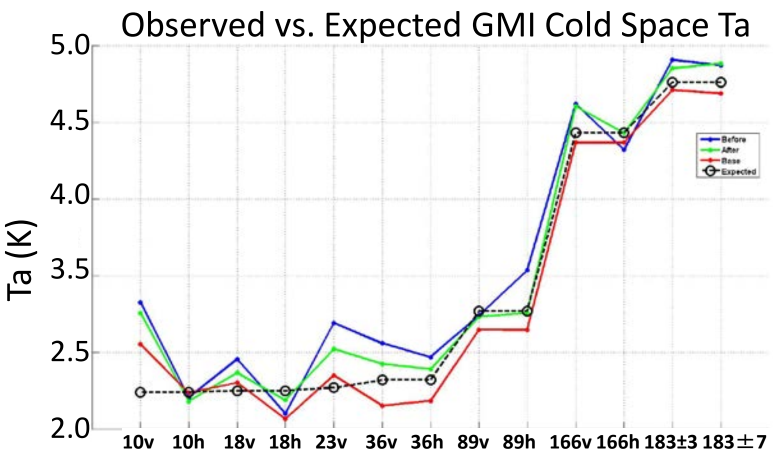

Observed vs. expected antenna temperatures by channel based on analysis of data from deep space calibration manuever (Courtesy Spencer Farrar, Univ. Central Florida).

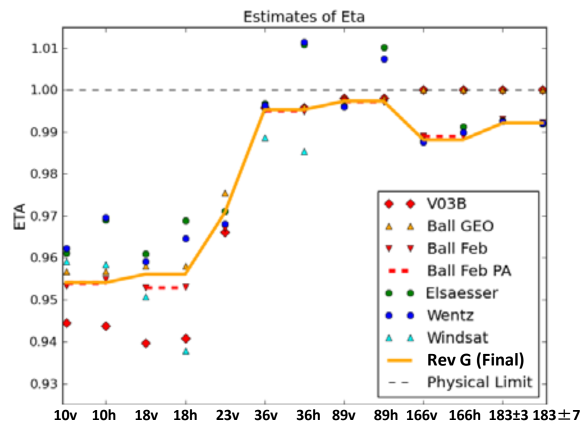

Various estimates for spillover correction (eta) for each GMI channel. Final values are indicated by solid yellow line (Courtesy Tom Wilheit).

Channel	Pre-Launch (η_F)	On-Orbit (η_G)	ΔTb (ocean)
10v	0.94435	0.95404	1.7
10h	0.94369	0.95404	1.0
18v	0.93968	0.95603	3.3
18h	0.94082	0.95603	2.0
23v	0.96601	0.97075	1.1
36v	0.99590	0.99535	-0.1
36h	0.99590	0.99535	-0.1
89v	0.99810	0.99734	-0.2
89h	0.99810	0.99734	-0.2
166v	1.00000	0.98814	-3.2
166h	1.00000	0.98814	-3.2
183±3v	1.00000	0.99212	-2.1
183±7v	1.00000	0.99212	-2.1

- On-orbit calibration maneuvers used to check for calibration anomalies and to develop corrections.
- Calibration Checks
  - Emissive Reflector (No evidence found)
  - Polarization Check (Differences < 0.3K at nadir)
- Calibration Corrections
  - Magnetic anomalies
    - Along-track due to spacecraft flying through Earth's magnetic field
    - Cross-track due to magnetic latches for GMI cover
    - Correction developed/applied. Residual anomalies are very small.
  - Spillover Corrections
    - Forward part of antenna pattern measured by Ball at near field range pre-launch, but spillover region could not be measured so they used two different models, which gave different answers.
    - Initial spillover corrections (Eta) for 166 and 183 channels were 1.0 (unphysical)
    - Data from 2 inertial hold maneuvers were analyzed by David Draper at Ball Aerospace, The resulting Eta values (see above table/figure) are based on physical observations rather than models (as used initially). These values are also not tuned to match any radiative transfer model.

Summary

- Significant changes were made to the spillover corrections (see above). Given limitations of pre-launch measurements this is a likely cause of significant calibration differences between sensors, particularly for lower frequency channels.
- Calibration corrections are based on data from on-orbit calibration maneuvers and are not dependent on radiative transfer models
- Independent comparisons with by both Ball/RSS and XCAL indicate that the GMI calibration is very consistent with clear-sky ocean simulated Tb.
- A conservative estimate for the absolute calibration errors of the GMI window channels are < 1K
- Comparisons of the GMI 166 and 183 GHz channels with the MHS and SAPHIR cross-track sounders indicate differences of < 0.5K

Total GMI On-orbit Calibration RMS Error

- Overall, the GMI RMS calibration error for on-orbit operations is 0.25K RMS bias and 0.14K RMS time-varying component
  - Note that these are considered as 1-sigma numbers, i.e. 68% probability of a particular channel falling within this error range.
  - An individual channel's error may be higher or lower.
- Comparison with Independently Calibrated Radiometers Suggests Absolute Accuracy Better than 1K RMS Across All Channels

	Magnetic Correction		TA Calibration		Antenna-Induced Bias		**Total TA ERROR (ocean)**		Spillover		Cross-pol		**Total TB ERROR (ocean)**	
Channel	Total Bias	Total Time-varying error	Total Bias	Total Time-varying error	Total Bias	Total Time-varying error	**Total Bias**	**Total Time-varying error**	Total Bias	Total Time-varying error	Total Bias	Total Time-varying error	**Total Bias**	**Total Time-varying error**
10V	0.09	0.09	0.12	0.07	0.00	0.03	**0.15**	**0.12**	0.29	0.02	0.07	0.00	**0.34**	**0.12**
10H	0.05	0.11	0.18	0.06	0.00	0.04	**0.18**	**0.13**	0.17	0.02	0.07	0.00	**0.26**	**0.13**
18V	0.05	0.05	0.09	0.08	0.00	0.02	**0.10**	**0.10**	0.26	0.02	0.05	0.00	**0.28**	**0.10**
18H	0.04	0.07	0.09	0.06	0.00	0.03	**0.09**	**0.09**	0.17	0.03	0.05	0.01	**0.20**	**0.09**
23V	0.06	0.08	0.09	0.09	0.00	0.01	**0.11**	**0.12**	0.23	0.03	0.02	0.03	**0.25**	**0.13**
36V	0.01	0.11	0.08	0.11	0.00	0.00	**0.08**	**0.16**	0.21	0.01	0.01	0.00	**0.23**	**0.16**
36H	0.02	0.07	0.07	0.08	0.00	0.00	**0.07**	**0.11**	0.15	0.02	0.01	0.00	**0.17**	**0.11**
89V	0.00	0.03	0.07	0.14	0.00	0.00	**0.07**	**0.14**	0.22	0.01	0.01	0.00	**0.23**	**0.14**
89H	0.02	0.09	0.08	0.12	0.00	0.01	**0.08**	**0.15**	0.20	0.02	0.01	0.00	**0.21**	**0.15**
166V	0.04	0.05	0.05	0.14	0.00	0.01	**0.06**	**0.15**	0.28	0.01	0.02	0.02	**0.29**	**0.16**
166H	0.04	0.09	0.05	0.14	0.00	0.01	**0.06**	**0.17**	0.28	0.02	0.02	0.02	**0.29**	**0.17**
183VA	0.02	0.06	0.04	0.14	0.00	0.01	**0.04**	**0.15**	0.24	0.01	0.01	0.07	**0.24**	**0.16**
183VB	0.02	0.09	0.03	0.14	0.00	0.01	**0.04**	**0.17**	0.24	0.01	0.01	0.07	**0.25**	**0.18**
RMS	0.04	0.08	0.09	0.11	0.00	0.02	**0.10**	**0.14**	0.23	0.02	0.03	0.03	**0.25**	**0.14**

TA BIAS

TB BIAS

*Results provided courtesy David Draper, Ball Aerospace & Technologies Corp. Boulder, Colorado USA

Pre-Screening

Dealing with Time-Dependent Calibration Errors

SSMIS Reflector Temperature vs. Sun Elevation/Azimuth

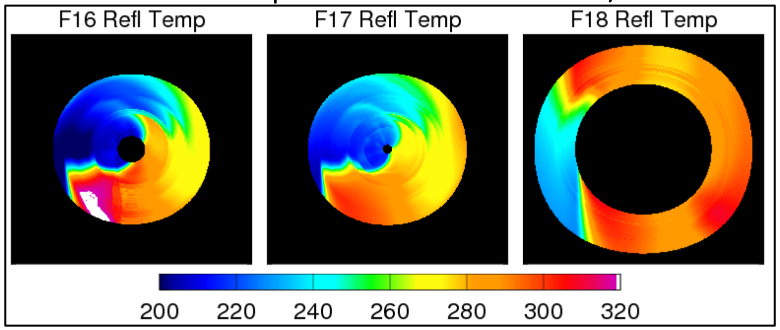

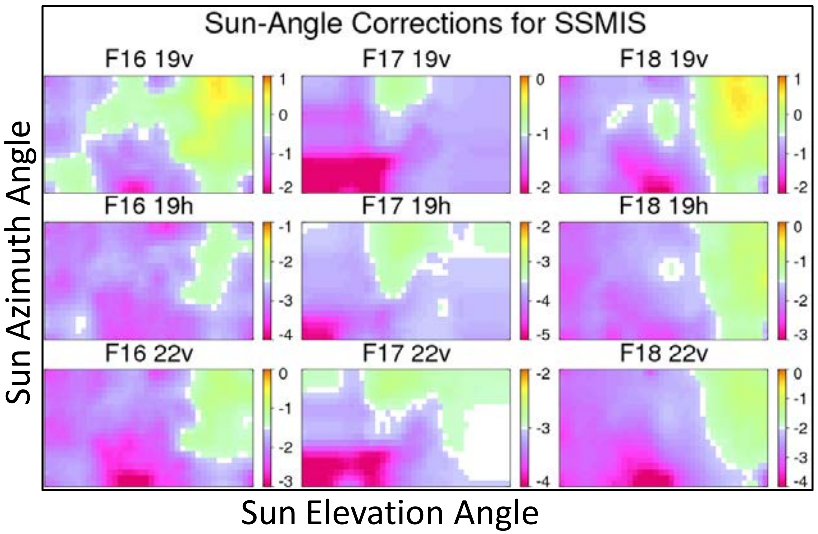

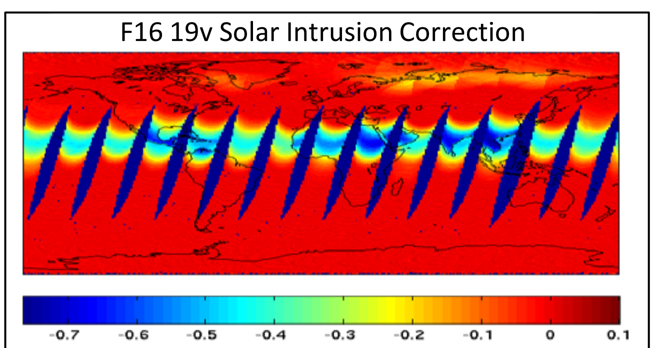

TMI Emissive Antenna Biases vs. Time

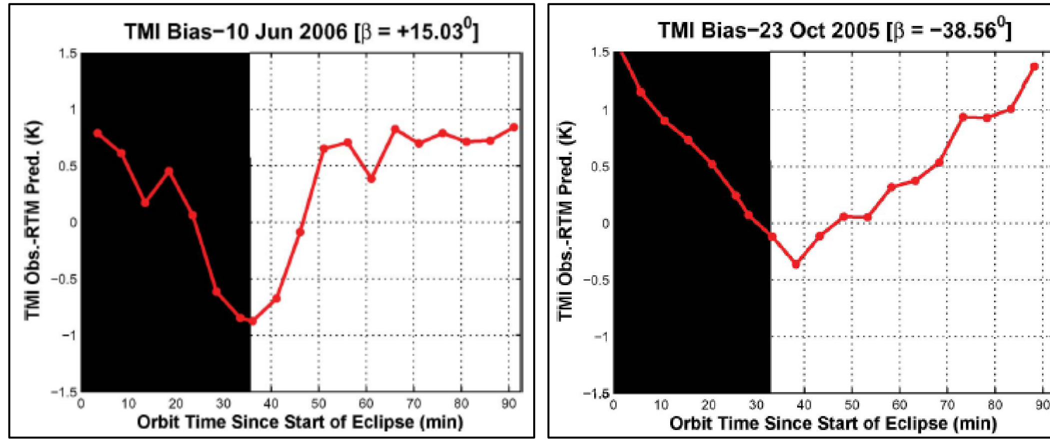

From Gopalan et al. 2009

- Emissive Antenna
  - TMI (~4% emissivity) correction by UCF applied to 1B11 v7 and GPM L1C
  - SSMIS -> Problem for F16 and F17. Difficult to correct for due to intrusions and other issues
  - **GMI looks good!**
- Solar/Lunar Intrusions
  - Solar intrusions into warm load lead to biases in warm calibration point
  - Lunar intrusions into cold-sky mirror bias cold end calibration
  - **No evidence of significant intrusion issues for GMI**
- SSMIS Sun-Angle Corrections
  - Combined corrections for emissive antenna, solar intrusions, and other instrument temperature-dependent biases
  - Computed from multiple years of data using double differences
  - Substantial (2-6K) corrections are different for F16, F17, and F18.
  - Eliminates biases between ascending and descending orbit passes

Intercalibration vs. GPM GMI

Double Difference Approach

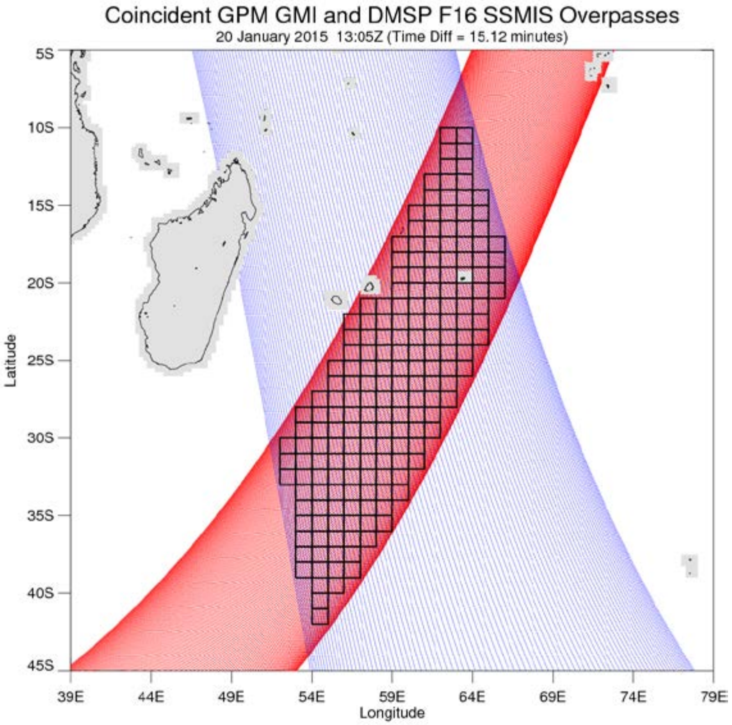

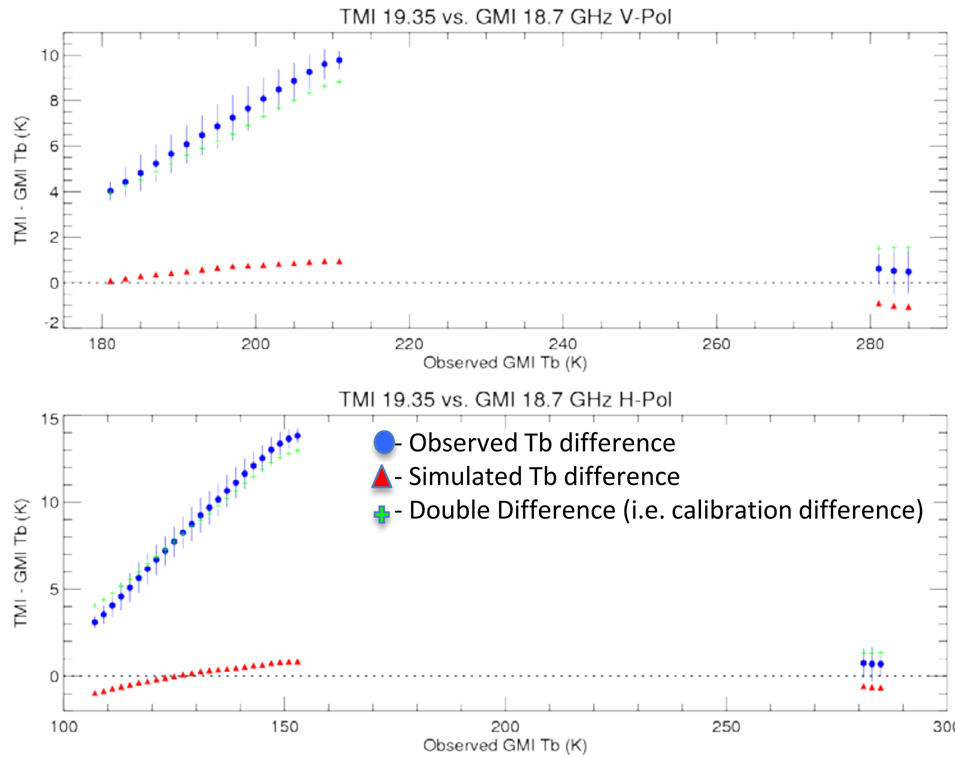

Double Difference Technique

- Identify and collect near-coincident observations between target sensor (e.g. TMI) and reference sensor (i.e. GPM GMI).
- Grid Tb into 1x1 degree boxes and screen for precipitation, land etc.
- Get geophysical parameters from global model analysis or use retrieval algorithm run on GMI for clear-sky scenes.
- Compute simulated Tb for target and reference sensors to account for differences in channel frequencies, bandwidths, view angles etc.
- Compute double difference as follows.

  - Tb_obs(DIF) = Tb_obs(REF) – Tb_obs(TGT)
  - Tb_sim(DIF) = Tb_sim(REF) – Tb_sim(TGT)
  - Ddiff = Tb_obs(DIF) – Tb_sim(DIF)

Intercalibration comparisons for the 19.35 GHz channels on TRMM TMI versus the equivalent channels on GPM GMI. The observed differences, simulated differences, and double differences (i.e. calibration differences), are shown as a function of Tb for the reference sensor (GMI). Cold temperature Tbs correspond to ocean scenes while warmer Tb values correspond to unpolarized vegetated scenes.

GPM Constellation Radiometer Intercalibration

Multiple Independent Techniques

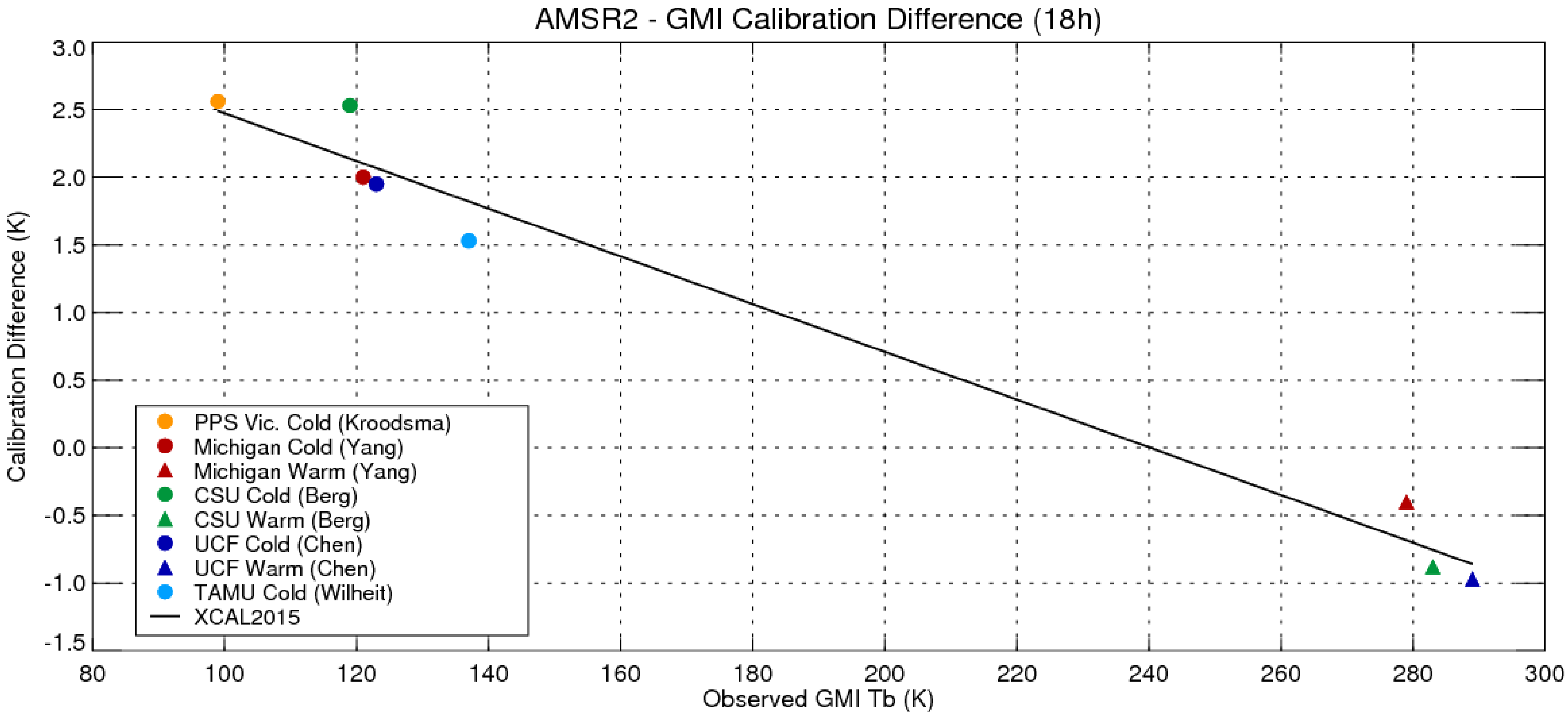

- The above example for the 18 GHz H-Pol channel on AMSR2 shows a “worst” case example of inconsistencies in the calibration between GMI and one of the constellation radiometers.
- Five groups within XCAL produced calibration offsets for cold ocean scenes and three groups produced offsets for warm land scenes.
- While this case exhibits both large biases relative to GMI as well as variations in the bias with scene temperature, the results between teams are consistent within 1K.
- While the XCAL team continues to investigate physical explanations for this discrepancy, we have a high degree of confidence that the adjusted Level 1C Tb values are consistent within 1K.

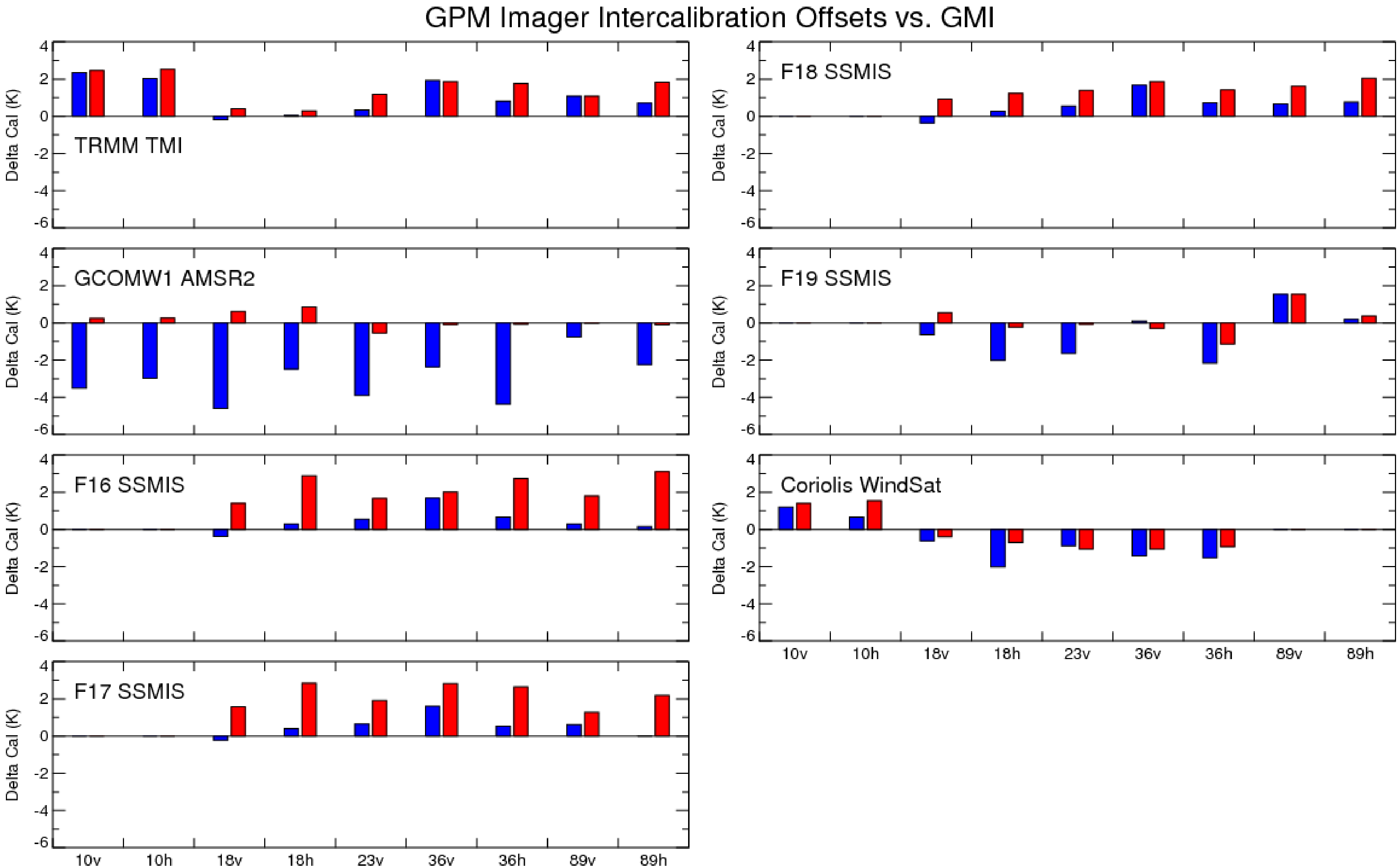
GPM Imager Intercalibration Offsets vs. GMI
TRMM TMI
GCOMW1 AMSR2
F16 SSMIS
F17 SSMIS
F18 SSMIS
F19 SSMIS
Coriolis WindSat
Delta Cal (K)
10v
10h
18v
18h
23v
36v
36h
89v
89h

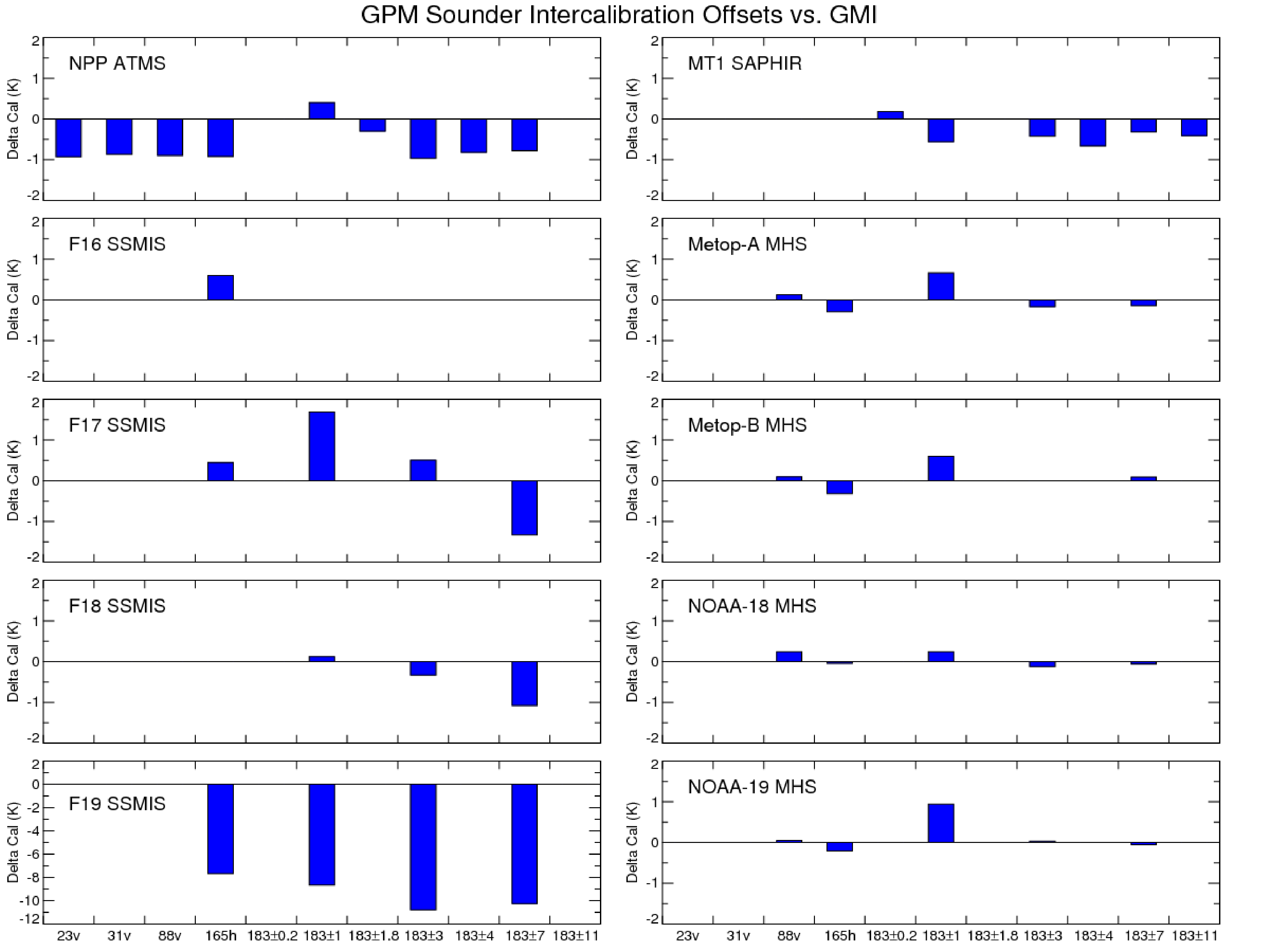

GPM Sounder Intercalibration Offsets vs. GMI
NPP ATMS
MT1 SAPHIR
F16 SSMIS
Metop-A MHS
F17 SSMIS
Metop-B MHS
F18 SSMIS
NOAA-18 MHS
F19 SSMIS
NOAA-19 MHS
Delta Cal (K)
23v 31v 88v 165h 183±0.2 183±1 183±1.8 183±3 183±4 183±7 183±11

Summary

- XCAL team lessons learned
  - Value of multiple approaches for calibration analysis
  - Importance of transparency
  - Value of working with instrument developers to identify instrument issues
- GPM GMI
  - Has both standard imager channels and several water vapor sounding channels
  - Four point calibration for lower frequency channels (standard cold/warm cal plus noise diodes)
  - On-orbit calibration maneuvers
    - Identification of and correction for magnetic interference
    - Adjustments to spillover corrections point to difficulties in characterizing antenna pattern pre-launch
    - Detailed GMI calibraiton uncertainty analysis
  - GMI appears to have the best calibration of any microwave imager to date
- Sounder intercalibration results
  - Very good consistency between current cross-track sounders (water vapor channels)
  - MHS instrument appears very well calibrated and consistent across four satellites
  - Slightly larger differences with NPP ATMS (still within 1K0
  - SSMIS calibration much more problematic
- Specific relevance to ATMS
  - Provide an independent calibration assessment relative to other microwave radiometers
  - Expertise related to the on-orbit identification and corrections for a variety of calibration errors
  - Currently investigating uncertainties in radiative transfer models (Thursday morning talk in GSICS microwave session)

Space Dynamics Laboratory
Utah State University Research Foundation

LW FOV5 Update

Introduction

- For S-NPP CrIS LW FOV5 has higher radiance than other FOVs at 668.125 cm^{-1} for cold scenes
- Numerous presentations on this anomaly
- Latest was from UW exploring unresolved channel spectrum
  - March 16, 2016
  - Beamsplitter gap causes a secondary “ZPD” spike at 0.88 cm OPD
- UW did analysis in the interferogram domain
- Spectral domain analysis should be identical
- Larabee provided monochromatic spectra for hot and cold scenes
- Results ambiguous
- Joe Predina proposed electrical crosstalk as root cause

Beamsplitter Gap Wedge Reduces Amplitude

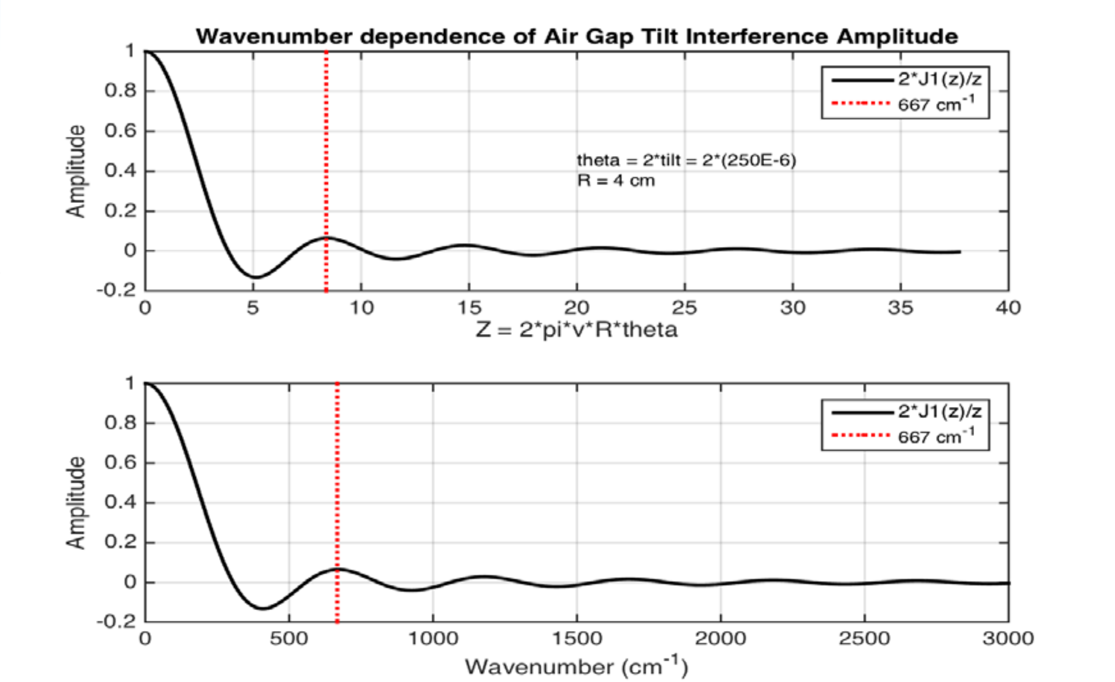

Normalization: 0.5*r ≅ (0.5) * [(n-1)/(n+1)]^2 =0.085 with n = 2.4

- From March 16, 2015 UW presentation
- Didn’t use normalization (conservative analysis)

Effect of Beamsplitter Gap Reflection

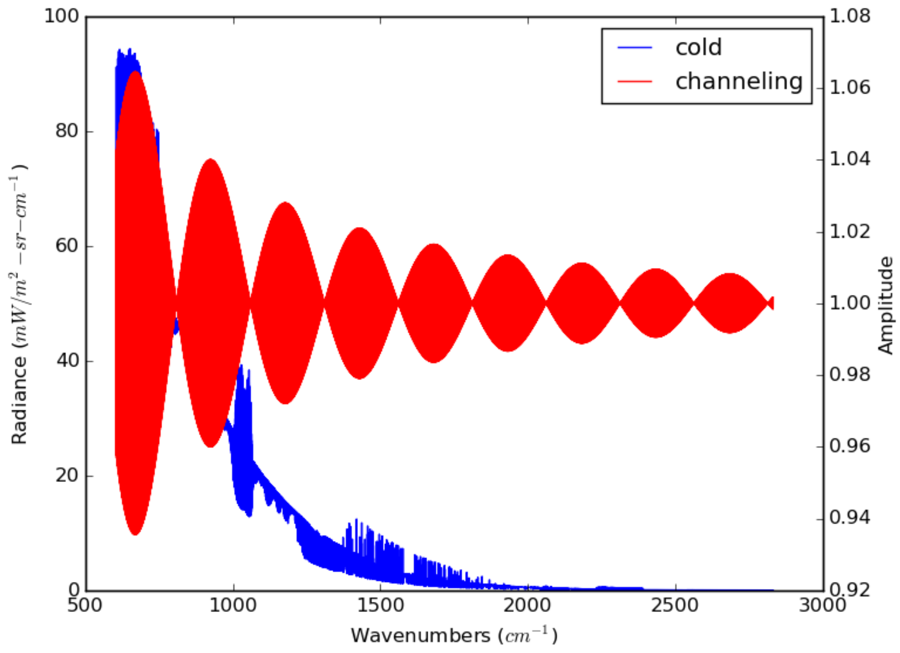

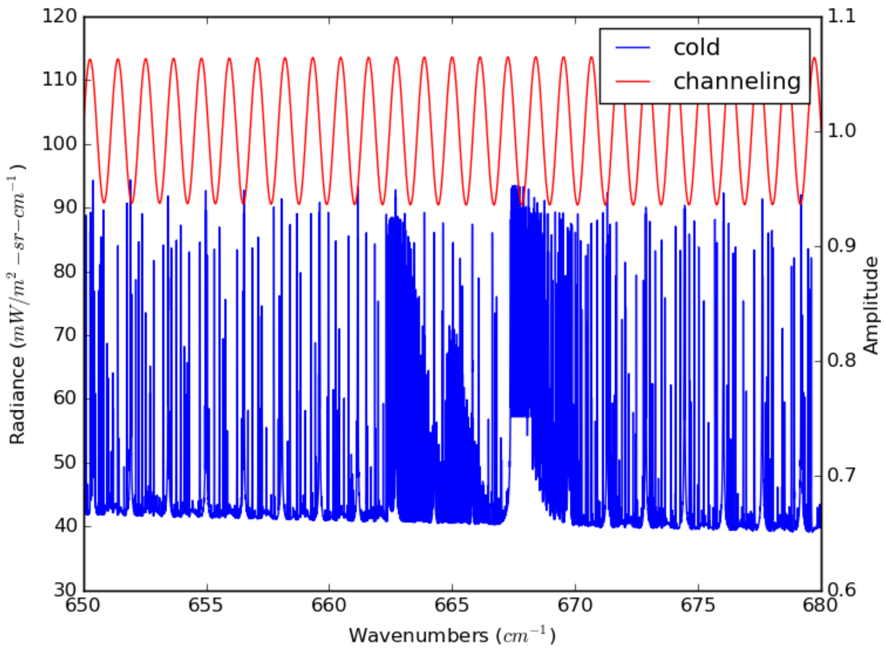

- High resolution spectra is modulated by channeling
- Phase of channeling is unknown

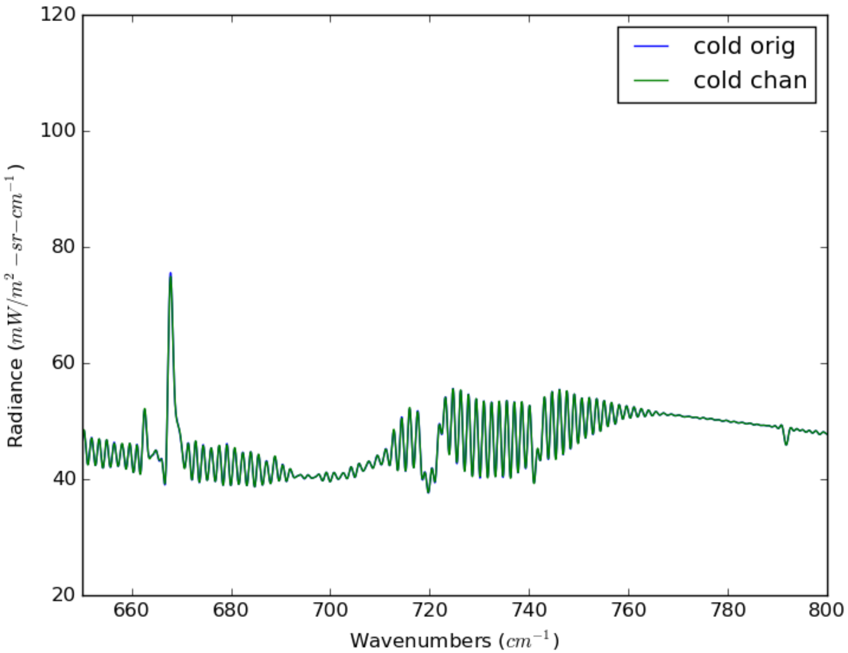

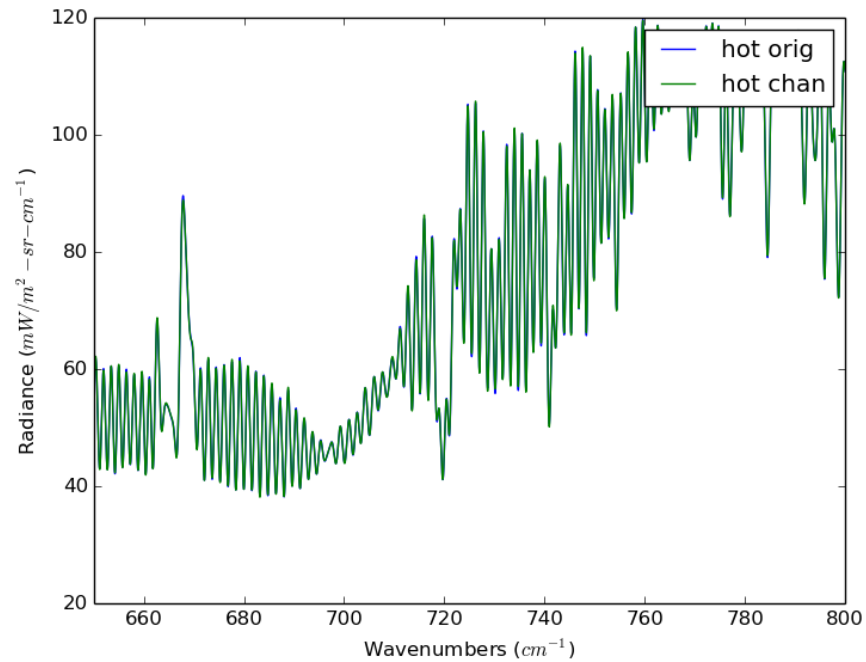

- Monochromatic spectra from Larrabee Strow
- Spectral resolution reduced to CrIS
- Modulation does not have a big affect

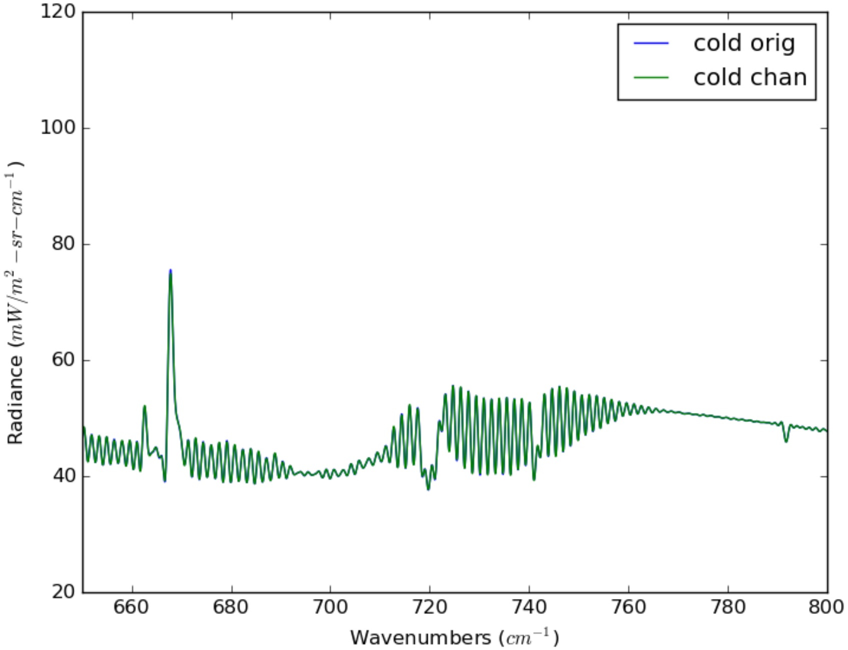

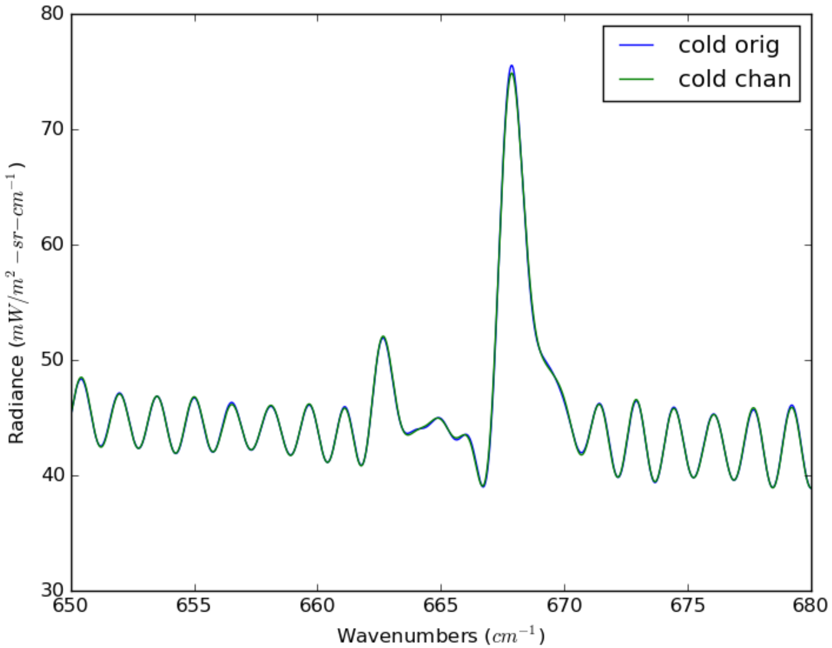

- Spectral resolution reduced to CrIS
- Modulation does not have a big affect

Observed Anomaly Doesn't Match Model

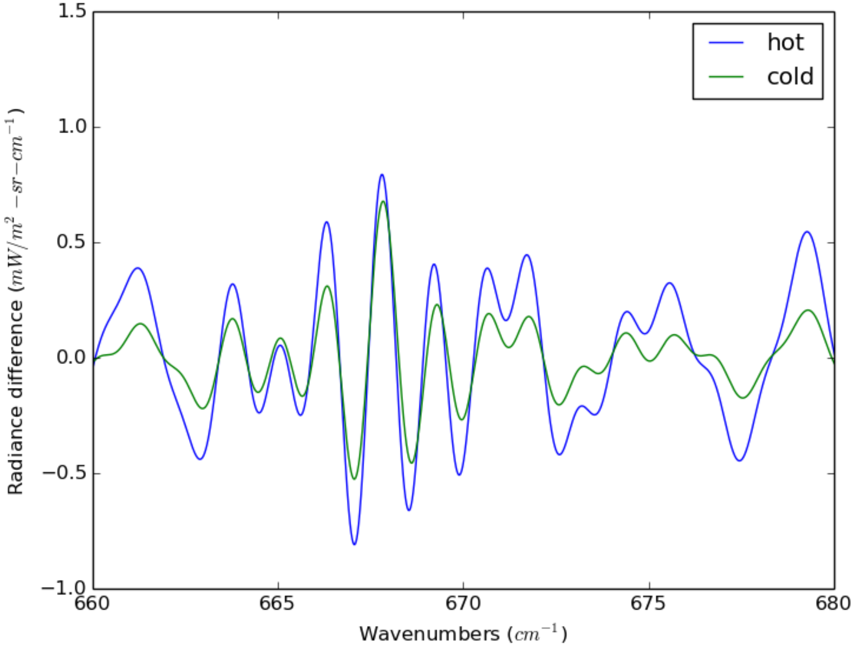

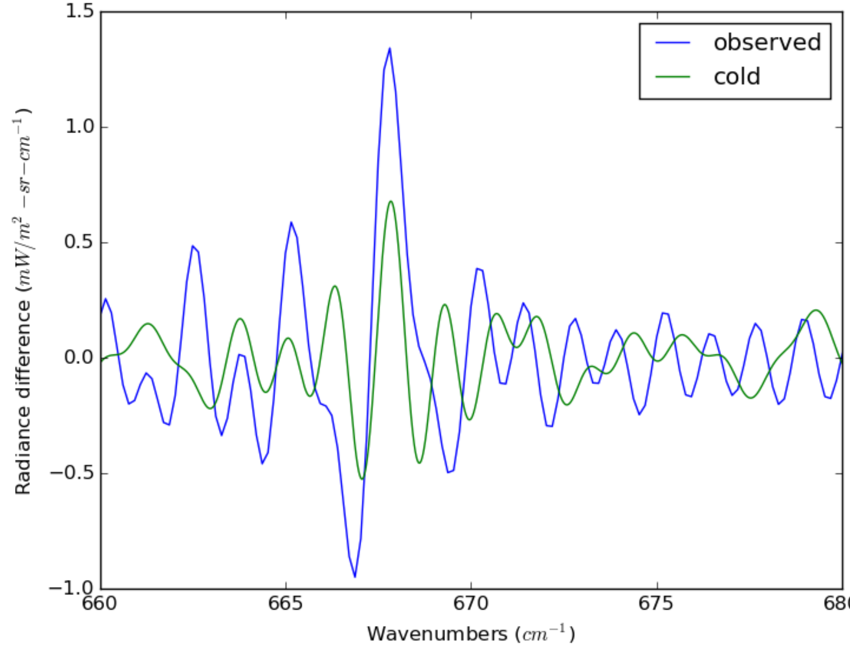

- Observed anomaly larger than modeled
- Larger affect seen for hot spectra than cold
- Shape not a very good match
- Could there be a non-LTE spectral line not in model

Spectral Shift of Anomaly

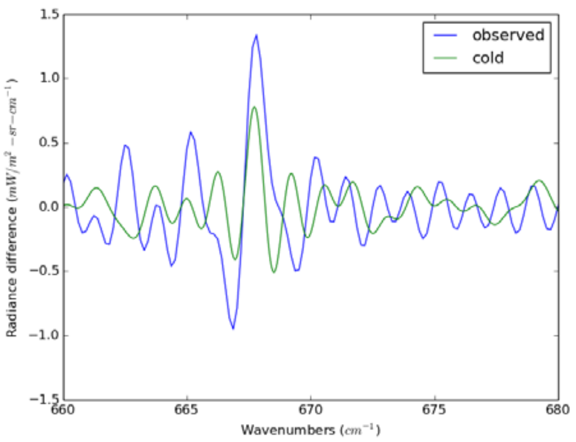

Phase 0

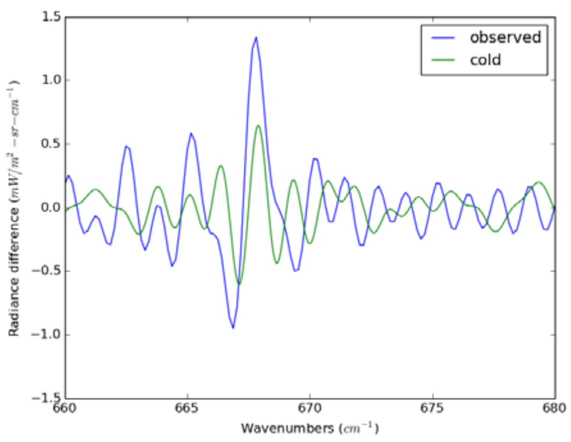

Phase -30

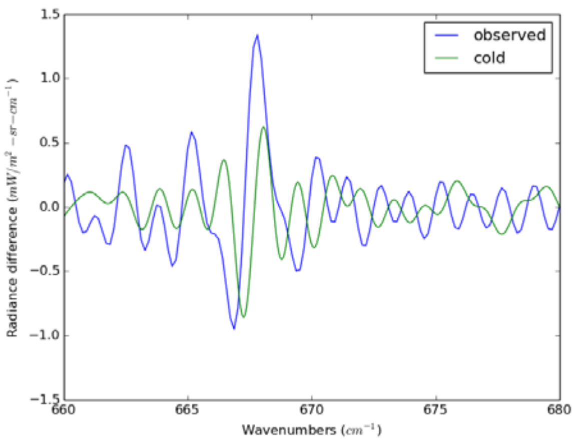

Phase -60

- Position of peak sensitive to the modulating phase
- Beamsplitter gap OPD is 0.88 cm^{-1} or 8800 μm
- Aluminum has thermal expansions of 24×10^{-6}/ºC at 20 C
- Change in length for 1 C change 0.21 μm compared to wavelength of 15 μm (5 degrees of phase)
- On orbit OMA temperature change not large enough to expect to see change

Electrical Cross-Talk

- Joe Predina proposed the effect could be due to electronic cross-talk
- General electronic pickup would likely not have same phase as optical signal and would show in imaginary spectra

Anomaly Only Visible in Real Spectrum

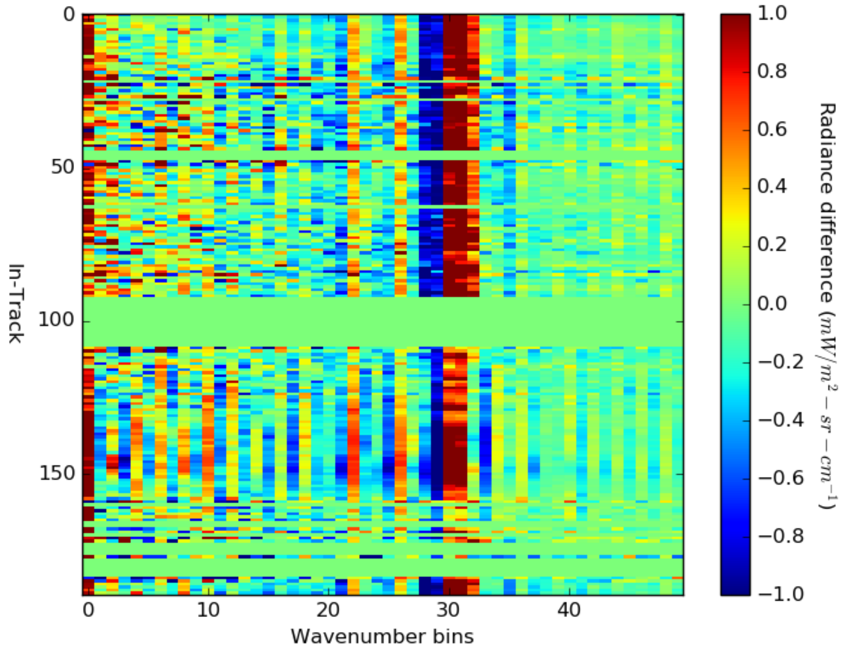

real

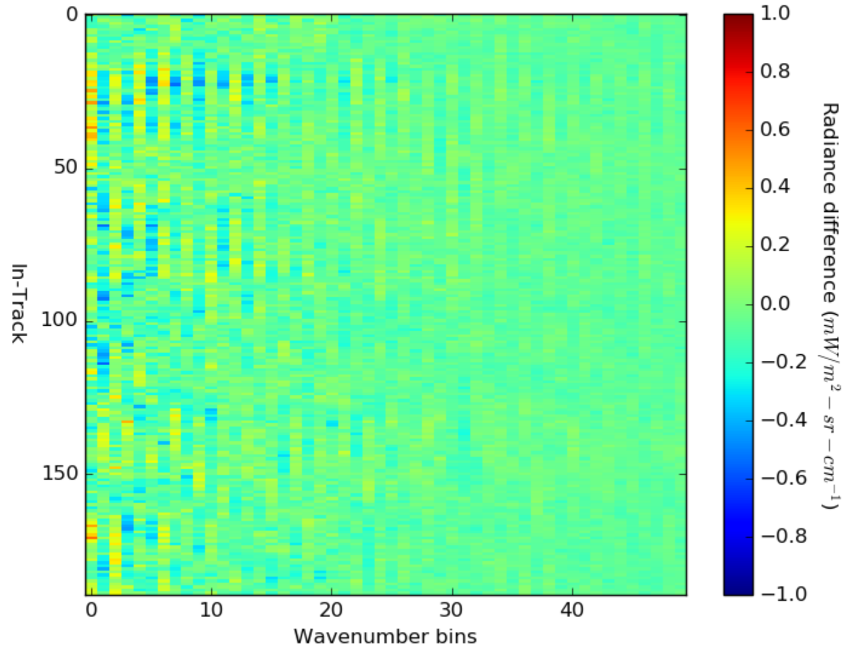

imaginary

- Difference between FOV5 and FOV6
- Anomaly shows up in real but not imaginary spectra
- August 1, 2015 orbit 19478

Electrical Cross-Talk

- If optical or detector electrical cross-talk were getting into FOV5 the line shape would be incorrect
- Synthesized spectra including SA matrix effects
  - From Larrabee Strow's high resolution spectrum
- Added small amount of FOV1 and FOV2 into FOV5
- Applied inverse SA matrix for FOV5
- Plot difference between correct FOV5 spectra

Adding Cross-Talk Not Consistent with Anomaly

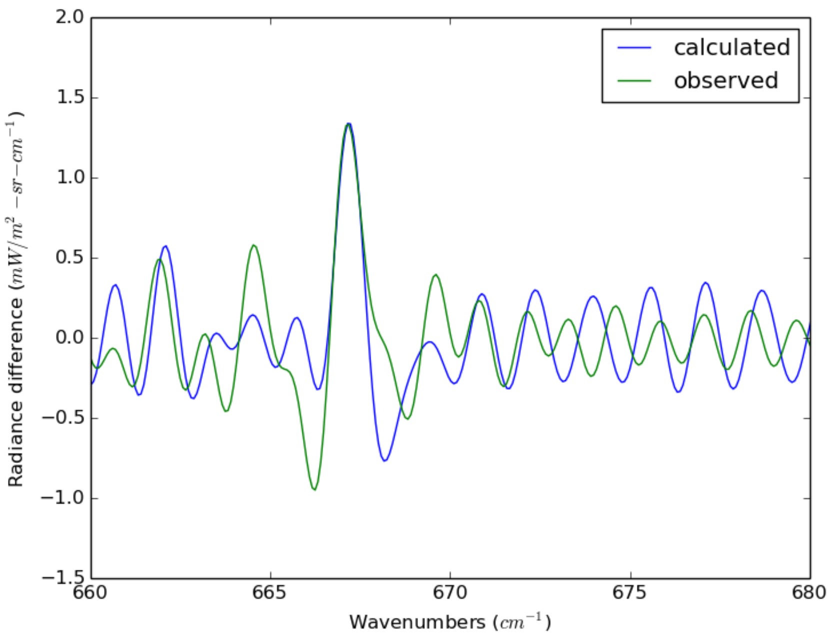

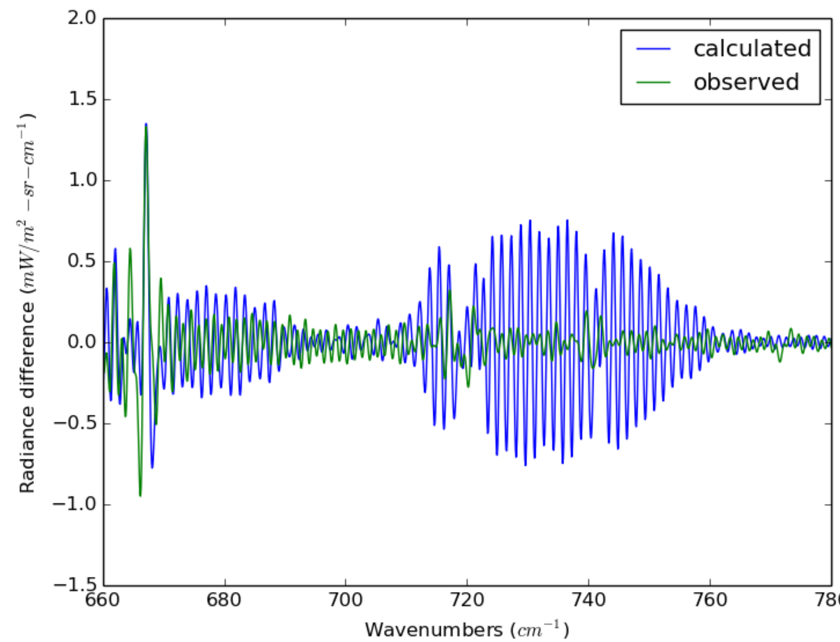

- 0.07 of FOV1 & FOV2 added to FOV5
- Biggest effect in 720 to 760 cm^{-1} region not 668 cm^{-1}
- Other combination of cross-talk also not a good fit

BACKUP

How Large is Anomaly?

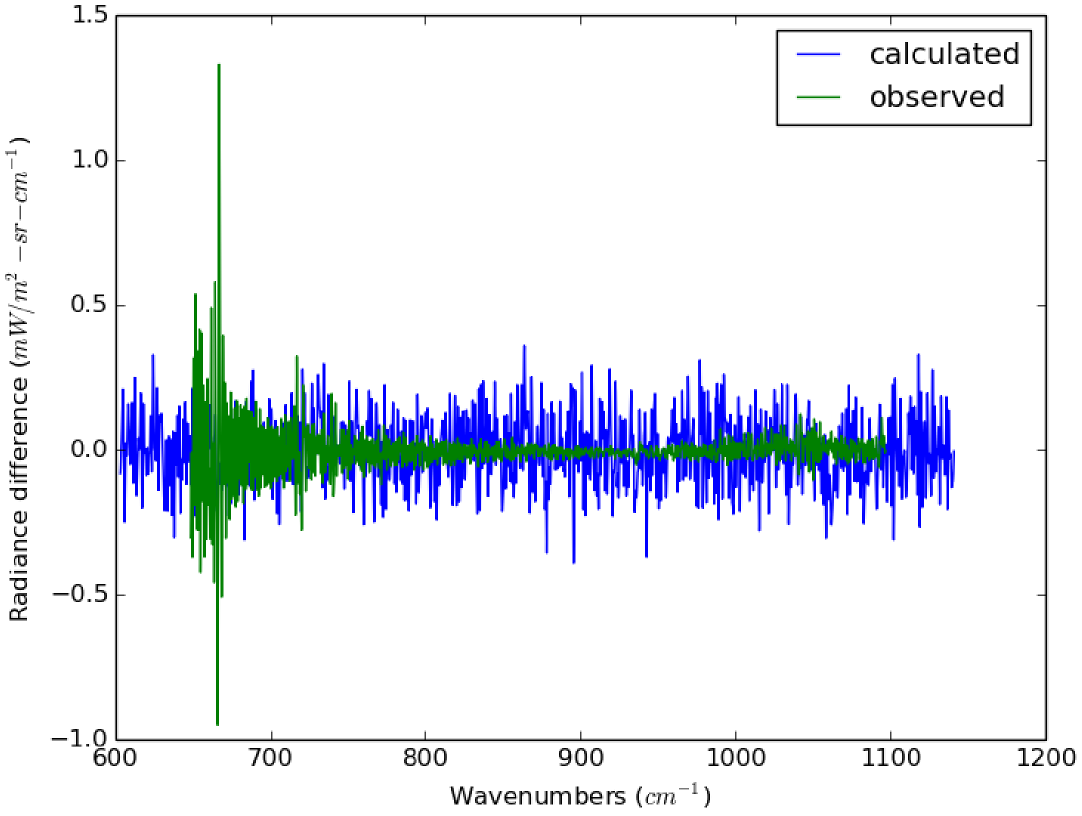

- Anomaly compared to a single pixel noise
- Anomaly was averaged over a granule

Anomaly Spectral Position not Constant

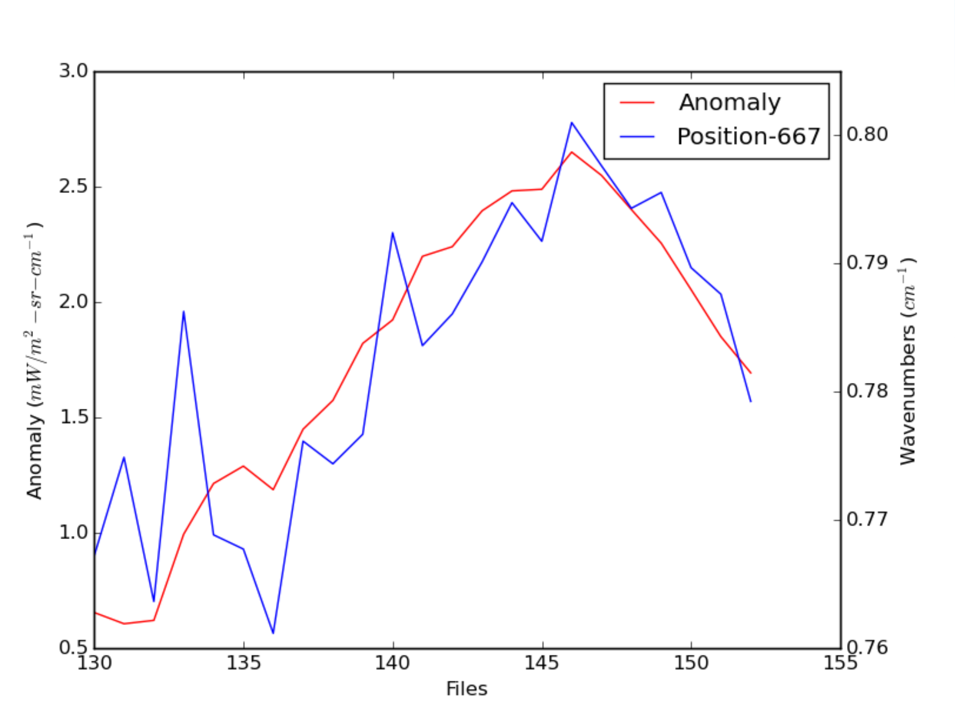

- Spectral position of anomaly correlated with amplitude
- Anomaly amplitude uses left axis, position right axis
- South pole region, averaged over each granule
- August 1, 2015 orbit 19480

Anomaly Spectral Position not Constant

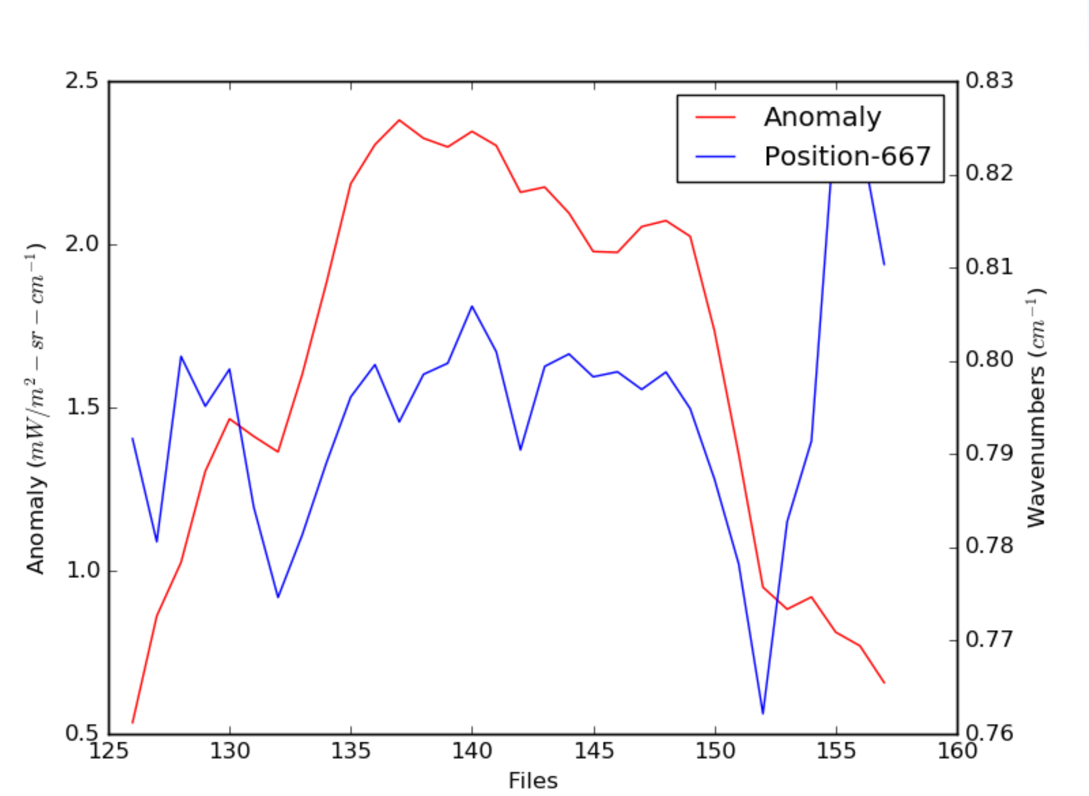

- Spectral position of anomaly correlated with amplitude
- Anomaly amplitude uses left axis, position right axis
- South pole region, averaged over each granule
- June 21, 2015 orbit 18900

Anomaly Spectral Position not Constant

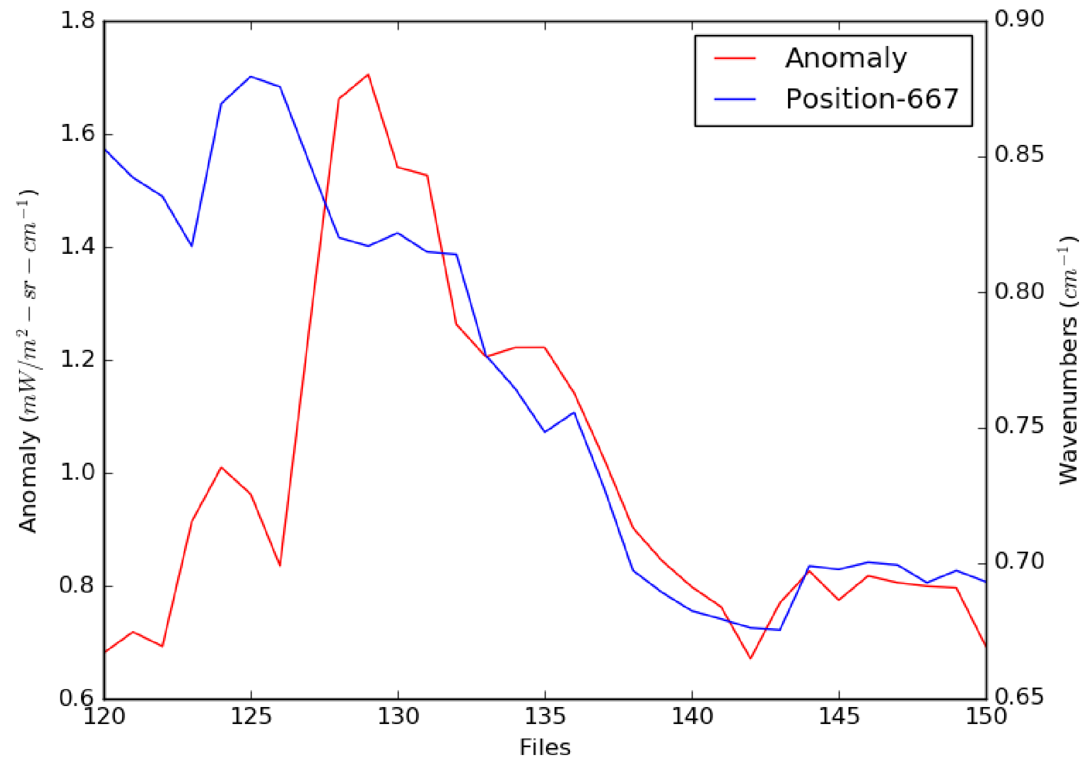

- Spectral position of anomaly correlated with amplitude
- Anomaly amplitude uses left axis, position right axis
- South pole region, averaged over each granule
- December 21, 2015 orbit 21496